Surfactant Based Enhanced Oil Recovery and Foam Mobility Control

3rd Annual & Final Technical Report

Reporting Period Start Date: July 2005

Reporting Period End Date: June 2006

Principal Authors:

George J. Hirasaki, Rice University

Clarence A. Miller, Rice University

Gary A. Pope, The University of Texas

Date Report was Issued: July 2006

DE-FC26-03NT15406

Rice University
Department of Chemical Engineering, MS-362
6100 Main Street
Houston, TX 77005-1892

The University of Texas
Department of Petroleum Engineering
P.O. Box 7726
Austin, TX 78713-7726

INTERA, Inc.
9111A Research Blvd.
Austin, TX 78758

DISCLAIMER

ABSTRACT

Surfactant flooding has the potential to significantly increase recovery over that of conventional waterflooding. The availability of a large number of surfactant structures makes it possible to conduct a systematic study of the relation between surfactant structure and its efficacy for oil recovery. A mixture of two surfactants was found to be particularly effective for application in carbonate formations at low temperature. The mixture is single phase for higher salinity or calcium concentrations than that for either surfactant used alone. This makes it possible to inject the surfactant slug with polymer close to optimal conditions and yet be single phase. A formulation has been designed for a particular field application. It uses partially hydrolyzed polyacrylamide for mobility control.

The addition of an alkali such as sodium carbonate makes possible in situ generation of naphthenic soap and significant reduction of synthetic surfactant adsorption. The design of the process to maximize the region of ultra-low IFT takes advantage of the observation that the ratio of soap to synthetic surfactant is a parameter in the conditions for optimal salinity. Even for a fixed ratio of soap to surfactant, the range of salinity for low IFT was wider than that reported for surfactant systems in the literature. Low temperature, forced displacement experiments in dolomite and silica sandpacks demonstrate that greater than 95% recovery of the waterflood remaining oil is possible with 0.2% surfactant concentration, 0.5 PV surfactant slug, with no alcohol.

Compositional simulation of the displacement process demonstrates the role of soap/surfactant ratio on passage of the profile through the ultralow IFT region, the importance of a wide salinity range of low IFT, and the importance of the viscosity of the surfactant slug.

Mobility control is essential for surfactant EOR. Foam is evaluated to improve the sweep efficiency of surfactant injected into fractured reservoirs as well as a drive fluid for ASP flooding.

UTCHEM is a reservoir simulator specially designed for surfactant EOR. It has been modified to represent the effects of a change in wettability produced by surfactant injection.

TABLE OF CONTENTS

TABLE OF TABLES

TABLE OF FIGURES

INTRODUCTION

Oil recovery by primary depletion and waterflooding recovers only about one third of the original in place, on the average. The remaining oil can be categorized into: (1) the residual oil in the regions swept by water and (2) the movable oil in the regions unswept or poorly swept by water. This project uses surfactants to reduce the residual oil saturation by both interfacial tension reduction and wettability alteration, the latter in cases where wettability is responsible for retaining oil in the matrix. A factor in the sweep efficiency of a reservoir is the mobility ratio between the resident fluids and the injected fluids. Polymer solution is the traditional method for mobility control in surfactant flooding. This project will evaluate foam as an alternate or supplement to polymer for mobility control. Our objective is to economically increase the recovery efficiency beyond that achieved by waterflooding.

Both unfractured and fractured formations will be addressed in this project. The driving force for displacement of oil in unfractured systems is primarily the pressure gradient developed by displacing fluids from the injection well to the production well. This pressure gradient may be only a small contributor in fractured formations. In this case, spontaneous imbibition is needed to exchange the injected fluid and oil between the fracture and matrix. The driving force for spontaneous imbibition includes capillary pressure gradients and buoyancy, or gravity drainage. The contribution due to capillary pressure gradients may be diminished because of low interfacial tension.

Both sandstone and carbonate formations will be considered. Carbonate formation usually tend to be more oil-wet and fractured compared to sandstone formations. In either case, surfactant adsorption on the mineral surfaces must be minimized. Sodium carbonate is used with anionic surfactants in carbonate formations to reduce adsorption. The alkalinity of the sodium carbonate also generates surfactants in situ by reacting with the naphthenic acids in the crude oil.

Scale-up from the laboratory to the field is a necessary part of developing an enhanced oil recovery process. The tool for this scale-up in the reservoir simulator, UTCHEM.

EXECUTIVE SUMMARY

Twenty four surfactants are compared for their efficacy for oil recovery by surfactant flooding. Surfactant structure–performance relationships are needed for applications with a specified crude oil composition, brine salinity, reservoir temperature, formation mineralogy, and recovery mechanism. The surfactants are characterized by the optimal salinity for different pure hydrocarbon oils, the solubilization ratio, which is an estimator of the level of interfacial tension at optimal conditions, and whether it forms viscous gel or liquid crystalline phases that cause slow emulsion coalescence. A combination of two surfactants, N67-7PO-S and IOS 15-18, was found to be particularly effective. N67-7PO-S has amoderately branched hydrophobe with 16-17 carbons, an average of 7 PO (propylene oxide) groups, and is sulfated. IOS 15-18 is an internal olefin sulfonate with 15-18 carbons. The location of the sulfonate in the IOS is distributed along the carbon chain and thus the result is a twin-tailed or branched hydrophobe. The branching reduces the tendency to form gels and viscous emulsions at low temperatures. EO and PO groups impart tolerance to divalent ions. PO is more lipophlic than the hydrophilic EO group and results in a lower optimal salinity requirement. The sulfate has an ester linkage and is subject to hydrolysis at high temperatures and low pH. Thermally stable sulfonates are evaluated for high temperature applications, as discussed more fully in an earlier report.

A surfactant-polymer formulation is being developed for a West Texas carbonate reservoir that has a pressure too low for CO_2 flooding. The formation has anhydrite, which will result in precipitation of sodium carbonate. The formulation has recovered up to 95% of the oil remaining after waterflooding in reservoir formation core material. The project team has met with the operator and partners to plan for a field test.

An alkaline surfactant process is also being developed for enhanced recovery in oil-wet, carbonate formations. The carbonate ion of sodium carbonate is a potential determining ion in carbonate formations such as calcite and dolomite. Alteration of the mineral surface to a negative charge aids in the wettability alteration and makes a dramatic reduction in the adsorption of anionic surfactants. Calcium ion concentration is sequestered because of the low solubility product of calcium carbonate. Also the alkali raises the pH, which results in saponification of naphthenic acids to naphthenic soap, a natural surfactant. The naphthenic soap is usually too lipophilic by itself and addition of a synthetic surfactant is needed. Ultra-low interfacial tensions are possible at synthetic surfactant concentrations as low as 0.05%. The system is complex because it is a mixture of naphthenic soap and synthetic surfactants with very different properties. This results in optimal salinity that depends on the water/oil ratio and surfactant concentration. However, these dependencies can be correlated by the ratio of soap/synthetic surfactant, as shown for two different crude oils. It was discovered that even for a fixed soap/surfactant ratio the range of salinities over which low IFT ($< 10^{-2}$mN/m) occurs is much wider than that expected for conventional akylaryl sulfonate surfactants.

The changing ratio of soap/surfactant during oil displacement can be utilized to have the composition pass through the low IFT region at the displacement front. This results in a robust recovery process that is not overly sensitive to salinity and surfactant

concentration. ASP formulations with 0.5 PV surfactant slug and low surfactant concentrations have recovered over 95% of the waterflood remaining oil from dolomite (0.2% surfactant) and silica (0.5% surfactant) sandpacks. This was possible at room temperature without need for alcohol. A one-dimensional simulator developed to describe the process yielded a cumulative oil recovery curve in agreement with results of the sandpack experiments.

Surfactant retention by adsorption and phase trapping determines the amount of surfactant required for a surfactant enhanced oil recovery process. We show that the adsorption of anionic surfactants on calcite and dolomite can be reduced by an order of magnitude by addition of sodium carbonate at low salinities. The reduction is smaller but still significant at higher salinities.

Mobility control is recognized as an essential element of surfactant EOR.Surfactant injection into fractured formations imposes a severe challenge for reservoir conformance or sweep efficiency. It was shown earlier that foam improves sweep in fracture systems. The apparent viscosity of bulk foam in fractures is evaluated in this report. The possibility of substituting the polymer drive with a foam drive is examined.

Foam was also evaluated as a possible replacement for polymer solution as the drive fluid in a forced convection alkaline/surfactant process. Sandpack experiments were performed in which a surfactant slug of the same composition as in the ASP sandpack floods mentioned above was injected in small increments separated by short intervals of air injection. This was followed by injection of alternating 0.1 PV increments of a polymer-free solution of IOS 15-18 and air. This surfactant was used alone because the foam generated was stronger than that for its mixture with N67-7PO-S as used in the surfactant slug. High oil recovery was obtained in these experiments with sands of two different permeabilities, showing that mobility control was adequate. Apparent viscosity of the foam was greater in the more permeable sand, indicating that use of foam should be particularly effective in heterogeneous reservoirs.

The reservoir simulator, UTCHEM will be used as the tool to scale-up from laboratory experiments to field design. An approach to model the change in wettability produced by an alkaline surfactant solution is presented. The model has been incorporated into UTCHEM, tuned to successfully match results of laboratory imbibition experiments conducted previously at Rice and used to simulate behavior in three dimensions of a process in which surfactant injection into a fractured carbonate reservoir alters matrix wettability, thereby greatly increasing oil recovery.

Task 1 Improved Surfactants and Formulations

We report results for a number of promising EOR surfactants based upon a fast, low-cost laboratory screening process that is highly effective in selecting the best surfactants to use with different crude oils. Initial selection of surfactants is based upon desirable surfactant structure. Phase behavior screening helps to quickly identify favorable surfactant formulations. Salinity scans are conducted to observe equilibration times, microemulsion viscosity, oil and water solubilization ratios and interfacial tension. Co-surfactants and co-solvents are included to minimize gels, liquid crystals and macroemulsions and to promote rapid equilibration to low-viscosity microemulsions. Branched alcohol propoxy sulfates, internal olefin sulfonates, and branched alpha olefin sulfonates have been identified as good EOR surfactants using this screening process. These surfactants are available at low cost and are compatible with both polymers and alkali such as sodium carbonate and thus are good candidates for both surfactant-polymer and alkali-surfactant-polymer EOR processes. One of the best formulations was tested in both sandstone and dolomite cores and found to give excellent oil recovery and low surfactant retention.

Recent advances including the development of new synthetic surfactants and increased understanding of the structure-performance relationship of surfactants have made it possible to rapidly identify promising high-performance surfactants for EOR. This process involves laboratory screening using knowledge of the molecular structure and cost of the surfactants as well as pertinent reservoir-specific information (i.e. temperature, salinity and crude oil properties).

The surfactant selection process starts with the screening of surfactants by phase behavior experiments and progresses to core floods with formulations that may incorporate co-surfactants, co-solvents, alkali, polymers and electrolytes as well. We illustrate the application of this approach to the selection of a surfactant formulation for use in both a sandstone outcrop and a West Texas dolomite reservoir, but focus mostly on the dolomite application because very few studies have been reported for carbonate (Adams, *et al*., 2006) or dolomite reservoirs. These laboratory data were used in a parallel simulation study of the same reservoir described by Anderson *et al*. (2006).

It is well known that the primary requirement needed to mobilize residual oil saturation is a sufficiently low interfacial tension (IFT) to give a capillary number large enough to overcome the capillary forces and allow the oil to flow (Stegemeier, 1976). Low IFT can be obtained with a wide variety of surfactants, but the best surfactant depends on the crude oil and reservoir conditions and must also satisfy several other stringent requirements. These requirements include low retention, compatibility with the electrolytes and polymer, thermal stability, aqueous stability, and low cost. Surfactant retention is due in part to adsorption on the rock surfaces, but other loss mechanisms including phase trapping can be just as important, or more so. There is a strong and well-established relationship between the microemulsion phase behavior and IFT (Winsor, 1954; Healy *et al*., 1976; Huh, 1979; Nelson and Pope, 1978; Pope *et al*., 1979; Bourrel and Schechter, 1988; Aoudia *et al*., 1995). This relationship can be used to great advantage to rapidly screen surfactants and predict which ones will likely perform best in the more difficult and expensive core floods.

Winsor (1954) described surfactant/oil/water microemulsions as type I (oil in water), type II (water in oil) or type III (bicontinuous oil and water in a third phase known as the middle phase microemulsion). The type III or middle phase microemulsions exhibit the lowest IFT. For anionic surfactants, increasing the salinity among other variables causes the characteristic transition from type I to type III to type II. Healy *et al*. (1976) presented the concept of optimum salinity as it applies to type III microemulsions. They observed the volumes of oil (V_o) and water (V_w) per unit volume of pure surfactant (V_s) in middle phase microemulsions and defined the optimum solubilization ratio (*) as the intersection of plots of V_o/V_s and V_w/V_s. Huh (1979) developed a theoretical relationship between the oil and water solubilization ratios, σ and IFT (γ):

$$\gamma = \frac{C}{\sigma^2},$$

where C is about 0.3 dynes/cm for typical crude oils and surfactants used for EOR. A very large number of papers published since 1979 have shown the Huh equation accurately models the IFT between equilibrium microemulsions and oil or water for numerous combinations of surfactants and crude oils over a wide range of concentration, salinity, temperature and other conditions typical of oil reservoirs. While IFT in the range of interest can be measured by the spinning drop method, using the Huh equation to calculate it from phase behavior data affords several significant advantages. These include the comparative ease and speed with which phase behavior experiments can be performed as well as the opportunity for easily taking repeated measurements over time.

It is desirable to quickly examine hundreds of combinations of surfactants, co-surfactants, co-solvents, numerous electrolytes in several different reservoir and injection brines, polymers, alkali such as sodium carbonate and sodium hydroxide, and different water-oil-ratios (WOR) for each specific crude oil. Thus, using simple observations of the microemulsion phase behavior in pipettes rather than measuring IFT for each combination is a very big advantage. Furthermore, IFT can be very difficult to measure with some crude oils and is subject to large uncertainty. IFT can vary with time for periods up to several months and may depend on precisely how the fluids are sampled and measured. It is of course a good idea to measure IFT on selected samples after the initial phase behavior screening, but it is not the most practical way to initially screen surfactants.

Using phase behavior to screen surfactants has other very significant advantages over IFT. It is easy to make qualitative observations of how fluid the interfaces are in the pipettes, how viscous the phases are, and how fast the emulsions equilibrate to microemulsions. These phenomena are as important to the selection of a suitable surfactant as IFT is. Highly viscous phases will not easily transport under low pressure gradients and will perform poorly in the reservoir where the pressure gradient is often on the order of 1 psi/ft or less.

High viscosity correlates with high surfactant retention. Thus, it is more efficient and effective to screen out such surfactants or to mitigate the problem by adding co-solvents or some other measure early in the screening process and not attempt to measure IFT until a microemulsion with a reasonable viscosity is identified. Core floods are expensive and core flood data are subject to uncertainty and misinterpretation unless

the phase behavior and physical properties such as viscosity have been measured and are well understood.

Extensive research on surfactants has established a clear relationship between surfactant structure and fluid properties and performance related to EOR (Bourrel and Schechter, 1988; Aoudia *et al*., 1995; Austad and Milter, 2000). For example, the solubilization ratio increases and the optimum salinity decreases with increasing hydrophobe length. Weakly hydrophobic functional groups such as propylene oxide (PO) have been characterized as having interface affinity, and as such increase the breadth of the ultra-low IFT region. The addition of these hydrophobic groups lowers the optimum salinity and adds calcium tolerance, so the degree of propoxylation can be used to tailor the surfactant to a given crude oil, temperature and salinity (Aoudia *et al*., 1995; Sanz and Pope, 1995; Wu *et al*., 2005; Jayanti *et al*., 2002; DOE, 2004; DOE, 2005). Similar statements can be made with respect to the addition of ethylene oxide (EO) or both EO and PO groups to the surfactant. Fortunately, both EO and PO are relatively inexpensive chemicals, so these are among the most practical ways to tailor a surfactant to the desired conditions as well as to improve its performance.

In this study, we focus on the use of POs to improve surfactant performance. Aoudia *et al*. (1995) showed the importance of hydrophobe branching with Guerbet alcohol propoxy sulfate surfactants that formed middle phase microemulsions. Branching decreases the order in the micellar structures, which tends to decrease the viscosity, reduce the time required for mixtures to equilibrate, and promotes the formation of microemulsions as opposed to undesirable liquid crystals, gels and other viscous phases. Co-surfactants that are branched or of differing structure are often added to further disrupt the orderly arrangement of surfactant molecules. Alcohols in the C4 range can be used to break viscous structures, but it is lower cost to use hydrophobe branching when possible. Polymers can also complicate the phase behavior and require the addition of co-solvent. Once again, the advantage of initially observing the phase behavior rather than measuring IFT is apparent since polymer typically has little if any effect on IFT.

Based upon this extensive knowledge base and understanding of surfactants and microemulsions, it makes sense to seek out or make surfactants with branched hydrophobes and screen them using the rapid phase behavior approach. The phase behavior is also needed for modeling purposes and is useful for interpreting the data from core floods to measure oil recovery and surfactant retention.

Subtask 1.1 Identifying and Synthesizing Improved, Cost-effective Surfactants

Isotridecanol (TDA) was initially considered to be the most suitable hydrophobe in terms of phase behavior for pure hydrocarbons ranging between hexane and decane (DOE, 2004; DOE, 2005). We started with TDA in part because it is the lowest cost commodity alcohol suitable for making synthetic surfactants with a sufficiently high carbon number for EOR of light crude oils. Formulations with this $C_{13}PO_x$-sulfate exhibited high optimum salinities with the C_6 to C_{10} hydrocarbons and may be a good candidate for some reservoirs. However, for some crude oils, temperatures, and salinities, the C_{13} hydrophobe is too short, so PO sulfates were made from a C_{16-17}

branched alcohol. Using this alcohol, 3, 5 and 7 propylene oxide units were added to make the three surfactants C_{16-17}-$(PO)_3$-SO_4, C_{16-17}-$(PO)_5$-SO_4 and C_{16-17} -$(PO)_7$-SO_4. Formulations with each surfactant were screened with several co-surfactants and co-solvents. The 7 PO sulfate when mixed with a C_{15-18}IOS emerged from the phase behavior screening tests as the best formulation for a crude oil from a low-temperature dolomite reservoir. For temperatures above about 60 C, sulfates will hydrolyze and cannot be used. For high temperature applications, similar surfactants can be made as sulfonates.

Table 1.1-1 gives the names and abbreviated chemical structures of some of the surfactants that have been screened for use with this West Texas reservoir (WT) crude using these new surfactants as well as some older generation surfactants such as branched alkyl benzene sulfonates and alpha olefin sulfonates (AOS). Similar screening has also been done with other crude oils at both UT and Rice University (DOE, 2004; DOE, 2005). The C_{20-24}AOS, C_{15-18}IOS, and the alcohol propoxy sulfates were synthesized specifically for testing in this project and are discussed below.

Table 1.1-1. Candidate Surfactants Tested for EOR

Descriptive Name	Abbreviated Chemical Formula (*b* = branching in the carbon chain)
C_{11-13} Alkyl Benzene Sulfonate (ABS)	$bC_{11-13}(C_6H_5)$-SO_3^-
C_{16} *o*-Xylene Sulfonate	C_{16}-(C_8H_{12})-SO_3^- where C_8H_{12} = *o*-xylene
Secondary Alkane Sulfonate (SAS)	R-CH(SO_3^-)-R' where R + R' = C_{14}-C_{17}
C_{14} Alpha Olefin Sulfonate (AOS)	bC_{11}-CH(OH)-CH_2-CH_2-SO_3^- (~75%) bC_{11}-CH=CH-CH_2-SO_3^- (~25%)
C_{16-18} Alpha Olefin Sulfonate (AOS)	bC_{13-15}-CH(OH)-CH_2-CH_2-SO_3^- (~75%) bC_{13-15}-CH=CH-CH_2-SO_3^- (~25%)
C_{20-24} Alpha Olefin Sulfonate (AOS)	bC_{17-21}-CH(OH)-CH_2-CH_2-SO_3^- (~75%) bC_{17-21}-CH=CH-CH_2-SO_3^- (~25%)
C_{15-18} Internal Olefin Sulfonate (IOS)	R-CH(OH)-CH_2-CH(SO_3^-)-R' (~75%) R-CH=CH-CH(SO_3^-)-R' (~25%), where R+R' = C_{12-15}
C_{16-17} Alcohol 3-Propoxy Sulfate (C_{16-17}-$(PO)_3$-SO_4)	bC_{16-17}-O-[$CH_2(CH_3)$CH-O]$_3$-SO_3^-
C_{16-17} Alcohol 5-Propoxy Sulfate (C_{16-17}-$(PO)_5$-SO_4)	bC_{16-17}-O-[$CH_2(CH_3)$CH-O]$_5$-SO_3^-
C_{16-18} Alcohol 5.7-Propoxy Sulfate (C_{16-18}-$(PO)_{5.7}$-SO_4)	C_{16-18}-O-[$CH_2(CH_3)$CH-O-]$_{5.7}$-SO_3^-
C16-17 Alcohol 7-Propoxy Sulfate (C16-17-(PO)7-SO4)	bC16-17-O-[CH2(CH3)CH-O]7-SO3-

1.1.1 Alcohol Propoxy Sulfate (APS) Surfactant

Commercially available branched alcohols were selected for synthesis of the alcohol propoxy sulfate (APS) surfactants. Isotridecyl (C_{13}) alcohols manufactured from oligomerization of C_3 groups (Exxal™) and of C_4 groups (Marlipal™) were propoxylated and sulfated by Sasol Chemical Co. or Stepan Chemical Co. Another hydrophobe selected for EOR applications was Shell Chemical Company's Neodol® 67, a C_{16-17} alcohol with an average of 1.5 methyl groups randomly positioned along the molecule. Branched, rather than linear alcohols were selected because branching decreases the formation of ordered structures/liquid crystals.

It was reasoned that the size of the hydrophobe (alcohol) was appropriate for light crude oils with typical equivalent alkane carbon numbers (EACN) ranging from C_8 to C_{12}. Alcohols were propoxylated with varying amounts of PO and sulfated with sulfamic acid or sulfur trioxide by Stepan Chemical Co. APS surfactants similar to these have been investigated in previous studies (Aoudia *et al*., 1995; Wu *et al*., 2005; Hirasaki and Zhang, 2004). An approximate structure of a C_{16-17}-$(PO)_7$-SO_4 molecule generated by a space filling, free-energy minimizing model is shown in Fig. 1.1-1 (a). The purpose of this illustration is to show the branching and compactness of the molecule and compare it with two others described next. The PO part of the molecule folds in a spiral. The hydrophobe here is shown with 16 carbon atoms and 3 methyl branches. Both features result in a molecule that is very different than typical linear hydrophobes. This is highly beneficial since the linear surfactants tend to form ordered structures that lead to liquid crystals and gels. This surfactant can be tailored by changing the number of POs.

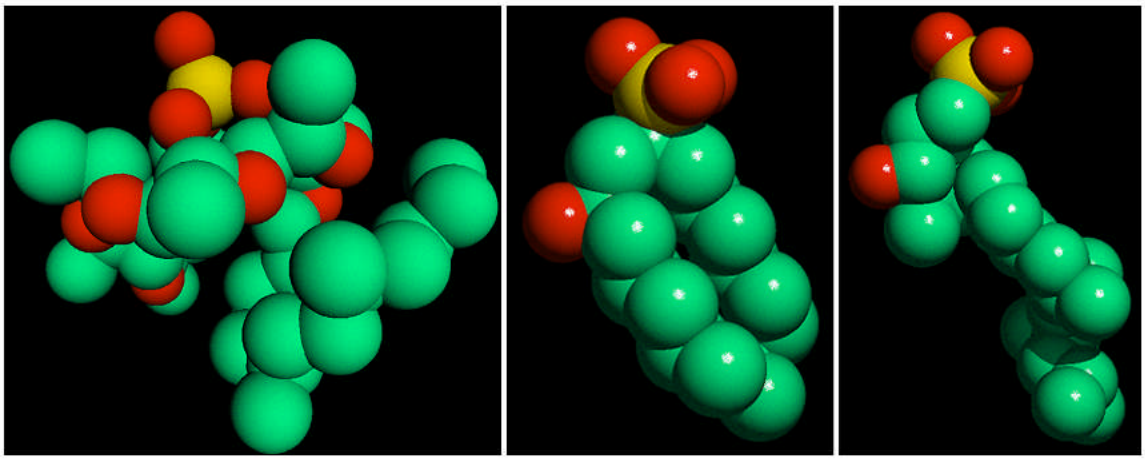

Figure 1.1-1 Possible structures of (a) C_{16-17} Alcohol 7-Propoxy Sulfate (C_{16-17}-$(PO)_7$-SO_4), (b) C_{15-18} Internal Olefin Sulfonate (IOS), and (c) C_{20-24} Alpha Olefin Sulfonate (AOS).

1. 1.2 C_{15-18} Internal Olefin Sulfonate (IOS)

This IOS was prepared by Stepan Chemical Co. using an internal olefin from Shell that is prepared via the oligomerization of ethylene by a process described as olefin metathesis. The internal olefin will have an overall size of C_{15} to C_{18} and a narrow range of internal, double-bond positions such that sulfonation with SO_3^{2-} will produce a variety of products. In addition to alkene sulfonate isomers produced by the position of the double bond, there are other surface-active products formed during the aging, neutralization and hydrolysis steps of commercial sulfonation. The first intermediates of sulfonation are β-sultones, which undergo transformation to alkene sulfonates or to γ- and δ- sultones. Neutralization and hydrolysis steps transform the γ- and δ- sultones to hydroxy alkane sulfonates. The proportion of alkene sulfonates to hydroxyl alkane sulfonates is roughly 60:40. The end result is a surfactant mixture with many different species of sulfonates, which is expected to minimize the formation of ordered structures such as liquid crystals and gels. The hydroxy alkane sulfonate form of a C_{15-18}IOS

molecule is shown in Fig. 1.1-1 (b) using the same approximate model as before for the purposes of visualization and comparison.

1. 1.3 C_{20-24} Alpha Olefin Sulfonate (AOS)

The C_{20-24} alpha olefin (AO) from BP is expected to be more highly branched than the AO from Shell Chemical. The AOS from this olefin was prepared by Stepan Chemical Co. The chemistry of sulfonation is the same as for IOS, and the expected products would be alkene-1-sulfonate and hydroxyl alkane sulfonates. The hydrocarbon length and unspecified branching of this AOS may contribute to its overall good performance. An approximate structure of a C_{20-24}AOS molecule in its hydroxyl alkane sulfonate form is shown in Fig. 1.1-1 (c) using the same model as before for the purposes of comparison.

Subtask 1.2 Phase Behavior Screening

Experiments were first performed to measure the phase behavior of surfactant-oil-water mixtures as a function of electrolyte concentration. Oil and water solubilization ratios were observed as salinity was increased causing a transition in phase behavior from Windsor type I to type III to type II. Two mL of each sample were pipetted into a thin, graduated, 5 mL borosilicate glass pipette with a flame-sealed bottom end. The level of the aqueous surfactant solution was recorded. Two mL of hydrocarbon was added and argon was used to displace volatile gas so that the tops of pipettes could be safely flame sealed. Pipettes were then placed in an oven at reservoir temperature. After reaching the desired test temperature, pipettes were inverted several times to facilitate mixing. Phase volumes were then observed and recorded over time. If the formation of viscous gels or macroemulsions appeared to inhibit mass transfer, pipettes were sometimes agitated again. Phase behavior of surfactant/co-surfactant/co-solvent formulations was evaluated using the following mostly qualitative criteria:

- How fast the emulsions break after gentle mixing and form a microemulsion in equilibrium with oil and/or brine and the absence of macroemulsions or gels, particularly at and below optimum salinity.
- High solubilization ratio at optimum salinity and hence low IFT. A solubilization ratio of 10 or greater corresponds to an IFT on the order of 0.003 dynes/cm or less.
- Microemulsion with low viscosity and the absence of high viscosity gels or other viscous phases, or rigid fluid interfaces, or interfaces with persistent, viscous macroemulsions next to them.
- Aqueous stability of surfactant/polymer solutions at required injection salinity (may be different from optimum salinity).

Preliminary phase behavior screening with the surfactants listed in Table 1.2-1 was performed with pure hydrocarbons. Some of the advantages of using pure hydrocarbons for initial screening include clarity of interfaces and other observations as well as the ability to compare the results with a large body of surfactant data with the

same pure hydrocarbons. The C_{16-17}-$(PO)_7$-SO_4 exhibited the most promising performance with both pure hydrocarbons and the West Texas crude oil (Table 1.2-1). Both C_{20-24}AOS and C_{15-18}IOS co-surfactants improved the performance of the C_{16-17}-$(PO)_7$-SO_4 with respect to equilibration time and the absence of gels and macroemulsions. The phase behavior of a mixture of C_{16-17}-$(PO)_7$-SO_4 and C_{15-18}IOS surfactants with the West Texas crude oil is shown as a volume fraction diagram in Fig. 1.2-1. The volume fraction data show the classical transition from type I to type III to type II microemulsion as the salinity increases. The optimum salinity shown in the tables and figures varies depending on the concentration of calcium in the samples.

Table 1.2-1. Some Formulations Screened with WT Crude Oil at 38 °C

Surfactant Formulation	Optimum Salinity S*, ppm NaCl	Optimum Sol. Ratio, σ, cc/cc	Equilibration Time at S*, days
2% *b*C_{12}-$(PO)_3$-SO_4, 2% TDA-$(PO)_3$-SO_4, 1% dihexyl-sulfosuccinate	75,000	3.5	<2
4% C_{20-24} AOS, 8% SBA	25,000	6	5
1.5% C_{16-17}-$(PO)_7$-SO_4, 0.5% C_{15-18} IOS	viscous/ slow equil.	-	-
0.75% C_{16-17}-$(PO)_7$-SO_4, 0.25% C_{20-24} AOS, 2% SBA	17,000	11	73
1.5% C_{16-17}-$(PO)_7$-SO_4 , 0.5% C_{15-18} IOS, 1% SBA, 1% Na_2CO_3	38,000	6	<1
0.375% C_{16-17}-$(PO)_7$-SO_4, 0.125% C_{15-18} IOS, 0.5% SBA	viscous/ slow equil.	-	-
0.75% C_{16-17}-$(PO)_7$-SO_4, 0.25% C_{15-18} IOS, 2% SBA, 1% Na_2CO_3	33,000	14	<1
1.5% C_{16-17}-$(PO)_7$-SO_4, 0.5% C_{15-18} IOS, 1% Na_2CO_3	35,000	12	2
0.75% C_{16-17}-$(PO)_7$-SO_4, 0.25% C_{15-18} IOS, 2% SBA, 1375 ppm $CaCl_2$	45,000	12	14

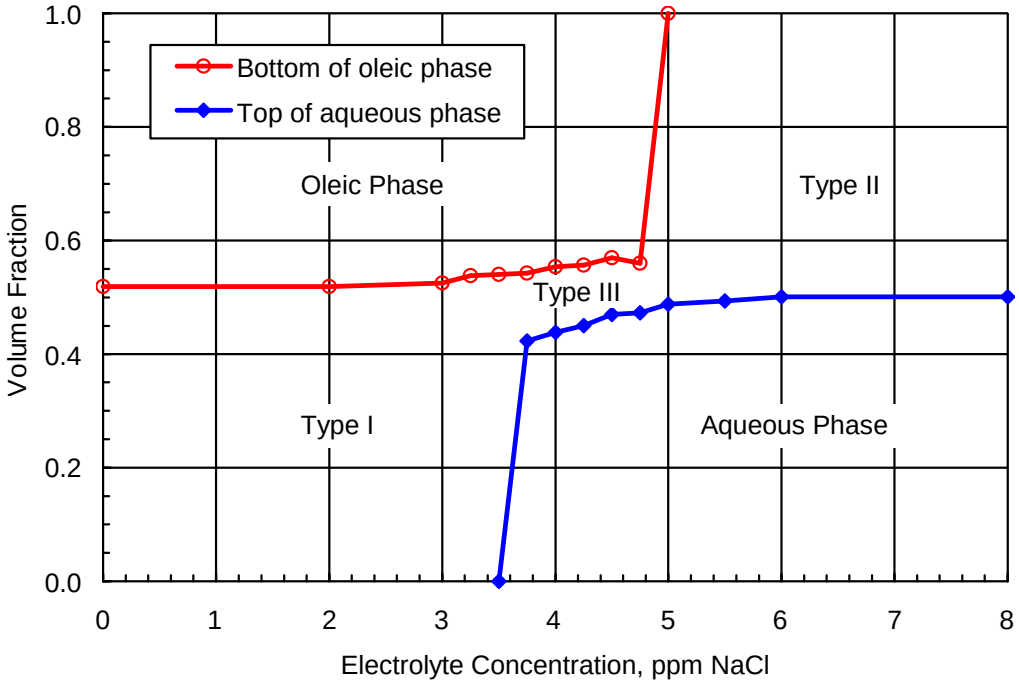

Figure 1.2-1. Volume fraction diagram for a 0.75% C_{16-17}-[PO]$_7$-SO_4, 0.25% C_{15-18} IOS, 2% SBA with WT crude at 38 °C after 21 days.

Mixtures with sodium carbonate (Na_2CO_3) exhibited shorter equilibration times (Fig. 1.2-2) as well as slightly higher solubilization ratios with both the West Texas crude oil (Fig. 1.2-3) and a crude oil from California (Fig. 1.2-4). However, most of the studies were done without sodium carbonate due to the presence of anhydrite in the West Texas dolomite reservoir and thus the risk of calcium carbonate precipitation. Most sandstone and carbonate reservoirs do not have anhydrite in them, so sodium carbonate could be used to great advantage since it reduces surfactant adsorption (DOE, 2004; DOE, 2005; Miller *et al*., 2006) and improves phase behavior. The *sec*-butanol (SBA) co-solvent could probably be eliminated from this formulation with sodium carbonate added, and this would reduce the cost since sodium carbonate is much less expensive than SBA, so for most reservoir applications the SBA would not be needed.

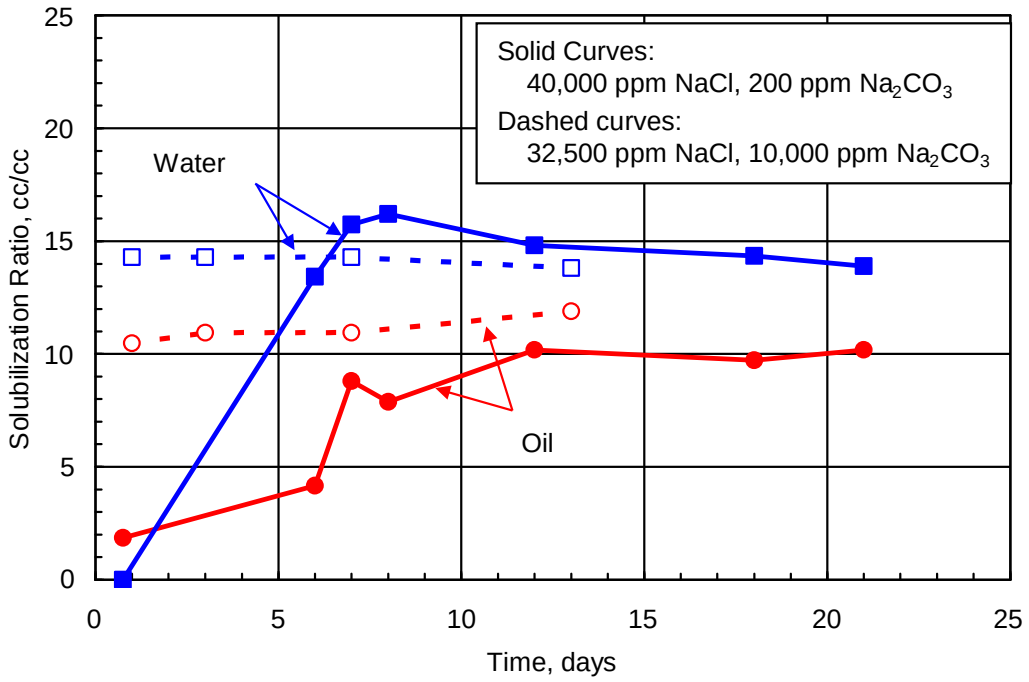

Figure 1.2-2 Equilibration of a surfactant formulation containing 0.75% C_{16-17}-$(PO)_7$-SO_4, 0.25% C_{15-18}IOS, 2% SBA with WT crude at 38 °C slightly below optimum salinity with and without sodium carbonate.

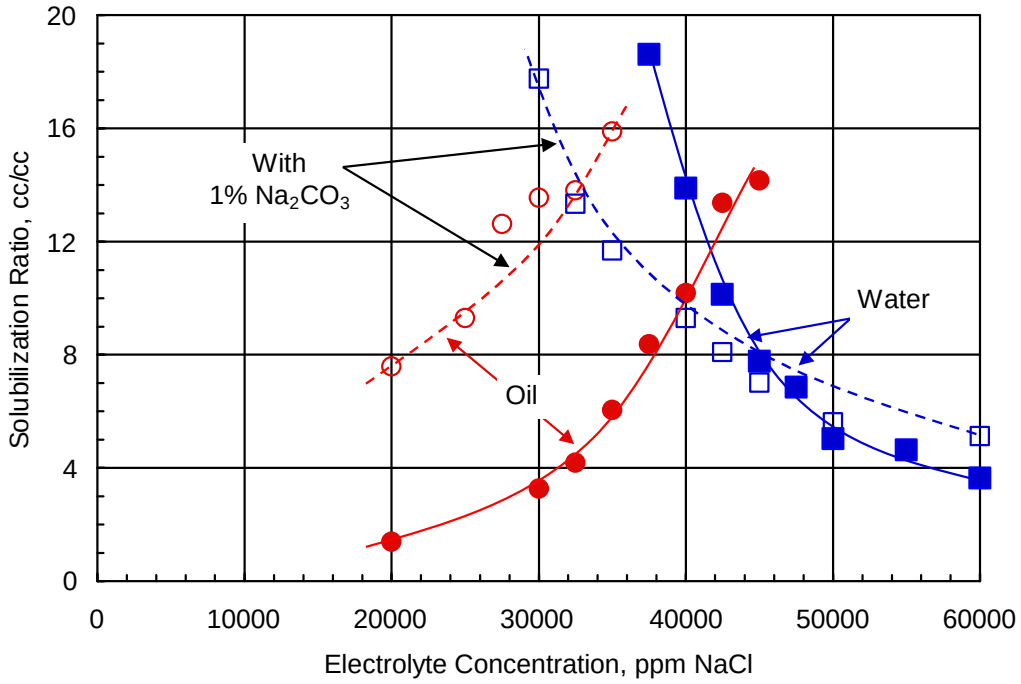

Figure 1.2-3 Solubilization ratio of 0.75% C_{16-17}-$[PO]_7$-SO_4, 0.25% C_{15-18} IOS, 2% SBA formulation with WT crude at 38 °C, with and without sodium carbonate.

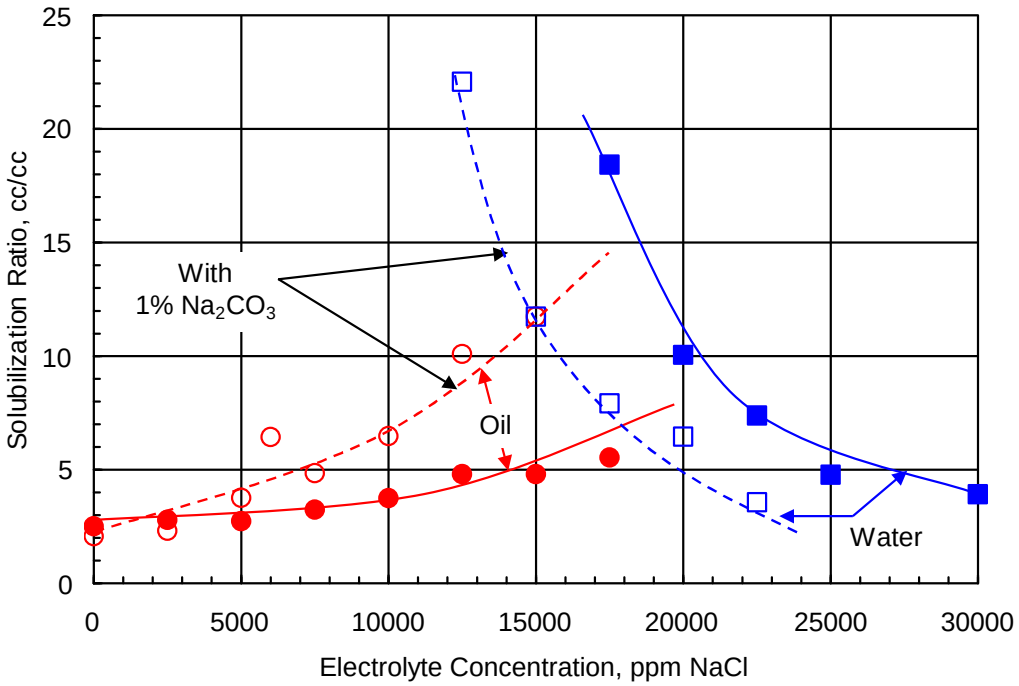

Figure 1.2-4 Solubilization ratios of 2% C_{20-24} AOS, 4% SBA formulation with a California crude at 100 °C, with and without sodium carbonate.

1.2.1 Co-Surfactant Selection

As part of the initial screening process, a comparison was made of the performance of the C_{15-18}IOS and C_{20-24}AOS co-surfactants with the C_{16-17}-$(PO)_7$-SO_4 primary surfactant. Phase behavior data for both formulations are presented in Figs. 1.2-5 and 1.2-6. Figures 1.2-7 and 1.2-8 show how the two formulations approached equilibrium for a near-optimum salinity. Optimum solubilization ratios measured with the C_{15-18}IOS co-surfactant are in the range of 10 to 12. The optimum solubilization ratio measured with the C_{20-24}AOS co-surfactant was about 11. The C_{15-18}IOS co-surfactant had a slightly more favorable solubilization ratio as well as a faster approach to equilibrium and less tendency to form viscous phases, so it is a better co-surfactant under these conditions. This behavior is consistent with the larger degree of hydrophobe branching of the C_{15-18}IOS surfactant. An additional observation that favored use of C_{15-18}IOS was the poorer performance of the C_{20-24}AOS when the total surfactant concentration was decreased. Several surfactant/co-surfactant ratios were evaluated in phase behavior experiments, and a ratio of 3:1 of the APS to IOS was found to give the best results.

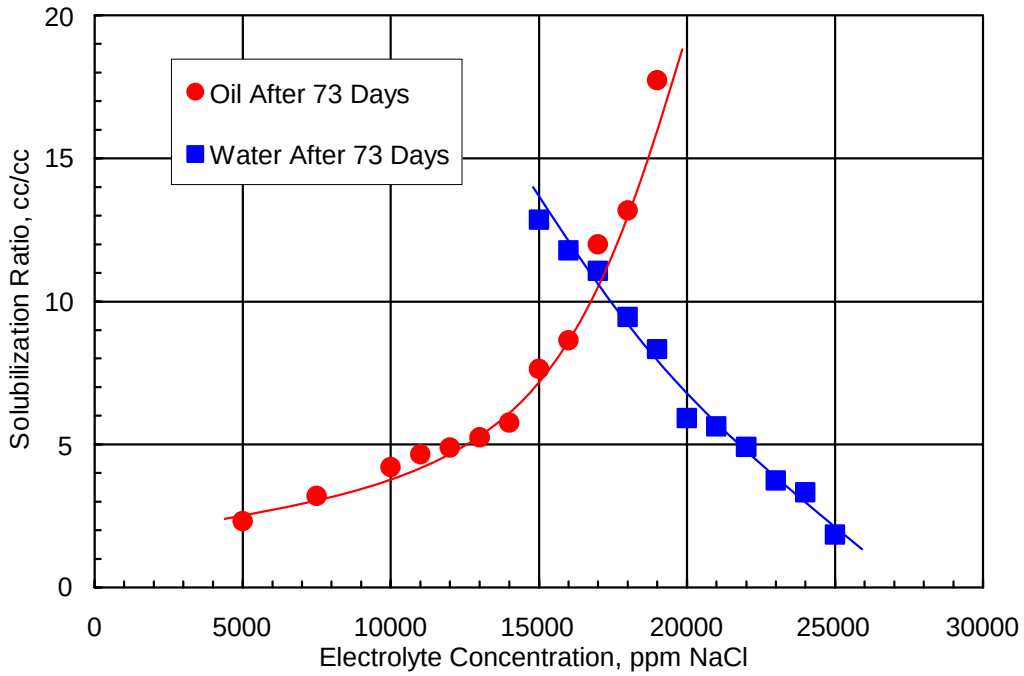

Figure 1.2-5 Phase behavior of 1.5% C_{16-17}-$(PO)_7$-SO_4, 0.5% C_{20-24} AOS, 4% SBA with WT crude at 38 °C.

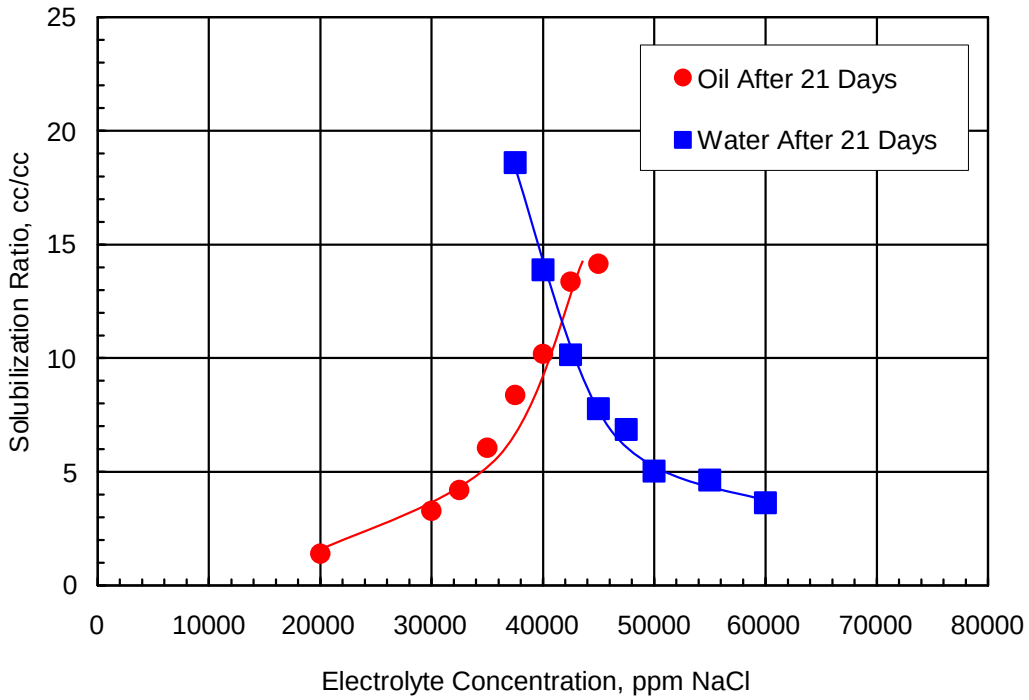

Figure 1.2-6 Solubilization ratio of 0.75% C_{16-17}-$(PO)_7$-SO_4, 0.25% C_{15-18} IOS, 2% SBA formulation with WT crude at 38 °C.

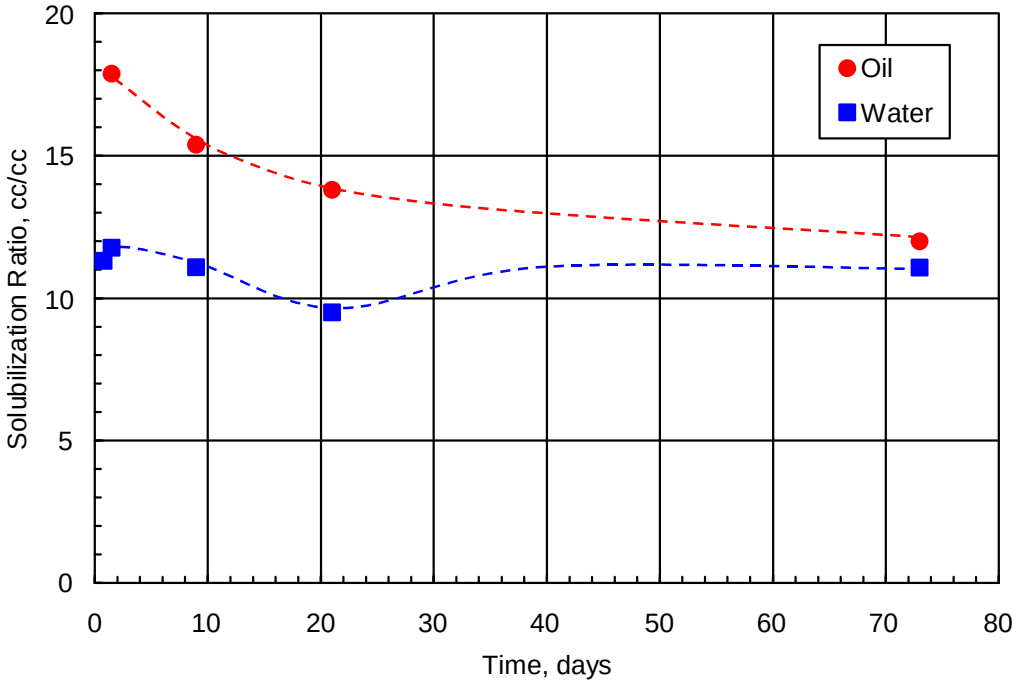

Figure 1.2-7 Equilibration of a surfactant formulation containing 1.5% C_{16-17}-$(PO)_7$-SO_4, 0.5% C_{20-24} AOS, 4% SBA, 1.7 wt% NaCl with WT crude at 38 °C.

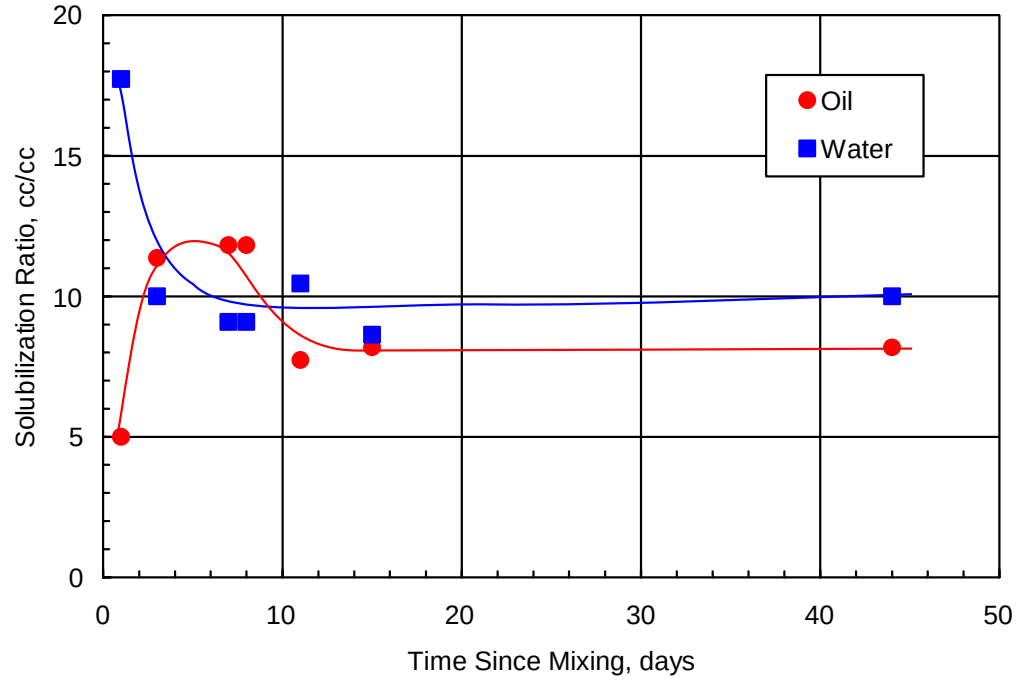

Figure 1.2-8 Equilibration of a surfactant formulation containing 0.75% C_{16-17}-$(PO)_7$-SO_4 and 0.25% C_{15-18} IOS with 4.5 wt% NaCl, 1375 ppm $CaCl_2$ and WT crude at 38 °C.

1.2.2 Co-Solvent, Surfactant/Co-Solvent Ratio, and Total Surfactant Concentration

Both *sec*-butanol (SBA) and isopropanol (IPA) were evaluated as co-solvents, and SBA proved superior. Increasing alcohol co-solvent concentration speeds up equilibration, reduces the viscosity and helps break macroemulsions, but invariably lowers the solubilization ratio at optimum salinity. Thus, a compromise must be made between maximum solubilization ratio (low IFT) and low viscosity and the other critical factors needed for good transport under low pressure gradients in oil reservoirs.

Initial phase behavior experiments were performed with 4 wt% total surfactant (surfactant + co-surfactant concentration) and a 1:2 total surfactant to co-solvent ratio. This had the advantage of generating large microemulsion volumes due to the high surfactant concentration plus rapid equilibration due to the high concentration of co-solvent. Once a promising surfactant and co-surfactant had been identified, additional phase behavior experiments were performed in order to optimize total surfactant to co-solvent ratio and total surfactant concentration.

The most promising formulation for application in the dolomite reservoir was a mixture of $C_{16\text{-}17}$-$(PO)_7$-SO_4, $C_{15\text{-}18}$IOS, and SBA. At 1 wt% surfactant concentration and 2 wt% SBA, this formulation equilibrates rapidly (Fig. 1.2-8) and exhibits a high solubilization ratio at optimal conditions (Fig. 1.2-6). This formulation is also tolerant of divalent cations such as calcium and magnesium. Most importantly, this formulation produces low viscosity microemulsions with fluid interfaces and little tendency to exhibit gels or macroemulsions. This can be observed qualitatively by tilting pipettes and observing the interface fluidity, as illustrated in Fig. 1.2-9. The microemulsion viscosity near optimum salinity without polymer was measured with a Contraves LS-30 low shear viscometer and found to be 10 cp. The dead crude oil viscosity is 11 cp.

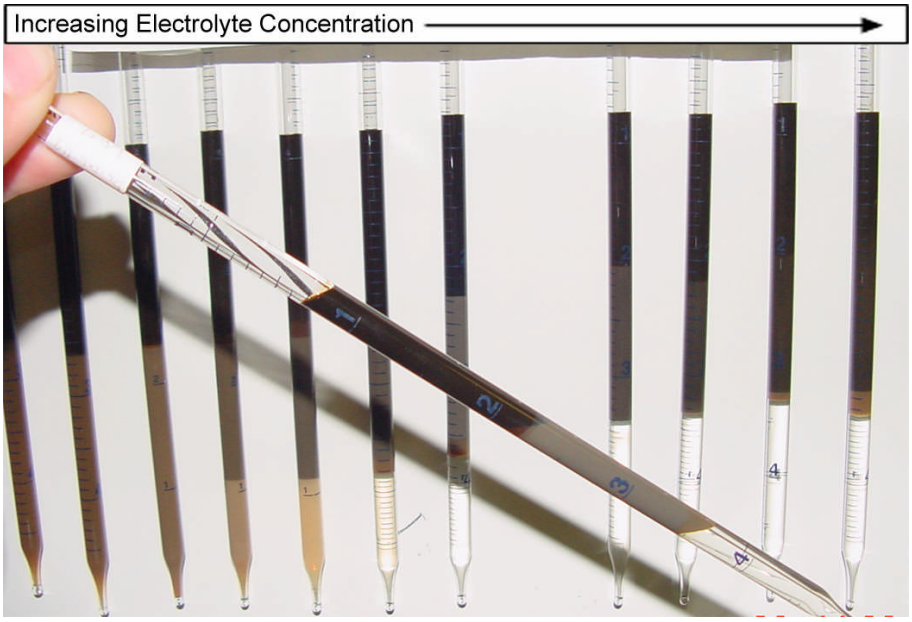

Figure 1.2-9 Qualitative observations of phase behavior, interface fluidity and viscosity by tilting pipettes.

Another important step in screening surfactants is to test their aqueous stability over a range of temperature and salinity appropriate to the field application. Some formulations show excellent behavior when mixed with crude oil, but show limited aqueous stability. The C_{16-17}-$(PO)_7$-SO_4/C_{15-18}IOS/SBA mixture formed a clear, stable aqueous phase at room temperature over a wide range of salinity, but it showed a cloud point as the temperature increased, which is more characteristic of non-ionic surfactants. We attribute this behavior to the large number of POs in the C_{16-17}-$(PO)_7$-SO_4 molecule since the same behavior was observed by Aoudia *et al*. (1995) when they increased the number of POs in a series of propoxy PO sulfate studies.

Subtask 1.3 Polymer Screening

Including polymer in a surfactant slug is essential for maintaining a favorable mobility ratio since the surfactant causes the water relative permeability to increase. This increase must be counterbalanced by decreasing the aqueous mobility with polymer (Hirasaki and Pope, 1974). Without polymer in the surfactant slug, the surfactant will finger into the oil bank and the reservoir sweep will be very poor. Furthermore, the polymer in both the slug and drive helps mitigate the effects of permeability variation and improves the overall sweep efficiency in the reservoir. Core floods show some but not all of the benefits of adding polymer, so acceptable results in a core flood without polymer can be misleading with respect to performance in the field.

Xanthan gum and hydrolyzed polyacrylamide (HPAM) polymers were selected for use with the SP core flood experiments in this study (DOE, 2004; DOE, 2005). Polymers were tested first in phase behavior experiments in order to determine compatibility with the surfactant solutions. In addition to compatibility testing, the relationship between viscosity, polymer concentration and salinity was measured. The variation in solution viscosity as a function of polymer concentration and electrolyte concentration for SNF's Flopaam 3330S HPAM is shown in Fig. 1.3-1. The Flopaam 3330S polymer solutions showed excellent filtration, which is another very important screening criterion before core flooding is started. The mobility of the surfactant-polymer slug and polymer drive is also affected by the permeability reduction caused by HPAM polymers. The permeability reduction factor for Flopaam 3330S in the dolomite reservoir rock is shown as a function of permeability in Fig. 1.3-2. This relationship is needed both for core flooding design and for modeling of the reservoir flood. Although the viscosity of the HPAM polymer is less than the xanthan gum polymer at high salinities corresponding to the formation brine and slug salinities, the HPAM is less expensive than the xanthan gum and thus is likely to be the more economical choice in this particular application. The HPAM is also less subject to biodegradation and has other advantages in this application.

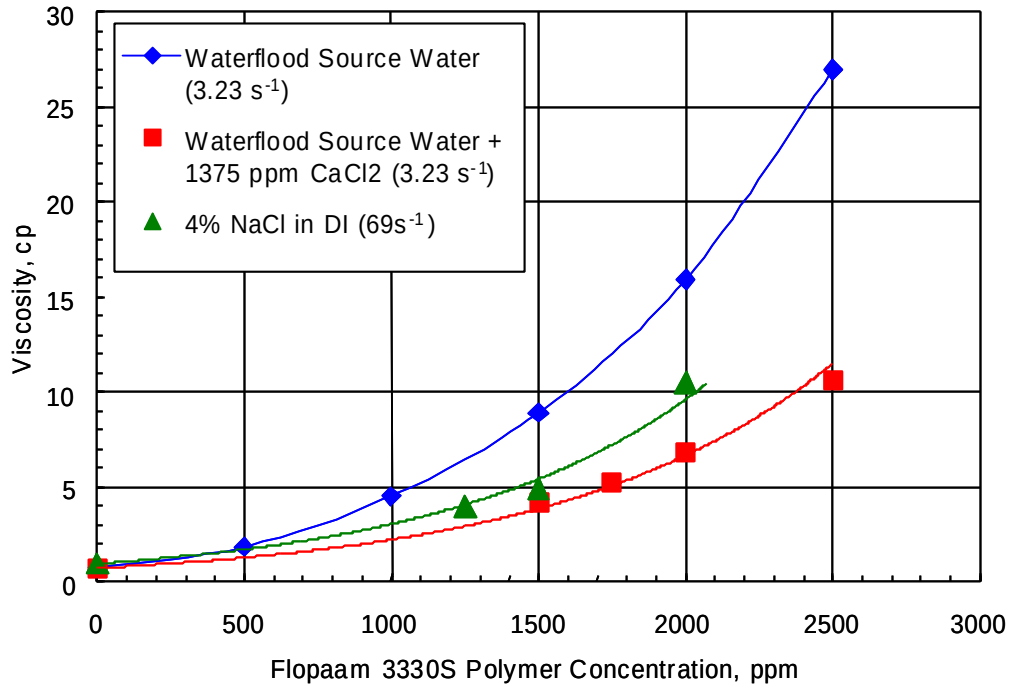

Figure 1.3-1. Viscosity for Flopaam 3330S in three different brines.

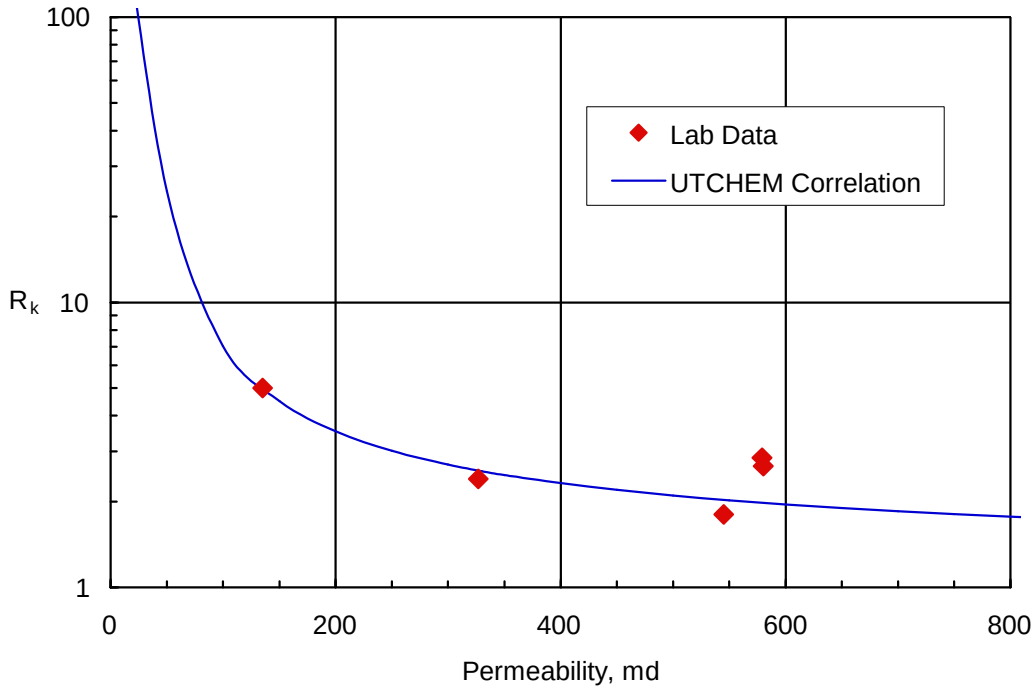

Figure 1.3-2. Permeability reduction factor for Flopaam 3330S polymer in dolomite cores.

Subtask 1.4 Core Flooding Experiments

A small number of core floods were performed as validation experiments for promising surfactants identified during phase behavior screening. Berea sandstone was used for the initial core floods. Later floods were performed in cores created from

combined reservoir plugs. These dolomite core plugs presented the additional complexities of low permeability, high heterogeneity including visible vugs and calcium pickup from anhydrite dissolution.

1. 4.1 Berea Core Preparation

Berea cores approximately 30 cm long and 5 cm in diameter were drilled, dried, and weighed. Lexan end pieces were attached to the core with five-minute epoxy and allowed to cure. Once the end pieces were attached, the core was placed inside a lexan tube, and the space between the core and the tube was filled with slow-setting epoxy. Once epoxy had set, pressure taps were added 5 cm from each face. A vacuum pump was used to evacuate air from the core and several pore volumes of CO_2 were flushed to remove the air. Next, the cores were brought up to 38 °C and flooded with synthetic formation brine (SFB) containing 60,000 ppm total dissolved solids (TDS) including 2600 ppm divalent cations (Ca^{++} and Mg^{++}). Pressure data were recorded and brine permeability calculated. The cores were then flooded with reservoir crude oil at a high pressure gradient (100 psi/ft) until no water was produced in the effluent. Produced brine was collected and pressure and flow rate were monitored. After aging between 2 and 30 days, cores were flooded with SFB at a pressure gradient similar to the reservoir away from the wells. Produced fluids and pressure were monitored until no additional oil was produced. Table 1.4-1 describes properties of a Berea sandstone core as well as other details of surfactant flood experiment B-1.

Table 1.4-1 Summary of Selected Core Flood Experiments

	B-1 (Berea Sandstone)	D-7C (Reservoir Dolomite)
Rock mass, g	1284	1482
PV, mL	113	143
□	0.18	0.21
k_{brine}, md	353	580
k_{rw}^*	0.05	0.04
S_{orw}	0.40	0.40
Surfactant Slug		
C_{surf}, wt%	1	1
C_{SBA}, wt%	2	2
$C_{Polymer}$, ppm	2000	2500
C_{NaCl}, ppm	45000	45000
C_{CaCl2}, ppm	1375	0
PV injected	0.5	0.5
Inj. rate, ft/day	0.6	0.6
Polymer Drive		
$C_{Polymer}$, ppm	2000	2500
C_{NaCl}, ppm	27000	27000
C_{CaCl2}, ppm	1375	0

1.4.2 Dolomite Core Preparation

Dolomite cores from the West Texas dolomite reservoir were prepared in a similar fashion to Berea sandstone cores with a few modifications. Due to the limited plug lengths, cores were prepared by combining several dolomite plugs to reach a total length of approximately 30 cm. The plugs were 3.8 cm in diameter in some experiments and 5.7 cm in diameter in other experiments. Due to the low permeability and high heterogeneity of many of the core plugs, they were first screened using an air minipermeameter and in a few cases with high-resolution X-Ray computed tomography (X-Ray CT).

The dolomite cores were then saturated and flooded with 2500 ppm TDS synthetic waterflood source water and effluent was collected and analyzed for Ca^{++} and SO_4^{2-} from anhydrite dissolution. In some cores, a small slug of isopropyl alcohol was injected as a tracer and displaced with additional brine to determine heterogeneity. Remaining preparations proceeded in a similar manner to those described for Berea cores.

Since a limited number of core plugs were available, some of the dolomite cores were cleaned for reuse by successive injections of several pore volumes of surfactant-polymer slug, polymer drive, freshwater, hypochlorite, freshwater, IPA, freshwater, and finally synthetic formation brine. The core was considered restored and ready for further use when the original brine permeability was restored. Experiment D-7C is an example of this; a core originally used for experiment D-7A was cleaned by this procedure and then used for experiment D-7C. Table 1.4-1 describes properties of a West Texas dolomite core as well as other details of surfactant flood experiment D-7C.

The specific BET surface area for an adjacent rock sample was measured at Rice University and found to be 0.13 m^2/g. Thin sections made from this rock were analyzed by Dr. Jerry Lucia at the Bureau of Economic Geology at the University of Texas and described as grain-dominated dolomitic packstone.

1.4.3 Surfactant-Polymer Flood Design

A salinity gradient was designed to maximize the region of ultra-low IFT (Pope *et al*., 1979). In order to make conditions in the sandstone flood similar to those in the reservoir dolomite core, calcium was added as $CaCl_2$ in an amount consistent with the solubility product of $CaSO_4$. Polymer was included in the slug and drive at a concentration that was determined necessary for favorable mobility control (Hirasaki and Pope, 1974). During surfactant-polymer slug and polymer drive injection, pressure was monitored and maintained at about 2 psi/ft by adjusting the flow rate. Frontal advance rates were on the order of 1 ft/day. Although it is common to do such core floods at this rate, the more important consideration is maintaining a low pressure gradient so the results will be scaleable to the field and useful in simulations studies.

Effluent was collected by a fraction collector and analyzed for oil and surfactant content. Some effluent samples were placed in an oven at 100 °C for 36 hours to hydrolyze the sulfate surfactant and allow easier reading of oil recovery. Table 1.4-1 summarizes the fluids injected in two typical core floods. Core floods were evaluated based upon oil recovery, pressure gradient and surfactant retention.

1.4.4 Berea Sandstone Core Flood Results

In experiment B-1, a 0.5 PV SP slug with 1 wt% surfactant concentration followed by a 2 PV polymer drive was injected into a Berea sandstone prepared as described above (Table 1.4-1). Oil recovery, pressure data, and surfactant recovery are presented in Figs. 1.4-1 through 1.4-3, respectively. About 91% of the water flood residual oil was recovered, which corresponds to a residual oil saturation to chemical (S_{orc}) of 0.03. Pressure drop remained on the order of 2 psi/ft. Approximately 90% of the injected surfactant was recovered. Only 0.08 mg of surfactant was retained per gram of rock. As discussed previously, mechanisms of surfactant retention include both adsorption on to rock surfaces and phase trapping. This extremely low retention value is indicative of minimal phase trapping, which we attribute to low microemulsion viscosity and minimal tendencies of this formulation to form viscous gels and macroemulsions. The favorable salinity gradient, with the drive salinity equal to about 0.6 times the optimum salinity (Table 1.4-1) is also beneficial in terms of low surfactant retention. When feasible, a salinity gradient will almost always result in a more efficient chemical flood.

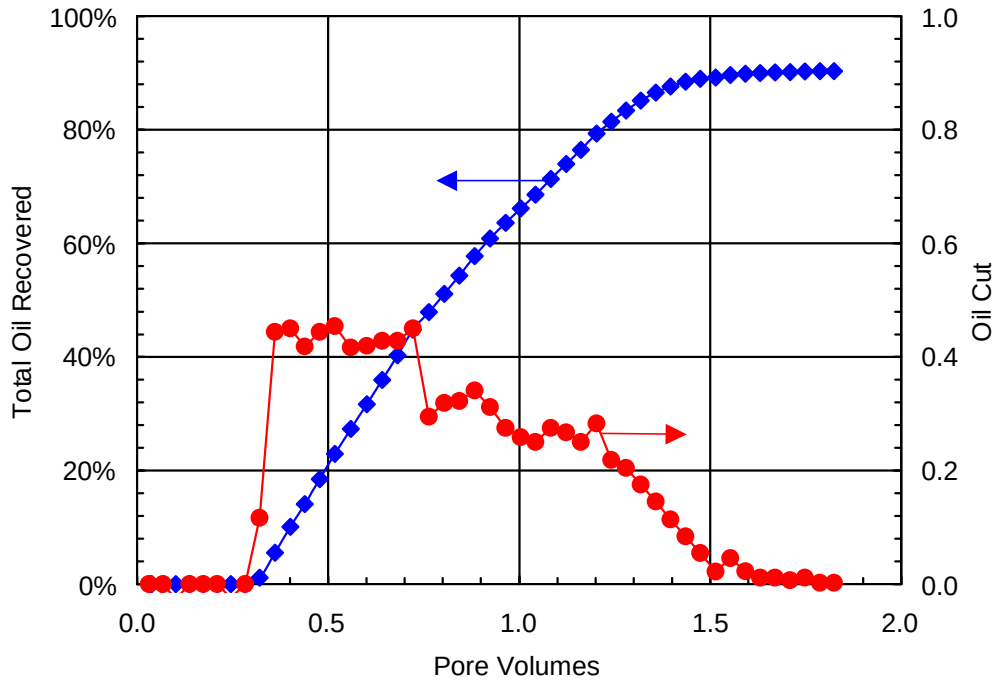

Figure 1.4-1 Oil recovery during Berea core flood B-1.

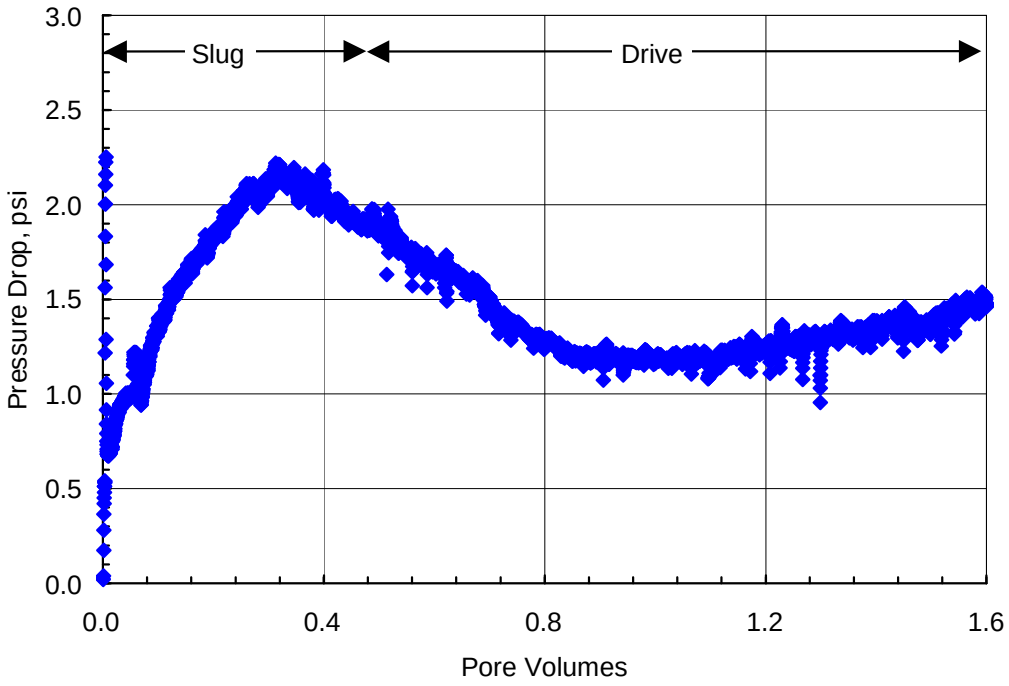

Figure 1.4-2 Pressure drop data for Berea core flood B-1 during surfactant flood and polymer drive.

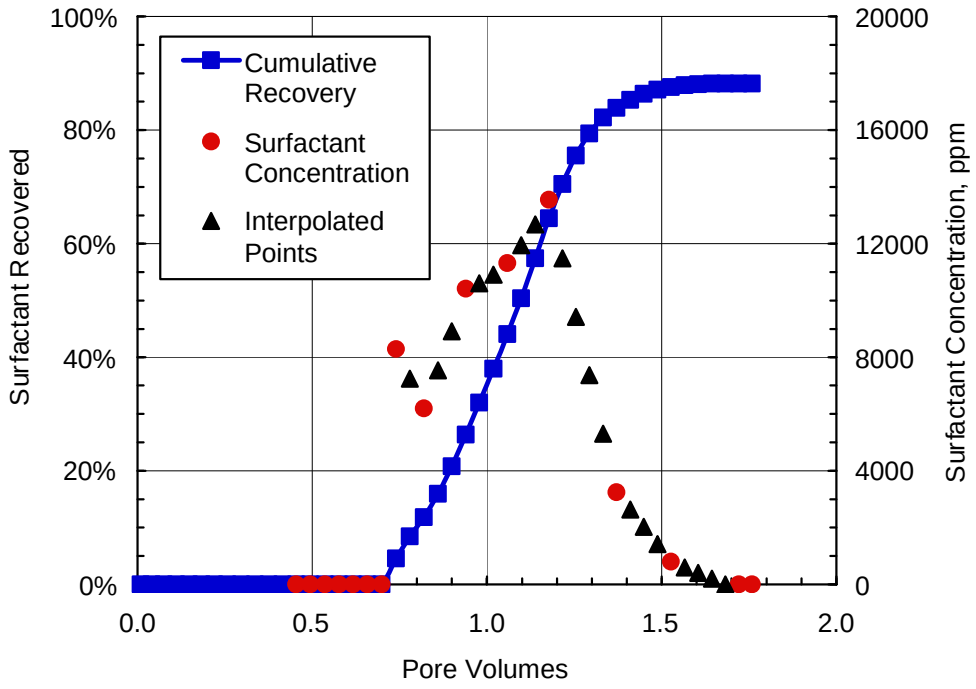

Figure 1.4-3. Surfactant Recovery during Berea core flood B-1.

1.4.5 West Texas Dolomite Core Flood Results

The reservoir targeted for surfactant EOR is a heterogeneous dolomite containing anhydrite, and thus presents several challenges to core flooding. The heterogeneous, vuggy nature of the rock, as seen clearly in CT scans (Fig. 1.4-4) can lead to channeling on the core scale due to the large size of the vugs with respect to the core. Although this is not expected to occur on larger scales corresponding to the actual reservoir, it can complicate interpretation of core flood results by leading to early tracer and surfactant breakthrough. A tracer was injected in to the core used in experiments D-7A and D-7C following a waterflood (S_o=0.4) and breakthrough was observed after only 0.25 PV (Fig. 1.4-5). This is equivalent to a breakthrough at 0.42 PV on a 100% water saturation basis. Such extreme heterogeneity can be partially mitigated by increasing polymer concentration, so high concentrations of polymer were used in most of the core flood experiments. Furthermore, the oil in the reservoir is less viscous (5 cp) than the dead crude (11 cp) used in the laboratory experiments and the brine relative permeability is higher in the mixed-wet dolomite reservoir than it is in the cleaned core plugs. Thus, higher polymer concentration is required in these particular core floods to maintain a favorable mobility ratio than it will be in the field. A better procedure would have been to age the cores at high temperature and convert them to mixed-wet condition, but such a procedure (Hirasaki and Zhang, 2004) is time consuming and was not used in this screening study since its focus was on surfactant selection, not mobility control.

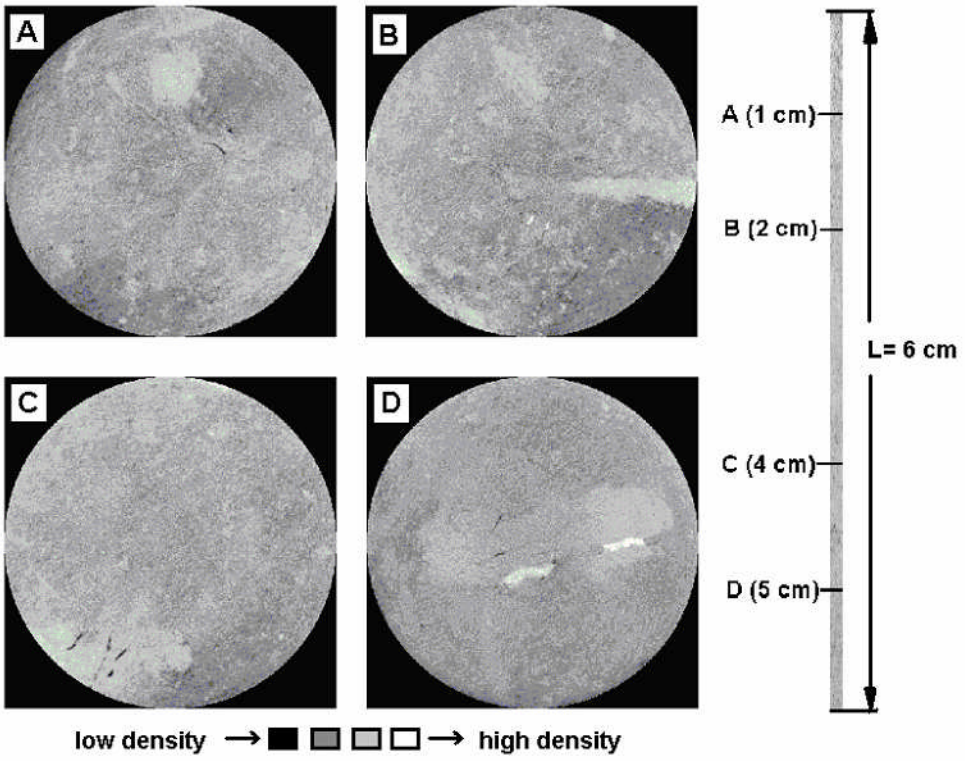

Figure 1.4-4 CT scans of a WT dolomite core plug. These data and images were produced at the High-Resolution X-ray Computed Tomography Facility of The University of Texas at Austin.

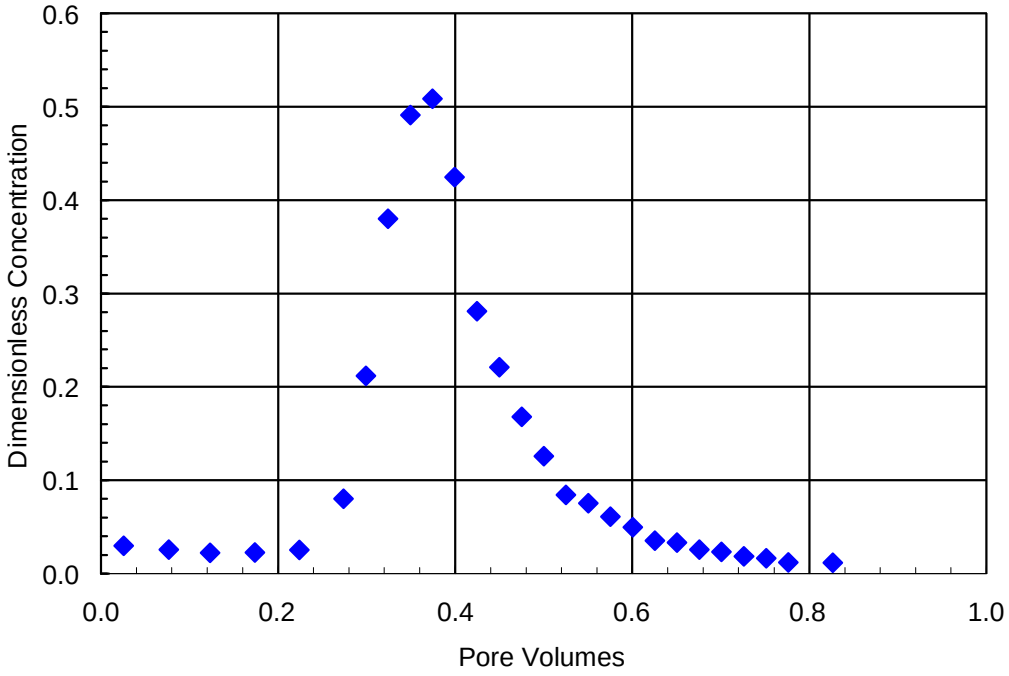

Figure 1.4-5 Tracer breakthrough data in dolomite core (D-7C) at S_{orw} = 0.4.

Anhydrite ($CaSO_4$) was detected visually from thin sections, by X-Ray diffraction (XRD), and by the presence of sulfate and increased concentrations of calcium in core flood effluent water samples at levels consistent with the solubility product of $CaSO_4$. This had several implications for the flood design. First, sodium carbonate was not included in the formulation because we expected the CO_3^{2-} would react with the dissolving anhydrite and precipitate as calcium carbonate. The economic benefits of using sodium carbonate are sufficiently large that we plan further investigations of its use, but it was not feasible or necessary to use it in this surfactant screening study. Also, the effect of this additional dissolved calcium on phase behavior and viscosity had to be taken into account.

In experiment D-7C, a 0.5 PV SP slug with 1 wt% surfactant concentration followed by a 2 PV polymer drive was injected into a West Texas dolomite core prepared as described above (Table 1.4-1). Oil recovery and pressure data for the West Texas reservoir dolomite core flood are presented in Figs. 1.4-6 and 1.4-7, respectively. Despite early surfactant breakthrough, 93% of water flood residual oil was recovered, leaving the S_{orc} at about 0.03. The pressure gradient was low at all times as it must be in the actual reservoir away from the wells. This is one of the most stringent requirements of a core flood experiment. In some ways it is even more important than high oil recovery because if the surfactant does not transport under low pressure gradient, then it will not even contact the oil deep in the reservoir with large well spacing.

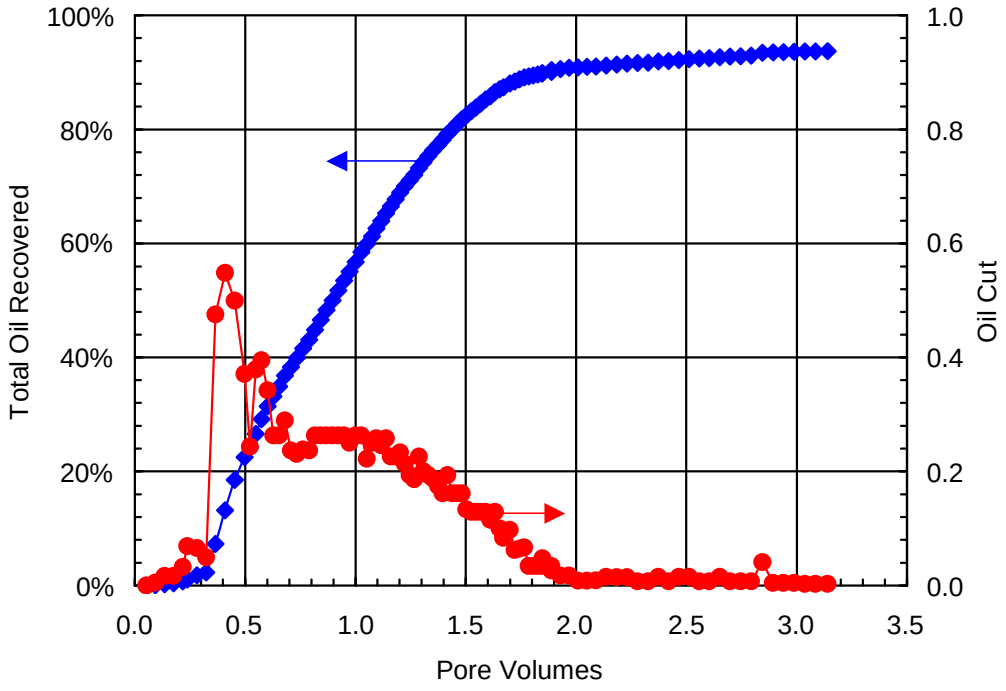

Figure 1.4-6. Oil recovery during dolomite core flood D-7C.

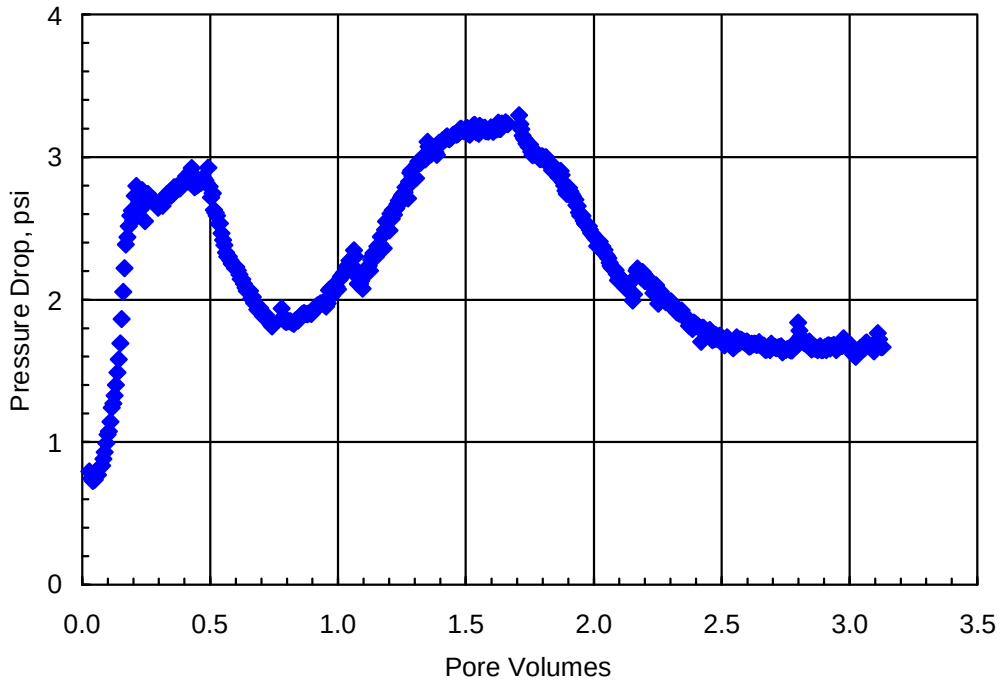

Figure 1.4-7. Pressure drop data for dolomite core flood D-7C during surfactant flood and polymer drive.

Surfactant retention in this experiment was 0.24 mg/g of rock. This is slightly higher than the mean of several experiments performed in this reservoir dolomite, with lower

and higher values obtained respectively when slug salinity was either significantly lower or slightly higher than optimum (S* in Table 1.4-2). The low retention may be due in part to the low specific surface area for the dolomite rock.

Table 1.4-2. Surfactant Retention in WT Reservoir Dolomite Cores

	Core Flood				
	D-5	D-6	D-7A	D-7C	D-11
Surfactant conc., wt%	2	1	2	1	2
Pore volumes injected	0.40	0.80	0.25	0.50	0.26
S*, ppm NaCl	40000	40000	40000	45000	40000
Slug salinity, ppm NaCl	23400	45000	9600	45000	3800
Retention, mg/g	0.21	0.43	0.12	0.24	0.01

Subtask 1.5 Calcium tolerance of NI surfactant blend

The NI blend consists of 80 wt% Neodol 67-7PO sulfate (N67) and 20 wt% internal olefin sulfonate 15-18 (IOS). It can not only provide good oil recovery but also improve the tolerance of surfactant to calcium.

From Figure 1.5-1, the concentration of calcium chloride for phase separation occurred at 0.5% and 0.1% respectively when N67 or IOS was used separately. The phase separation behaviors of the two surfactants were different: IOS was precipitated by calcium, while N67 formed cloudy solutions. However, when they were mixed at different weight ratios, they stayed in the single-phase region over a much wider calcium range than for IOS or N67 only. For the 4:1 ratio, which we used for forced displacement experiments, the upper limit concentration of $CaCl_2$ to keep the solution clear is 1.0%.

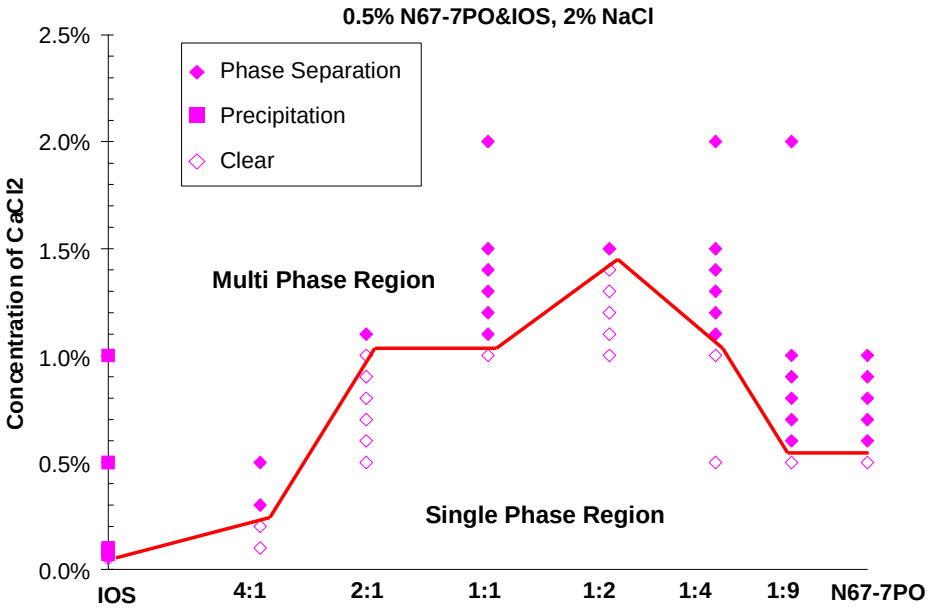

Figure 1.5-1 Phase diagram of NI blend

Summary

Several high-performance, low-cost surfactants for EOR have been identified and tested starting with an efficient and effective laboratory screening process that emphasizes observations of phase behavior and viscosity. This screening process has been shown to provide reliable selection of cost effective surfactants, co-surfactants and polymers as a function of salinity, hardness, alkali, temperature, and rock type. Surfactant structures with branched hydrophobes are the most suitable for EOR because microemulsions made from these surfactants show little tendency to form viscous phases such as gels and liquid crystals that result in high surfactant retention. Adding propylene oxide to the surfactant improves its performance with little increase in cost and is a very practical approach to tailoring the surfactant to the specific crude oil and reservoir conditions. The surfactants investigated gave high oil recoveries and low residual oil saturation (S_{orc}=0.03) in both Berea sandstone and a dolomite reservoir rock flooded under low pressure gradients typical of values in oil reservoirs. These surfactants also showed low retention in both Berea sandstone (0.08 mg/g) and in the dolomite reservoir rock (0.24 mg/g). The low surfactant retention is attributed in part to low viscosity microemulsions that were selected using the qualitative phase behavior testing described in this report. Sodium carbonate was observed to speed up coalescence to equilibrium microemulsions and is also expected to decrease surfactant adsorption on both sandstone and carbonate rocks, so its use in some applications should provide additional benefits. A simulation study presented in a companion paper (Anderson *et al*., 2006) indicates that the economics of such high-performance synthetic surfactants are very attractive at crude oil prices of about 30 $/Bbl or more even in a heterogeneous dolomite reservoir, and would be much more so in many sandstone and carbonate reservoirs where sodium carbonate could be used.

Mixtures of N67 and IOS have higher calcium tolerance than N67 and IOS used separately.

Nomenclature

γ = interfacial tension (IFT)
σ = solubilization ratio
S* = optimum salinity
S_{orc} = residual oil saturation to chemical
S_{orw} = residual oil saturation to water
k_{rw}^* = relative permeability endpoint to water
R_k = permeability reduction factor

References

Adams, W. T. and Schievelbein, V. H: “Surfactant Flooding Carbonate Reservoirs,” *SPERE* (November 1987), 619.

Anderson, G. A., Delshad, D., King, C. B., Mohammadi, H., and Pope, G. A.: "Optimization of Chemical Flooding in a Mixed-Wet Dolomite Reservoir," paper

SPE 100082 presented at the 2006 SPE/DOE Symposium on Enhanced Oil Recovery, Tulsa, OK, April 22-26.

Aoudia, M., Wade, W. H., and Weerasooriya, V.: "Optimum Microemulsions Formulated with Propoxylated Tridecyl Alcohol Sodium Sulfates," *Journal of Dispersion Science and Technology* (16(2) 1995), 115.

Austad, Tor and Milter, Jess: "Surfactant Flooding in Enhanced Oil Recovery," *Surfactants: Fundamentals and Applications in the Petroleum Industry*, L.L. Schramm (ed.), Cambridge University Press, Cambridge, UK, 2000.

Bourrel, M. and Schechter, R. S.: "*Microemulsions and Related Systems*", Marcel Dekker, Inc., New York, NY (1988).

DOE: First Annual Technical Report on Surfactant Based Enhanced Oil Recovery and Foam Mobility Control; prepared for U.S. DOE (DE-FC26-03NT15406), Rice University, Houston, TX (June 2004).

DOE: Second Annual Technical Report on Surfactant Based Enhanced Oil Recovery and Foam Mobility Control; prepared for U.S. DOE (DE-FC26-03NT15406), Rice University, Houston, TX (June 2005).

Healy, R. N., Reed, R. L. and Stenmark, D. K.: "Multiphase Microemulsion Systems," *SPEJ* (June 1976) 147.

Hirasaki, G. J and Pope, G. A.: "Analysis of Factors Influencing Mobility and Adsorption in the Flow of Polymer Solution Through Porous Media," *SPEJ* (August 1974), 337.

Hirasaki, G., and Zhang, D. L.: "Surface Chemistry of Oil Recovery From Fractured, Oil-Wet, Carbonate Formations," *SPEJ* (June 2004), 151.

Huh, C.: "Interfacial Tensions and Solubilizing Ability of a Microemulsion Phase That Coexists with Oil and Brine," Journal of Colloid and Interface Science (September 1979), 408.

Jayanti, S., Britton, L. N., Dwarakanath, V., and Pope, G. A.: "Laboratory Evaluation of Custom Designed Surfactants to Remediate NAPL Source Zones," *Environmental Science and Technology* (December 2002), 5491.

Miller, C. A., Hirasaki, G. J., Zhang, D., Liu, W., Yan, M., and Puerto, M.: "Favorable Attributes of Alkali-Surfactant-Polymer Flooding," paper SPE 99744, presented at the 2006 SPE/DOE Symposium on Enhanced Oil Recovery, Tulsa, OK, April 22-26.

Nelson, R. C. and Pope, G. A.: "Phase Relationships in Chemical Flooding," *SPEJ* (Oct. 1978), 325.

Pope, G. A., Wang, B., and Tsaur, K.: "A Sensitivity Study of Micellar/Polymer Flooding," *SPEJ* (December 1979), 357.

Sanz, C.A. and Pope, G.A., "Alcohol-Free Chemical Flooding: From Surfactant Screening to Coreflood Design," Proceedings of the SPE International Symposium on Oilfield Chemistry, San Antonio, TX, February 14-17, 1995.

Stegemeier, G. L.: “Mechanisms of Oil Entrapment and Mobilization in Porous Media,” presented at the 1976 AIChE Symposium on Improved Oil Recovery By Surfactant and Polymer, Kansas City, Missouri, April 12-14.

Winsor, P. A.: "*Solvent Properties of Amphiphilic Compounds*," Butterworths, London (1954).

Wu, Y., Shuler, P., Blanco, M., Tang, Y., Goddard, W. A.: "A Study of Branched Alcohol Propoxylate Sulfate Surfactants for Improved Oil Recovery," paper SPE 95404, presented at the 2005 Annual Technical Conference and Exhibition, Dallas, Texas, October 9-12.

Task 2 Phase behavior, adsorption, and composition changes during displacement

Subtask 2.1 Surfactant Adsorption

Surfactant adsorption is crucial to surfactant recovery processes including the alkali-surfactant process. Both alkali concentration and salinity influence surfactant adsorption significantly. The presence of Na_2CO_3 can reduce surfactant adsorption. However, higher salinity causes higher surfactant adsorption and counteracts the adsorption reduction by carbonate. Thus, it is better to implement the alkali-surfactant process at low salinity. The effect of soap on synthetic surfactant adsorption was also tested. No synthetic surfactant adsorption reduction was found by using sodium oleate or sodium naphthenates from Fisher Scientific.

2.1.1 Low surfactant adsorption domain

Figure 2.1-1 shows the adsorption of synthetic surfactant [4:1 Neodol 67-7PO sulfate (N67):internal olefin sulfonate 15-18(IOS)] on calcite powder for different salinity and alkalinity. At the same alkalinity, adsorption increases with increasing salinity. By adding Na_2CO_3, the adsorption can be reduced. However, this adsorption reduction effect will be weakened under higher salinity. At 5% NaCl, the adsorption is reduced to $2.5*10^{-3}$ mmol/m^2 by adding 1.21% Na_2CO_3, while the adsorption at 0% NaCl will be $0.2*10^{-3}$ mmol/m^2 with the presence of 1% Na_2CO_3. These results indicate that it's better to implement the alkali-surfactant process at low salinity (<3%) because low surfactant adsorption can be achieved at this condition. Figure 2.1-2 illustrates the adsorption isotherms at 5% NaCl. It shows that no more than 0.2% Na_2CO_3 is needed for the adsorption reduction effects. Adding Na_2CO_3 at higher concentrations up to 1.2% Na_2CO_3 does not further reduce adsorption. As shown in the previous annual report, only 0.1% Na_2CO_3 is needed for the adsorption reduction at 0% NaCl. Figure 2.1-3 shows contours of maximal (plateau) adsorption for N67:IOS (4:1) by summarizing all the adsorption data. This plot shows that the domain with low surfactant adsorption is: [Na_2CO_3]>0.2% and [NaCl]<3%. Hence, the alkali-surfactant process with the current surfactant should be performed in this concentration domain to have low surfactant adsorption.

Figures 2.1-1, 2.1-2 and 2.1-3 are for the 4:1 N67 and IOS mixture. N67 and IOS were also tested individually to verify the adsorption reduction effect by Na_2CO_3, Figures 2.1-4 and 2.1-5 show that the presence of Na_2CO_3 can reduce the adsorption for N67 and IOS respectively significantly. The adsorption for N67 with Na_2CO_3 is 1/10 of that without Na_2CO_3, while the adsorption for IOS with Na_2CO_3 is 1/7 of that without Na_2CO_3 in the absence of NaCl.

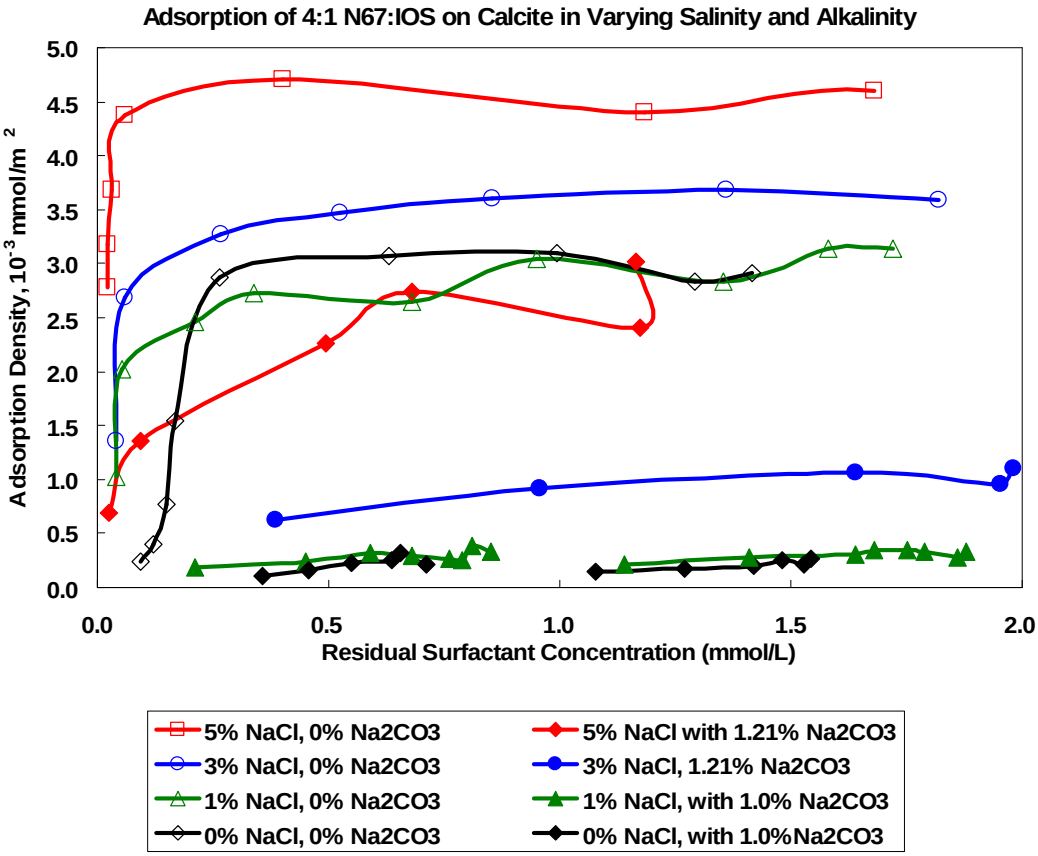

Figure 2.1-1 Adsorption of 4:1 N67:IOS on calcite in varying salinity and alkalinity

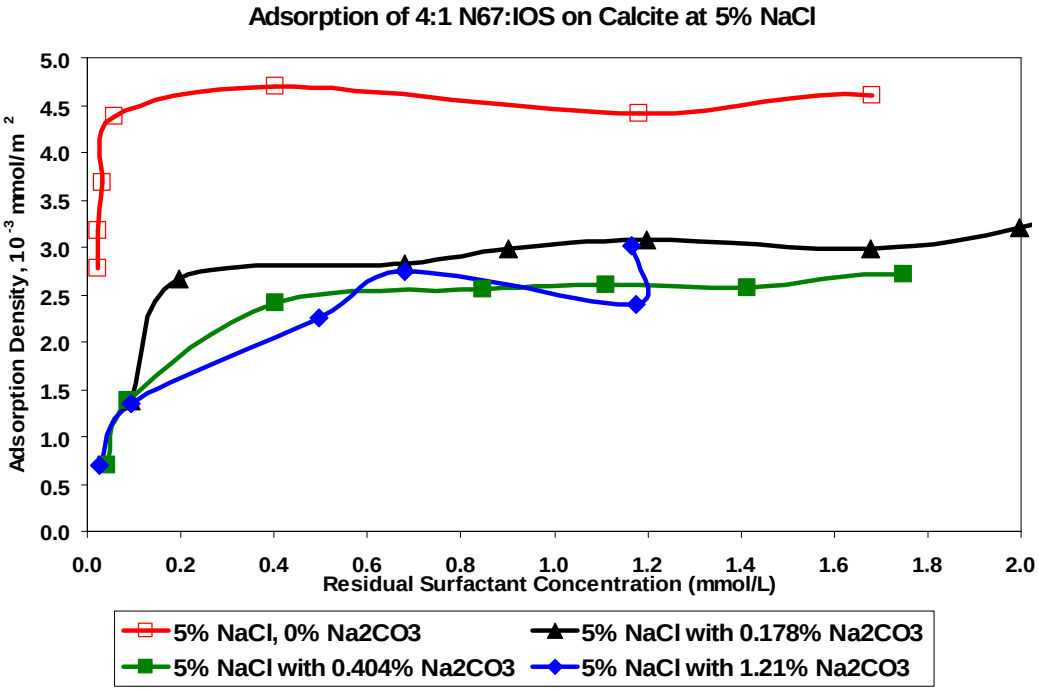

Figure 2.1-2 Adsorption of 4:1 N67:IOS on calcite in varying alkalinity at 5% NaCl

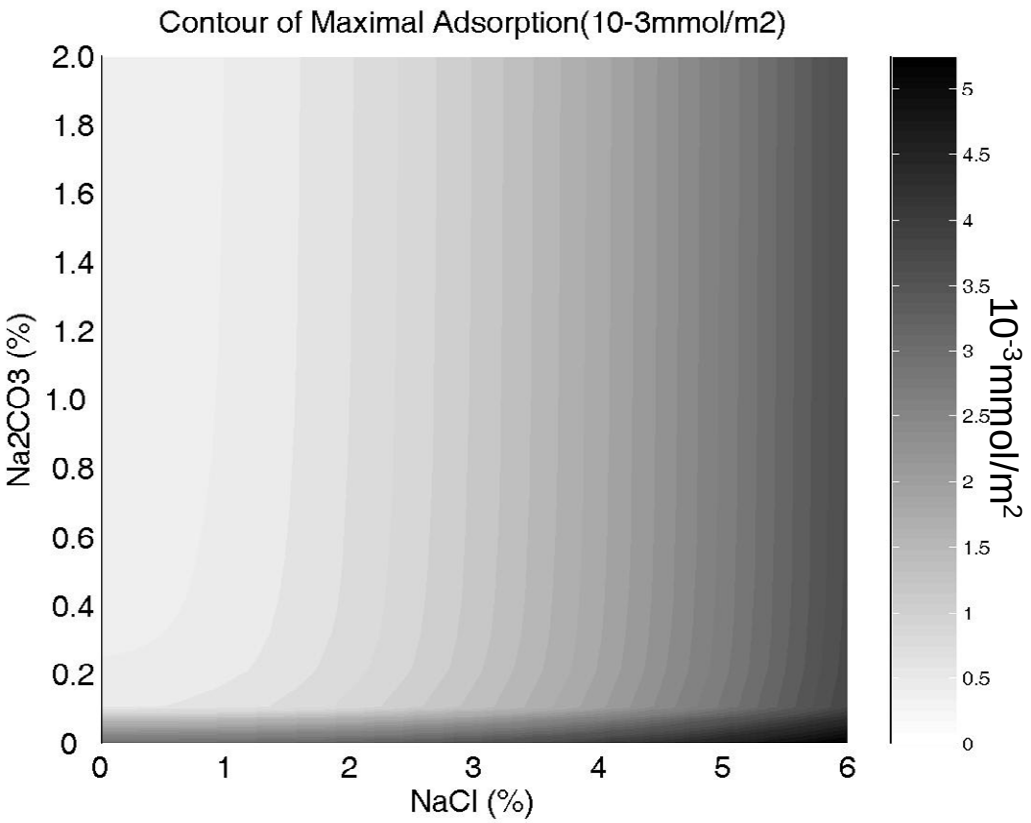

Figure 2.1-3 the contour of maximal adsorption for N57 IOS(4:1)

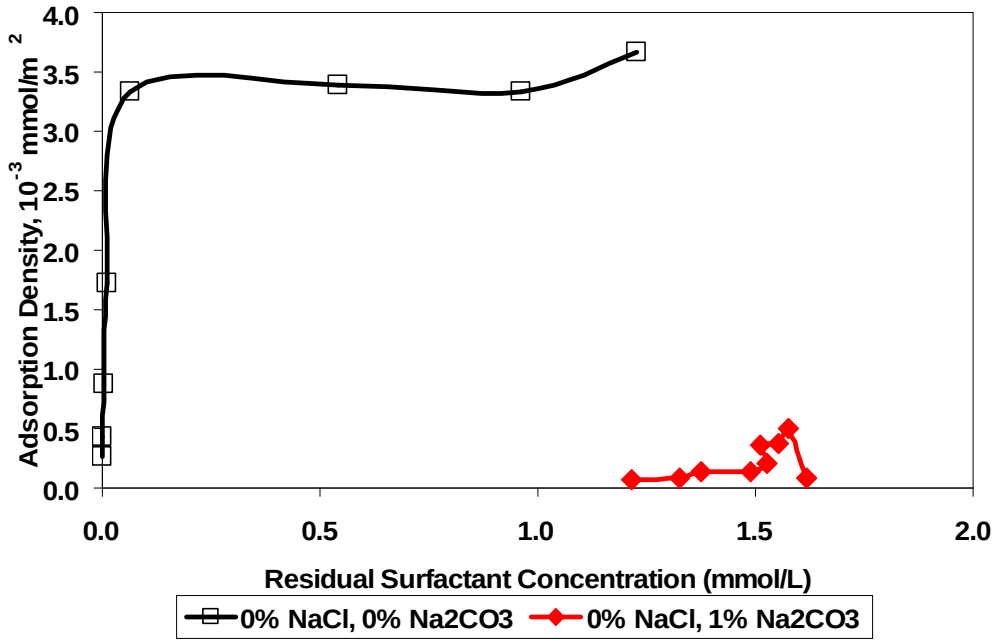

Figure 2.1-4 Adsorption of N67 on calcite powder

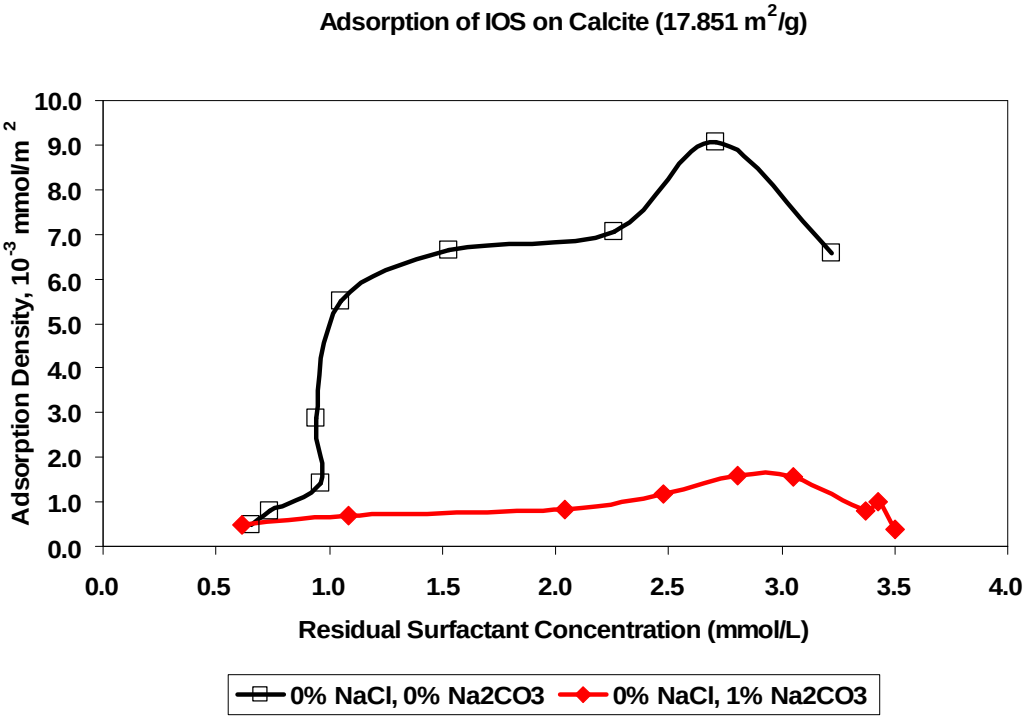

Figure 2.1-5 Adsorption of IOS on calcite powder

2.1.2 Surfactant adsorption with different soaps

If soap is present, the surfactant adsorption may change. Two soaps were tested. The first was sodium oleate. Solutions of sodium oleate having a concentration of 1.4 mmol/L and different amounts of calcite powder (0.2~8g) were prepared. After one day of mixing, the residual solutions were titrated. However, no soap could be detected. Meanwhile, a white paste material was found at the air-liquid interface and on the tube side. This material seemed hydrophobic because it adhered to the polypropylene tube surface even after centrifuging. Since the solubility product of $CaCO_3$ is 3.8 x 10^{-9} and the solubility product of calcium oleate is 3.98 x 10^{-13} (from reference [1]), the precipitation reaction of Eq. (1) below must happen during the mixing. The white material is calcium oleate. According to the solubility product, the minimum Na_2CO_3 concentration that restrains $Ca(oleate)_2$ precipitation can be calculated by equation (3). For a 0.1% sodium oleate solution (3.29 mmol/L), 1.1% Na_2CO_3 is needed to suppress the calcium ion concentration so that no $Ca(oleate)_2$ will precipitate. The experiment shows that no soap was detected with 1% Na_2CO_3 and white material was found inside the tube. Only after adding 5% Na_2CO_3 was no white material formed.

$$2Na^+ + Oleate^- + \quad Ca^{2+} \Leftrightarrow Ca(Oleate)_2 \downarrow +2Na^+ \qquad (1)$$

$$Ca^{2+} + CO_3^{2-} \Leftrightarrow CaCO_3 \qquad (2)$$

$$[CO_3{}^{2-}] = [Oleate^-]^2 \frac{K_{spCaCO_3}}{K_{spCa(Oleate)_2}} = 9500 * [Oleate^-]^2 \qquad (3)$$

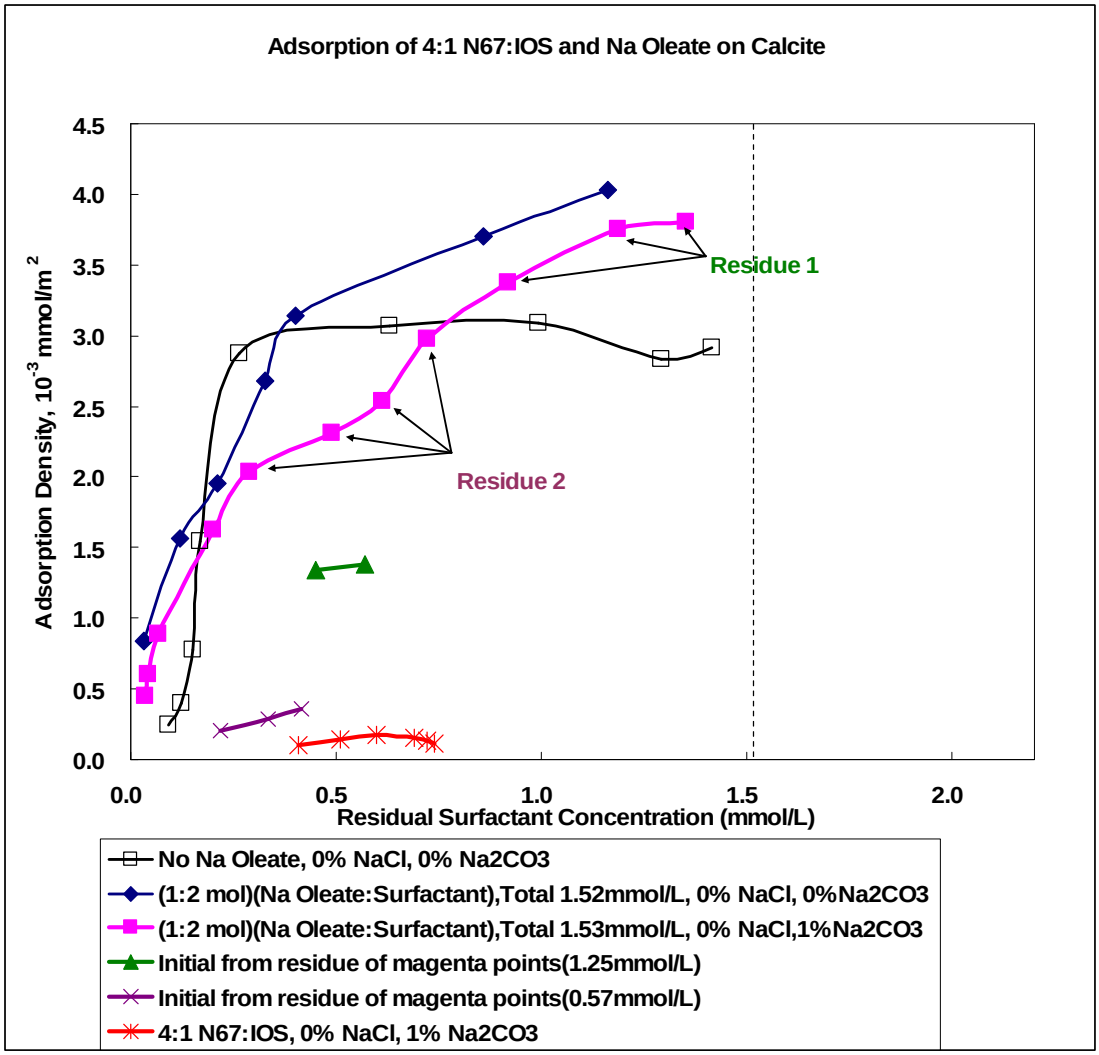

Figure 2.1-6. Adsorption of NI blend and NI blend/sodium oleate mixture on calcite with and without added sodium carbonate

Figure 2.1-6 shows adsorption on calcite from a solution initially containing 0.96 mM NI blend and 0.56 mM sodium oleate, both with and without addition of 1% Na_2CO_3. Both the amount adsorbed and the residual surfactant concentration represent the total of NI blend plus oleate since the titration method used cannot distinguish between the two. No precipitate was observed in either experiment. For comparison the corresponding curves for NI blend alone are also shown.

Comparison of the curves without Na_2CO_3 present shows that adsorption is about the same or somewhat higher for the surfactant/soap mixture than for surfactant alone for a given residual concentration. In view of the discussion in the following paragraph, one might speculate that oleate reduces surfactant adsorption in this case due to competition for sites on the solid. However, no definite conclusions can be made without additional data on the relative amounts of soap and surfactant in the residuals, a topic for further research.

In the presence of Na_2CO_3 figure 2.1-6 shows that adsorption for the surfactant/soap mixture is much greater than that for the NI blend alone, indicating that oleate is adsorbed more strongly on calcite than the synthetic surfactant blend. Indeed, a mass balance for the two situations shows that, whatever is assumed about the amount of oleate adsorbed, adsorption of NI blend from the mixture is greater than that from its own solution for total residual surfactant concentrations below about 0.9 mM. The same is likely true at higher residual concentrations as well, but the additional data mentioned above are required to make conclusive statements. As indicated in Figure 2.1-6, two samples were formed, each by mixing some residuals from the surfactant/soap experiments with Na_2CO_3. Then adsorption on calcite of these mixed samples was measured. The sample consisting of the residuals with the lowest amounts of soap plus surfactant showed much lower adsorption, comparable to that of the NI blend alone in the presence of Na_2CO_3. This result suggests that this sample contained relatively little oleate, which is consistent with the above conclusion that oleate adsorbs more strongly than the NI blend under these conditions.

One possible interpretation of this behavior is that oleate has a much stronger affinity for calcium than the sulfates/sulfonates of the NI blend, as indicated by the much lower solubility of calcium oleate than calcium sulfates or sulfonates (see subtask 1.5). As a result, some oleate ions may adsorb on calcium sites even though overall surface charge may be negative. Such adsorbed oleate ions may lead to formation of admicelles on the solid surface, which surfactant ions can join with a lower adsorption energy than would be required on a clean calcite surface.

The other soap tested was sodium naphthenates from Fisher Scientific. For this mixture of sodium naphthenates, a small amount of white precipitate was also observed when it was mixed with calcite powder. However, the amount of this precipitate was much less than that in the sodium oleate experiments, suggesting that calcium naphthenates are more soluble than calcium oleate. It was found that dissolved sodium naphthenates exhibited absorption in the UV-vis spectrum. However, the absorbance curve was broad without sharp peaks, as perhaps would be expected for such a mixture. The residual solution after being mixed with calcite showed lower absorption, suggesting that some adsorption on calcite occurred, but it was not possible to assess the results quantitatively.

Before the adsorption experiments with mixtures of the NI blend and sodium naphthenates, two samples were titrated. One was 0.1% N67:IOS (4:1), and the other was 0.1% N67:IOS (4:1) with 0.05% sodium naphthenates. The titration results for these two samples were quite close to each other. The end point for the two samples were1.50±0.02 mmol/L and 1.49±0.03 mmol/L. Thus, the presence of sodium naphthenates did not change the titration results, demonstrating that the synthetic surfactant adsorption can be measured. The surfactant adsorption does not change much with the presence of sodium naphthenates. as figure 2.1-7 shows. Na_2CO_3 still reduces synthetic surfactant adsorption by about the same amount whether or not sodium naphthenates are present.

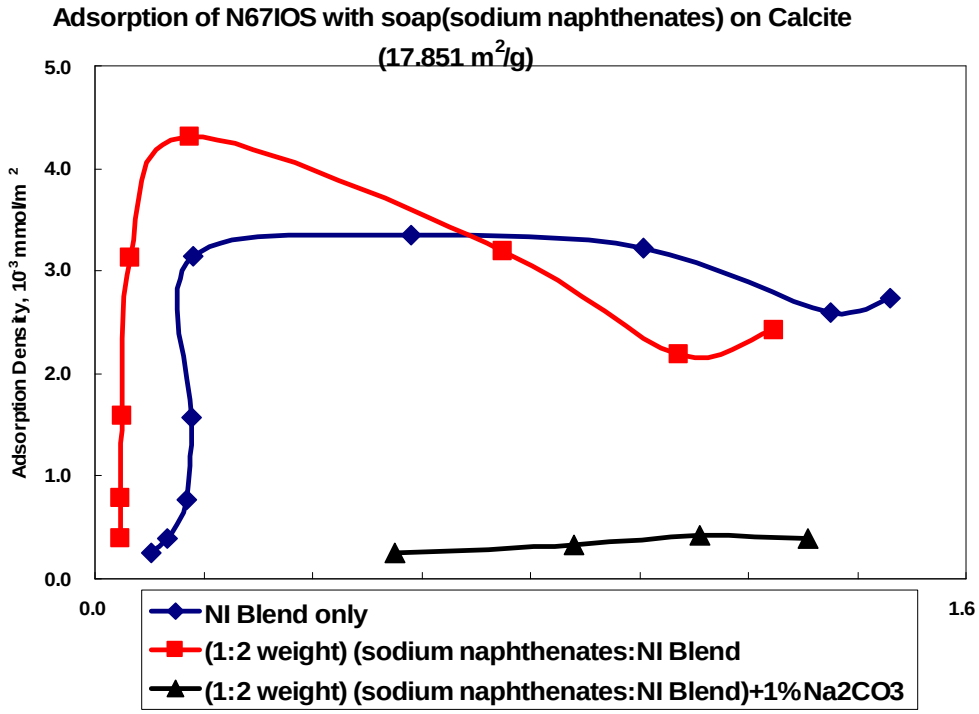

Figure 2.1-7 Adsorption of 4:1 N67:IOS on calcite with sodium naphthenates

Conclusions

1. Both sodium carbonate concentration and salinity influence surfactant adsorption on calcite significantly. The presence of Na_2CO_3 reduces surfactant adsorption. However, higher salinity increases surfactant adsorption and counteracts the adsorption reduction by Na_2CO_3.
2. The concentration domain with low surfactant adsorption for the current surfactant blend is: [Na_2CO_3]>0.2% and [NaCl]<3%.
3. The presence of Na_2CO_3 reduces the adsorption for N67 and IOS respectively significantly.
4. In the absence of sodium carbonate, sodium oleate may reduce adsorption of the NI blend although further data are required to make conclusive statements. Adsorption of NI blend increases, however, when both sodium carbonate and sodium oleate are present. Possibly oleate adsorbs owing to a strong affinity for surface calcium ions,

allowing surfactant molecules to adsorb nearby with a lower adsorption energy and form admicelles.

5. The presence of sodium naphthenates from Fisher Scientific does not significantly affect synthetic surfactant adsorption either with or without sodium carbonate present.

Subtask 2.2 IFT measurement, phase behavior and ultra-low IFT region

2.2.1 IFT measurement for crude oil-alkali-surfactant system

Interfacial tension (IFT) is one of the key factors in the alkali-surfactant process. However, it's difficult to obtain reproducible results in our IFT measurement because there is not enough surfactant to generate enough middle phase microemulsion phase for IFT measurements. Also, a colloidal dispersion was found in the alkali-surfactant system as figure 2.2-1 shows. This is a creamed layer of emulsion between the excess oil and lower phase microemulsion. Since the color of this emulsion is darker than the lower phase microemulsion and it is less dense than the lower phase microemulsion, the oil concentration in this emulsion is expected to be higher than that in the lower phase microemulsion. The presence of this colloidal dispersion significantly changes the IFT results.

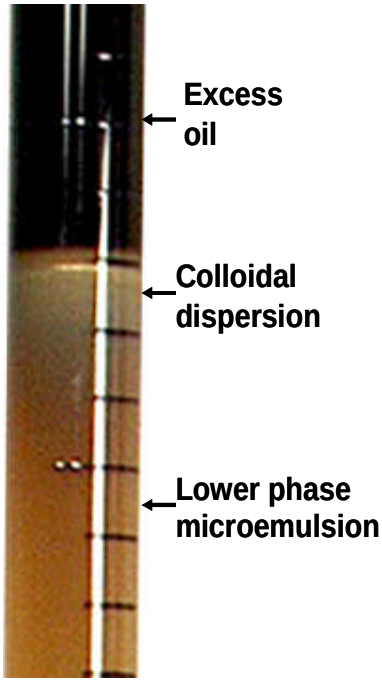

Figure 2.2-1 Phase behavior of 0.2% NI blend / 1% Na_2CO_3 / 2% NaCl (23 days settling)

The colloidal dispersion can also be observed during spinning drop interfacial tension measurements. Figure 2.2-2 shows that during spinning drop tension measurement of 0.2 % NI blend/1% Na_2CO_3 /2% NaCl, there are three regions: aqueous phase, middle layer (colloidal dispersion) and oil. As shown in figure 2.2-1, the volume of the colloidal dispersion is not enough for accurately measuring the density. In calculation of the interfacial tension, the diameter of the oil phase, and the density difference between oil and the aqueous solution were used.

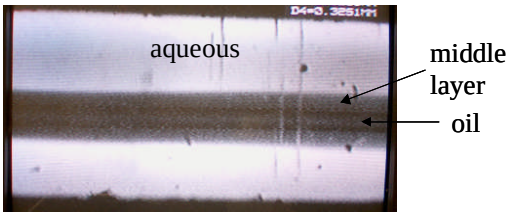

Figure 2. 2-2 spinning drop measurement of 0.2 % NI blend/1% Na_2CO_3/2% NaCl, 4 hours' settling. There are three layers.

The microstructures of colloidal dispersion and lower phase microemulsion are different as figure 2.2-3 and figure 2.2-4 show. The sample was the alkaline/surfactant solution which contained 0.2% NI blend, 1% Na_2CO_3 and 2% NaCl mixed with MY4 (WOR=3). After 24 hours mixing, the lower phase was sampled by syringe and put into spinning tube to centrifuge. The colloidal dispersion and clear lower phase separated after centrifuging in the tensiometer. These two regions were sampled and sealed into different capillary

chambers. The photos were taken under the microscope. In the colloidal dispersion, the amount of dispersed drops in colloidal dispersion is much more than that in clear lower phase. The sizes of most drops in colloidal dispersion are around 1 micron. In the clear lower phase, there are some vesicles in the clear lower phase. They are not oil drops because they did not settle after centrifuging.

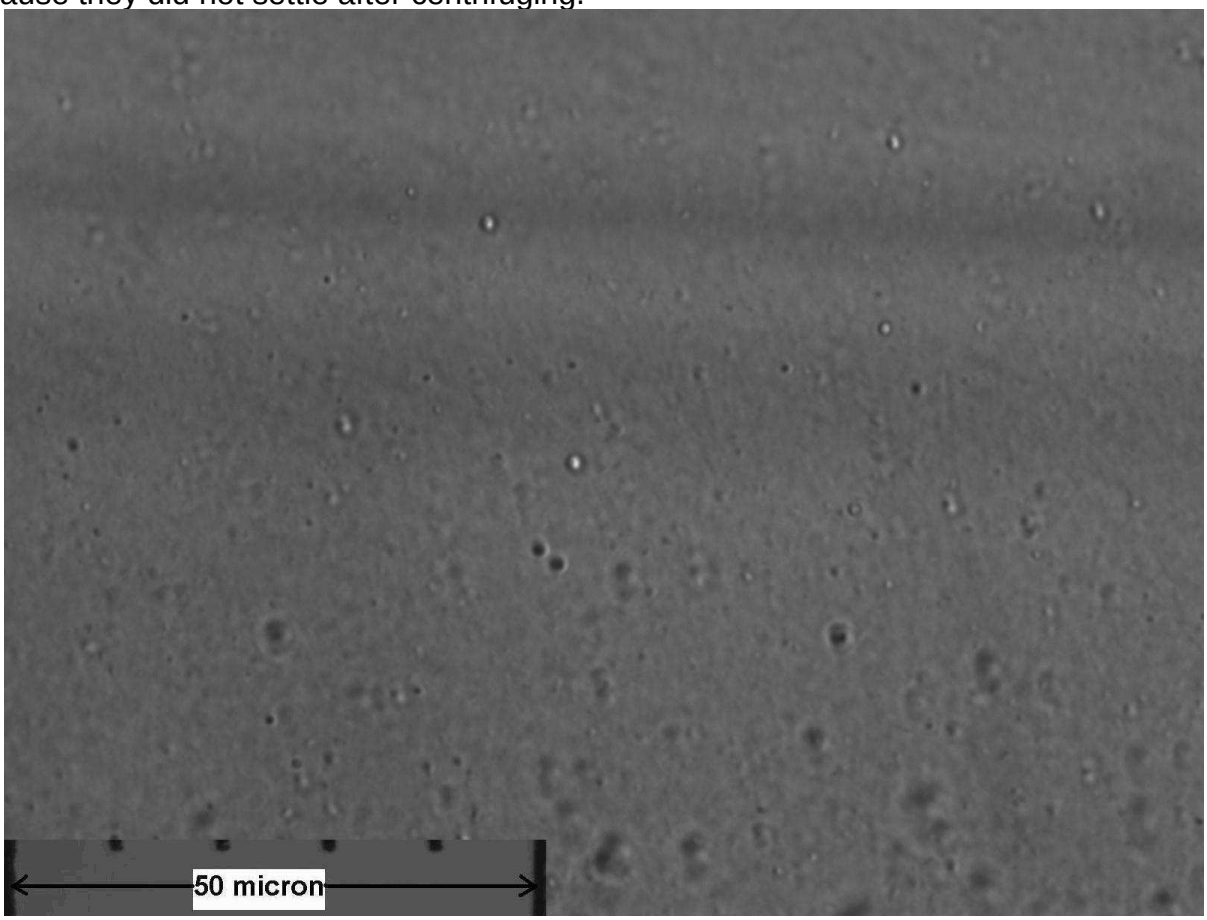

Figure 2. 2-3 Microstructure of colloidal dispersion

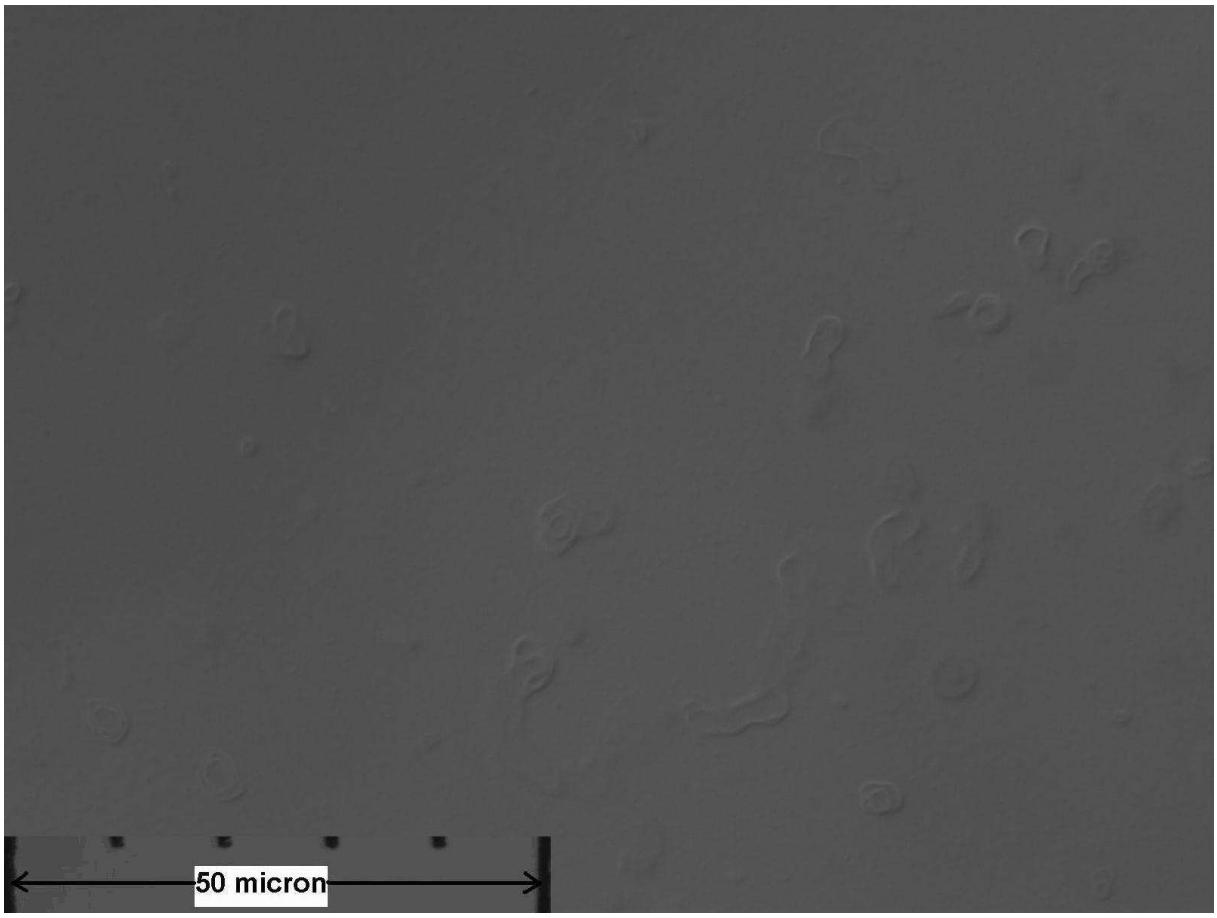

Figure 2. 2-4 Microstructure of clear lower phase

Several experiments were carried out for the system which contains 0.2% NI blend, 1% Na_2CO_3 and 2.0% NaCl at WOR = 3 (soap/surfactant=0.35). The excess oil and aqueous phase were sampled at different settling times, and the dynamic IFT plot is shown as figure 2.2-5. This plot indicates the dynamic IFT is a function of settling time. The photo of a drop after 2 hours settling is shown as figure 2.2-6 for different times of spinning. It is difficult to see the oil drop when its diameter is less than that of the colloidal dispersion because the latter is opaque. It was found that colloidal dispersion was the most important factor for the low tension as figure 2.2-7 shows. There are two drops with different diameters in figure 2.2-7. The two drops both come from a larger drop. The drop with more colloidal dispersion has a smaller diameter and hence lower IFT than the other with less colloidal dispersion. The smaller drop on the left of figure 2.2-7 is obscured by the opaque colloidal dispersion. Figure 2.2-8 shows that the equilibrium low IFT can be reached more quickly if the colloidal dispersion is added.

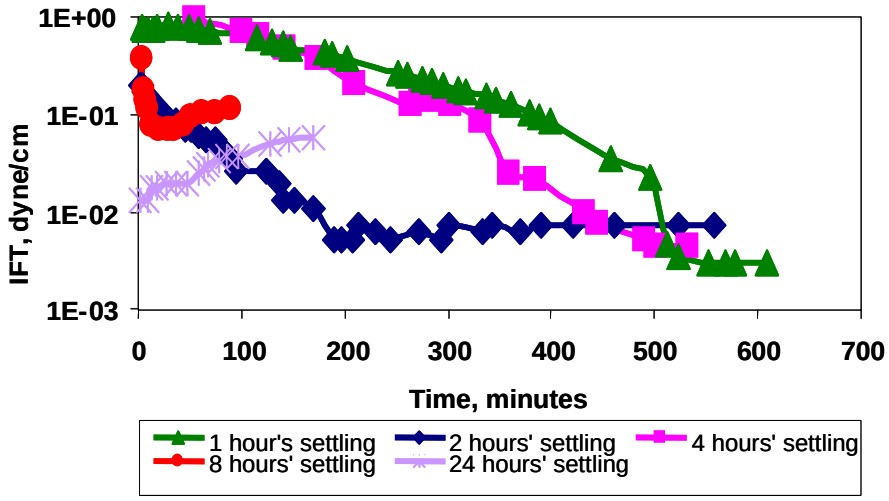

Figure 2.2-5 IFT of 0.2% NI blend / 1% Na2CO3 / 2% NaCl with different settling time

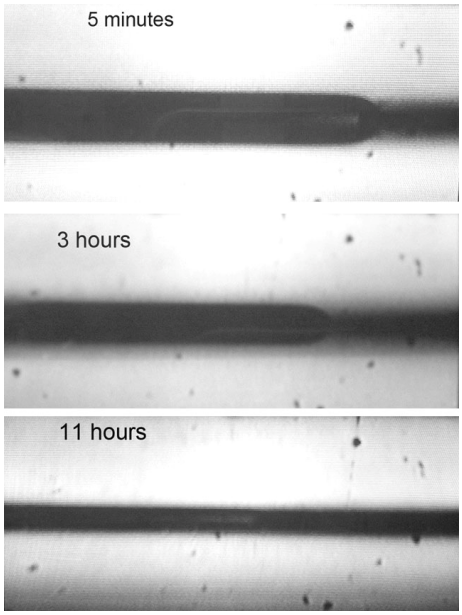

Figure 2.2-6 Photos of spinning drop of IFT of 0.2% NI blend / 1% Na2CO3 / 2% NaCl

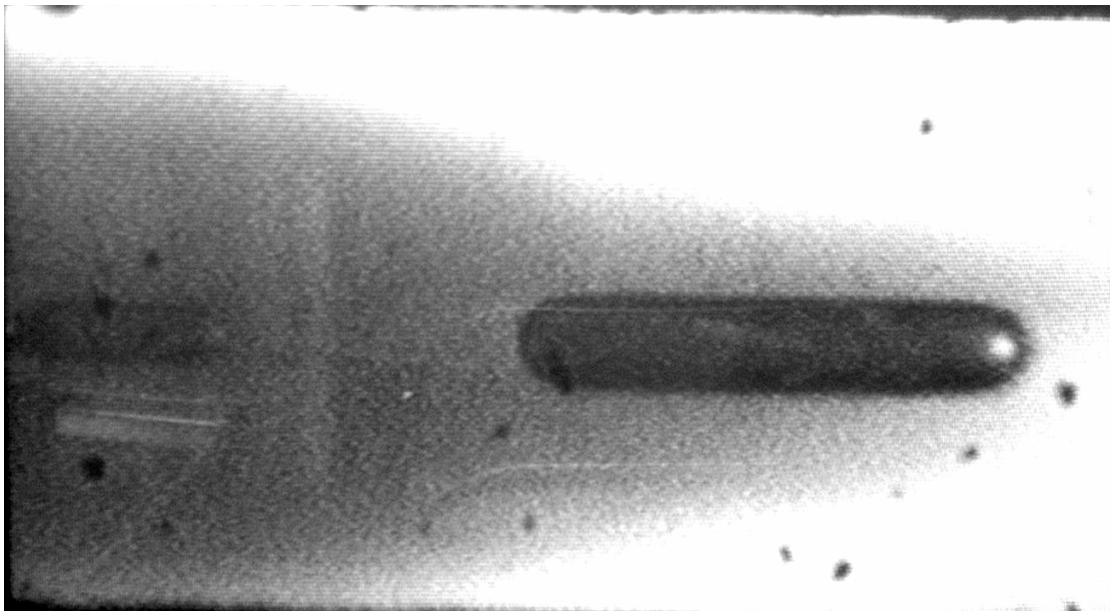

Figure 2.2-7 Photo of two different spinning drops of 0.2% NI blend / 1% Na_2CO_3 / 2% NaCl

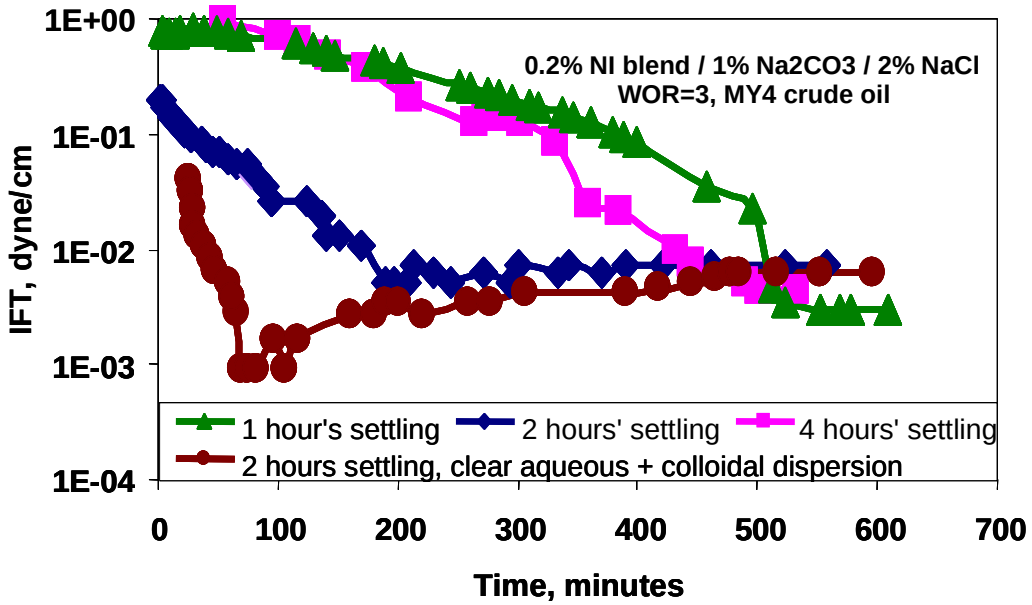

Figure 2.2-8 IFT of 0.2% NI blend / 1% Na_2CO_3 / 2% NaCl with different settling time

It was found that the settling time for colloidal dispersion is different at different salinity as figure 2.2-9 shows. For the samples where salinity is less than 3.0% NaCl, the colloidal dispersion settled between the excess oil and lower phase microemulsion after 23 days. However, the colloidal dispersion did not settle for the 3.4% NaCl sample after 23 days. By centrifuging this sample, colloidal dispersion was found as figure 2.2-10 shows. Thus, the density of colloidal material for the 3.4% NaCl sample is close to that of the lower phase microemulsion. For IFT measurement, the colloidal dispersion is still important no matter what its density. If the colloidal dispersion was removed by centrifuging before the IFT experiment as figure 2.2-11, the time that was needed to reach the equilibrium low IFT became longer.

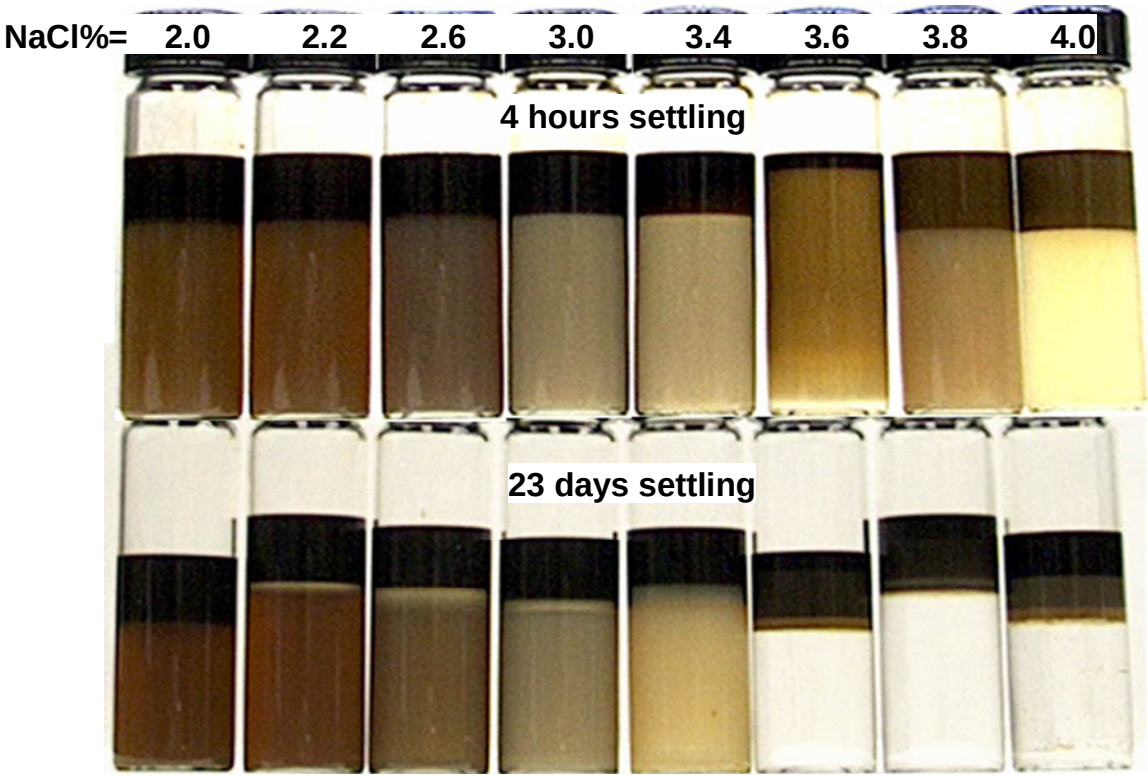

Figure 2.2-9 Comparison of phase appearance of 0.2% NI / 1% Na_2CO_3 / x % NaCl at different time

0.2% NI blend /1% Na_2CO_3 / 3.4% NaCl, 23 days settling with oil-rich emulsion

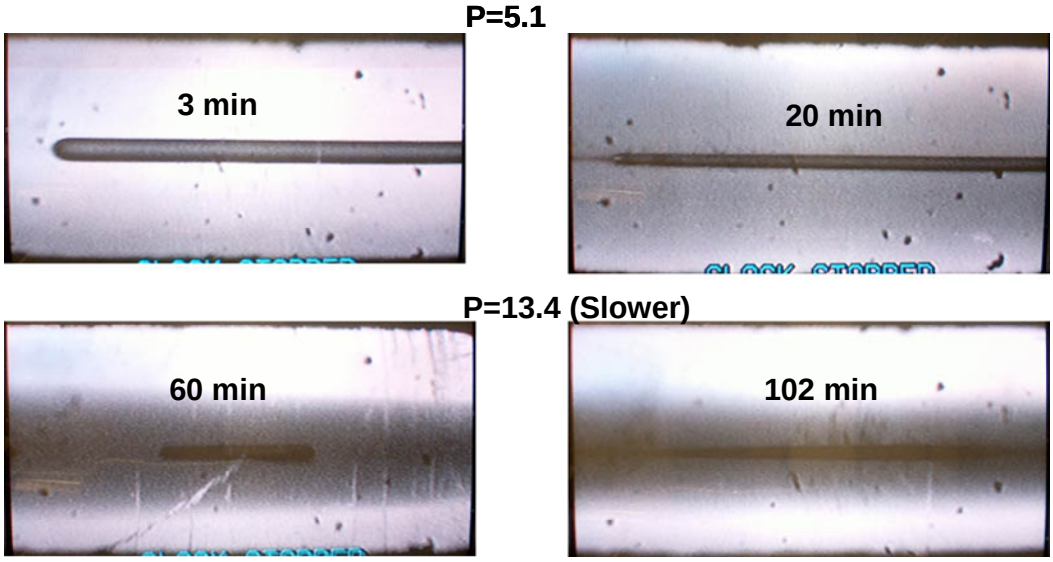

Figure 2.2-10 Photos of spinning drop of 0.2% NI blend / 1% Na2CO3 / 3.4% NaCl with all the colloidal dispersion

0.2% NI blend /1% Na2CO3 / 3.4% NaCl, 23 days settling
Remove most oil-rich emulsion

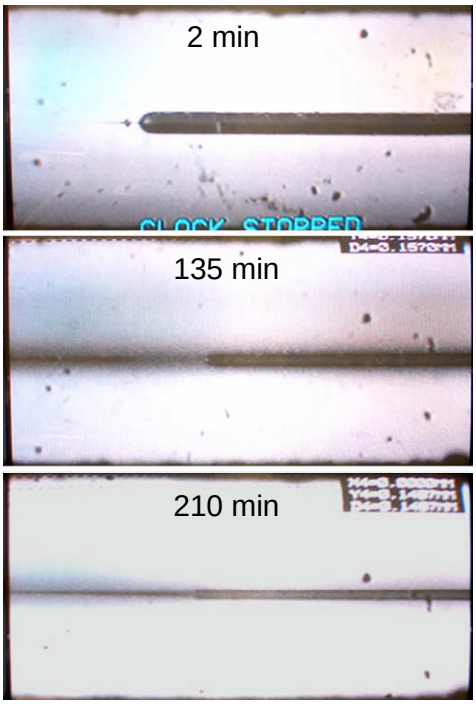

Figure 2.2-11 Photos of spinning drop of 0.2% NI blend / 1% Na2CO3 / 3.4% NaCl
Remove most colloidal dispersion (P=5.1)

Colloidal dispersion is very important for the IFT measurement. However, the spinning drop cannot be seen if the colloidal dispersion surrounds the oil drop and extends to the end of the tube. The oil drops in figures 2.2-6 and 2.2-11 can be seen because the amount of colloidal dispersion is no more than the amount of oil drop. The colloidal dispersion needs time to coalesce with occupy the oil-water interface. It's better to let the oil drop and the colloidal dispersion settle in the spinning tube for some time before the spinning experiments. Otherwise, the phenomena in figures 2.2-7 and 2.2-10 will occur, and a longer spinning time is needed to reach equilibrium IFT.

A standard method, which can quickly provide reproducible equilibrium IFT values, is introduced. The spinning drop IFT experiments should be conducted as follows:

1. Mix the crude oil with the alkaline surfactant solutions containing 0.2% NI blend and 1% Na_2CO_3 at WOR = 3. These solutions have different salinity (0%NaCl~5%NaCl).
2. Rotate the mixture for 24 hours to reach equilibrium.
3. After letting the mixture settle for 4 hours, take samples of oleic and aqueous phases into different syringes. The phase appearances of these samples are shown as figure 2.2-12. If settling time is longer than 24 hours, the aqueous phase will clear up due to separation of the colloidal dispersion. The low IFT may not be observed as discussed in previous annual report.
4. Since these samples may continue to settle and the settling time in the two syringes may be different, shake them before the IFT spinning drop measurement, so that they can be considered as the same sample that was obtained after 4 hours settling.
5. Put some of the aqueous phase (but no oil) into the capillary tube for the spinning drop device and centrifuge it in the device. Remove some of the colloidal dispersion from the

central portion of the capillary tube because the sample will be too dark if too much colloidal dispersion is left. The remaining colloidal dispersion should have less volume than the volume of the excess oil drop that is added into the spinning drop tube.

6. Inject an oil drop into the vertically oriented tube and let it settle for some time (~12 hours), so that the colloidal dispersion can equilibrate with the oil and the lower phase microemulsion.

7. Begin the spinning drop IFT measurement.

Step 5 and 6 will be shown to be a necessary procedure in the following. Figures 2.2-13~2.2-18 show the dynamic IFT of the samples with different salinities (0%~5%). For 0% NaCl, 1% NaCl, 2% NaCl and 4% NaCl samples, step 6 reduces the time that is needed to reach the equilibrium low tension. However, there is no significant difference for 3% NaCl sample by using step 6. This can be explained by phase behavior in figure 2.2-12. The lower phase content is similar to the colloidal dispersion so that low tension can be achieved even without the occupation of the colloidal dispersion in the interface. For 5% NaCl sample, step 6 was not used because there is no colloidal dispersion in this sample and the aqueous phase is clear. This sample exhibits overoptimum phase behavior with some emulsion in the oil-continuous region, as shown in figure 2.2-12.

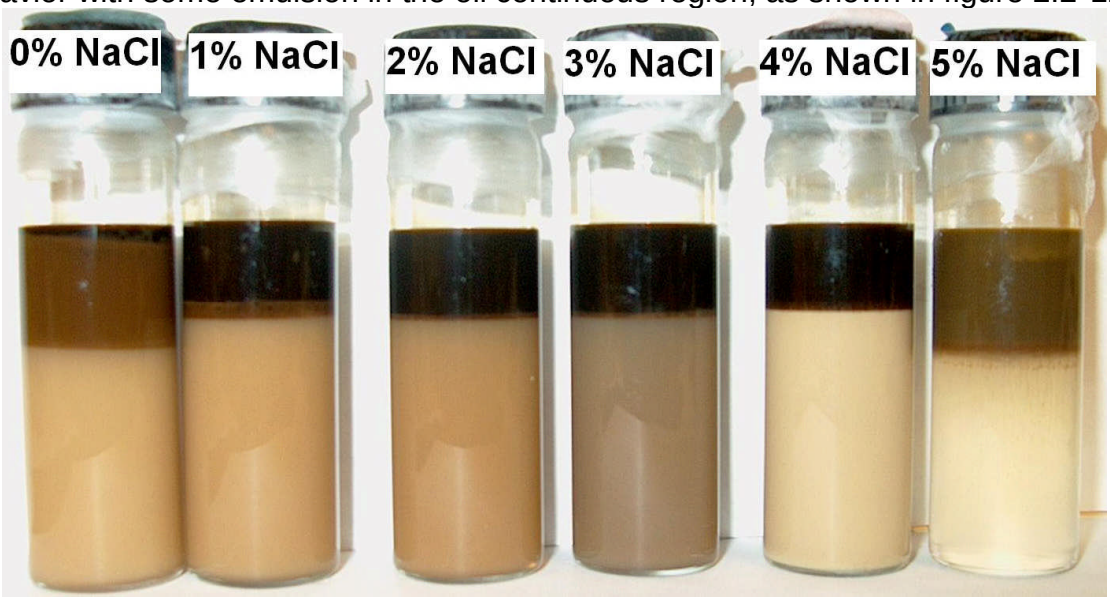

Figure 2.2-12 Phase behavior of 0.2% NI blend/1% Na_2CO_3 (24 hours mixing, 4 hours settling)

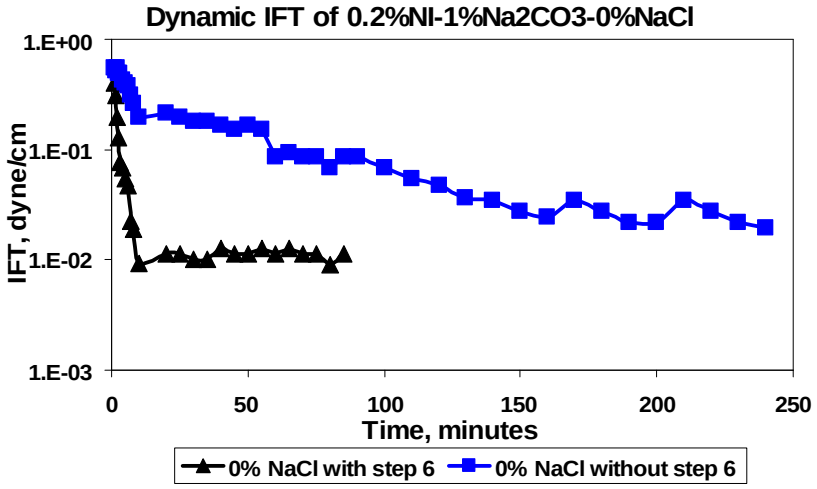

Figure 2.2-13 IFT of 0.2% NI blend/1% Na_2CO_3/0%NaCl as a function of time

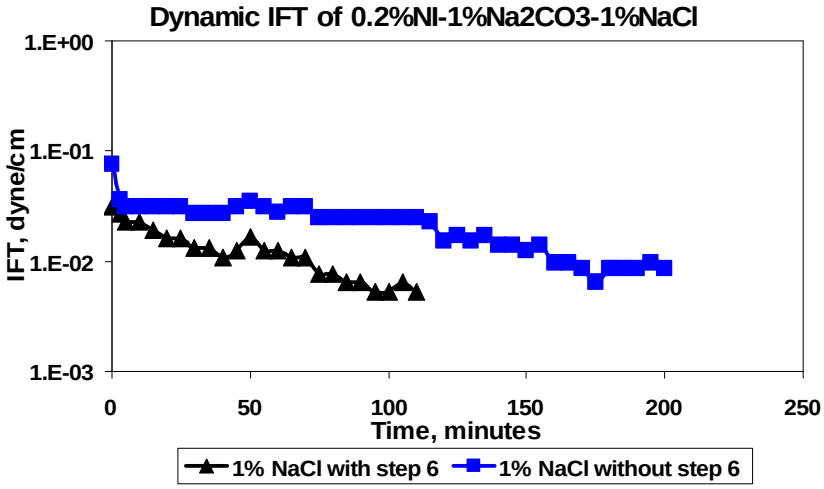

Figure 2.2-14 IFT of 0.2% NI blend/1% Na_2CO_3/1%NaCl as a function of time

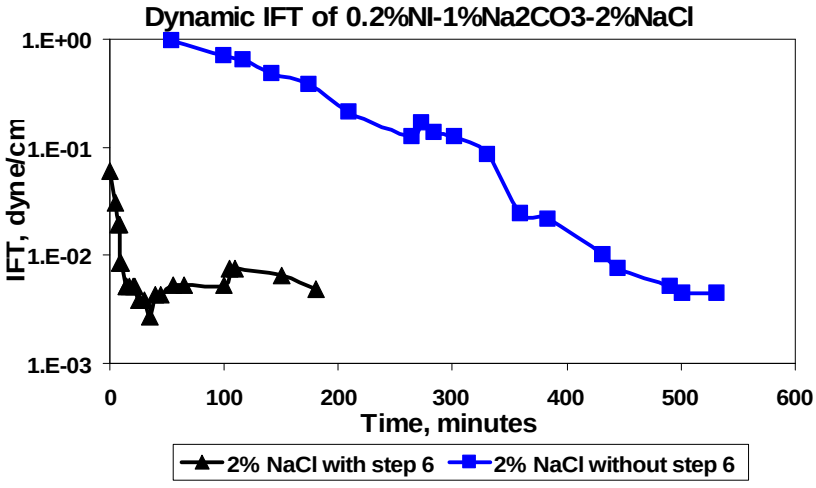

Figure 2.2-15 IFT of 0.2% NI blend/1% Na_2CO_3/2%NaCl as a function of time

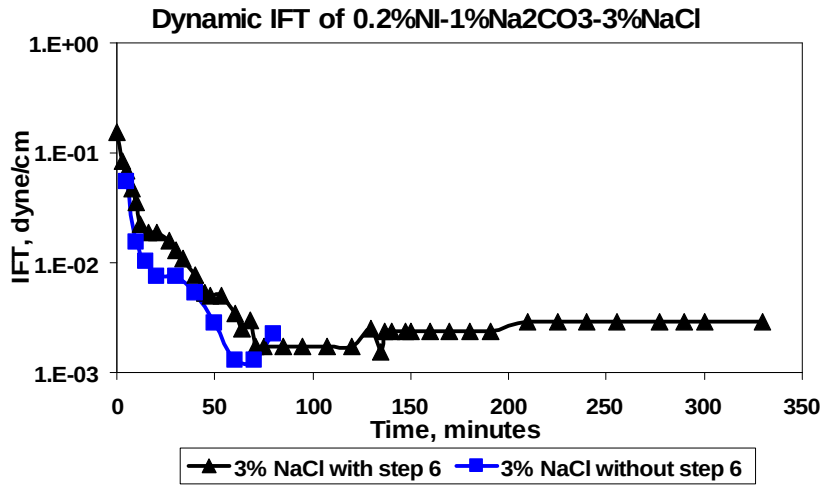

Figure 2.2-16 IFT of 0.2% NI blend/1% Na_2CO_3/3%NaCl as a function of time

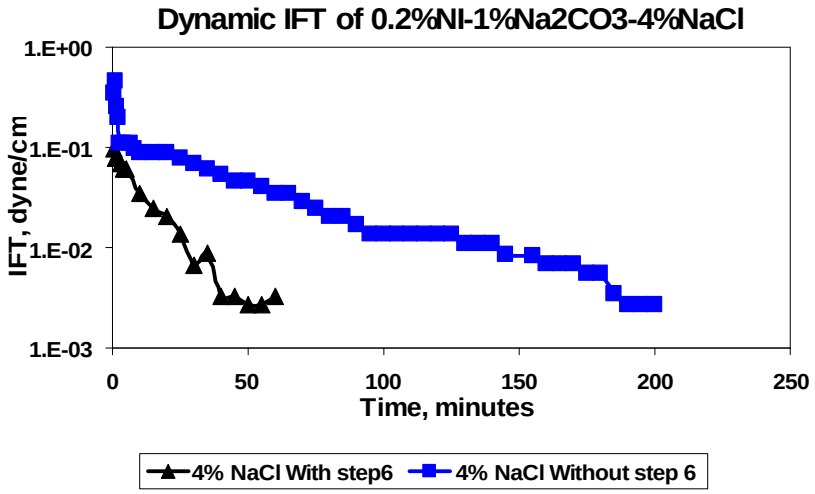

Figure 2.2-17 IFT of 0.2% NI blend/1% Na_2CO_3/4%NaCl as a function of time

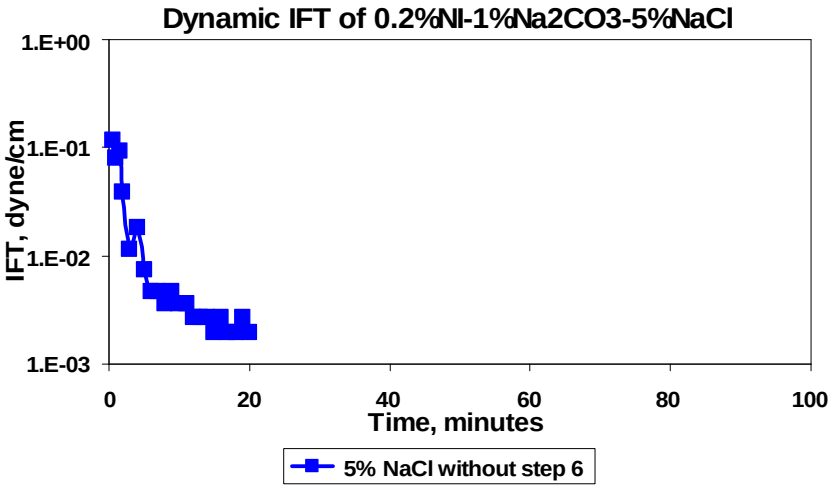

Figure 2.2-18 IFT of 0.2% NI blend/1% Na_2CO_3/5%NaCl as a function of time

Figure 2.2-19 shows the equilibrium IFT measured using different procedures. It demonstrates conclusively that the colloidal dispersion is essential for achieving ultralow IFT. It also shows that step 6 does not change the equilibrium IFT in most cases although, as indicated above, the equilibrium IFT is reached in much less time. Finally, the settling time of step 3 has a significant effect on the equilibrium IFT near optimal salinity, just as it has for lower salinities (fig. 2.2-5). This is because the colloidal dispersion was not present in the lower phase at long settling times and low tensions could not be achieved.

Figure 2.2-19 also shows how IFT changes with salinity. This result implies that the low IFT region of two-surfactant (soap and synthetic surfactant) system is much wider than that of one-surfactant system. From this figure, the width of low IFT region is from 2%NaCl to 5% NaCl. And according to reference [1], the width of low IFT region for single surfactant system is only around 0.3% NaCl. In section 2.3, the importance of the wide salinity range of low IFT will be discussed.

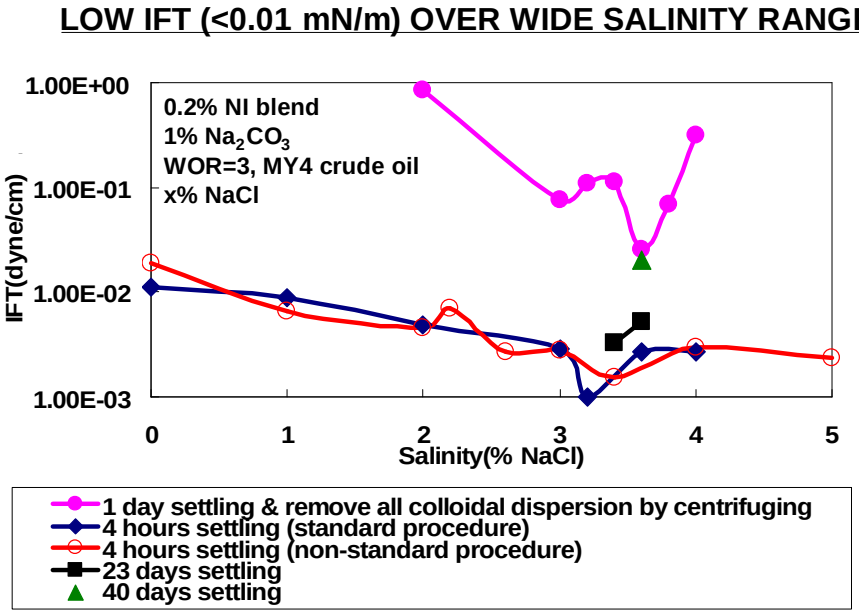

Figure 2.2-19 IFT change with salinity for 0.2NI-1%Na_2CO_3/WOR=3

2.2.2 Correlation between phase behavior and IFT

The solubilization ratios of 0.2% NI blend/1% Na_2CO_3/NaCl are calculated from the phase behavior shown in figure 2.2-20 and plotted in figure 2.2-21. In the calculations the colloidal dispersion layer volume was counted towards the volume of the lower phase. The error of reading the volumes of oil and aqueous phase was estimated to be 0.01 ml. The error of solubilization ratios thus was calculated to be 1.3. The solubilization ratios of this system are very high. Even at a low salinity of 2% NaCl, the ratio of oil to surfactant is close to 7.

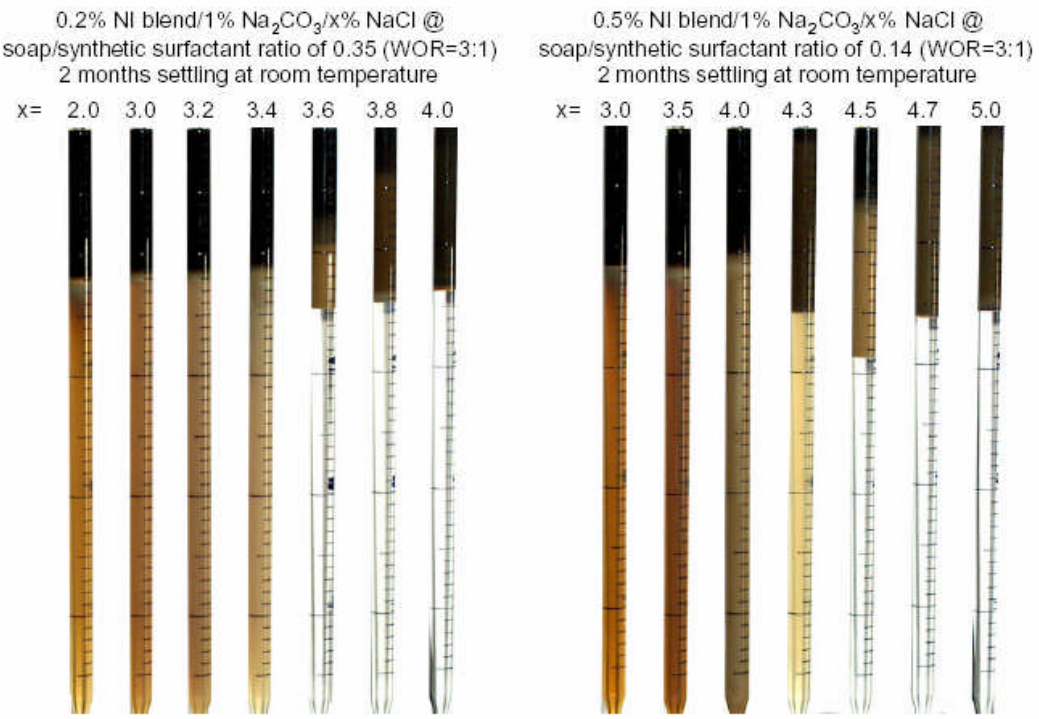

Figure 2.2-20 Phase behavior after 2 months with 0.2% and 0.5% NI blend.

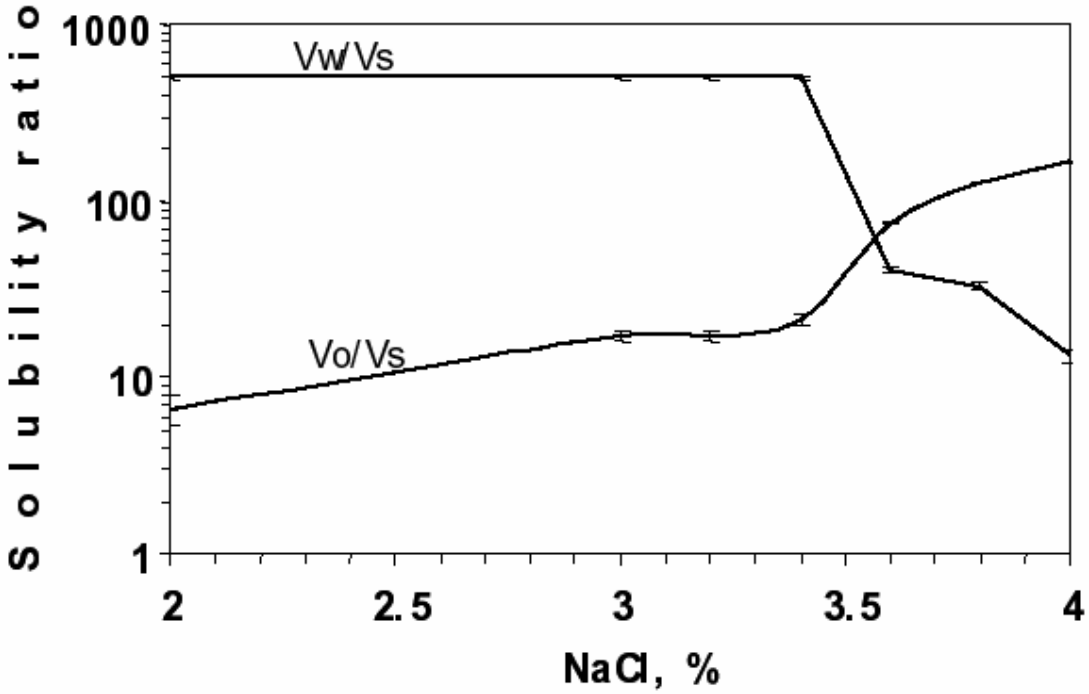

Figure 2.2-21 Solubility ratios of 0.2% NI blend/1% Na_2CO_3/NaCl

Interfacial tension can be estimated from Chun-Huh correlation:

$\sigma_{l3} = \frac{C}{R_{l3}^2}$ (Huh, 1979) .....(2.2-1)

where σ_{l3}: interfacial tension between excess oil or aqueous phase and middle

phase,

R_{l3}: solubilization ratio of oil or water by surfactant,

c: a constant with a typical value of 0.3.

Interfacial tensions of 0.2% NI blend/1% Na_2CO_3/NaCl estimated from Chun-Huh correlation with c=0.3 are plotted in Fig 2.2-22. At salinity of 2% - 4% NaCl, IFT measured by spinning drop method and that estimated from Chun-Huh correlation are close.

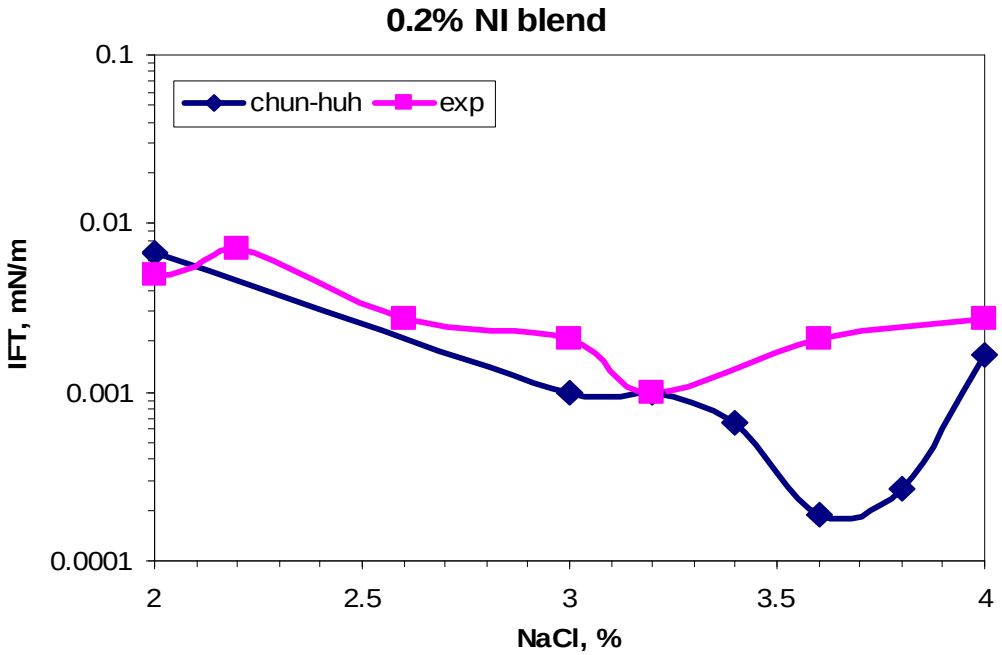

Figure 2.2-22 Comparison of IFT measured by spinning drop measurements using standard procedure and that estimated by Chun-Huh correlation of 0.2% NI blend/1% Na_2CO_3/NaCl. c=0.3.

The phase behavior, with increased concentration of 0.5% NI blend is shown in the right of figure 2.2-20. The solubilization ratios and IFT estimated from Chun-Huh correlation with c=0.3 are plotted in figures 2.2-23 and 2.2-24, respectively. Both the solubilization ratios and the estimated IFT are similar to those with 0.2% surfactant, but the optimal salinity has increased with increased surfactant concentration.

The remarkable observation of the phase behavior (Figure 2.2-20), IFT measurements and estimations (Figures 2.2-20, 2.2-22) is that low IFT (i.e., below 10^{-2} mN/m) appears not to be limited to the three-phase or Winsor III region but also occurs well into the lower-phase microemulsion or Winsor I region. We interpret this by looking at the close-up of the phase behavior in Fig. 2.2-1. A system that appears to be a lower-phase microemulsion has a colloidal dispersion at the top just beneath the oil phase. This colloidal dispersion appears to be a “middle” phase between the lower-phase microemulsion and the excess oil phase. It was observed in the IFT measurements that the presence of this colloidal dispersion was necessary for low tensions in most cases. We speculate that this colloidal dispersion may be due to the naphthenic soaps formed from action of the alkali on the naphthenic acids in the oil. If this is the case, we would expect more of this colloidal dispersion to be present if the

amount of crude oil is increased. That appears to be the case in Figure 2.2-25. The left two tubes both have a salinity of 2% NaCl but have soap/surfactant ratio of 1:1 and 0.35:1 respectively. The left tube with more crude oil does appear to have more colloidal dispersion.

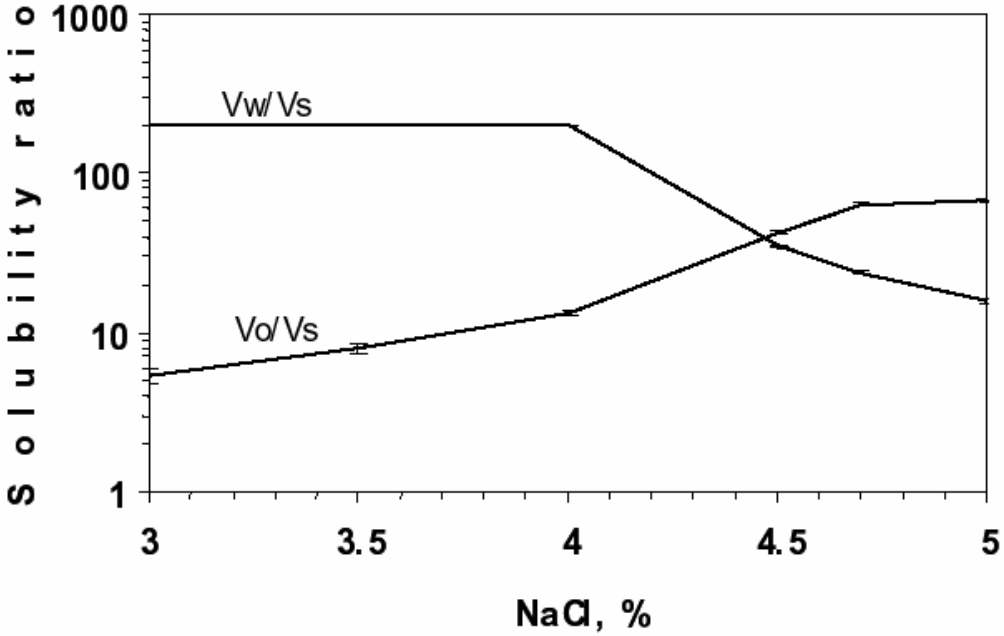

Figure 2.2-23 Solubility ratios of 0.5% NI blend/1% Na_2CO_3/NaCl

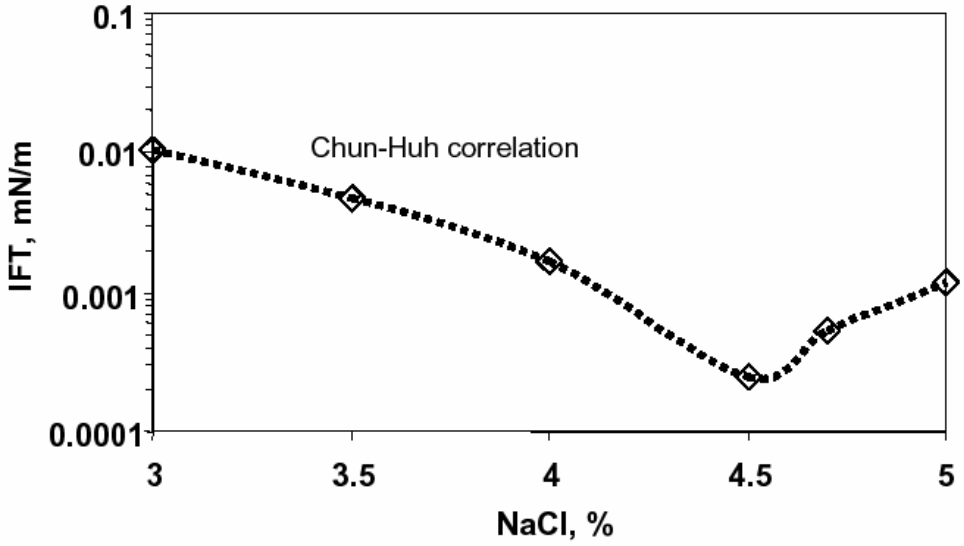

Figure 2.2-24 IFT estimated by Chun-Huh correlation of 0.5% NI /1% Na_2CO_3/NaCl, c=0.3.

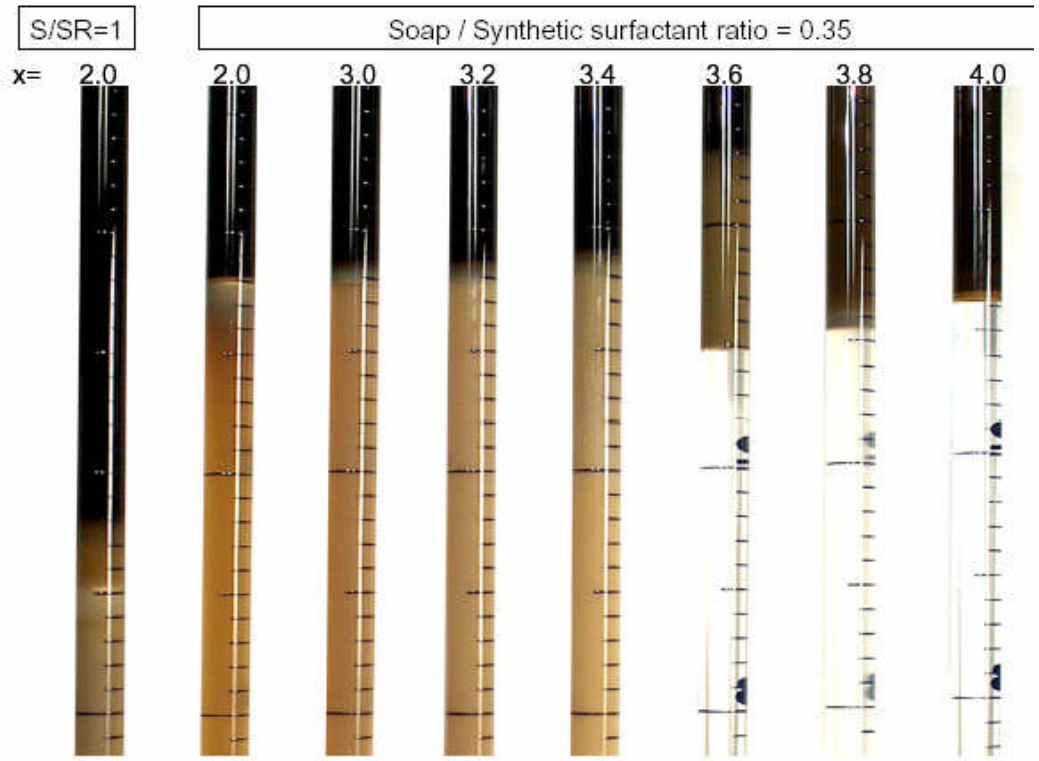

Figure 2.2-25 Phase behavior of 0.2% NI blend/1% Na_2CO_3/x% NaCl, 40 days of settling. Thin colloidal dispersion layers exist at salinity of 2-3.4% NaCl.

2.2.3 Birefringence of MY4-NI Blend system

Birefringence was observed in the 0.2% NI blend salinity scan at 1% Na_2CO_3, WOR=3, as shown in figure 2.2-26. There is strong birefringence for the sample 3.2 % NaCl, which is close to the optimal condition.

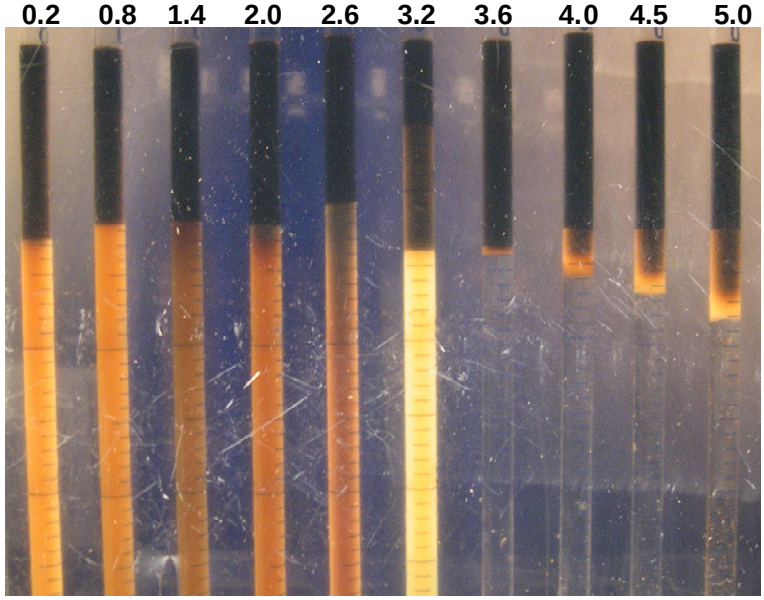

Figure 2.2-26 Appearance of 0.2% NI blend / 1% Na_2CO_3 / x% NaCl, WOR=3:1, 24 hours mixing, 40 days settling under polarized light

Birefringence might indicate that liquid crystalline material is present. Some liquid crystalline phases are very viscous and could not propagate through porous media. Several experiments were done using different viscometers. With both the Brookfield viscometer and the RDA III rheometer, the viscosities of the birefringent lower phase at different shear rates were measured. Figure 2.2-27 shows that this birefringent solution is a Newtonian fluid with roughly the viscosity of water. The viscosity is 1.07 cP $\pm$ 0.07 at shear rates of 100-1000 s^{-1}. For lower shear rates uncertainty in viscosity increases owing to less accuracy in measuring torques, but it never exceeds ±20%. Thus, the sample with strong birefringence is not highly viscous. It may be that liquid crystalline material is dispersed (perhaps along with some oil drops) in the lower phase microemulsion in the form of particles or of vesicles such as those shown in figure 2.2-4 at 2.0% NaCl. In that case the concentration of particles or vesicles must be considerably larger at 3.2% NaCl to exhibit birefringence.

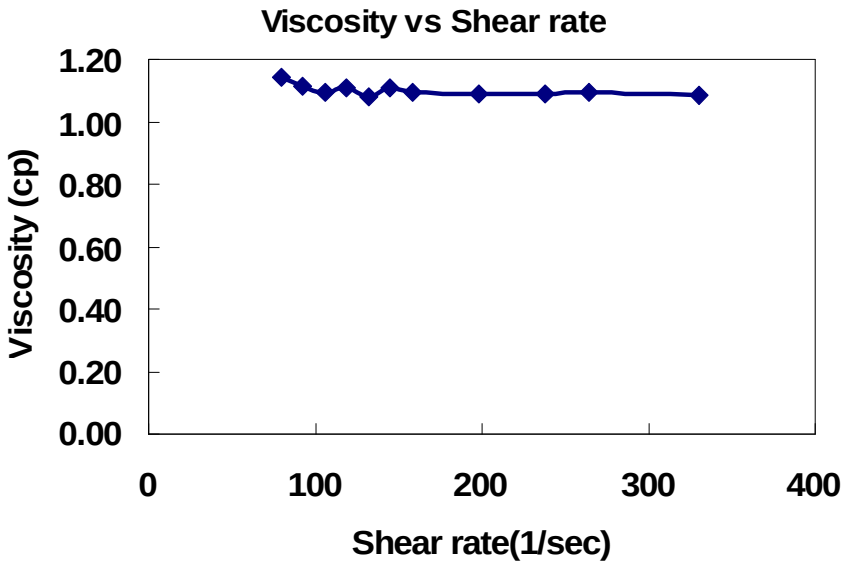

Figure 2.2-27 Viscosities of 0.2% NI / 1% Na_2CO_3 / 3.2 % NaCl at different shear rates

Conclusions

1. In the alkali-surfactant system, colloidal dispersion plays an important role in achieving low values of IFT.
2. A spinning drop IFT measurement procedure, which can reach the equilibrium IFT quickly for alkali-surfactant system, was introduced.
3. The NI Blend-MY4-Na_2CO_3 system has a wider low IFT region than normally seen for single surfactant systems.
4. IFT for NI Blend-MY4-Na_2CO_3 system can be correlated with solubilization ratios that are obtained from the observed phase behavior by using Chun-Huh correlation with c=0.3
5. There is birefringence near the optimal salinity for NI Blend-MY4-Na_2CO_3 system. The sample exhibiting birefringence is still a low-viscosity Newtonian fluid.

Subtask 2.3 Characteristics of Alkali-Surfactant-Polymer process

By using the one-dimensional ASP simulator that was discussed in the previous annual report, some important characteristics of the ASP process are discussed in this section. Based on the data of Subtask 2.2 presented above, which shows a wide range of low IFT in the lower phase region, a contour plot of IFT was generated as figure 2.3-1. The narrow range of low IFT in the upper phase region used previously was retained for these simulations because data reported above showing low tensions for high salinities was not then available. Figure 2.3-1 is clearly different from the narrow low IFT region contour plot, figure 2.3-2 that was used in the previous annual report.

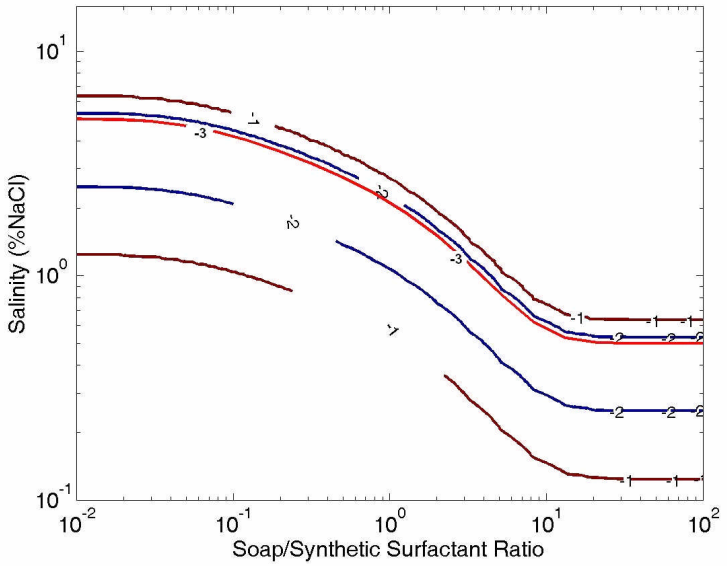

Figure 2.3-1 Contour of interfacial tension with wide low IFT region (log_{10}(IFT)) (IFT: dyne/cm)

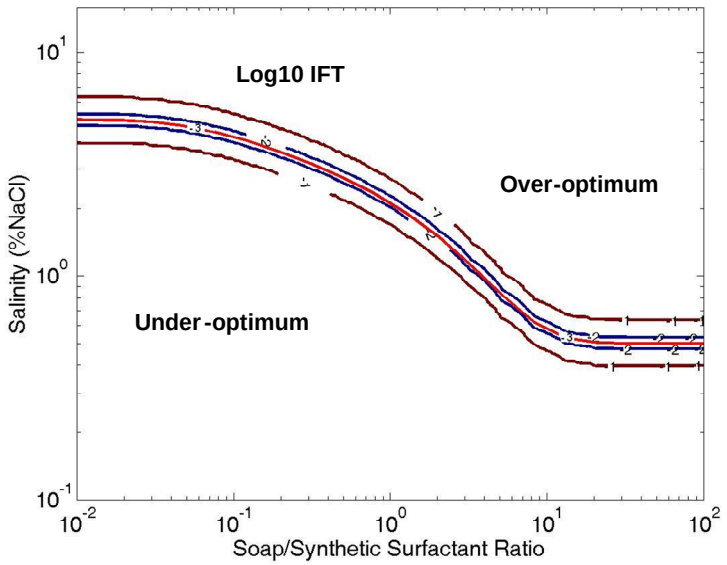

Figure 2.3-2 Contour of interfacial tension with narrow low IFT region (log_{10}(IFT)) (IFT: dyne/cm) (The width of low IFT region is base on reference [1])

Initial Oil Saturation	Formation Brine	Acid No. of Crude oil	Injecting Na_2CO_3 concentration	Injecting Salinity
0.3	2.0%	0.2 mg KOH/g	1.0%	2.0% NaCl
Surfactant concentration	Surfactant Slug Size	Injecting Polymer (flopaam3330S)	Injecting solution viscosity:	Crude Oil viscosity
0.5%(NI blend)	0.5 PV	5000ppm	40 cp	19.7 cp
Polymer adsorption	Surfactant Adsorption	NX (Grid block No.)	dt/dx	Peclet No
20 μg/g	0.2mg/g	100	0.05	500

Table 2.3-1 Other major parameters for the example

These two different models of IFT behavior were compared by the ASP simulator. Other major parameters are the same and are shown in Table 2.3-1. The simulation results show that the recovery will be 95.6% with wide low IFT region and be only 62.3% with narrow low IFT region. This result can be explained by figure 2.3-3. The left two figures show the oil saturation profile and IFT profile respectively for the wide low IFT region when the dimensionless time equals 0.5 PV. The right two figures show the same profiles at same time but with narrow IFT region. The low tension region ($<10^{-2}$ dyne/cm) in the left profile is around 0.1 dimensionless distance, while low tension region in the right profile is only 0.03 dimensionless distance. The oil saturation in the left profile is much less than that in the right profile. Narrow low IFT region will have less recovery because oil will be trapped again when the IFT increases. When the low IFT region is wide, less oil is trapped after the low tension region and recovery increases.

In the previous annual report, high oil recovery was achieved only around optimal salinity of the injected surfactant because of the narrow low IFT region assumption. However, with the wide low IFT region in the alkali-surfactant system, high oil recovery can be achieved for a large range of salinities. Figure 2.3-4 illustrates this phenomenon. Thus, salinities with high surfactant adsorption could be avoided by injecting at salinities well below the optimal value for the synthetic surfactant alone. Also the ASP process is more robust because of its large operational salinity region.

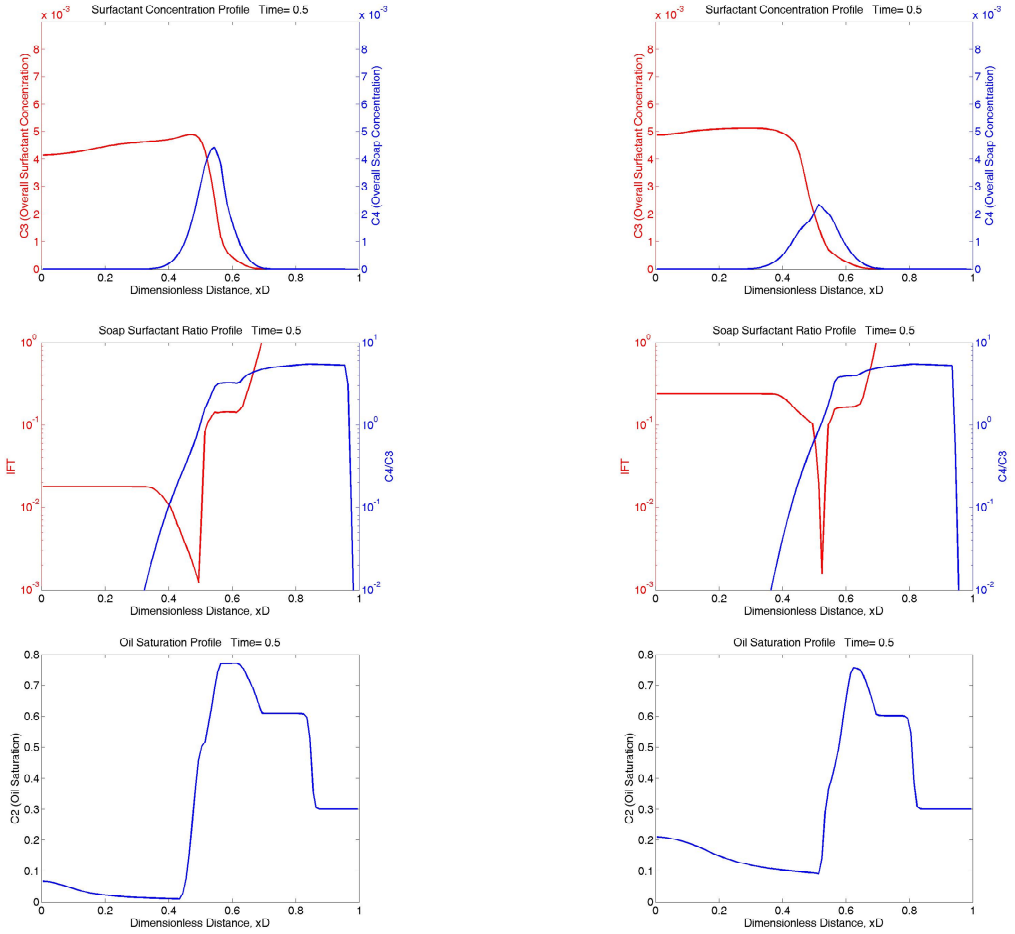

Figure 2.3-3 Comparison of profiles between wide low IFT region and narrow low IFT region

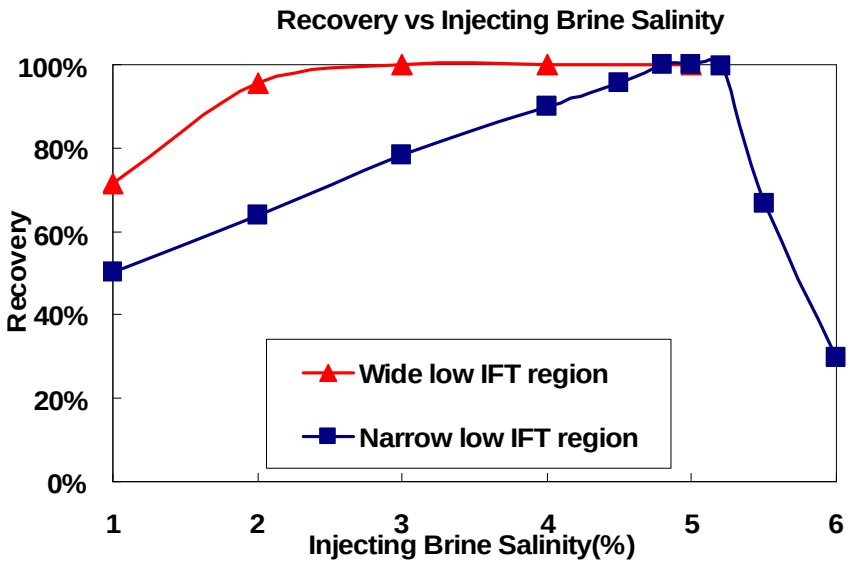

Figure 2.3-4 Oil recoveries vs. injecting brine salinities

The other important parameter is viscosity. The injection solution viscosity can change the oil recovery significantly as figure 2.3-5 shows. The wide low IFT region was used in all the figures of figure 2.3-5. All the other parameters are the same as Table 2.3-1 except the injection solution viscosities. The left two figures are calculated by using 40 cp as the injection solution viscosity, while the right two used 24 cp as the injection solution viscosity. The IFT profiles of these two conditions are similar to each other. However, the oil saturation profiles are different, thus the oil recoveries are different. This is because the injection solution viscosity has significant effect on recovery because it is related to mobility ratio. Because the oil fractional flow increases with increasing aqueous phase viscosity, the oil in the low tension region can flow more easily. Figure 2.3-6 illustrates this effect. Lower aqueous phase viscosity, i.e., higher mobility ratio, has lower oil recovery even with wide low IFT region because it takes a greater distance to displace the oil before the IFT increases. Thus, the injection solution viscosity should be large enough to obtain high oil recovery.

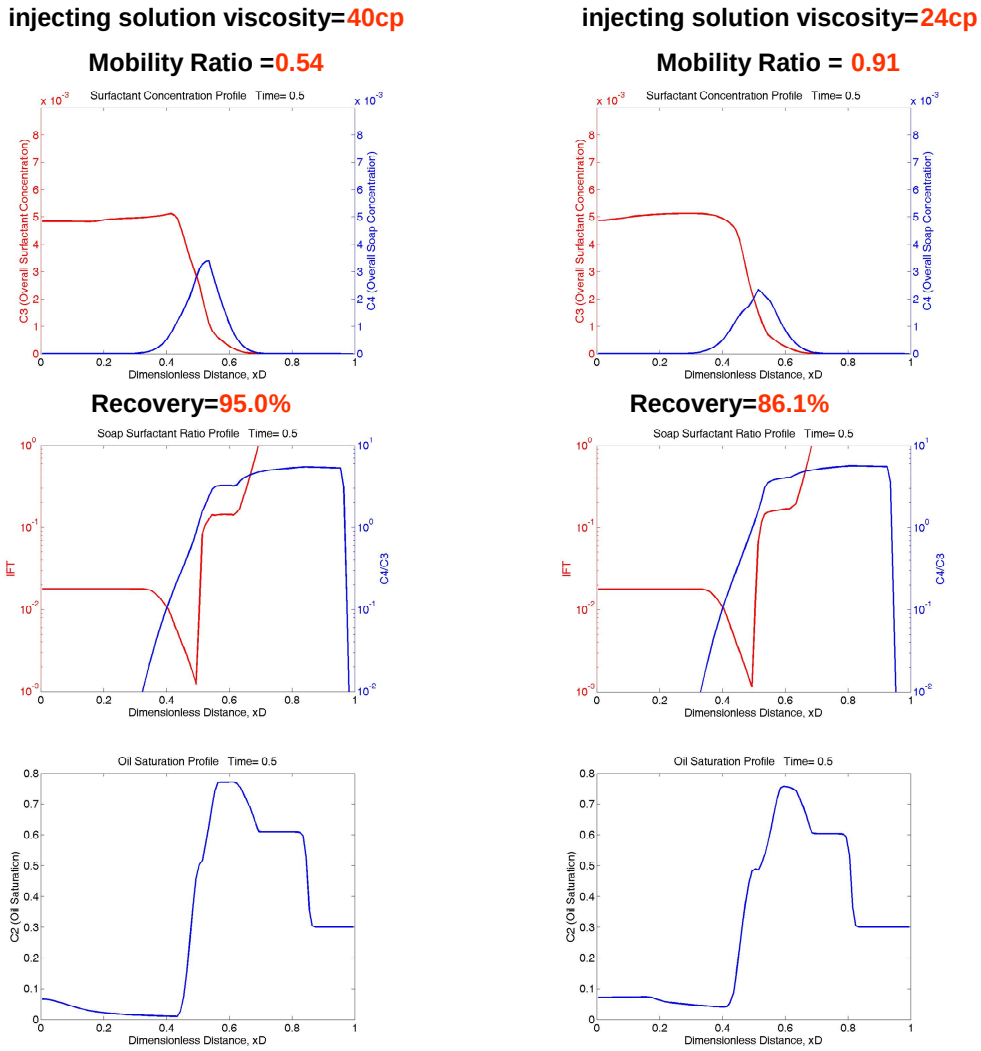

Figure 2.3-5 Comparison of profiles between varied injecting solution viscosities

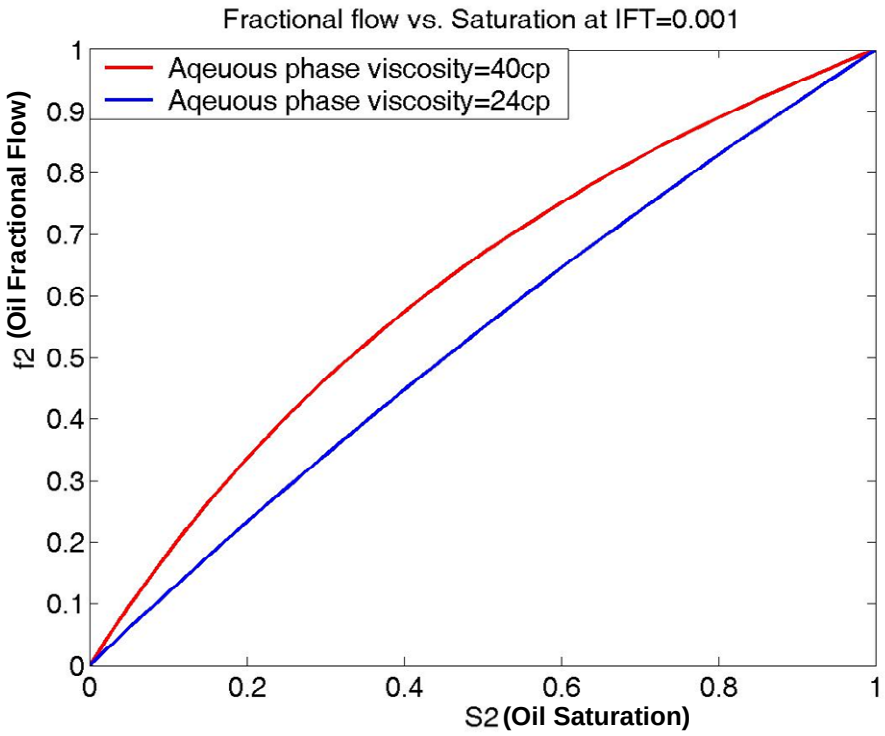

Figure 2.3-6 Oil Fractional Flow vs. Saturation at IFT=0.001dyne/cm (Oil viscosity =19.7 cp)

Conclusions

1. The width of the low IFT region is a key factor for recovery. Narrow low IFT region will have lower recovery because oil will be trapped again when the IFT increases. When the low IFT region is wide enough, less oil will be trapped after the low tension region. The current system has wide low IFT region.
2. The injection solution viscosity has significant effect on recovery. Lower aqueous phase viscosity, i.e., higher mobility ratio, has lower oil recovery even with wide low IFT region. This is because the oil fractional flow increases with the aqueous phase viscosity.

Subtask 2.4 Alkaline-Surfactant Polymer Forced Displacement

2.4.1 Dolomite sand pack

An alkaline-surfactant-polymer process was performed on a one-dimensional dolomite sand pack column. The permeability of the dolomite was 35 darcy. Before the alkaline-surfactant process, the water-flooding was conducted by the following procedure:

1. The sand pack was saturated with CO_2 so that there was no air left in the sand pack.
2. Brine with 2% NaCl was injected at the velocity 0.5 ml/min (interstitial velocity = 14 ft/day) until the column was saturated by the brine.
3. Crude oil (MY4) was injected at the velocity 0.5 ml/min (interstitial velocity = 14 ft/day) until the oil broke through. The oil cut was 100% immediately after breakthrough. The oil saturation after the oil flooding was 0.98.
4. The oil-saturated column was placed into a 60 ℃ oven for 60 hours. The purpose of this aging procedure was to change the wettabilty of the substrate (dolomite) to mixed-wet.
5. After aging, brine with 2 % NaCl was pumped into the column at velocity 0.5 ml/min (interstitial velocity = 14 ft/day) until there was no oil in the effluent.

Figure 2.4-1 show the photos of oil flooding and water flooding. The left one is the photo for oil flooding. The right five photos show the water flooding at different pore volume injected. The flow is upward.

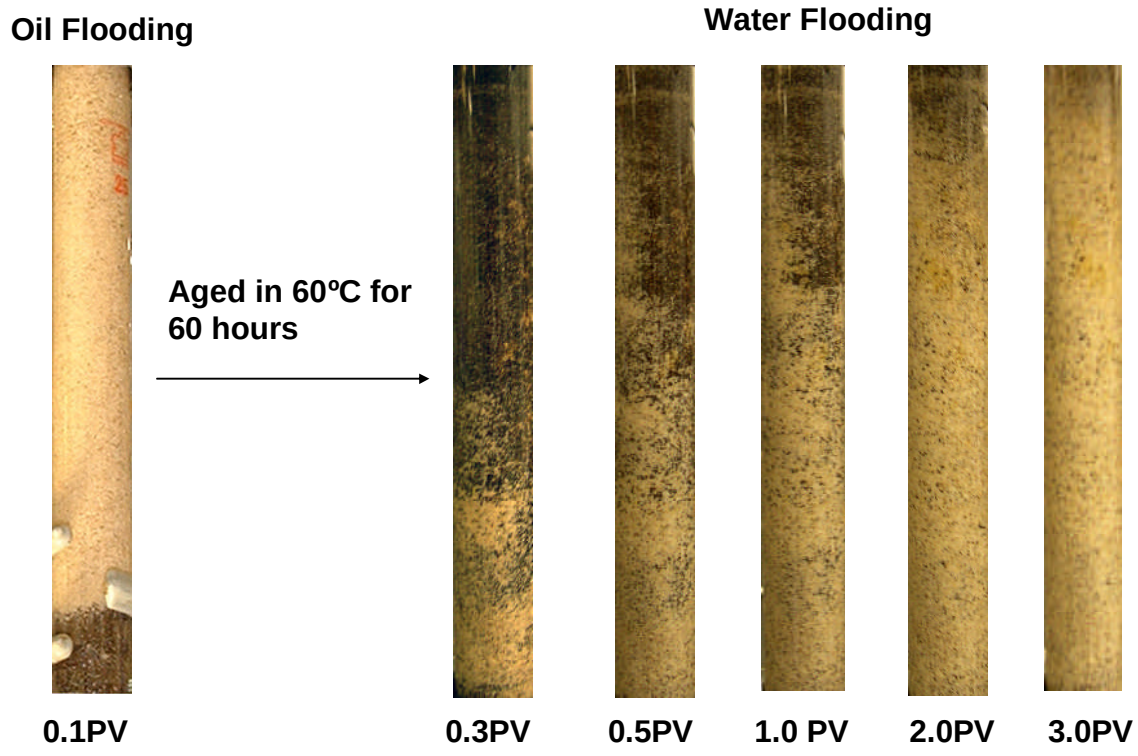

Figure 2.4-1 Photos of oil flooding and water flooding

The cumulative oil recovery and the fractional flow of oil are shown on figure 2.4-2. In this figure, the oil saturation is 0.177 (S_{or}=0.177) after 3.2PV was injected. Further injection of water would not be expected to recover much more oil.

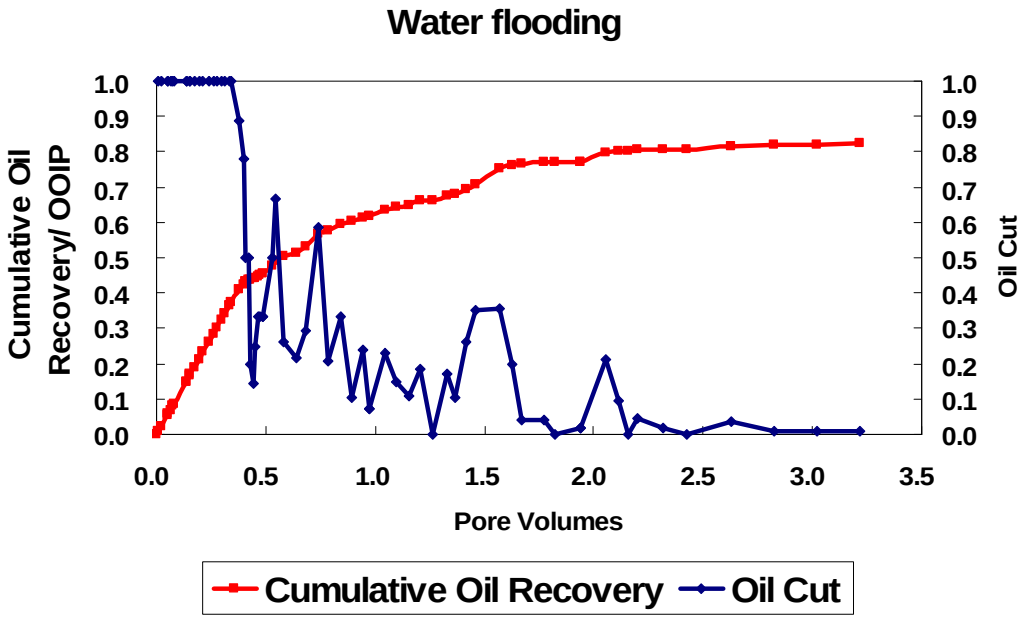

Figure 2.4-2 Oil Recovery of Water Flooding in Dolomite Sand Pack (OOIP: Original Oil in Place)

After water-flooding, the alkaline-surfactant process was implemented on the dolomite sand pack. A 0.50 PV slug of alkaline surfactant polymer solution was injected into the sand pack followed by a 1.0 PV polymer drive. The formulation of alkaline-surfactant-polymer solution is shown in Table 2.4-1. The viscosity of this solution was 45.1 cp at the shear rate of 66 sec^{-1}. The reason that such high viscosity was used is that the crude oil viscosity was 19.4 cp. The polymer drive consists of 5000 ppm polymer and 2.0% NaCl.

Chemicals	Concentration
Alkali (Na_2CO_3)	1.0 %
NaCl	2.0%
Surfactant **(4:1 NEODOL 67:IOS)**	0.2%
Polymer (Flopaam 3330S)	5000ppm

Table 2.4-1 formulation for the alkaline surfactant polymer solution

The photos in figure 2.4-3 illustrate how the oil bank forms and propagates in the ASP process. Figure 2.4-4 shows the cumulative oil recovery and the fractional flow of oil. Figure 2.4-5 shows the effluent. The oil bank breaks though at 0.8 PV. The surfactant breaks through at 0.99 PV because we can find lower phase micro-emulsion in the effluent at 0.99 PV. The incremental oil recovery is 98.1% and the clean oil recovery is 61.3%. There may be some oil in the aqueous phase because the color of the aqueous phase of some effluent is brown. The history of pressure drop is shown in figure 2.4-6. The pressure increased with the injection because the surfactant slug and polymer drive were designed to have a favorable mobility ratio. The pressure became stable and did not increase any more after the surfactant broke through because the whole column was

occupied by the surfactant slug and polymer drive. Further injecting the polymer solution did not change the viscosity of the system.

The one-dimensional simulator was used to simulate this experiment. Figure 2.4-7 compares the simulation results and the experimental results. This plot shows the simulation result matches the experimental results quite well.

Figure 2.4-3 Photos of dolomite pack at different injecting pore volumes

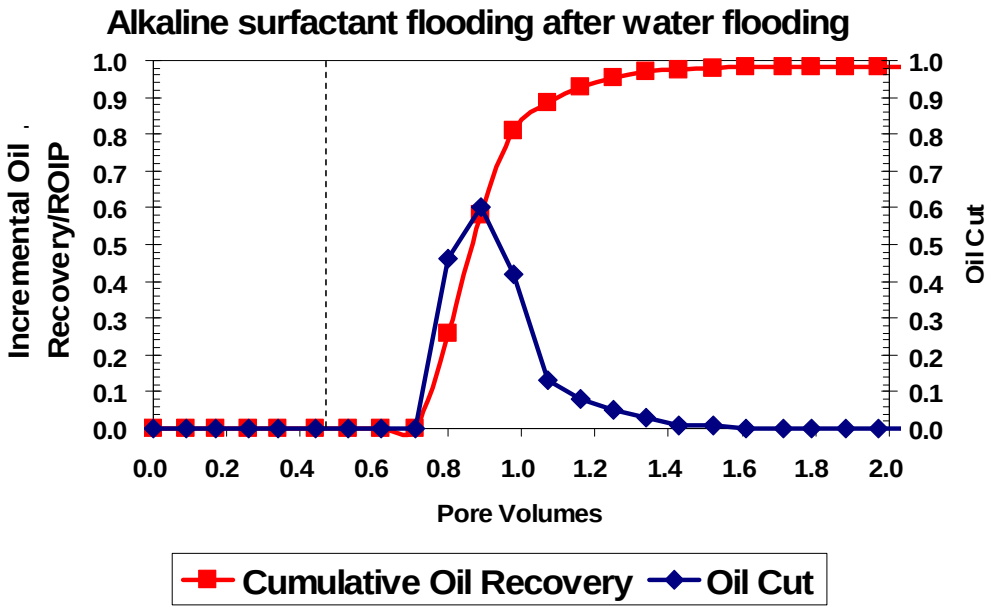

Figure 2.4-4 Oil Recovery of ASP Flooding in Dolomite Sand Pack (ROIP: Residual Oil in place)

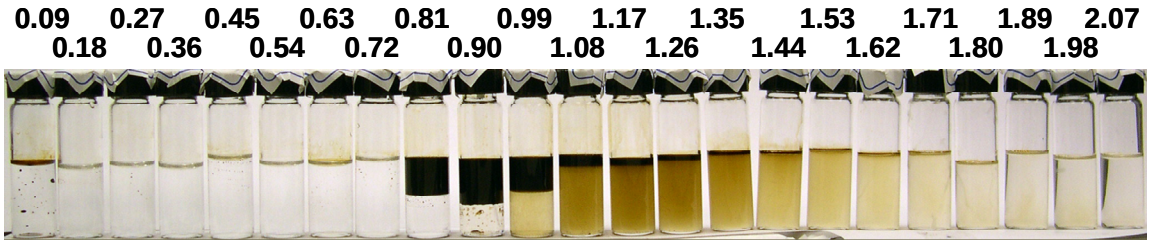

Figure 2.4-5 Effluent of ASP Flooding in Dolomite Sand Pack

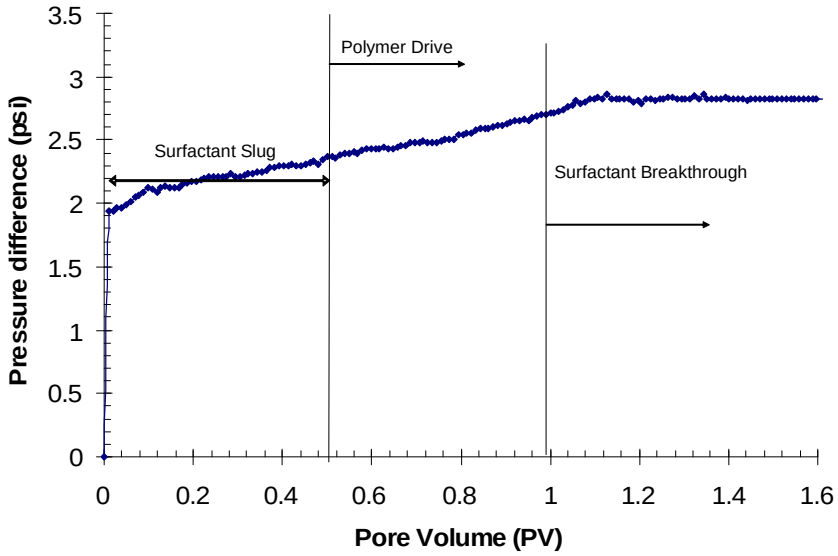

Figure 2.4-6 History of pressure drop for dolomite pack

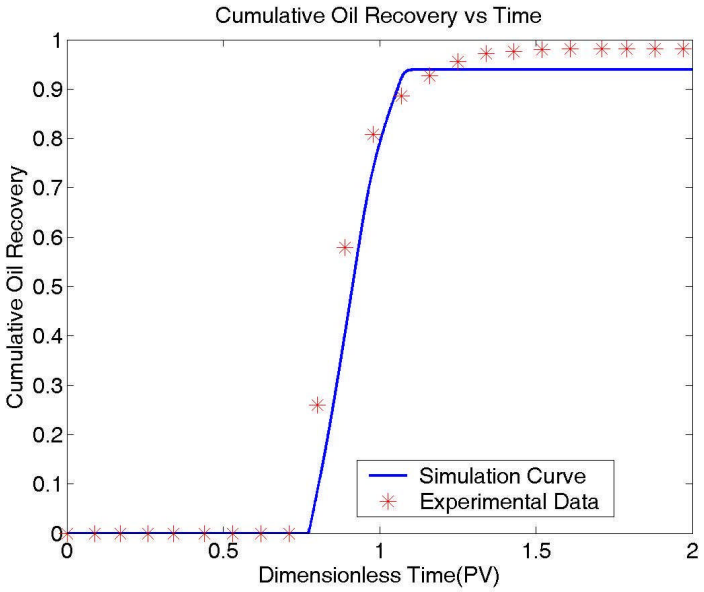

Figure 2.4-7 Comparison between simulation and experiments for dolomite pack

2.4.2 Silica sand pack

An Alkaline-surfactant-polymer (ASP) flooding experiment was performed in a silica sand pack. The sand pack's permeability was 40 darcy and the waterflooding remaining oil saturation was 0.25. The operation parameters in this experimental were the same as in the previous experiment except that the surfactant concentration was 0.5% and the injection solution viscosity was 43 cp at the shear rate of 66 sec^{-1}. The photos in figure 2.4-8 illustrate how the oil bank forms and propagates in the silica pack. From figure 2.4-9, it took about 1.3 pore volumes to get an incremental recovery of 98% of the remaining oil after waterflooding. The pressure drop history is shown as figure 2.4-10, which is similar to figure 2.4-6.

Figure 2.4-11 also shows that the simulation result matches the experimental results with the exception of the early oil production. The early oil breakthrough in this experiment is because the remaining oil saturation after waterflooding is slightly greater than the residual oil saturation after water flooding.

Figure 2.4-8 Photos of silica sand pack at different injecting pore volumes

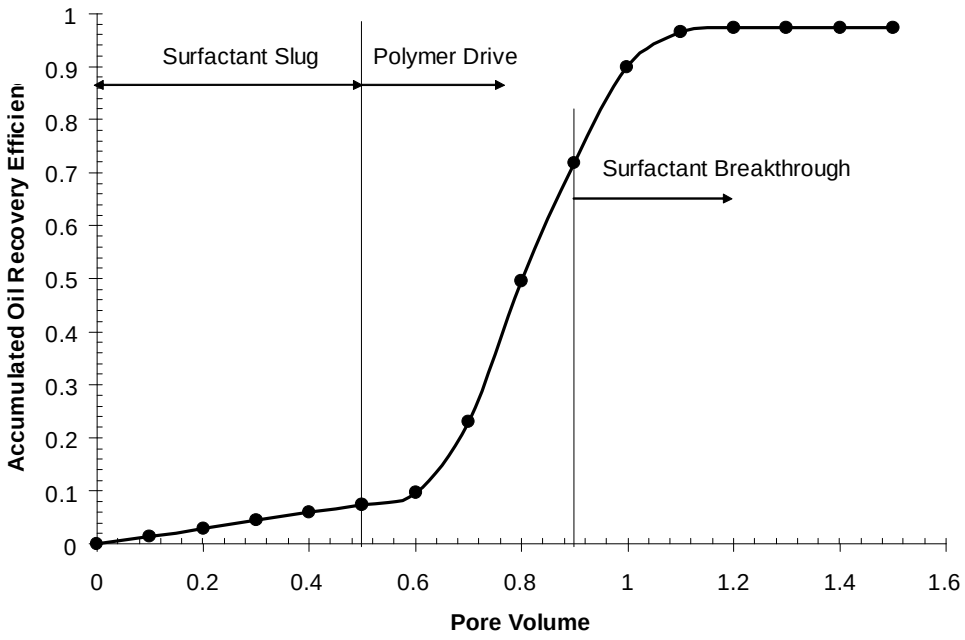

Figure 2.4-9 Oil Recovery of ASP flooding in silica sand pack

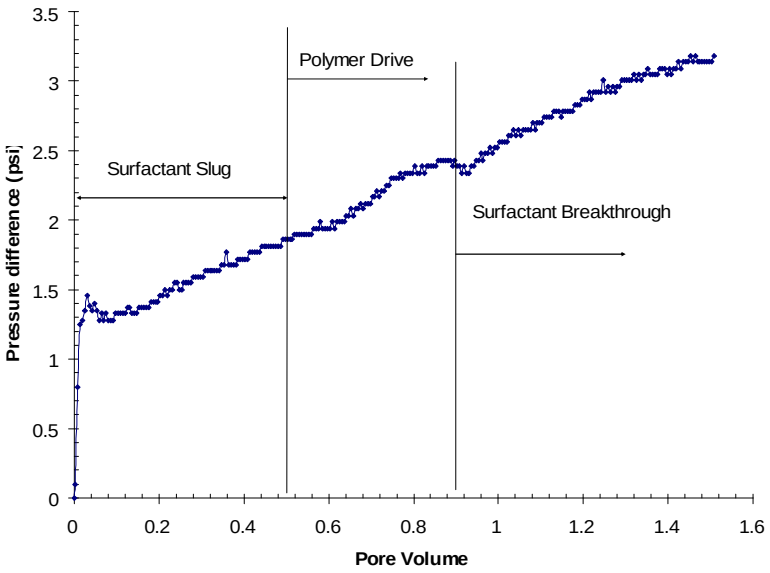

Figure 2.4-10 History of pressure drop for silica pack

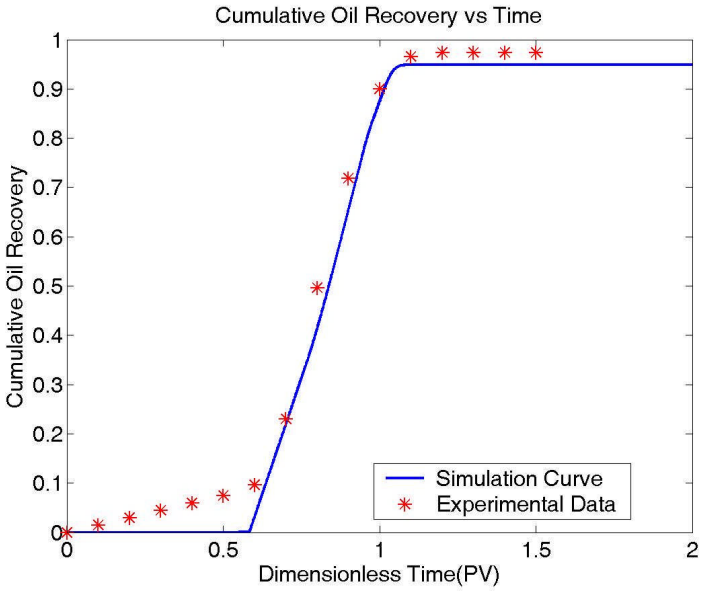

Figure 2.4-11 Comparison between simulation and experiments for silica pack

2.4.3. Polymer/Surfactant phase separation

Before the prior experiment in silica sand, an experiment was done at the same condition as in figure 2.4-8 except the injection salinity was 4.0% NaCl. This was thought to be optimal salinity based on the phase behavior experiments without presence of polymer. Before injection, the ASP solution (4%NaCl) looked a bit turbid while the 2% NaCl ASP solution was clear. After injection, no oil bank was found, as shown in figure 2.4-12. It seems the surfactant is ahead of polymer front. The mobilized oil appears to be behind the surfactant front as if there was lack of mobility control. The pressure history in figure 2.4-13 shows that the pressure drop in this experiment is around 10 times of that in figures 2.4-6 and 2.4-10. This implies that there is a more viscous phase in the experiment of figure 2.4.13 since the flow rates are same in all experiments. After one week settling of the ASP solution, phase separation can be observed, as on the left of figure 2.4-14. There is a separated layer in that sample. The injected solution should be a clear, one-phase system. Otherwise, phase separation may occur during the flooding process. Lower injection salinity would be a good way to avoid the phase separation.

Figure 2.4-12 Photos of silica sand pack at different injecting pore volumes when injecting salinity = 4.0%

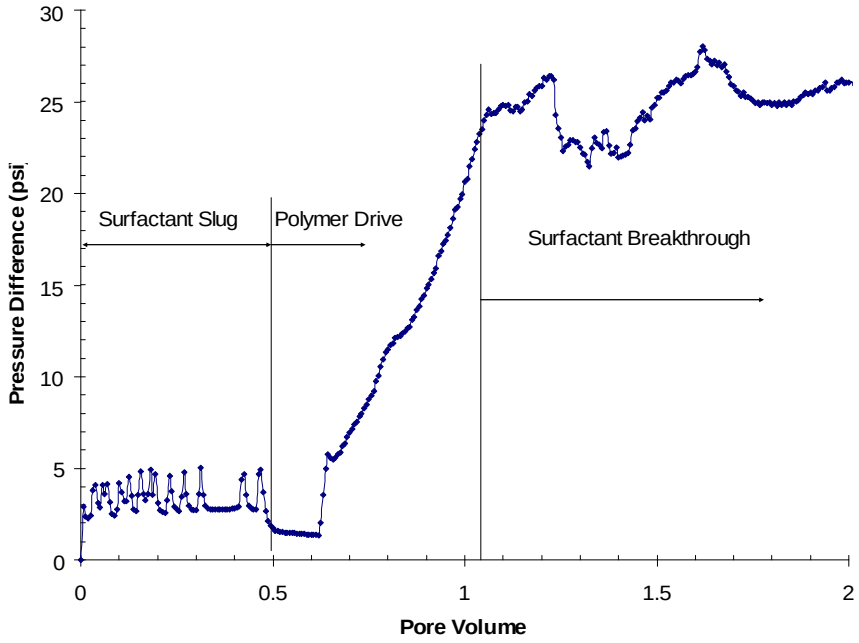

Figure 2.4-13 Pressure difference vs. pore volume when polymer/surfactant separation

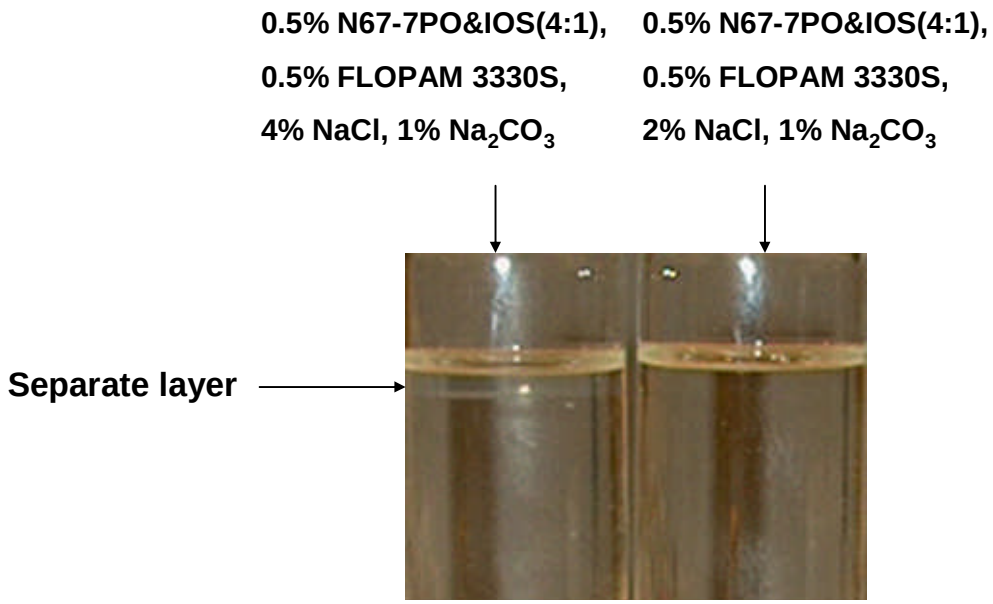

Figure 2.4-14 Phase behaviors of different ASP solutions after one week

Conclusions

1. Experimental results show that the ASP process with only 0.2% surfactant recovers 98% of the oil that is trapped after water-flooding. Good recoveries (>95%) were obtained in both dolomite sand pack and silica sand pack.
2. High salinity causes the phase separation for alkaline surfactant polymer solution. This results in loss of mobility control.
3. The simulation matches the experimental data.

Subtask 2.5 NI blend with other oils (White Castle, Midland Farms)

Crude oils other than Yates, such as White Castle and Midland Farms, were also investigated with the NI blend (4:1 N67:IOS + 1% Na_2CO_3 + x% NaCl). The phase behavior of White Castle is similar to that of the Yates oil. Figure 2.5-1 shows a salinity scan with WOR =3, 40 days settling time. It seems that the optimal salinity is near 0.9% NaCl. Figure 2.5-2 shows the same system with WOR = 9 and with a different settling time. It is found that the sample (2.0%NaCl) forms a middle layer after 40 days settling. From the phase behavior, the optimal salinity is approximately 2.2 % when WOR = 9. Figure 2.5-3 shows the solubilization ratios for the photo (40 days settling) on the right of figure 2.5-2. This plot confirms that the optimal salinity is 2.2%.

According to the literature (SPE 24117), the acid number of White Castle crude oil is 1.5 mg KOH/gram oil. The soap amount of the system can be calculated with this number, as can the soap/surfactant ratio. The black curve in figure 2.5-4 is the optimal salinity vs soap/surfactant ratio curve for Yates crude oil (MY4) as discussed in the previous annual report. Figure 2.5-4 indicates that the White Castle oil follows the same curve when the soap/surfactant ratio has values near or greater than unity.

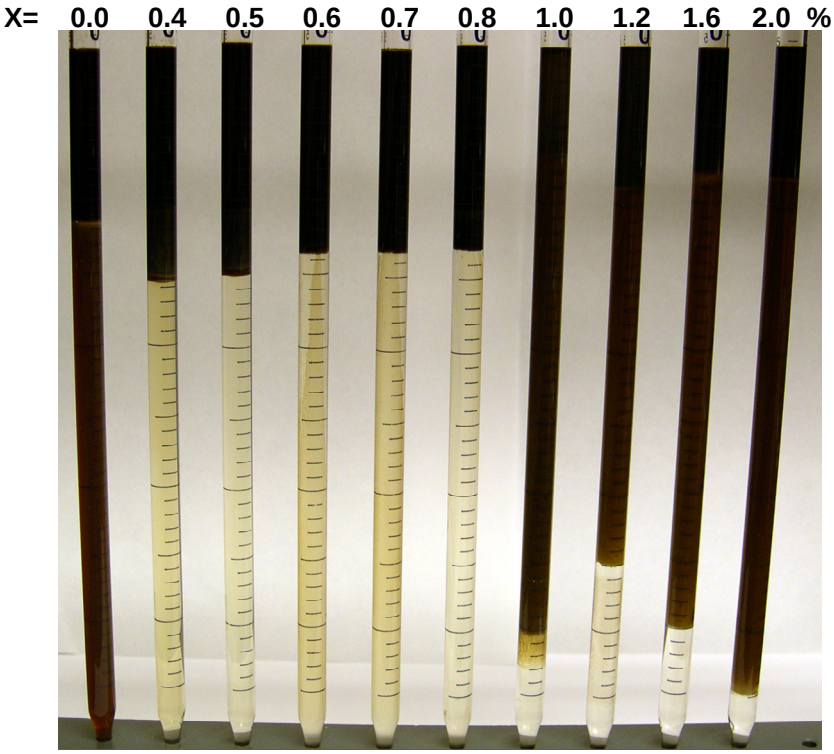

Figure 2.5-1 Phase behavior of White Castle with 0.2% NI / 1% Na_2CO_3 / x% NaCl, WOR=3:1, 24 hours mixing, 40 days settling

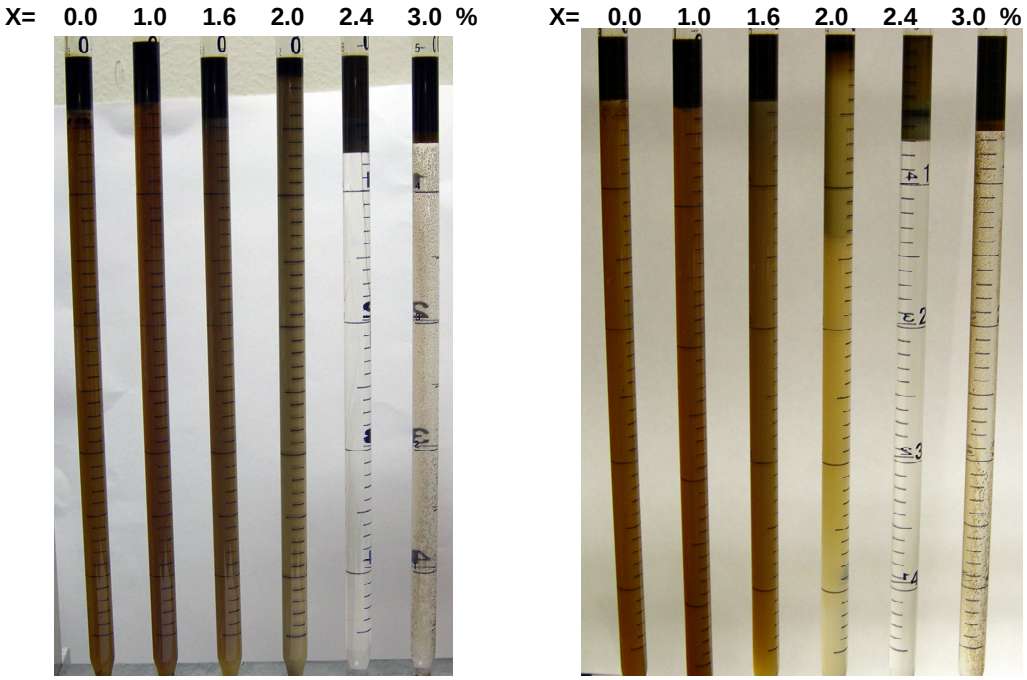

Figure 2.5-2 Phase behavior of White Castle with 0.2% NI / 1% Na_2CO_3 / x% NaCl, WOR=9:1, 24 hours mixing at different settling time.

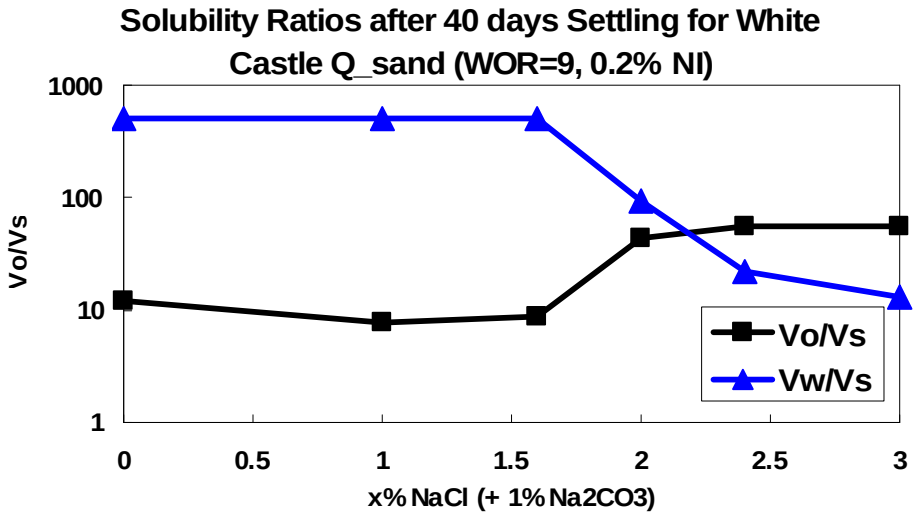

Figure 2.5-3 Solubility ratios for salinity scan of the 40 days settling sample in Figure 2.5-2

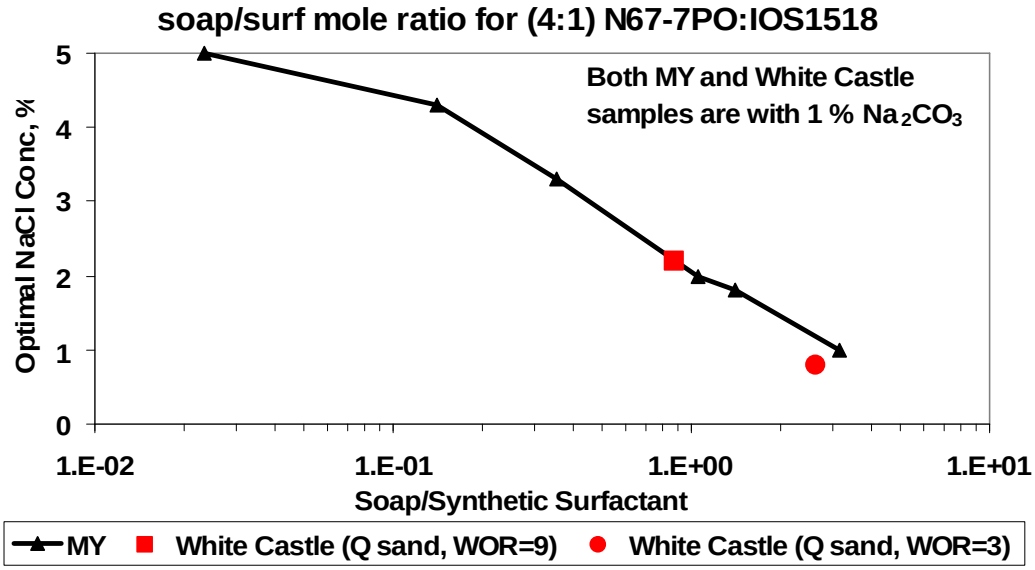

Figure 2.5-4 Optimal Salinity vs soap/synthetic surfactant ratio for Yates (MY4) and White Castle (Q_sand)

Midland Farms crude oil was also tested. In the previous report, this oil was tested by using the same NI blend with high surfactant concentrations. The lowest surfactant concentration was 1%. In the following phase behavior samples, the surfactant concentration is only 0.2%. Figure 2.5-5 compares the phase behavior of Midland Farms oil without Na_2CO_3 and with 1% Na_2CO_3. Figure 2.5-6 shows the solubilization ratios of the series without Na_2CO_3. Figure 2.5-7 shows the solubilization ratios of the series with 1% Na_2CO_3. The phase behavior and solubilization ratio plots indicate that the optimal salinity without Na_2CO_3 is approximately 4.4% and the optimal salinity with 1% Na_2CO_3 is approximately 3.2 %. In the previous annual report and paper SPE100089, the optimal salinities without Na_2CO_3 and with 1% Na_2CO_3 by using 1% NI surfactant are 4.2% and 3.3% respectively. Also at the optimal condition, the solubilization ratios are nearly the same with different surfactant concentrations. In the previous report, the solubility ratios of 1% NI blend at the optimal conditions are around 10 to 15, which are close to those obtained with 0.2% NI blend.

The IFT of 0.2% NI blend/1% Na_2CO_3/3.2% NaCl, WOR=3 was measured by following the procedure discussed in Subtask 2.2. The dynamic IFT curve is shown as figure 2.5-8, and equilibrium IFT is $4.8*10^{-3}$ mN/m. The solubilization ratio at this condition is around 13. According the Chun-Huh correlation, the equilibrium IFT should be $2*10^{-3}$ dyne/cm, in reasonable agreement. That is, ultra-low tension can be achieved for Midland Farms oil by using only 0.2% NI Blend, and the IFT can be predicted by using Chun-Huh correlation.

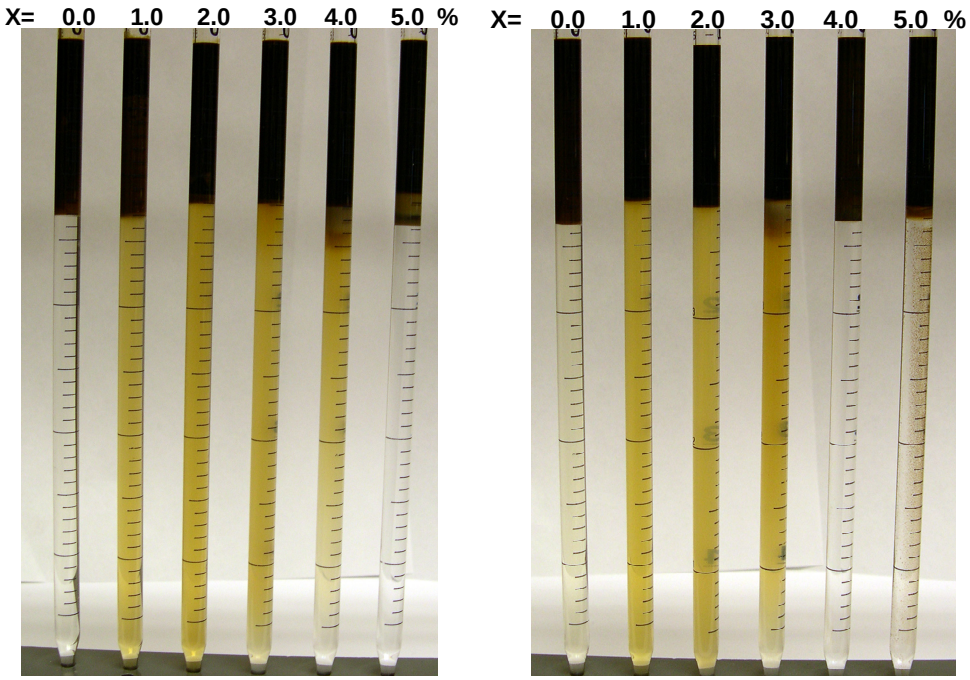

Figure 2.5-5 Phase behaviors of Midland Farm with 0.2% NI blend / x% NaCl, WOR=3:1, 24 hours mixing, 40 days settling

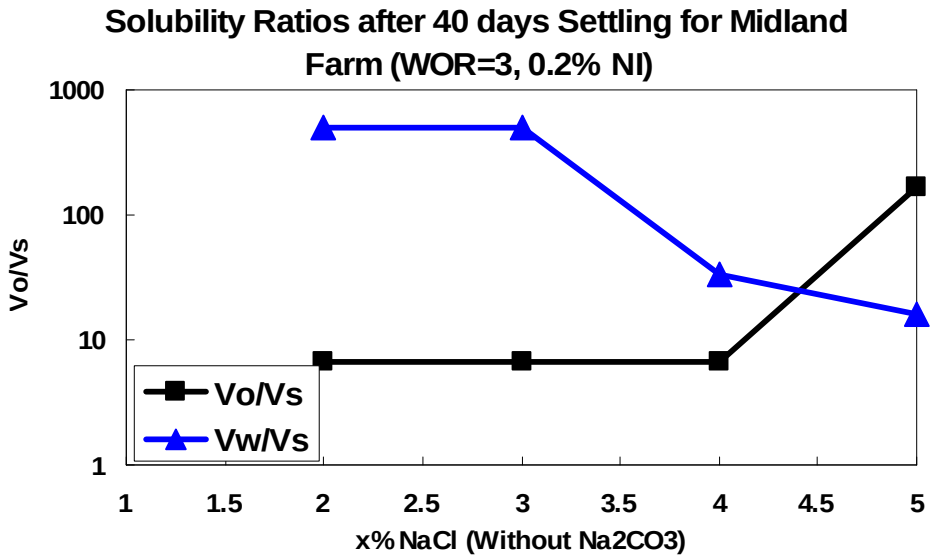

Figure 2.5-6 Solubility ratios for salinity scan of 0.2% NI / 0% Na_2CO_3 / x% NaCl

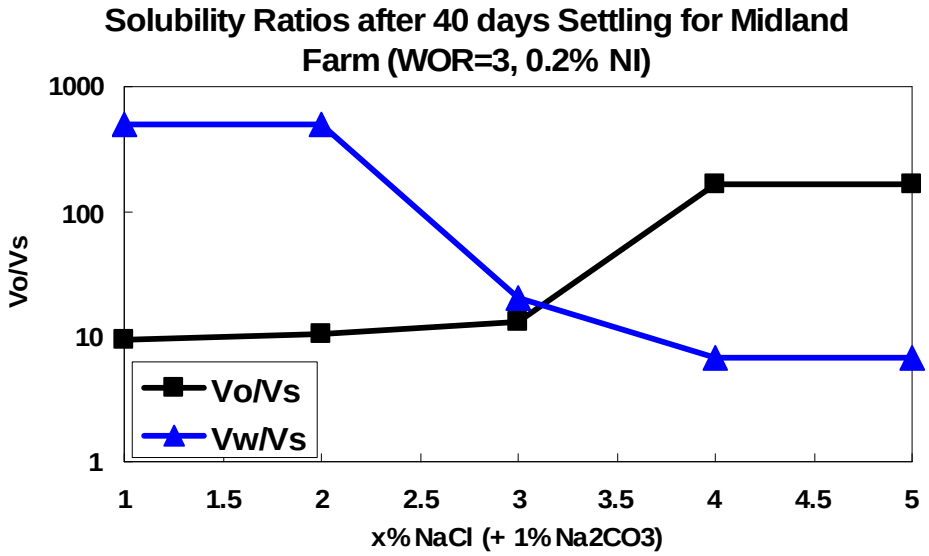

Figure 2.5-7 Solubility ratios for salinity scan of 0.2% NI / 1% Na_2CO_3 / x% NaCl

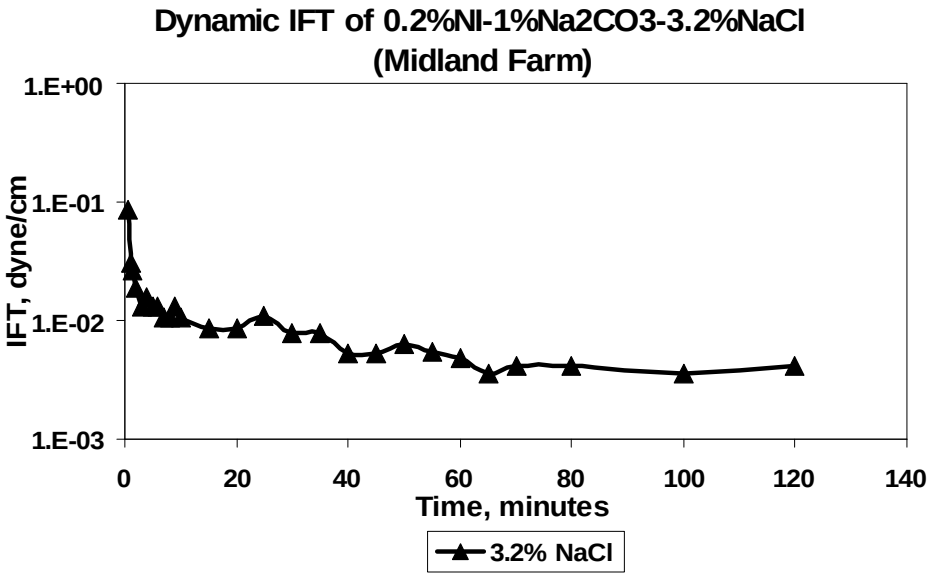

Figure 2.5-8 IFT of 0.2% NI /1% Na_2CO_3/3.2%NaCl /Midland Farm as a function of time

Conclusions

1. For White Castle oil, the change of optimal salinity with soap/surfactant ratio follows the optimal salinity/ratio curve of Yates oil for soap/surfactant ratios near or greater than unity.
2. For Midland Farms oil, surfactant concentration does not influence optimal salinity even when alkali is present, which indicates that this oil contains very little acid. Changing surfactant concentration does not change the solubilization ratio significantly.
3. Ultra-low tension can be achieved by using only 0.2% NI blend for Midland Farms oil. The IFT can be predicted by using the Chun-Huh correlation.

Task 3 Foam for Mobility Control

Subtask 3.1 Bulk foam in fractures

In our previous work, we found the factors that can affect foam apparent viscosity in fractures when the foam bubble diameter is larger than the fracture aperture. Two mechanisms – liquid between bubbles and bubble deformation -- were found to contribute to the foam apparent viscosity in this case. Predictions of a theory modeling these two mechanisms fit experimental data. But when the foam bubble diameter is significantly less than the aperture, bulk foam exists throughout the fracture. Further experiments were performed and a different model used for this case as discussed below.

Experimental technique

The fracture model shown in Fig. 3.1-1 has been described in previous reports. It mainly consists of two parallel plates. Changing the gasket thickness between the plates can change the aperture of the fracture. The set-up diagram of the equipment for the foam experiments is shown in Fig. 3.1-2. A Harvard syringe infusion pump (Model 22) is used to inject surfactant solution, and a Matheson mass flow controller (Model 8270) is used to inject air into the foam generator. Relatively uniform size bubbles can be generated only when the air and liquid are introduced on opposite sides of the frit in the foam generator. Choosing frits with different pore size can generate different sizes of bubbles. Two grooves were made along the inlet and outlet of the fracture model to ensure a uniform pressure at the inlet and outlet.

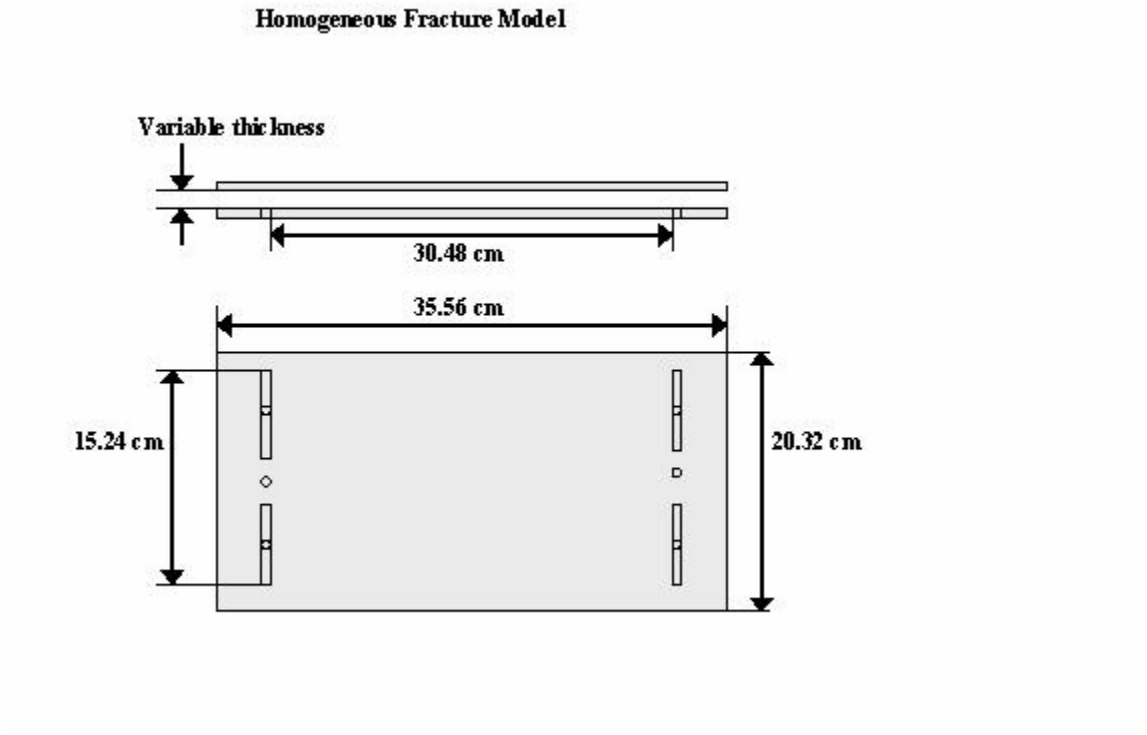

Figure 3.1-1 Detailed fracture model

The surfactant solution in the experiments was 0.5% C13-4PO and 0.5% STEOL CS330. C13-4PO is from Harcros Chemicals and its chemical description is propoxylated C13 alcohol ether sulfate, ammonium salt. STEOL CS330 is from Stepan and its chemical description is C12-3EO sulfate. The salinity was 0.23% NaCl, 0.07% $CaCl_2$ and 0.04% $MgCl_2$. The mean bubble diameters in the experiment were 0.04 and 0.06 mm. The aperture is 0.2 mm or 0.4 mm for homogeneous fracture experiments. The gas fractional flow range was from 0.0 to 0.67. The viscosity and surface tension were 1.0 mPa.s and 28 mN/m, respectively.

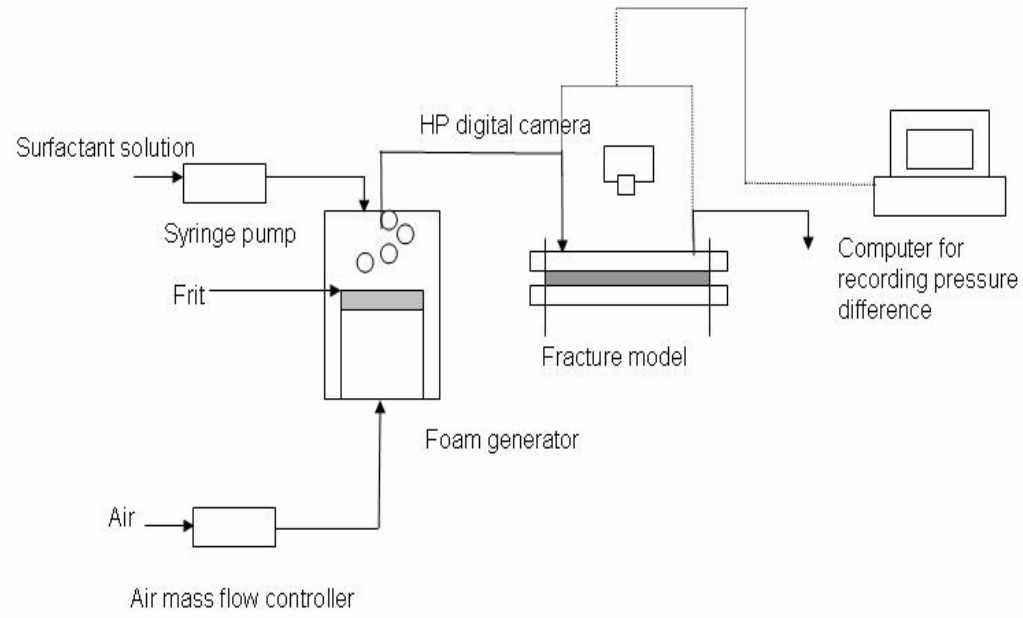

Figure 3.1-2 Diagram for experiment in fracture model

Theory

Princen [1982] developed a theory for rheology of foams and highly concentrated emulsions. Hirasaki and Lawson [1989] developed a theory to describe the apparent viscosity of bulk foam in a capillary tube with plug flow and high gas fraction. But the theory can be applied only to bubbles with the shape of pentagonal dodecahedrons, which are obtained only at quite high gas fractional flow when all the bubbles in the system are closely-packed.

Many semi-empirical expressions are available for describing the shear viscosity of concentrated dispersions of hard spheres. The most widely used is the functional form suggested by Krieger and Dougherty [1959].

$$\eta_r = (1 - K\phi)^{-2.5/K} \qquad (1)$$

Where η_r is the relative viscosity, which is the ratio of the viscosity of emulsion to the viscosity of water. ϕ is the volume fraction of the dispersed phase of the emulsion. K is the crowding factor and equal to the reciprocal of the dense random packing limit volume fraction $\phi_{\max}$, at which η_r diverges to infinity. For random close packing of monodisperse hard spheres, they found $\phi_{\max}$ = 0.64 and K =1.56.

Mooney [1951] developed another expression for the relative viscosity of emulsions where the particles behave as rigid spheres.

$$\eta_r = \exp[\frac{2.5\phi}{1-K\phi}] \qquad (2)$$

The crowding factor *K* in the above two equations can be smaller when the particles are not uniformly distributed or the particles are deformable because these factors can cause an increase of the dense random packing limit volume fraction.

Pal [1992] studied the rheology of polymer-thickened emulsions and found that the effect of internal circulation within the drops was sometimes important. He suggested the following equation:

$$\eta_r^{1/K_I} = \exp[\frac{2.5\phi}{1-K\phi}] \qquad (3)$$

where K_I is a factor which takes into account internal circulation effects and is given by

$$K_I = [\frac{1+0.4(\eta_c/\eta_d)}{1+(\eta_c/\eta_d)}]$$

In the above equation, η_c is the viscosity of the continuous phase and η_d is the viscosity of the dispersed phase. Pal [1992] also suggested a crowding factor K = 1.04, which means the dense random packing limit volume fraction $\phi_{\max}$ = 0.96.

Results and discussion

The apparent viscosity for bulk foam flow in fractures was measured at different aperture, flow velocity and bubble size as shown in Fig. 3.1-3. The highest gas fractional flow is 0.67 because we found that bubbles began to coalesce for gas fractional flows exceeding 0.67.

The predictions from Krieger and Dougherty equation, Mooney equation and Pal's model are also plotted in Fig. 3.1-3. For the first two equations $\phi_{\max}$ has been increased to 0.99 and K decreased to 1.01 because we deal with deformable bubbles, not hard spheres. Even with this change there are still significant deviations between the predictions and experimental results although agreement is much better than with the corresponding hard sphere values given above. In contrast, the experimental measurements match well the prediction of Pal's model.

Because the viscosity of water is much larger than that of gas, K_I is close to 0.4. We still use 0.96 as the dense random packing limit volume fraction. Then the crowding factor K is 1.04. Because the viscosity of the dispersed phase is small in the foam case, internal circulation doesn't contribute significantly to the viscosity. .

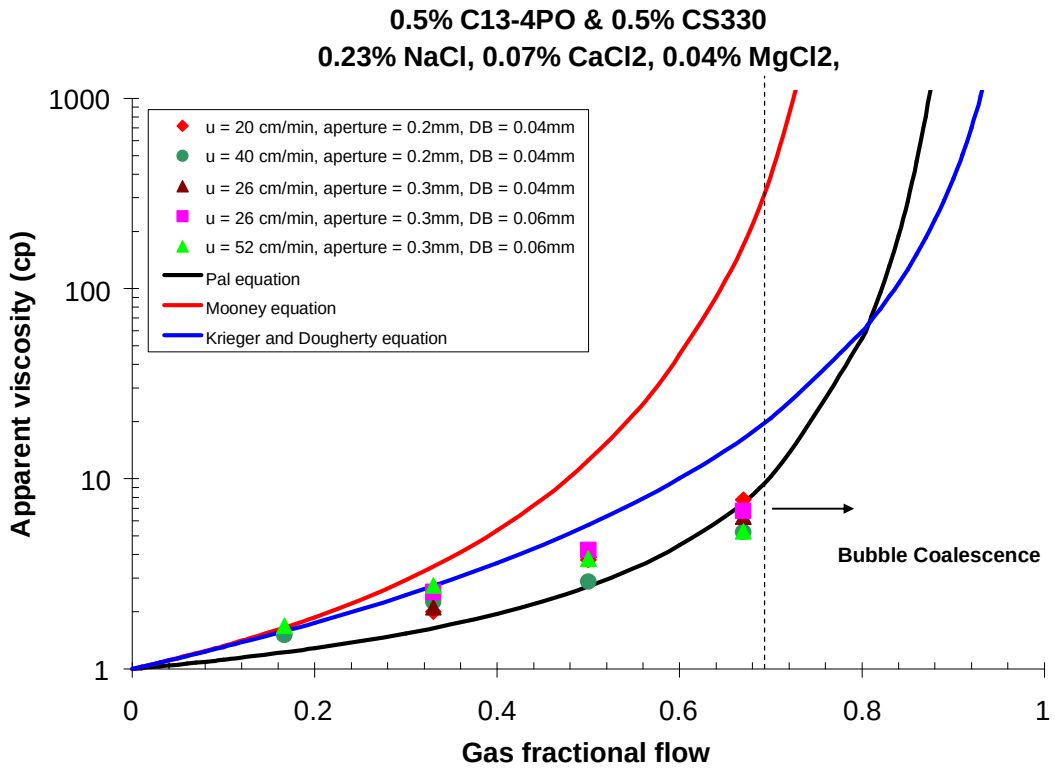

Figure 3.1-3 Bulk foam apparent viscosity in fractures; measurement and prediction. K=1.01 for Mooney and Krieger and Dougherty equations.

Subtask 3.2 Foam Drive for ASP Process

In the alkaline/surfactant/polymer process polymer is used as a mobility control agent to be injected together with surfactant and also as drive. However, polymer is expensive. In this section we discuss experiments to investigate the possibility of using foam to replace polymer as drive.

3.2.1 Displacement of Surfactant Slug with Foam

Initial experiments were performed in a horizontal, one-dimensional, one-foot-long sand pack, which had a permeability of 40 darcies. It was presaturated with a surfactant/polymer solution to simulate a situation where residual oil saturation was zero behind the surfactant/polymer slug. The solution contained 0.5% N67-7POS:IOS15-18 (4:1), 0.5% FLOPAM 3330S, 1% Na_2CO_3 and 2% NaCl. Its viscosity was 43 cp at 24C and a shear rate of 66 s^{-1}.

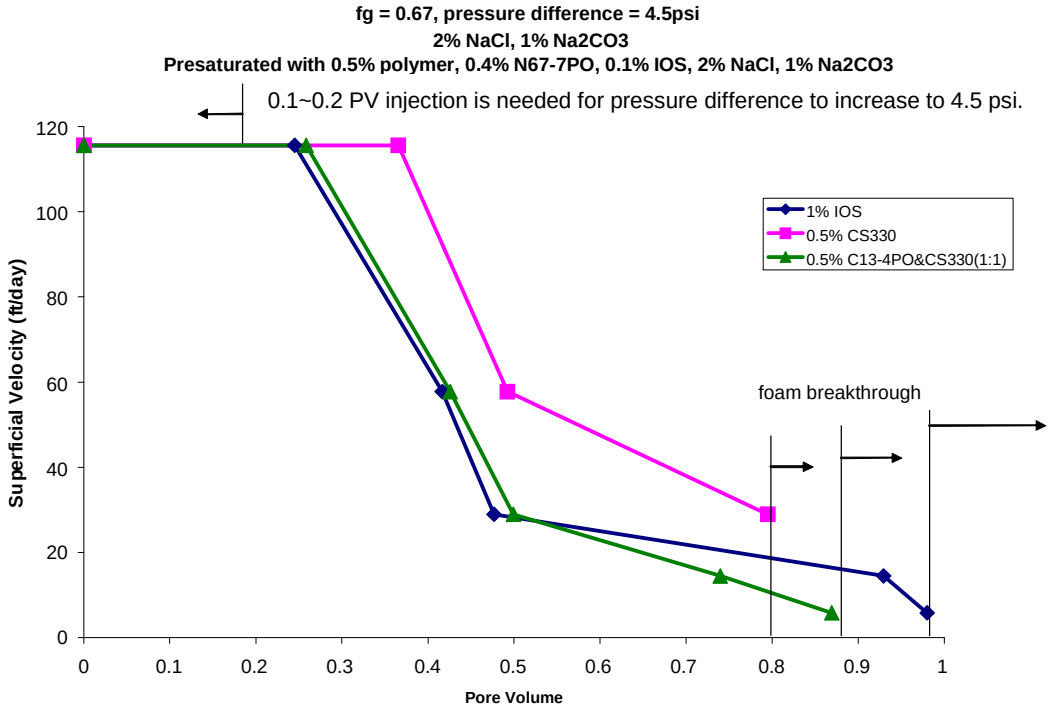

Figure 3.2-1 Foam sweep of the sand pack presaturated with polymer/surfactant

Experiments were carried out at constant pressure drop between 4.0 and 4.5 psi. Foam was generated in the sand pack by co-injection of surfactant solution and air at a gas fractional flow of 0.67. Three different surfactants were used in the drive with the same salinity as in the slug: 1% IOS, 0.5% CS330, and 0.5% C13-4PO:CS330 (1:1). The results are shown in Fig. 3.2-1. Some 0.1-0.2 PV of co-injected fluid was required to raise the pressure drop to 4.0-4.5 psi. Subsequently flow rate was varied as necessary to maintain this pressure drop. The foam produced by IOS, CS330 and the C13-4PO mixture broke through at approximately 1.0 PV, 0.8 PV, and 0.9 PV respectively. The same surfactant blend as in the slug was also tried, but its foam broke through before pressure drop exceeded 1.5 psi. This last result is consistent with

experiments described in the previous annual report showing that this blend is a poor foamer.

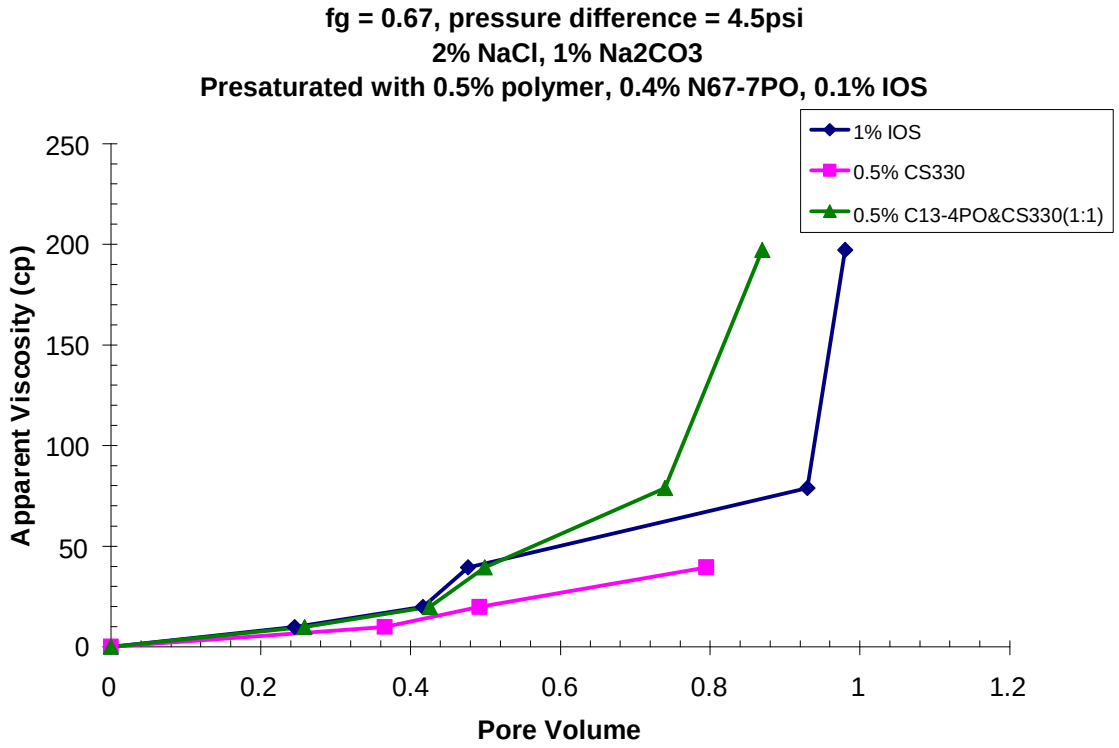

Figure 3.2-2 Apparent viscosity during the sweeping the sand pack presaturated with polymer/surfactant

Fig. 3.2-2 shows the apparent viscosity during sweeping of the sand pack. At the time of foam breakthrough apparent viscosity was about 40 cp for CS330 and 200 cp for the other two surfactants. If we take these values as approximately equal to the apparent viscosities of the respective foams, we find that they are either about the same or greater than slug viscosity, indicating a favorable mobility ratio. However, we did see fingering at the front between the foam and slug. The reason may be that foam at the front was weakened locally by some mixing with the N67-7POS in the slug.

The results of Fig. 3.2-1 show that it is possible to use foam instead of polymer as drive in the ASP process. Although the cost of surfactant is comparable to that of foam at the same concentration, lower surfactant concentrations than used here may be possible. Moreover, a substantial portion of the drive fluid in foam is gas in the bubbles.

3.2.2 ASP Flood Using Foam in Drive

To continue to investigate the possibility of using foam to replace polymer as drive in ASP process, we did an experiment which involved crude oil. The experiment was performed in a one-dimensional silica sand pack in vertical orientation. The sand pack was 1 foot long with a permeability of 40 darcies. The procedure for the experiment was:

1. Fill the sand pack with CO_2;
2. Fill the sand pack with water;

3. Displace water with crude oil;
4. Use brine to flood the sand pack at 10 ft/day superficial velocity until no oil comes out, the residual saturation after brine flooding was 25% from material balance calculation.;
5. Inject alkaline/NI blend/polymer solution into sand pack to displace oil for 0.5 PV at superficial velocity 5 ft/day;
6. Inject IOS/polymer solution as drive for 0.2 PV at superficial velocity 5 ft/day;
7. Co-inject IOS solution and air into sand pack as drive at gas fractional flow 0.67 and superficial velocity 20 ft/day.

The slug composition was the same as in the preceding section. The crude oil was MY-4 with a viscosity of 19cp. The surfactant/polymer solution in step 6 was 0.5% IOS and 0.5% polymer at 2% NaCl. Its viscosity is 46.1cp from measurement. The reason that we included step 6 was that we wanted to construct a barrier between the NI blend of the slug and the IOS in the foam drive because N67-7POS can weaken the foam as indicated above. The co-injection of air and surfactant solution was at gas fractional flow 0.67. The surfactant solution in step 7 was 0.5% IOS at 2% NaCl and 1% Na_2CO_3.

Photographs of the displacement are shown in Fig. 3.2-3. They show that the oil bank is pretty clear, but there was a tail after the oil bank. The reason may be that the injected crude oil for this experiment (but not for others) contained some viscous emulsion. But we can see that the shape of the tail didn't change after the foam drive began. This shows the foam drive moves by plug flow in the sand pack. From Fig. 3.2-4, at around 1.5 PV, almost all the residual oil was recovered. The effect of the tail can also be found from the effluents shown in Fig. 3.2-5.

Fig. 3.2-6 shows the pressure history during the experiment. The first 0.7 PV is alkaline/surfactant/polymer slug and polymer drive injection. The pressure difference during this time period gradually increases. When the air/surfactant co-injection begins, the pressure difference decreases first, then increases up to around 3 psi and remains there. This behavior shows that foam that forms has fairly uniform properties .

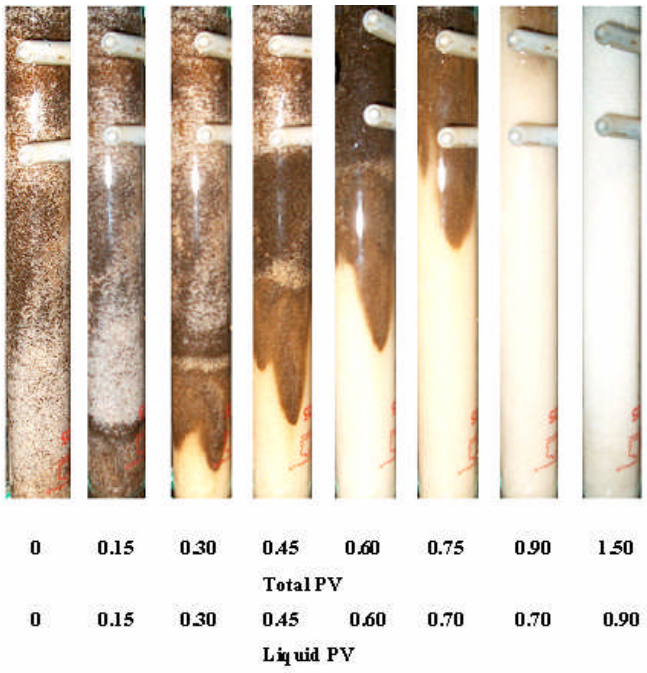

Fig. 3.2-3. Photos showing behavior during ASP flood with foam drive

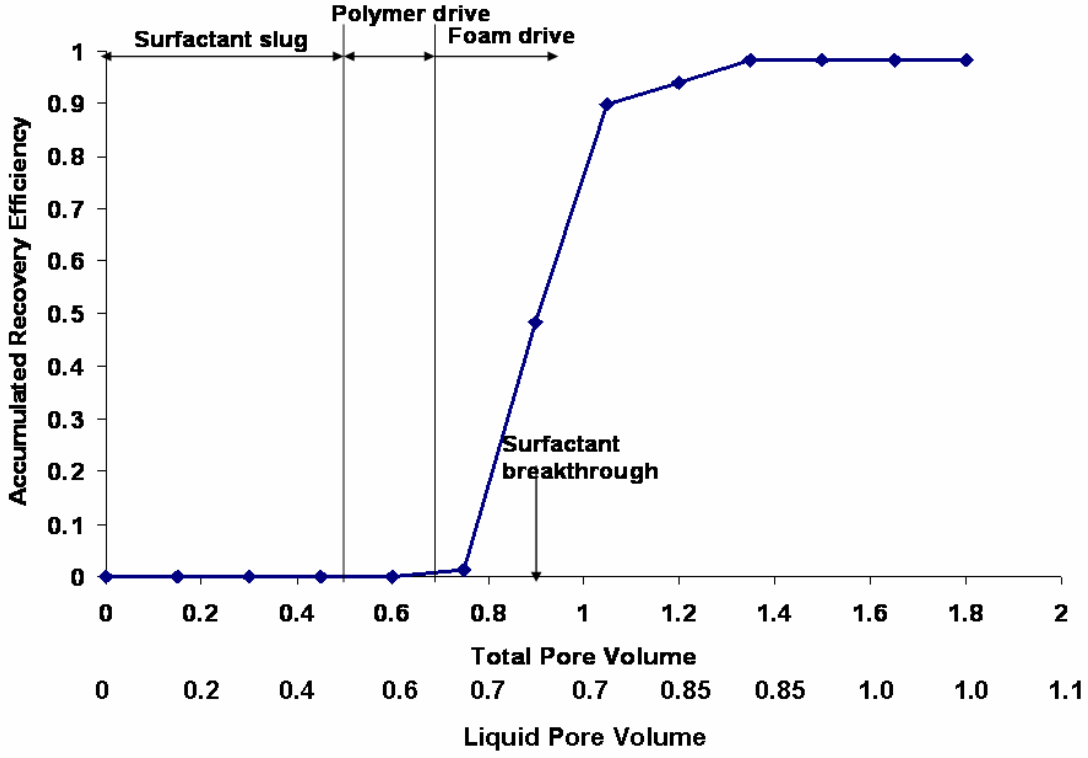

Fig. 3.2-4. Recovery history for foam drive experiment

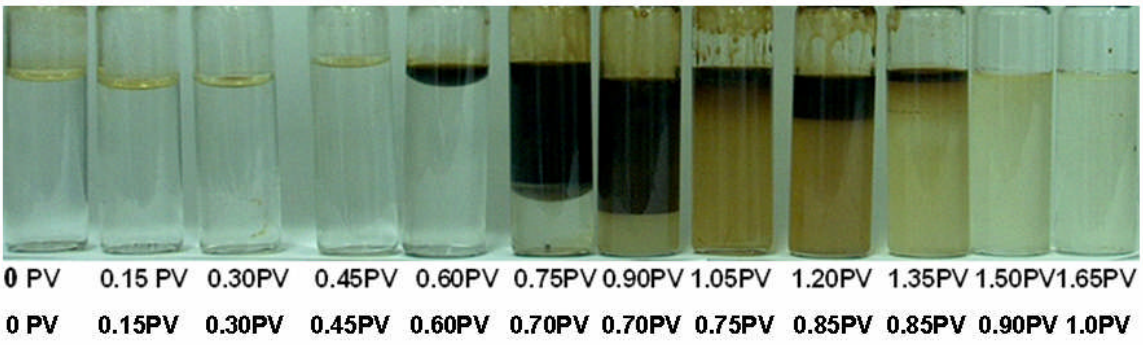

Fig. 3.2-5. Effluent history for foam drive experiment

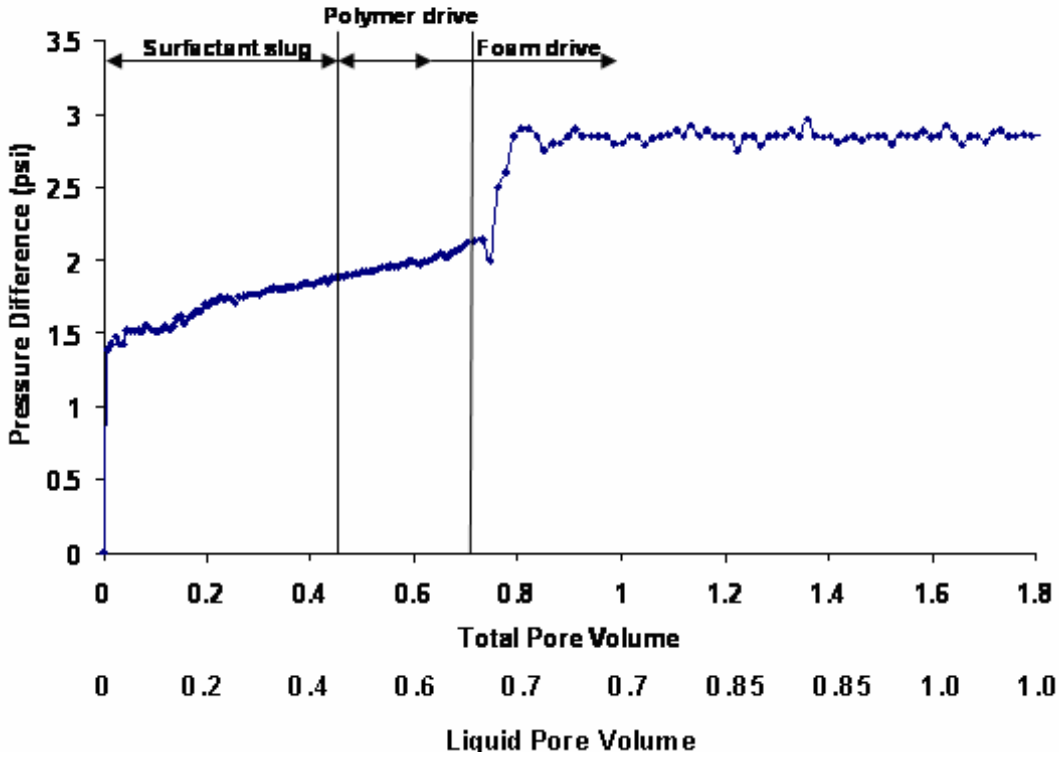

Fig. 3.2-6. Pressure history for foam drive experiment

Another experiment was performed for two reasons: first to test the reproducibility of the above results, second to improve process cost effectiveness by using less surfactant slug and lower IOS concentrations in the buffer solution and drive. Hence, the second experiment used only 0.3 PV of the same surfactant slug followed by 0.2 PV IOS/polymer solution containing only 0.2% IOS and 2% NaCl. The polymer concentration in both surfactant slug and polymer drive was 0.5%, which provides 47 cp viscosity. The foam was generated by alternating injection of air and 0.2% IOS at 2% NaCl at the volume ratio of 2:1. The superficial velocity for the injection of surfactant slug and polymer drive was 5 ft/day. Air was injected at 20 ft/day, and surfactant solution was injected at 10 ft/day.

From the pictures in Fig 3.2-7 showing the behavior during the flood, the oil bank is not as sharp as in Fig. 3.2-3. The reason may be that the surfactant slug is small, and the oil recovered in the oil bank is less than in the previous experiments with 0.5 PV surfactant slugs (see Fig. 3.2-8). From Fig. 3.2-9, which shows the pressure history, the pressure difference increased after air injection began, then leveled off, confirming that foam was formed.

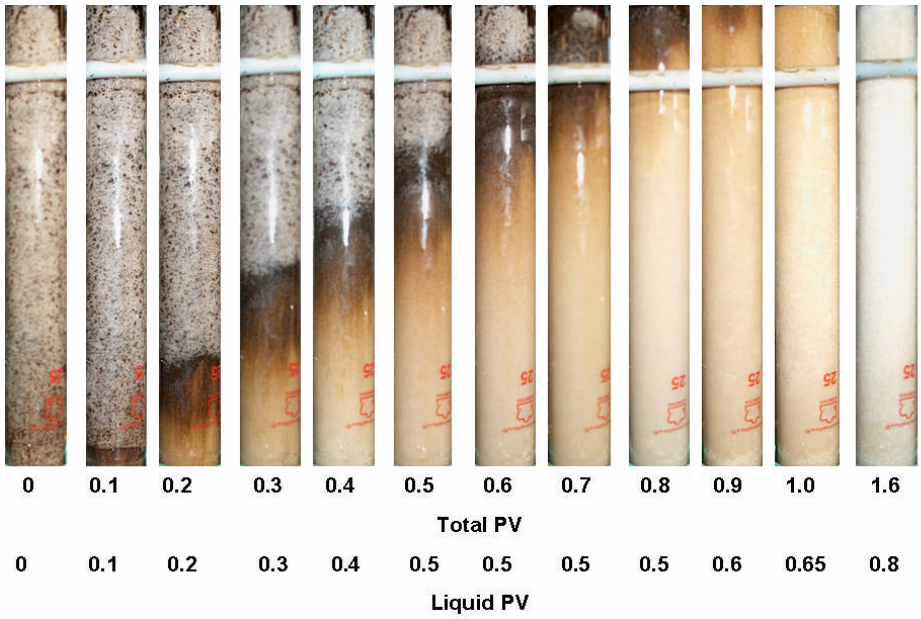

Fig. 3.2-7. Photos showing behavior during experiment with smaller slug and lower IOS concentration.

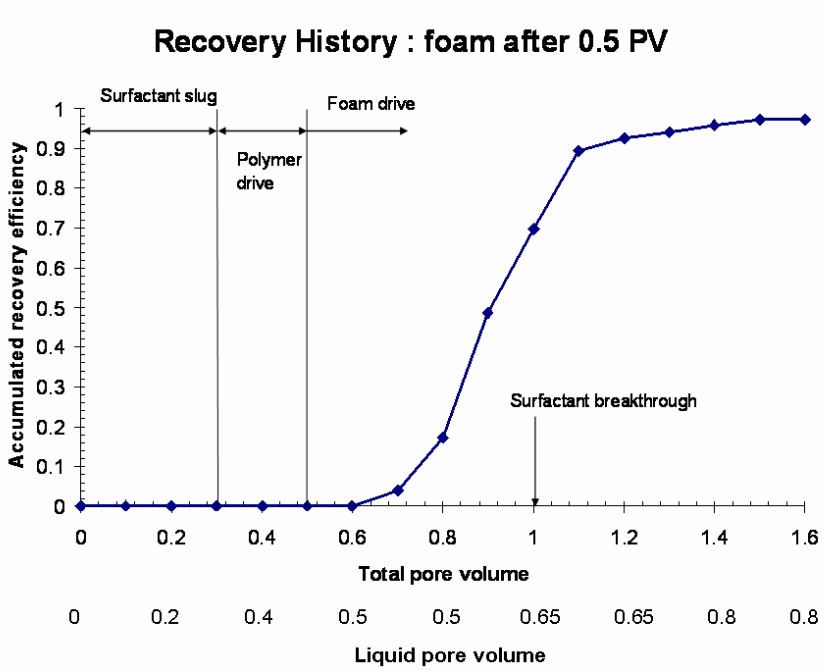

Fig. 3.2-8. Recovery history for the experiment of Fig. 3.2-7.

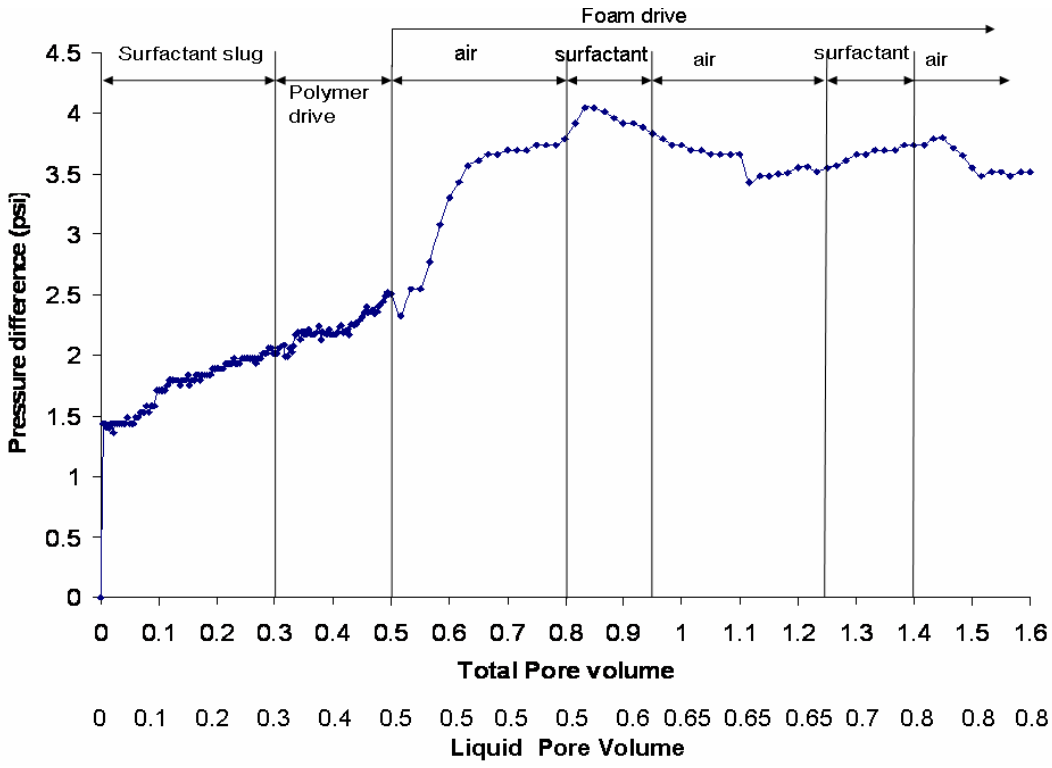

Fig. 3.2-9. Pressure history for the experiment of Fig. 3.2-7.

The above two experiments give similar results: the recovery efficiency is above 90%, more than 70% of recovered oil is clean oil, and all the oil is recovered within 1.6

total pore volume and most within 1.1 total pore volume. The differences between the two experiments are that the surfactant slug in the second experiment is 0.3 PV, which is 0.2 PV less than in the first experiment, and the foam in the second experiment is generated by surfactant/air alternate injection while in the first the foam is generated by co-injection of surfactant solution and air. The 0.3 PV surfactant slug is enough to recover the waterflood residual oil. The pressure difference during the foam injection increases up to 2 times of that during surfactant slug and polymer slug injection, which shows that foam apparent viscosity is somewhat greater than the viscosity of the polymer drive.

3.2.3 Formation of Foam During Slug Injection: the ASPF Process

Although the experiments of 3.2.2 show that it is possible to use foam drive instead of polymer drive, the unique advantage of foam is not fully utilized if foam is used only as drive. The reason is that the entire alkaline /surfactant slug is injected before the foam drive begins with the result that foam has no effect on slug distribution among layers. The foam has higher apparent viscosity in the high permeability layers, so foam with slug injection should be able to divert more of the slug into low permeability layers. Then foam can work best in the heterogeneous system to get higher oil recovery by increasing the sweep efficiency. We did two experiments to test the foam strength in two sand packs with different permeability. As indicated above, NI blend is a weak foamer. However, the surfactant slug, which also contains polymer, may generate stronger foam than the surfactant solution alone.

Experiments to investigate crude oil displacement with foam in both the surfactant slug and the drive, the ASPF process, were performed in a one-dimensional vertical sand pack as before. The procedure for doing the experiment was:

1. Fill the sand pack with CO_2.
2. Fill the sand pack with brine at 2% NaCl.
3. Flood the sand pack with MY-6 crude oil at 10 ft/day.
4. Use brine (2% NaCl) to flood the sand pack at 10 ft/day until no oil comes out.
5. Alternate the injection at 20 ft/day into the sand pack of 0.2% NI blend with 0.5% polymer at 1% Na_2CO_3 and 2% NaCl for 0.1 PV, and air for 0.1 PV. Altogether 0.6 PV of NI/polymer and air is injected.
6. Alternate the injection into the sand pack of 0.2% IOS at 1% Na_2CO_3 and 2% NaCl for 0.1 PV, and air for 0.1 PV. The superficial velocity is 20 ft/day.

3.2.3.1. 40 darcy sand pack

Photographs taken during the experiment are shown in Fig 3.2-10. The sand pack had 25% residual oil saturation after water flooding. The cumulative recovery efficiency for the flooding is shown in Fig 3.2-11, and the pressure history is shown in Fig 3.2-12.

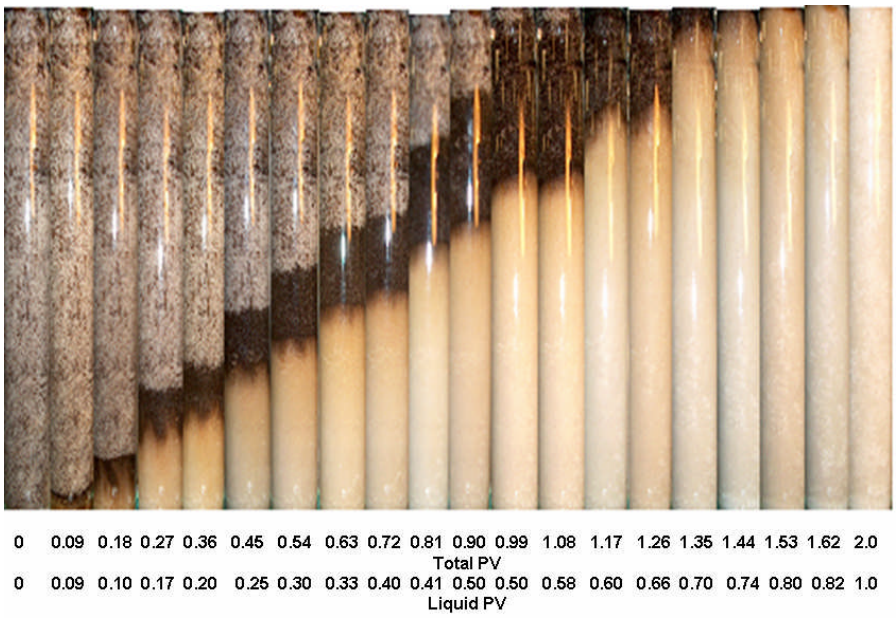

Fig. 3.2-10 Displacement of residual crude oil by ASPF process in 40 darcy sand pack

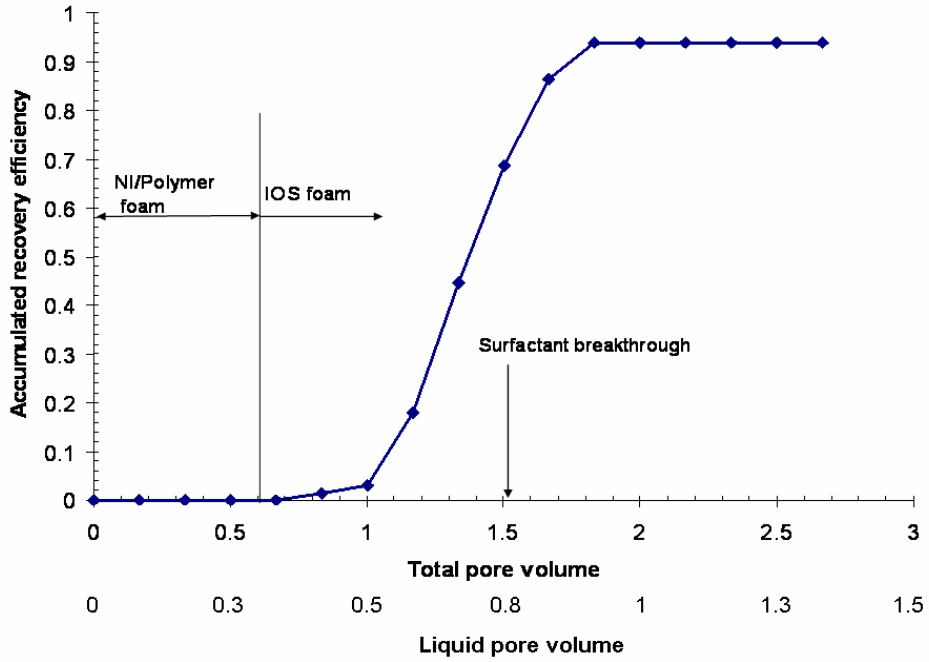

Fig. 3.2-11 Recovery efficiency for ASPF process in 40 darcy sand pack

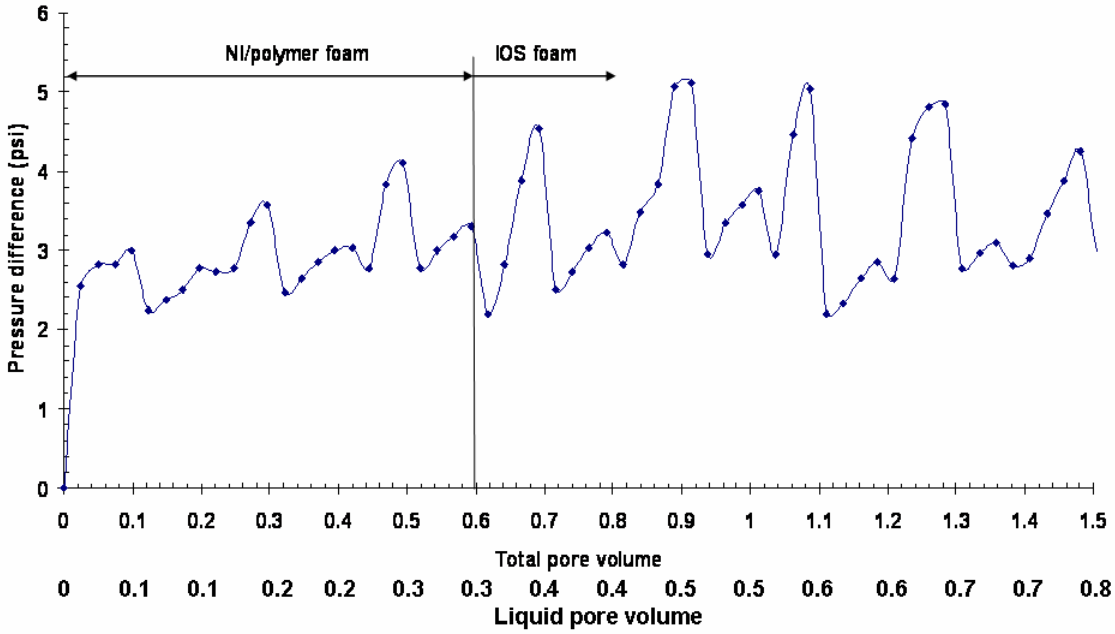

Fig. 3.2-12 Pressure history for ASPF process in 40 darcy sand pack

In all 94% of the residual crude oil was recovered by the ASPF process. Most of the crude oil was recovered between 1 and 1.6 total PV. The pressure differences for the foam from the slug for the first 0.6 total PV and from the subsequent IOS solution in the drive are close, which means that the apparent viscosities of NI/polymer foam and IOS foam are close. In experiments where foam displaces water, the NI/polymer foam has an apparent viscosity of 44 cp -- well above that for the surfactant alone -- while that of the IOS foam is 81 cp. But in the ASPF process, the IOS foam will contact some N67-7POS and perhaps a little crude oil left after oil displacement by the slug, which may decrease the strength of the IOS foam. During the experiment, air (not bubbles) breaks through at about 0.9 PV. The reason for early air breakthrough is that some air gets into the oil bank and perhaps even slightly ahead of it.

3.2.3.2 200 darcy sand pack

A similar ASPF flooding experiment was performed in a sand pack having a permeability of 200 darcies. Figures 3.2-13 – 3.2-15 show photographs of the progress of the flood, cumulative oil recovery, and pressure drop during the experiment.

The residual oil saturation after water flooding is 30% in this case. Approximately 96% of this residual crude was recovered. The oil breakthrough occurs near 0.8 PV, which is earlier than 1.0 PV in the 40-darcy sand pack. The reason is that the mobility ratio between the foam and the oil bank is smaller in the 200-darcy sand pack. The NI/polymer foam exhibits an apparent viscosity of 215 cp in the 200-darcy sand pack at 20 ft/day in an experiment where foam displaces brine. The apparent viscosity of IOS foam in the 200-darcy sand pack is about the same because it exhibited the same pressure difference (Fig. 3.2-15). Air breaks through at around 0.7 PV, which is earlier

than in the 40-darcy sand pack. Here too air gets into the oil bank and even some distance ahead of oil bank. Because the oil bank breaks through earlier in the 200-darcy sand pack, the air also breaks through earlier.

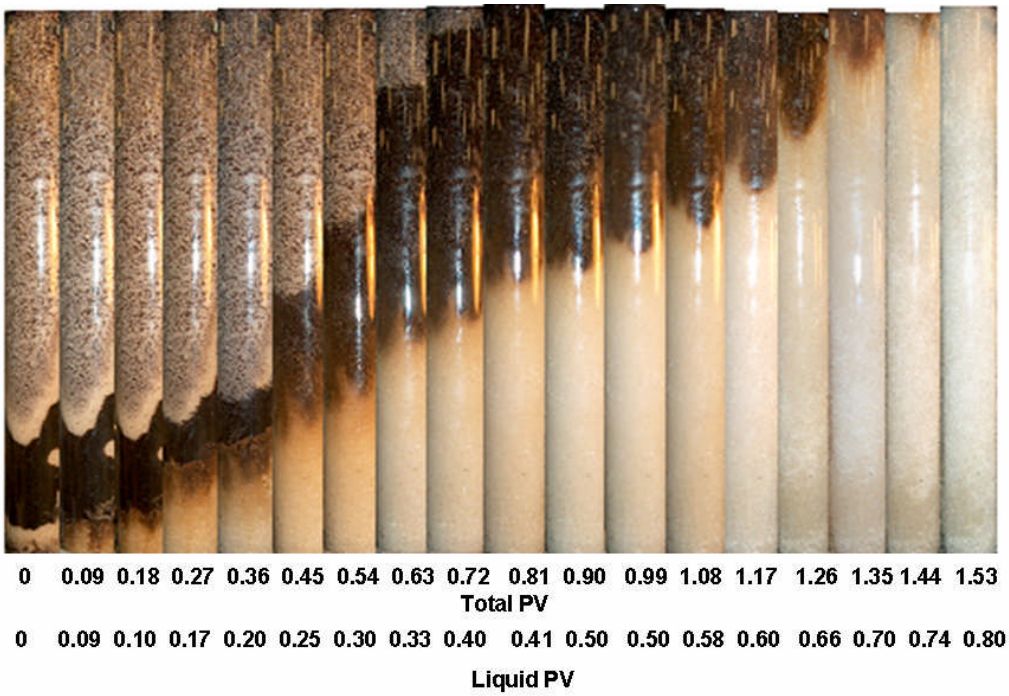

Fig. 3.2-13 Displacement of residual crude oil by ASPF process in 200 darcy sand pack

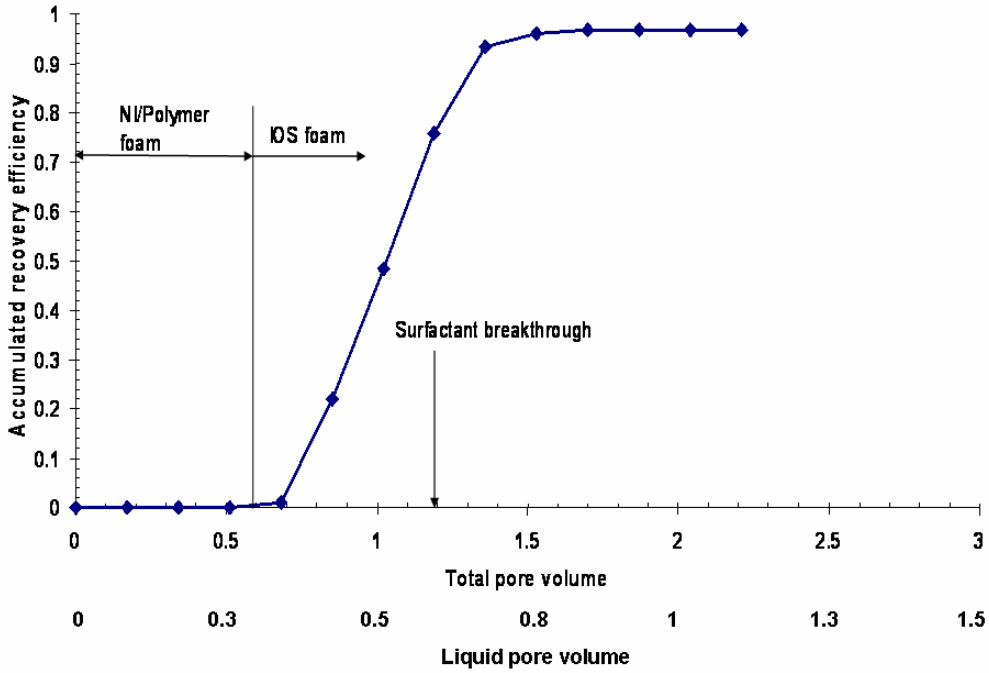

Fig. 3.2-14 Recovery efficiency for ASPF process in 200 darcy sand pack

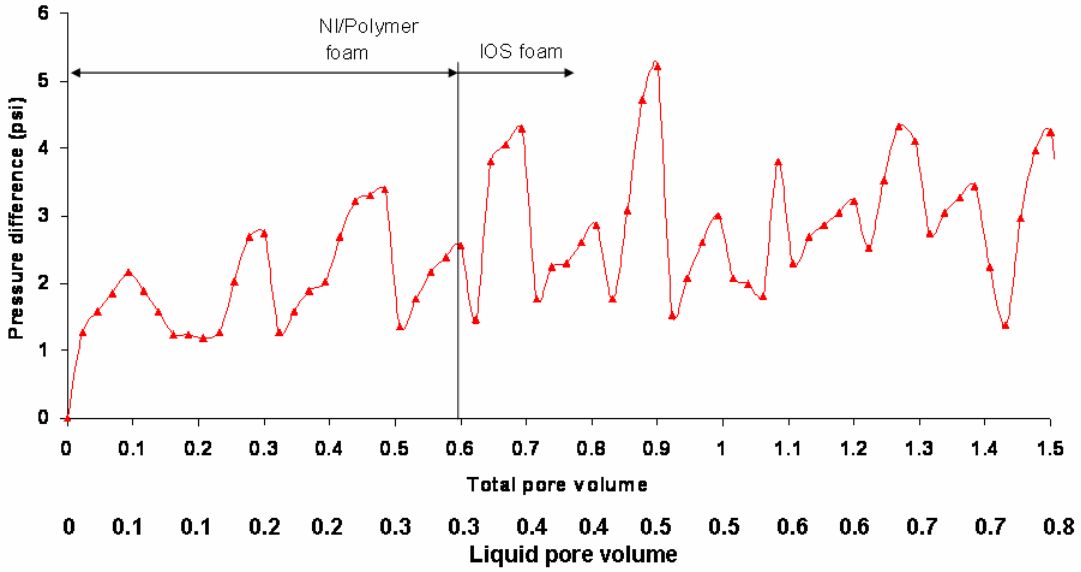

Fig. 3.2-15 Pressure history for ASPF process in 200 darcy sand pack

3.2.3.3 Comparison between the foam flooding in 40 darcy and 200 darcy sand packs

Fig. 3.2-16 shows overall apparent viscosity as a function of PV fluid injected during ASPF flooding in the 40-darcy and 200-darcy sand packs. The apparent viscosity in the latter is about 4~5 times the apparent viscosity in the former. A schematic description of the different regions during ASPF flooding is shown in Fig. 3.2-17. The apparent viscosity for IOS foam at 20 ft/day is 81 cp for the 40-darcy region and 284 cp for the 200-darcy region from separate experiments where foam displaced brine. However, as shown in Fig. 3.2-16, the apparent viscosity of IOS foam was somewhat lower than these values during the ASPF flood – especially for the 40-darcy experiment -- apparently owing to some contact with N67-7POS and crude oil. Moreover, Fig. 3.2-16 shows that the apparent viscosities of IOS foam and NI/polymer foam are nearly the same in both experiments.

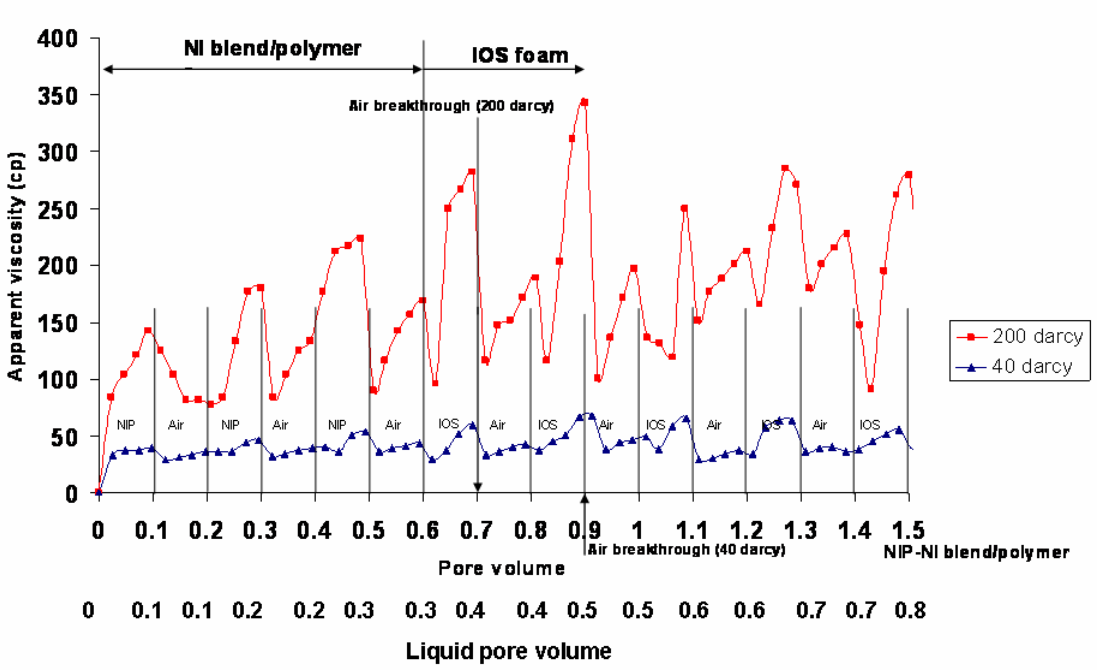

Fig. 3.2-16 Apparent viscosity during ASPF process for both 40 and 200 darcy sand packs

The relative mobility of the foam is obtained from the pressure difference after the foam has filled the sand pack using equation (3.2.1):

$$\lambda_{foam} = \left(\frac{k}{u} \frac{\Delta p_{foam}}{L} \right)^{-1} \qquad (3.2.1)$$

Here λ_{foam} is the relative mobility of the foam in the sand pack, u is the superficial velocity, k is the permeability of the sand pack, Δp_{foam} is the pressure difference after the foam has filled the sand pack, and L is the length of the sand pack.

The relative mobility of water in a region which has residual oil saturation is calculated from the pressure difference during water flooding using equation (3.2.2). The relative mobility of water with residual oil in 40-darcy and 200-darcy sand packs are 0.05 cp^{-1} and 0.025 cp^{-1} respectively.

$$\lambda_{rw} = \left(\frac{k}{u} \frac{\Delta p_{w}}{L} \right)^{-1} \qquad (3.2.2)$$

where λ_{rw} is the relative mobility of the water in the sand pack with water flood residual oil, and Δp_w is the pressure difference at steady state after water flooding.

The length of the oil bank is obtained from measurement of the oil bank front and a material balance. That is, the oil content in the oil bank should be calculated from the residual oil content of the swept and being swept zones as in equation (3.2.3).

$$L_{ob} = \frac{(L_{foam1} + L_{foam2})S_{or}}{S_{ob} - S_{or}} \qquad (3.2.3)$$

$$L = L_w + L_{ob} + L_{foam1} + L_{foam2} \qquad (3.2.4)$$

Where S_{or} is the water flood residual oil saturation, S_{ob} is the oil saturation in the oil bank, L_w is the length of the water region having residual oil saturation, L_{ob} is the length of the oil bank, L_{foam1} is the length of the NI/polymer foam region and L_{foam2} is the length of the IOS foam region. Because the relative mobility of NI/polymer foam and IOS foam are equal, the length of the NI/polymer foam and IOS foam regions can be combined into a foam region as in equation (3.2.5).

$$L_{foam} = L_{foam1} + L_{foam2} \qquad (3.2.5)$$

The total relative mobility of the sand pack can be obtained from equation (3.2.6), where Δp is the pressure difference across the sand pack. The relative mobility of oil bank is obtained from equation (3.2.7). The relative mobility of the oil bank is found to be 0.022 cp^{-1} in the 40-darcy sand pack and 0.012 cp^{-1} in the 200-darcy sand pack.

$$\lambda_r = \left(\frac{k}{u} \frac{\Delta p}{L} \right)^{-1} \qquad (3.2.6)$$

$$\frac{L_{ob}}{\lambda_{ob}} = \frac{L}{\lambda_r} - \frac{L_w}{\lambda_{rw}} - \frac{L_{foam}}{\lambda_{foam}} \qquad (3.2.7)$$

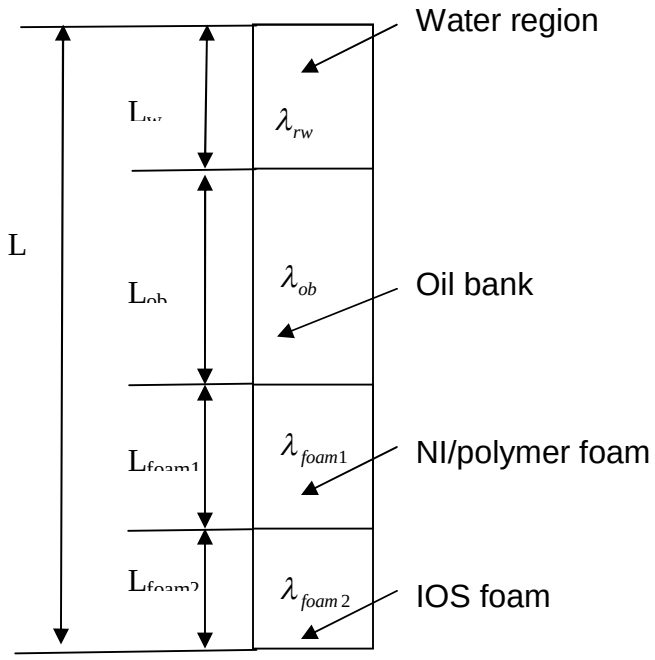

Fig. 3.2-17 Schematic diagram of the different regions during the ASPF process in sand pack

Table 3.2-1 summarizes results for the apparent viscosities and relative mobilities in the two experiments. It shows that the relative mobilities of water and oil bank in the 200-darcy sand pack are about half of those in the 40-darcy sand pack. One reason may be that the residual oil saturation is larger in the 200-darcy pack. The foam relative mobility in the 40-darcy sand pack is 1/5 of that in the 200-darcy sand pack. This ability to generate a higher apparent viscosity in more permeable regions is a key advantage of using foam instead of polymer for mobility control.

Permeability	S_{or}	μ_w (cp)	μ_{ob} (cp)	μ_{foam} (cp)
40 darcy	25%	20	46	47
200 darcy	30%	40	83	215

Table 3.2-1 Summary of the apparent viscosity for the ASPF experiments in 40 darcy and 200 darcy sand packs

3.2.3.4 Calculations of ASPF Performance in Hypothetical Heterogeneous System

The main advantage of the ASPF process is in heterogeneous systems. Foam has higher apparent viscosity in the high permeability regions than in the low permeability regions, which diverts the fluid into the latter. Consider a reservoir with 100 feet width, 100 feet thickness and 2000 feet length. The pressure of the reservoir is 1000 psia and its temperature is 80F, like conditions in Yates Field, West Texas. The reservoir has a

porosity of 35% and two layers with different permeabilities. The thickness h_1 of layer 1 is 20 feet with 200 darcy permeability, and the thickness h_2 of layer 2 is 80 feet with 40 darcy permeability, as shown in Fig. 3.2-18. The ASPF process to recover the residual oil in the reservoir consists of:

1. Alternate injection of a NI blend/polymer slug and air at 20 ft/day in 0.1 PV increments for a total 0.6 PV. The slug includes 0.2% N67-7PO and IOS at 4:1 ratio, 0.5% polymer, 2% NaCl and 1% Na_2CO_3.
2. Alternate injection of IOS and air in 0.1 PV increments to generate IOS foam as drive. IOS solution includes 0.2% IOS at 2% NaCl and 1% Na_2CO_3.

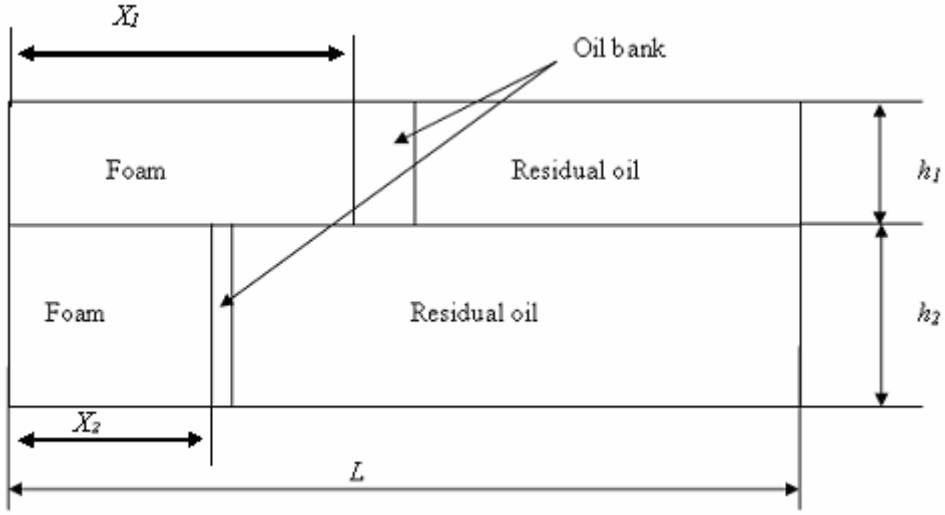

Fig. 3.2-18 Schematic of a reservoir with 2 layers of different permeabilities

Crude oil viscosity is 19 cp. From the results of experiments in section 3.2.3.3, the relative mobility of the residual oil region is 0.05 cp^{-1} when the residual oil saturation is 25%, and the relative mobility of the oil bank is 0.022 cp^{-1}. The foam apparent viscosity is 215 cp in the 200-darcy layer and 46 cp in the 40-darcy layer.

The calculation can be made with the assumptions:

1. Piston-like displacement;
2. The same pressure difference in each layer;
3. No crossflow;
4. All the oil has been recovered in the region after the oil bank.
5. The foam apparent viscosity of IOS foam is the same as the NI/polymer foam.

The foam front position can be calculated from Darcy's law:

$$\frac{dx_l}{dt} = -k_l \lambda_{rl} \frac{\Delta p}{L} \qquad l = 1, 2 \qquad (3.2.8)$$

Four regions exist in the sand pack during ASPF flooding as in Fig. 3.2-19. They are: water flood residual oil, oil bank, NI blend/polymer foam, and IOS foam. The relative mobility in each layer can be obtained from (3.2.8). The result is

$$\overline{\lambda_{rl}} = [\frac{x_{foam1l}}{\lambda_{foam1l}} + \frac{x_{foam2l}}{\lambda_{foam2l}} + \frac{x_{obl}}{\lambda_{obl}} + \frac{x_{rol}}{\lambda_{rol}}]^{-1} \qquad l = 1, 2 \qquad (3.2.9)$$

where $x_{foam1,}\, x_{foam\,2,}\, x_{ob,}\, x_{ro}$ are the lengths of IOS foam, NI blend/polymer foam, oil bank and water flood residual oil phases respectively and $\lambda_{foam1,}\, \lambda_{faom\,2,}\, \lambda_{ob,}\, \lambda_{ro}$ are the relative mobilities for these phases.

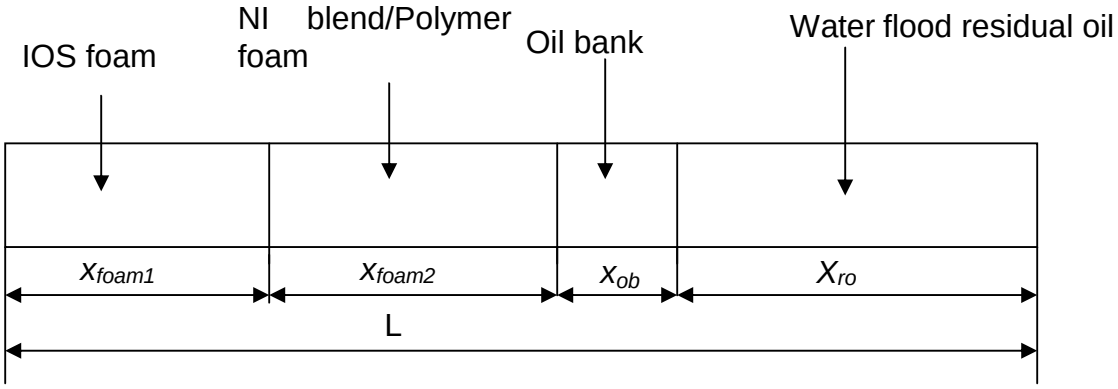

Fig. 3.2-19 schematic illustration of ASPF flooding

In this particular case, the relative mobility of IOS foam λ_{foam1l} is equal to that of the NI blend/polymer foam $\lambda_{foam\,2l}$. Because all the oil after the oil bank has been recovered, the oil bank length x_{ob} can be related to the length of the length of foam $(x_{foam1l} + x_{foam\,2l})$ by the material balance.

$$x_{obl} = \frac{(x_{foam1l} + x_{foam\,2l})S_{orl}}{(S_{obl} - S_{orl})} \qquad l = 1, 2 \qquad (3.2.10)$$

where S_{orl} is the water flood residual oil saturation and S_{obl} is the oil saturation in oil bank.

Taking the ratio of the velocities in the two layers will eliminate time and pressure drop since both layers experience the same Δp. Then in two layers with different permeability,

$$\frac{dx_1}{dx_2} = \frac{k_1}{k_2}\frac{\overline{\lambda_{r1}}}{\overline{\lambda_{r2}}} \qquad (3.2.11)$$

where x_1 and x_2 are the dimensionless front positions of foam in high permeability and low permeability layers, k_1 and k_2 are the permeabilities of the two layers, $\overline{\lambda_{r1}}$ and $\overline{\lambda_{r2}}$ are the relative mobilities in the different layers.

Using numerical methods, we can find the front positions of foam in layer 1 and layer 2 at different pore volumes.

$$x_1(i) = \Delta x \cdot i \qquad (3.2.12)$$

$$x_2(i+1) = x_2(i) + \Delta x \frac{k_2}{k_1}\frac{\overline{\lambda_{r2}}}{\overline{\lambda_{r1}}} \qquad (3.2.13)$$

where Δx is the dimensionless step length in layer 1 which is set to be 0.01 and i is the time indexing. x_1 can be over 1 and it is the hypothetical front of the foam out of the

layer 1 to track the volume of fluid injected. When $x_1 > 1$, $\bar{\lambda}_{rl}$ is based on the fluids preset for $x_1 \leq 1$.

The sweep efficiency is obtained as:

$$\text{Sweep efficiency} = \frac{(x_1 h_1 + x_2 h_2)}{h_1 + h_2} \quad \text{when} \quad x_1 < 1 \qquad (3.2.14)$$

$$\text{Sweep efficiency} = \frac{(h_1 + x_2 h_2)}{h_1 + h_2} \quad \text{when} \quad x_1 \geq 1 \qquad (3.2.15)$$

The sweep efficiency for the ASPF process calculated in this way is shown in Fig. 3.2-20 and compared with that for the ASP process with a 0.3 PV surfactant/polymer slug followed by a polymer drive, both having a viscosity of 46 cp. Fig. 3.2-20 shows that less than 1.06 total pore volume of foam is needed to sweep the heterogeneous system while 1.36 pore volume of polymer is needed to get the same sweep with ASP process. The foam breaks through layer 1 around 0.85 total pore volume and the polymer breaks through around 0.45 total pore volume. An important difference between the processes is that the polymer has the same viscosity in different layers.

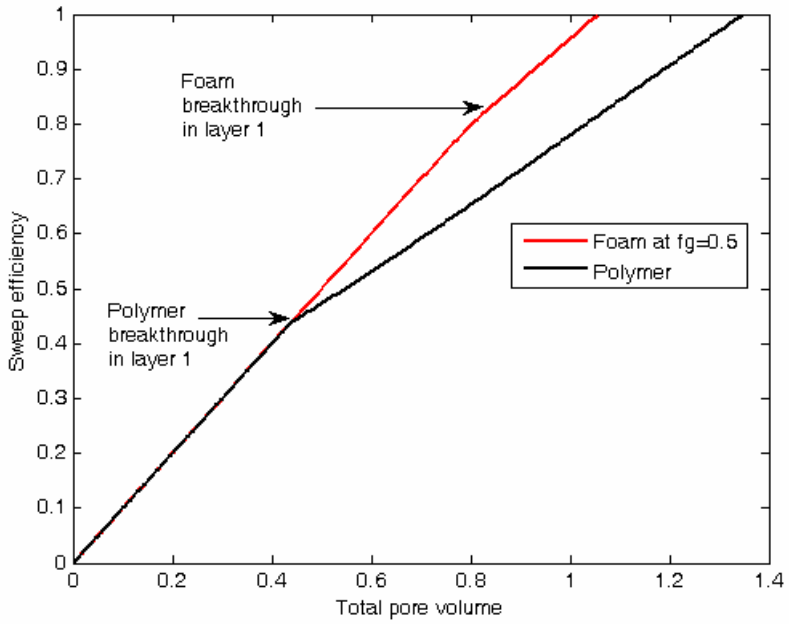

Fig. 3.2-20 Sweep efficiency of foam or polymer sweep in a heterogeneous system with 5:1 permeability ratio and 1:4 thickness ratio

Because the foam is injected at gas fractional flow of 0.5, 0.53 PV of liquid injection is needed, which includes 0.3 PV polymer-surfactant solution at 0.5% polymer and 0.2% NI blend, and 0.23 PV 0.2% IOS solution. For a conventional ASP process, 1.36 PV of liquid is needed which includes 0.3 PV polymer-surfactant solution at 0.5% polymer and 0.2% NI blend, and 1.23 PV of polymer solution at 0.5% concentration.

In each process, a total 0.3 PV NI blend was injected in the heterogeneous system. By tracking the foam front of the IOS foam in ASPF or the polymer drive front in ASP, one finds that there was 0.08 PV of NI blend/polymer solution flowing into layer 1 (higher

permeability) and 0.22 PV into layer 2 (lower permeability) in ASPF compared to 0.17 PV of NI blend/polymer solution flowing into layer 1 and only 0.13 PV into layer 2 with ASP. Thus, the foam diverted more surfactant solution from the high permeability layer to the low permeability layer. 73% of NI blend solution flows into layer 2, which contains 80% of the residual oil, by ASPF process while only 43% of NI blend solution gets into layer 2 by ASP process. The diversion effect by ASPF process is important because enough surfactant must be injected in a real reservoir to overcome the loss by the adsorption of surfactant. This example with a permeability ratio of 5 is not as severe as may be encountered in many formations, where thief zone (high permeability region) could be an order of magnitude or more greater than mean permeability. Then the ASPF process could be even more beneficial.

Tables 3.2-2 and Table 3.2-3 list assumptions and results of calculations illustrating the difference between revenue and chemical expenses for ASPF and ASP processes in this hypothetical reservoir. The cost of natural gas represents the largest part of the chemical cost of ASPF, which is $2.47 per barrel of oil recovered (assuming that all waterflood residual oil is recovered). The price of natural gas assumed is near the current market price and could be considerably less in a reservoir where natural gas co-exists with crude oil. The corresponding cost for ASP is $2.93 per barrel. Although these numbers show a savings of only 16% by using ASPF instead of ASP, a key advantage of ASPF is that more surfactant solution is diverted into the low permeability layer. In actuality a larger surfactant slug would likely be needed in the ASP process to overcome adsorption losses in the lower permeability layer if all oil there is to be recovered. Alternatively, with the same slug size for both processes total oil recovery for ASP would likely be lower. The ASPF process should be especially attractive for a reservoir where there is no nearby pipeline to transport produced gas but where there is a way to transport oil produced by EOR.

	Natural gas	N67-7PO	IOS	Polymer	Crude oil
Unit price	$7.28	$3.00	$1.00	$1.00	$35.00
	/MCF	/pound	/pound	/pound	/bbl
Amount	234,130	211,860 pounds	92,806 pounds	662,080 pounds	1,251,600
	MCF				bbl
Revenue or expense	$1,704,500	$635,580	$92,806	$662,080	$43,805,000
Revenue minus expense	$40,710,034	Revenue minus expense per bbl crude oil	$32.53/bbl	Expense per bbl crude oil	$2.47/bbl

Table 3.2-2 Revenue and expense calculation for ASPF process after water flooding on a reservoir with 2000 ft length, 100 ft thickness, 100 ft width, 35% porosity, 1:5 permeability ratio and 25% residual oil

	N67-7PO	IOS	Polymer	Crude oil
Unit price	$3.00 /lb	$1.00/lb	$1.00 /lb	$35.00/bbl
Amount	211,860 lb	42,372 lb	2,983,300 lb	1,251,600 bbl
Revenue or expense	$635,580	$42,372	$2,983,300	$43,805,000

Revenue minus expense	Revenue minus expense per bbl crude oil	Expense per bbl crude oil
$40,143,748	$32.07/bbl	$2.93/bbl

Table 3.2-3 Revenue and expense calculation for ASP process after water flooding on a reservoir with 2000 ft length, 100 ft thickness, 100 ft width, 35% porosity, 1:5 permeability ratio and 25% residual oil

Subtask 3.3 Foam stability with the presence of residual oil

The stability of foam by different surfactants in the presence of residual oil was tested. A short sand pack is used to avoid the long periods of time that would have been required to test various surfactants in the 1-ft long sand pack. The set up for the experiment is shown in Fig. 3.3-1.

The porous medium consists of a 1.5 inch long and 0.5 inch diameter cylinder packed with 50-mesh sand. Pore volume for the short sand pack is about 5ml. Foam is generated in the sand pack by co-injection of surfactant solution and air. The surfactant is injected by an Isco pump, and air is injected by an air flow controller. Two pressure transducers measure the pressure drop across the tubing and the injection pressure to the sand pack. Foam quality is measured by passing foam from the tubing through an inverted burette containing IPA/water mixture, which breaks the foam. The ratio of the volume of air collected to the amount of liquid displaced gives the quality of foam.

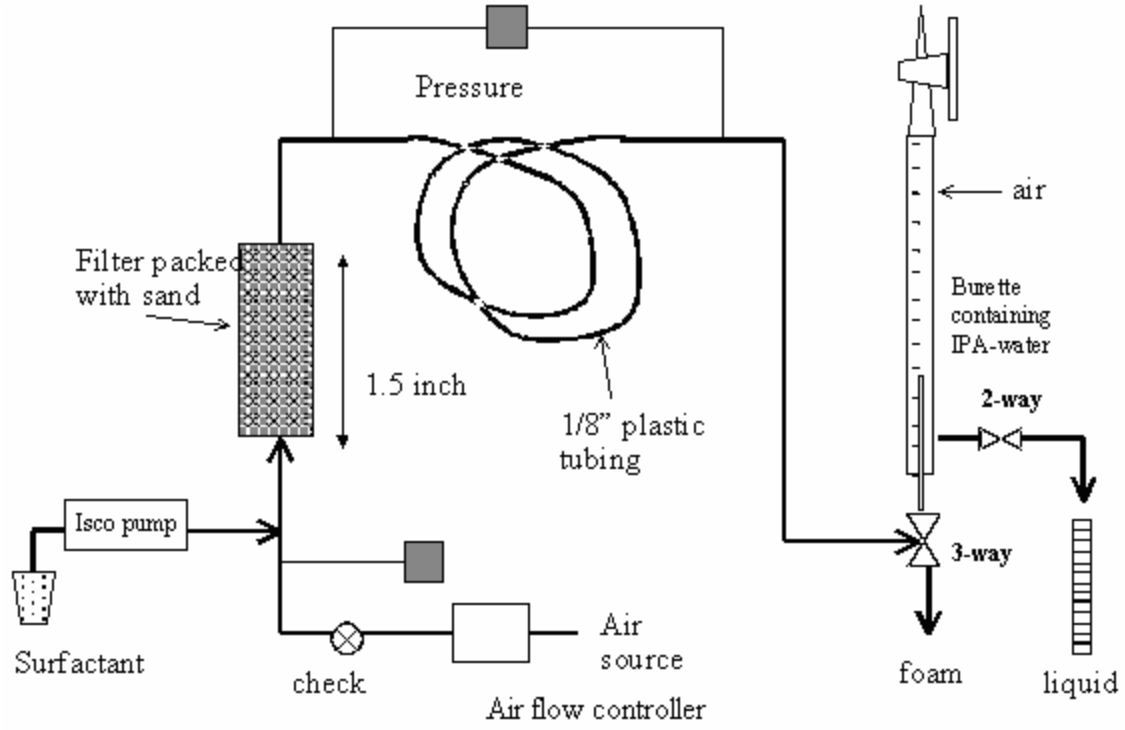

Figure 3.3-1 Short sand pack

To test the foam stability in the presence of residual oil, first, the foam strength without the presence of oil is measured for comparison at some constant gas fractional flow. Second, the water-saturated pack is filled with hexadecane. Then water is used to flush the sand pack to achieve residual oil saturation. Foam is then generated at the same gas fractional flow. The steady state pressure readings are recorded to compare the foam strength with or without residual oil in the sand pack.

The results are shown in Fig.3.3-2. IOS seems to be the best foamer among all the surfactant candidates. Even after contacting with residual crude oil, the foam produced by IOS still has a higher apparent viscosity than that formed by any other foamer. N67 and the blend of N67/IOS(4:1) has almost the same apparent viscosity with or without residual crude oil. But that doesn't necessarily mean that foam generated with N67 or the N67/IOS(4:1) is stable when the residual oil is present. Because the salinity we used is close to the optimal salinity of N67-7PO and N67-7PO&IOS(4:1), almost all residual oil is displaced by the initial surfactant injected so that little oil is present at the final steady state conditions. And the foam of both N67 or N67/IOS(4:1) is weak compared with that of IOS. Therefore IOS is the best candidate of the evaluated surfactants as a foamer.

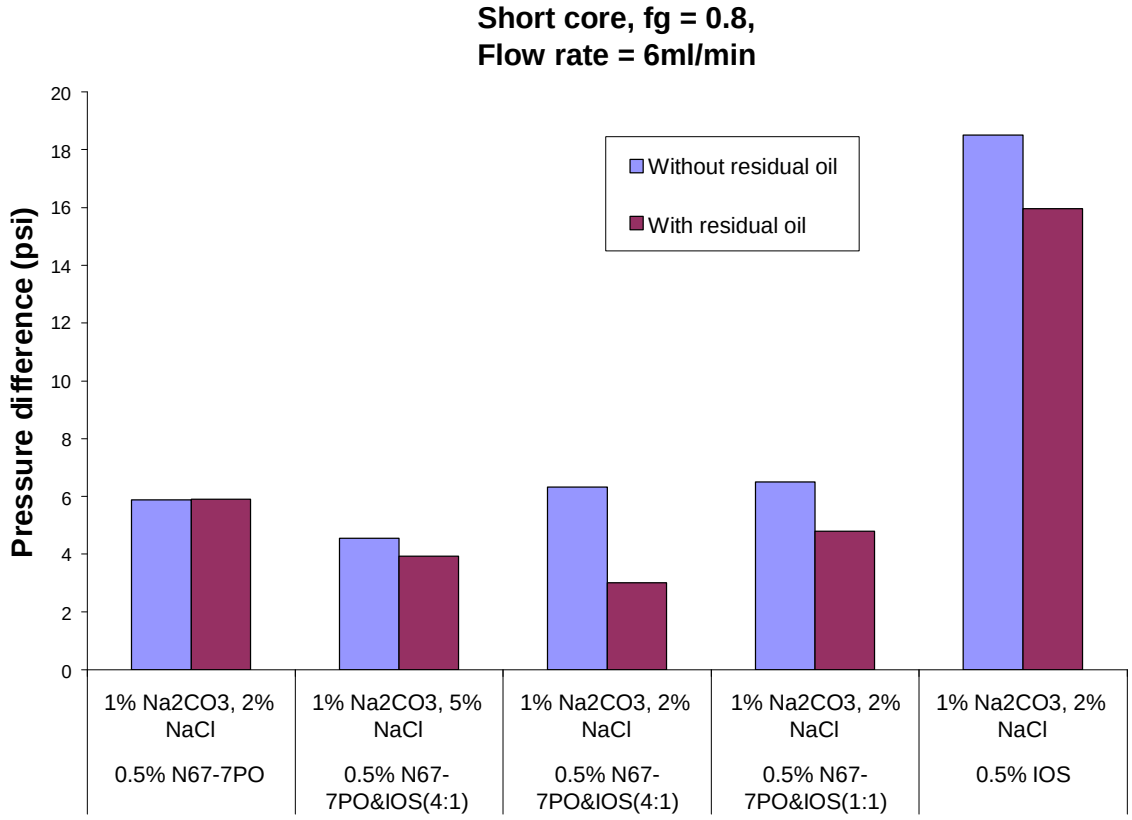

Figure 3.3-2 Comparison of foam strength with or without residual oil by different surfactants

Reference

G.J. Hirasaki and J.B Lawson, Mechanisms of Foam Flow in Porous Media: Apparent Viscosity in Smooth Capillaries, *Society of Petroleum Engineers Journal*, 25 (2), 1985, 176-190.

H.M. Princen, Rheology of Foams and Highly Concentrated Emulsions, I. Elastic Properties and Yield Stress of a Cylindrical Model System, *Journal of Colloid Interface Science* (1983) 91, No. 1 160-175.

I.M. Krieger, Rheology of Monodisperse Latices, *Advances in Colloid and interface Science*, 1972, 3, 111-136.

M.J. Mooney, The Viscosity of a Concentrated Suspension of Spherical Particles, *Journal of Colloid Science*, 1951, 6, 162-170.

R. Pal, Rheology of Polymer-thickened Emulsions, *Journal of Rheology*, 36(7), 1992.

TASK 4: SIMULATION OF FIELD-SCALE PROCESSES

Subtask 4.1 Wettability Alteration Model

As a result of an extensive literature survey and test simulations, the effects of wettability on residual oil saturation, relative permeability curves, and CDCs are clear. However, a mathematical relationship to link the changes of each property with changes in wettability due to surfactant injection is still unclear. A method has been established in an attempt to fulfill this complex task.

Wettability alteration is modeled with changes in relative permeability and capillary pressure. A brief description of the model is given here. Corey-type relative permeabilities are calculated for each gridblock as follows:

$$k_{r\ell} = k^{o}_{r\ell} S^{e\ell}_{n\ell} \quad \ell = 1,2,3 \tag{4.1}$$

where ℓ is either water, oil or microemulsion phases, $k^{o}_{r\ell}$ is the relative permeability endpoint for phase ℓ, $e\ell$ is the Corey exponent of phase ℓ and $Sn\ell$ is the normalized saturation of phase ℓ calculated as follows:

$$S_{n\ell} = \frac{S_\ell - S_{\ell r}}{1 - \sum_{\ell=1}^{3} S_{\ell r}} \quad \ell = 1,2,3 \tag{4.2}$$

where S_ℓ is the saturation of phase ℓ and $S\ell r$ is the residual saturation of phase.

In addition to the wettability alteration effect, surfactants also reduce the interfacial tension between oil and aqueous phases and help in the oil mobilization. This effect is modeled by means of a dimensionless number called trapping number, which is a combination of capillary number and bond number and can adequately model the combined effect of viscous, capillary, and buoyancy forces in three dimensions (Delshad et al., 1996; Delshad, 1990; Jin, 1995). As the surfactant enters a gridblock, it reduces the interfacial tension and as a result, trapping number increases. Interfacial tension reduction and oil mobilization effect of surfactants, affects the residual phase saturations, endpoint relative permeabilities, and exponents. Mobilization effect on residual phase saturations is modeled in UTCHEM (Delshad et al., 1986) as follows:

$$S_{\ell r} = \min\left[S_\ell, \left(S^{high}_{\ell r} + \frac{S^{low}_{\ell r} - S^{high}_{\ell r}}{1 + T_\ell N_{T\ell}} \right) \right] \quad \ell = 1,2,3 \tag{4.3}$$

where $S^{high}_{\ell r}$ and $S^{low}_{\ell r}$ are residual saturations of phase ℓ at high and low trapping numbers respectively (given as input parameters), T_ℓ is the input trapping parameter of phase ℓ and $NT\ell$ is trapping number of phase ℓ. $S^{high}_{\ell r}$ is typically zero. The trapping number for phase ℓ displaced by phase ℓ' is defined as follows (Delshad et al., 1986):

$$N_{T\ell} = \frac{\left| \vec{k} \cdot \left(\vec{\nabla}\Phi_{\ell'} + g\Delta\rho\vec{\nabla}D \right) \right|}{\sigma_{\ell\ell'}} \quad \ell = 1,2,3 \tag{4.4}$$

Mobilization effects on endpoint relative permeabilities are modeled using the following correlation (Delshad et al., 1986):

$$k_{r\ell}^{o} = k_{r\ell}^{o\,low} + \frac{S_{\ell'r}^{low} - S_{\ell'r}}{S_{\ell'r}^{low} - S_{\ell'r}^{high}} \left(k_{r\ell}^{o\,high} - k_{r\ell}^{o\,low} \right) \quad \ell = 1,2,3 \tag{4.5}$$

where $S_{\ell'r}$ is the residual saturation of the conjugate phase e.g. oil is the conjugate phase for microemulsion phase and $k_{r\ell}^{o\,low}$ and $k_{r\ell}^{o\,high}$ represent the endpoint relative permeability of phase ℓ at low and high trapping numbers respectively. Equation 4.6 gives the relative permeability exponents as a function of trapping number (Delshad et al., 1986).

$$e_{\ell} = e_{\ell}^{low} + \frac{S_{\ell'r}^{low} - S_{\ell'r}}{S_{\ell'r}^{low} - S_{\ell'r}^{high}} \left(e_{\ell}^{high} - e_{\ell}^{low} \right) \quad \ell = 1,2,3 \tag{4.6}$$

where e_{ℓ}^{low} and e_{ℓ}^{high} represent the relative permeability exponents for low and high trapping numbers respectively specified as input parameters.

Equations 4.1 to 4.6 are solved once for the initial reservoir wettability condition $(k_{r\ell}^{initial})$ and once for the altered condition of strongly water-wet $(k_{r\ell}^{final})$. Two sets of relative permeability ($k_{r\ell}^{o}$, $S_{\ell'r}$, e_{ℓ}) and trapping parameters (T_{ℓ}) are required as input parameters corresponding to each wettability state. The relative permeability in each gridblock $(k_{r\ell})$ is then obtained by linear interpolation between the relative permeability corresponding to the two different wettability conditions, provided that the concentration of surfactant in the gridblock is greater than the critical micelle concentration. Interpolation is made based on the scaling factor .

$$k_{r\ell} = \omega\, k_{r\ell}^{final} + (1-\omega)\, k_{r\ell}^{initial} \quad \ell = 1,2,3 \tag{4.7}$$

where ω is the interpolation scaling factor and $k_{r\ell}^{final}$ and $k_{r\ell}^{initial}$ represent the relative permeabilities corresponding to the two extreme wetting states, i.e. final and initial wettability states, respectively. The scaling factor is either a constant user input parameter or is related to the concentration of surfactant adsorbed in each gridblock as follows:

$$\omega = \frac{\hat{C}_{surf}}{\hat{C}_{surf} + C_{surf}} \tag{4.8}$$

where $\hat{C}_{surf}$ and C_{surf} represent the adsorbed and total concentration of surfactant, respectively.

The capillary pressure as a function of wettability is also modeled using linear interpolation between the capillary pressure of the initial wetting state and the final condition.

$$P_c = \omega P_c^{final} + (1-\omega) P_c^{initial} \tag{4.9}$$

where the capillary pressure Pc is a scaled with the interfacial tension as follows:

$$P_c = P_{cow} \frac{\sigma_{om}}{\sigma_{ow}} \tag{4.10}$$

where

$$P_{cow} = C_{pc} (1 - S_{n\ell})^{E_{pc}} \tag{4.11}$$

Examples of wettability effects on oil/water relative permeability and oil capillary desaturation curve in Berea sandstone are those measured by Mohanty (1983) and Morrow et al. (1973). The effect of wettability on the capillary desaturation curve for oil in a carbonate rock is has been reported by Kamath et al. (2001).

Capillary desaturation curves, relative permeability endpoints, and relative permeability exponents as a function of trapping number for different wettability conditions of water wet and mixed wet are given in Figs. 4.1-1 through 4.1-3. Relative permeabilities are then calculated using Eqs. 4.1 to 4.7 with a constant wettability scaling factor of □= 0.5. The base relative permeability parameters listed in Table 4.1 for water-wet and mixed-wet conditions are based on the relative permeability measurements of Morrow et al. (1973). Relative permeabilities are calculated for different trapping numbers of 10-7, 10-5, and 10-3 given in Figs. 4.1-4 through 4.1-6. Figure 4.1-7 shows the capillary pressure curves calculated for water wet and oil wet conditions using Eq. 4.11 and a mixed wet curve using the scaling factor of 0.5 in Eq. 4.9. Table 4.1-1 lists the capillary pressure parameters.

	Oil-Wet		Water-Wet	
	Oil	Water	Oil	Water
Residual saturation	0.28	0.12	0.25	0.12
Endpoint relative permeability	0.80	0.56	1	0.26
Relative permeability exponent	3.3	1.4	1.3	3
Trapping parameters (T_ℓ)	1,000	20,000	200	1,500
Capillary pressure endpoint (CPC)	-15		7	
Capillary pressure exponent (EPC)	6		2	

Table 4.1-1 Relative Permeability and Capillary Pressure Parameters (Low Trapping Number in Matrix)

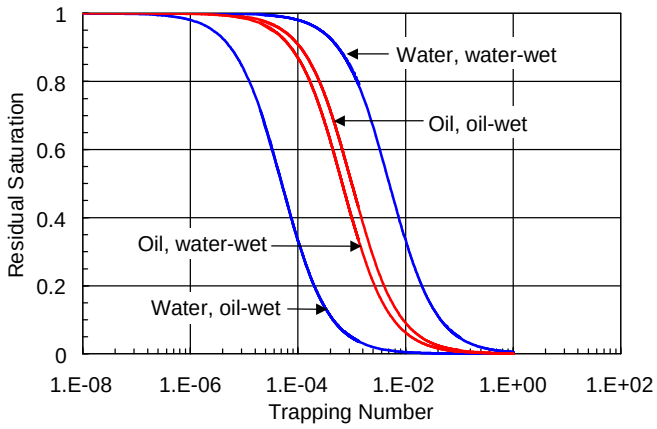

Fig. 4.1-1 Capillary Desaturation Curves used in Simulations.

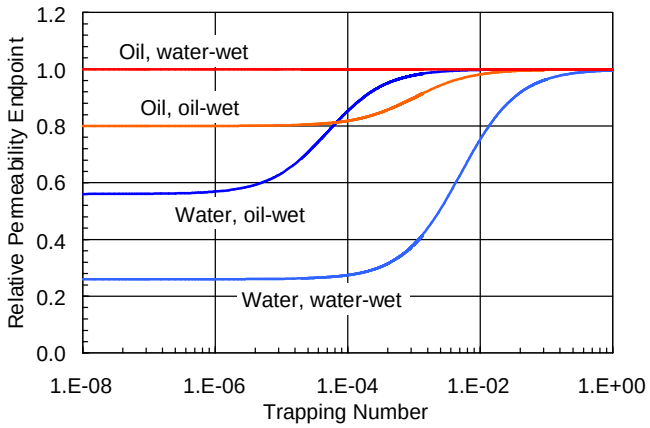

Fig. 4.1-2 Endpoint Relative Permeability.

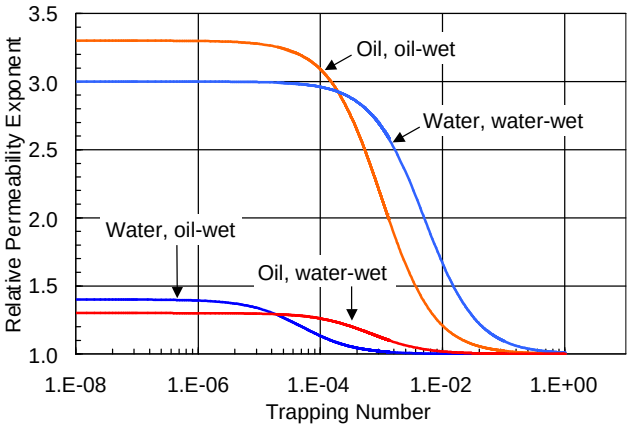

Fig. 4.1-3 Relative Permeability Exponent.

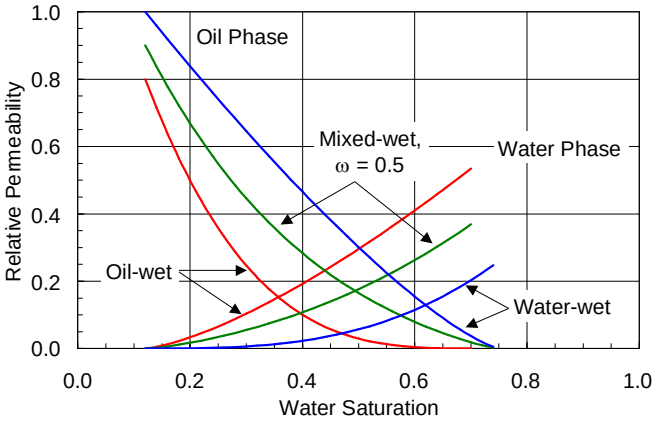

Fig. 4.1-4 Calculated Relative permeability Curves for Different Wettability Conditions at Low Trapping Number of 10^{-7}.

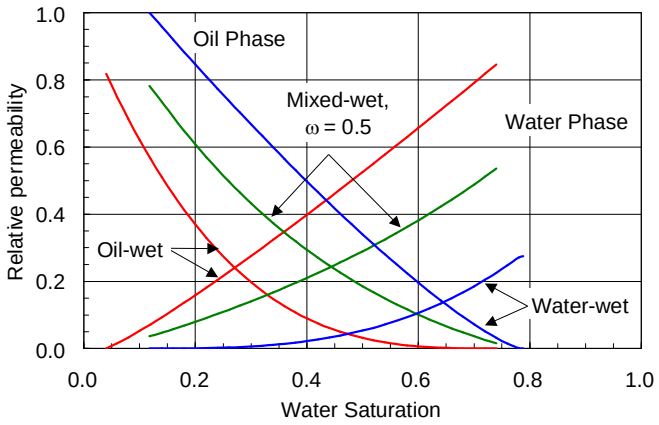

Fig. 4.1-5 Calculated Relative Permeability Curves for Different Wettability Conditions at Trapping Number of 10^{-5}.

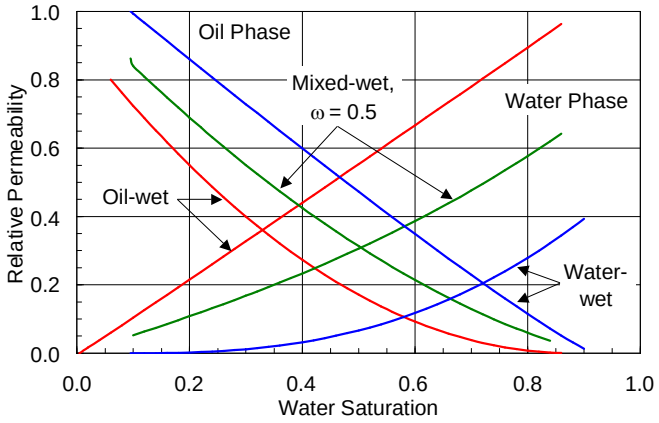

Fig. 4.1-6. Calculated Relative Permeabilities for Different Wettability Conditions at Trapping Number of 10^{-3}.

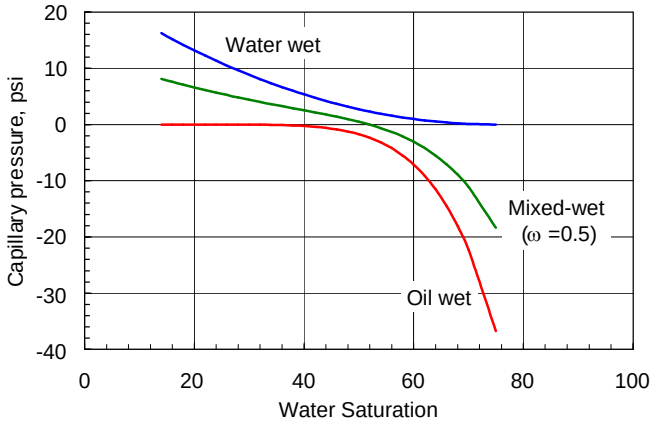

Fig. 4.1-7 Calculated Capillary Pressure Curves for Different Wettability Conditions.

Subtask 4.2 Simulation of Imbibition Cell Experiment

The data of interest used in the modeling study consists of spontaneous imbibition tests using both brine and alkali/surfactant solution conducted at Rice University (Hirasaki and Zhang, 2003; Hirasaki et al., 2004). The experiments were comprised of dead crude oil, formation brine, and reservoir cores from the Yates oil reservoir in West Texas. The Yates field was discovered in 1926 and is a massive naturally fractured carbonate reservoir located at the southern tip of the Central Basin Platform in Permian Basin of West Texas (Chen et al., 2001). The matrix permeability ranges from 50 to 250 md and the average fracture permeability is 1000 md. The matrix porosity ranges from 15 to 22%.

The crude oil used in the laboratory studies had an API gravity of 30^o (0.88 g/cc) and a viscosity of 19.1 cp. The formation brine used in the experiment contained mostly NaCl and small concentrations of $CaCl_2$ and $MgCl_2$. Several reservoir cores were used in different laboratory experiments under slightly different conditions. The cores were carbonates with moderate porosity and low permeability. The core samples were oil flooded to residual water saturation and some were aged for 24 hours at 80 °C. Data from two of these imbibition cell experiments were used in this study. The first, called Core C, is a 40 md core that was saturated but not aged in crude oil prior to the imbibition tests. The second, called Core B, is a 122 md core that was aged in the crude oil at 80°C prior to the imbibition tests. Oil recovery by spontaneous imbibition was measured by placing the oil-saturated cores in imbibition cells filled with either formation brine or alkaline/surfactant solution.

The first experiments conducted were imbibition cell tests using brine as the fluid surrounding the cores in each cell. After one to two weeks, no oil was recovered from either core and the experiments were stopped. A picture of the imbibition cell for brine imbibition and alkali/surfactant is shown in Figure 4.2-1. The lack of oil recovery was attributed to the wettability of the reservoir cores. They anticipated the cores to be mixed-wet or oil-wet. However, the length of time allowed for the imbibition experiment was relatively short for this low permeability rock.

The next set of experiments conducted were spontaneous imbibition cell tests using the same Yates cores and an alkali/surfactant solution as the fluid surrounding the cores in each cell. The surfactant solution was a mixture of 0.025 wt% CS-330 (C_{12}-3EO-sulfate) and 0.025 wt% TDA-4PO-sulfate (C_{13}-4PO- sulfate). In addition, a 0.3 M sodium carbonate alkali solution was also added to the aqueous solution used to reduce the surfactant adsorption. The sodium carbonate generates soaps in-situ by reacting with the naphthenic acids in the Yates crude oil, which has an acid number of 0.2 (Hirasaki and Zhang, 2003).

Shortly after the beginning of the experiment they observed oil appearing at the top of each core. Both cores were allowed to imbibe the alkali/surfactant solution for more than 100 days. The surfactant imbibition test for Core C, which was not aged in crude oil, recovered 14% of the oil. The test for Core B, which was aged in crude oil, recovered 44% of the oil. Based on the appearance of oil at the top of the core, the

imbibition process was heavily gravity dominated. Hirasaki *et al.*, 2004 attributed the increase in recovery for Core B to higher permeability and lower initial oil saturation. However, the difference in oil recovery seems to be more significant than small variations in permeability and initial oil saturation. One important fact is that Core B was aged and Core C was not. An alternate explanation can be that the wettability of Core B was altered to more oil-wet during the aging process and was then altered back to a mixed-wet state or water wet state during the surfactant imbibition test. This change in wettability could have enhanced the oil mobilization by means of redistribution of fluid phases as well as by lower IFT. On the other hand, the wettability of Core C was either not altered or was altered to a lesser extent during the surfactant imbibition test and resulted in lower oil recovery.

Although several experiments were conducted for different surfactant formulations, initial oil saturations, and permeability, we picked Cores B and C for the simulation study. The purpose of matching Core C was to obtain rock and fluid properties that were not measured or not available. Conversely, the intent of matching Core B was to validate the wettability alteration model implemented in UTCHEM.

4.2.1 Numerical model

The most challenging part of developing the simulation model is that the laboratory experiment was an oil-saturated core placed inside an imbibition cell at ambient conditions rather than in the more conventional setup where the core is confined in a core holder or sleeve. The simulation model was set up to simulate both the core and surrounding fluid in the imbibition cell. Therefore, the grid consisted of fluid gridblocks (hereinafter referred to as "non-rock" gridblocks) and rock gridblocks. The grid was Cartesian with 7x7x7 gridblocks as shown in Figure 4.2-2. The purpose of this grid was to simulate fluid flowing from the open imbibition cell into the rock and expelling oil to the top. The imbibition cell dimensions were approximately 2 inches in diameter and 12 inches tall (9 inches of which is a graduated collection tube). Both Core C and Core B had the same dimensions: 1.5 inches in diameter and 3 inches in length. The grid in this model was square but the rock gridblocks had dimensions that honored the pore volume and original oil in place of the cylindrical core.

The non-rock gridblocks of this model were located at the top and on the sides of the grid. The thickness of the top two layers of the grid was 3.6 and 1.2 inches to allow for oil to accumulate at the top. The remaining grid thickness was derived from the core dimensions. The thickness of the bottom five layers was 0.6 inches. Therefore, the total thickness of the grid is 7 inches. Since the actual height of the imbibition cell was 12 inches, the model was assumed to be at a depth of 5 inches in order to simulate the actual hydrostatic head at the top of the core. Each non-rock gridblock was given a set of petrophysical properties with the intent of simulating flow through the open imbibition cell. Table 4.2-1 shows a summary of the properties used to define the non-rock gridblocks.

The rock gridblocks were present in the middle, bottom portion of the grid. This 5x5x5 area was given petrophysical properties indicative of the core, which will be

discussed in the next section. The dimensions of the rock gridblocks were 0.2664 inches by 0.2664 inches by 0.6 inches giving the simulated core total dimensions of 1.332 inches by 1.332 inches by 3 inches. The bulk volume of the simulated square core is 1.774 inches^3 compared to the actual circular volume of 1.767 inches^3. A visual representation of the grid is shown in Figure 4.2-2. This figure shows the location of the non-rock and rock gridblocks within the grid.

Based on the gridblock configuration and lack of simulated wells, a method had to be established to process the output of each imbibition simulation. One focus of this study was to match the oil recoveries. In the actual experiments, the volume of oil in the graduated collection tube of the imbibition cell was recorded over time. This value was then divided by the known original oil in place to determine the cumulative oil recovery. A similar approach was taken to determine the cumulative oil recovery of each simulation. After the simulation was completed, the concentration output file of UTCHEM (.CONCP) was copied into an Excel worksheet. Then a macro was written to calculate the volume of oil in the top two layers (non-rock layers) of the simulation model. Oil volumes were calculated as a function of time and divided by the original oil in place. The oil recoveries as a fraction of OOIP were then plotted against time for comparison with the laboratory oil recovery data.

4.2.2 Petrophysical and chemical properties

Some of the petrophysical and chemical properties were obtained from Hirasaki *et al.*, 2004. These properties included porosity, permeability, initial water saturation, and brine composition. The core was assumed to be homogeneous and isotropic. In addition, the non-rock and rock gridblocks were assumed to have the same salinity. The properties used for Core C and Core B are shown in Table 4.2-2. The initial water saturation and the residual water saturation were assumed to be the same because the cores were oil flooded at very high pressure gradients to saturate the core. Lastly, remaining oil saturations at the end of the surfactant spontaneous imbibition were also provided. These values are used as the residual oil saturations for the numerical model as a preliminary assumption.

4.2.3 Model assumptions

To complete the development of the simulation model several assumptions had to be made to describe other petrophysical and chemical behaviors that were not measured. The following is a list of assumed matching parameters:

- Relative permeability parameters;
- Capillary pressure parameters;
- Surfactant molecular diffusion;
- Surfactant critical micelle concentration (CMC);
- Capillary desaturation parameters; and

- Surfactant phase behavior parameters.

The initial relative permeability curves used in this model were based on an analog West Texas mixed-wet reservoir described in the next section. The capillary pressure curve was set up to be oil-wet from the understanding that the cores produced no oil during spontaneous imbibition tests with brine solution. The parameters used to develop these two petrophysical processes are shown in Table 4.2-2. These properties are depicted graphically in Figures 4.2-3 and 4.2-4, respectively. In addition, the capillary desaturation curve used for the initial simulations is shown in Figure 4.2-5. The remaining properties are shown in Table 4.2-3 and will be discussed in more detail in a later section. These four parameters are expected to be the most significant parameters for this study. The results of the surfactant imbibition tests will be strongly dependent on the rate of formation of microemulsion within the core, which is controlled by surfactant molecular diffusion and the critical micelle concentration (CMC). The results will also be strongly dependent on the ability of the surfactant to reduce the capillary forces and mobilize the oil, which is controlled by the surfactant phase behavior and capillary desaturation.

Four final assumptions were made during the development of this simulation model. In the actual spontaneous imbibition experiment, sodium carbonate was added to the surfactant solution to reduce surfactant adsorption and generate in-situ soap. For this study, it is assumed that the amount of generated soap is negligible and that the primary effect of the alkali is surfactant adsorption reduction. Based on this, the surfactant adsorption is assumed to be zero. Next, it was assumed that the surfactant forms a Type II(-) microemulsion where oil and microemulsion are in equilibrium during the simulation rather than a Type III where microemulsion is in equilibrium with both excess oil and brine phases. This is a reasonable assumption based on the salinity of the surfactant solution and the phase behavior data used in the experiment. Lastly, the physical dispersion was assumed to be negligible and only an effective surfactant molecular diffusion was used.

4.2.4 Water spontaneous imbibition simulation

After the imbibition simulation model was established, the first step was to simulate the experiment with brine solution in the non-rock gridblocks. The purpose of this simulation was to compare the simulated oil recovery with the laboratory experimental data showing zero oil recovery. The simulation was run using the Core C properties for 14 days. The result of the simulation was no oil recovery in agreement with the experiment, so this was the initial validation of the model.

4.2.4.1 Core C surfactant simulations

The next step was to simulate surfactant imbibition for Core C. Recall that Core C was not aged and was assumed to maintain its original wettability during the surfactant experiment. Based on this assumption, obtaining a match of the experimental results will give insight into the correctness of some of the assumed parameters used in the

simulation model. Some of the key parameters such as surfactant molecular diffusion, CMC, and capillary desaturation curves can be obtained for this core once a match was obtained. To complete this task, a sensitivity study was conducted for each petrophysical and chemical parameter. The base case values for surfactant diffusion, CMC, and trapping parameters are given in Table 4.2-3. The surfactant phase behavior parameters were adjusted to obtain a value of IFT (0.02 dynes/cm) that matched the laboratory results (Hirasaki *et al.*, 2004). Since the surfactant spontaneous imbibition simulations were conducted at a constant salinity, matching the IFT at one salinity was sufficient. By adjusting the UTCHEM input parameters, an IFT value of 0.022 dynes/cm was obtained with an oil solubilization ratio of 3.7 cc/cc at a constant salinity of 0.3 meq/mL. The UTCHEM phase behavior input parameters are shown in Table 4.2-3.

The final step for the Core C surfactant imbibition simulations was to consider changes to multiple key parameters with the intent of matching the laboratory data. The key parameters - surfactant effective diffusion coefficient, CMC, and CDC - were adjusted until a satisfactory match with the laboratory data was obtained. Recall that the purpose of these simulations was to obtain values for the key parameters. The Core C laboratory data were used because it was assumed that wettability alteration was not occurring. The values obtained in this study could then be applied to Core B, which did have wettability alteration during the surfactant imbibition experiment.

The Core C laboratory data were matched by adjusting the surfactant effective diffusion coefficient and CDCs. The CMC value of $5x10^{-5}$ (volume fraction) turned out to be the best match. The value of surfactant effective diffusion coefficient used in the simulation match was $6.5x10^{-5}$ ft^2/day ($6x10^{-3}$ cm^2/sec). The CDC parameters were T_w = 10,000 and T_o = 10,000. The result of the simulation match is shown in Figure 4.2-6. A good match was obtained with this simulation and gave encouraging results to use in the wettability alteration simulations in the subsequent sections.

4.2.4.2 Core B Surfactant Imbibition Simulations

In the previous section, a surfactant imbibition simulation study was performed with the intent of obtaining an understanding of the transport mechanisms and unknown petrophysical and chemical properties. The Core C experiment was successfully matched by adjusting the surfactant diffusion and CDCs. The Core C experiment was assumed to retain its initial wettability throughout the imbibition process. On the other hand, the Core B experiment was said to have altered its wettability by interaction with surfactant during spontaneous imbibition. This section focuses on simulating the Core B surfactant imbibition experiment. The first step was to use the matching parameters obtained from the Core C simulations and apply them to the Core B simulation assuming no wettability alteration occurred. Following the results of this simulation, the modified UTCHEM will be used to model wettability alteration during the surfactant spontaneous imbibition.

The purpose of simulating the Core B experiment assuming no wettability alteration is to show that IFT reduction, gravity, and buoyancy are not the only process accounting for the increase in oil recovery for this experiment. The simulation model used to match the Core C experiment was adjusted to consider the known properties of

Core B. The differences in the two models were the permeability, initial oil saturation, residual oil saturation, residual water saturation, and simulation time. The property differences were summarized in Table 4.2-2.

The Core B laboratory data and the results of this simulation are shown in Figure 4.2-7. It is apparent that the laboratory data cannot be matched without simulating wettability alteration. The oil recovery response time is much too late and the ultimate oil recovery is too low. However, a brief sensitivity analysis was conducted to test the effects of the key parameters on this simulation.

Based on the results from the capillary pressure and CDC sensitivity, a simulation was run allowing for wettability changes in both properties. In other words, the capillary pressure curve was allowed to change from oil-wet to more water-wet and the CDC was allowed to change from oil-wet to mixed-wet with changes in wettability. The result of this simulation is shown in Figure 4.2-7. As you can see from this figure, a very close match of the Core B experimental data was obtained by simulating wettability alteration corresponding to changes in capillary pressure and CDCs.

The final step was to test the sensitivity to the interpolation wettability scaling factor. The simulation with the best match of experimental data with the scaling factor of □ = 0.5 was used. Two additional simulations using 0.3 and 0.7 were run to test the sensitivity to the rate at which the wettability alteration changes the modeled properties. The results are shown in Figure 4.2-8. A small sensitivity to the interpolation scaling factor was observed. However, by increasing the scaling factor from 0.5 to 0.7, a slightly better match of the experimental data was obtained.

Table 4.2-1 Non-Rock Gridblock Properties for Spontaneous Imbibition Simulations

Property	Value
Porosity	1
Permeability (md)	100,000
Initial Water Saturation	1
Salinity (meq/mL)	0.3
Residual Phase Saturations	0.0001
Endpoint Relative Permeabilities	1
Relative Permeability Exponents	1
Capillery Pressure Endpoint (CPC)	0

Table 4.2-2 Rock Gridblock Properties for the Spontaneous Imbibition Simulations

Property	Value (Core C / Core B)
Porosity	0.24
Permeability (md)	40 / 122
Initial Water Saturation	0.18 / 0.32
Salinity (meq/mL)	0.3
Residual Water Saturation	0.18 / 0.32
Residual Oil Saturation	0.7 / 0.38
Water Endpoint Relative Permeability	0.23
Oil Endpoint Relative Permeability	0.59
Water Relative Permeability Exponent	2.9
Oil Relative Permeability Exponent	3.3
Capillery Pressure Endpoint (CPC)	-2.86 / -5
Capillary Pressure Exponent (EPC)	2

Table 4.2-3 Properties for the Core C Base Case Spontaneous Imbibition Simulations

Property		Value
Surfactant Diffusion Coefficient (ft^2/day)		$5x10^{-5}$
Surfactant CMC (volume fraction)		$5x10^{-5}$
Trapping Parameter for Water CDC		59074
Trapping Parameter for Oil CDC		1865
Trapping Parameter for Microemulsion CDC		364
Surfactant Phase Behavior Parameters Used to Obtain Constant IFT value.	HBNC70	0.001
	HBNC71	0.008
	HBNC72	0.1
	CSEL (meq/mL)	0.4
	CSEU (meq/mL)	0.8
	Interfacial Tension (dynes/cm)	0.02

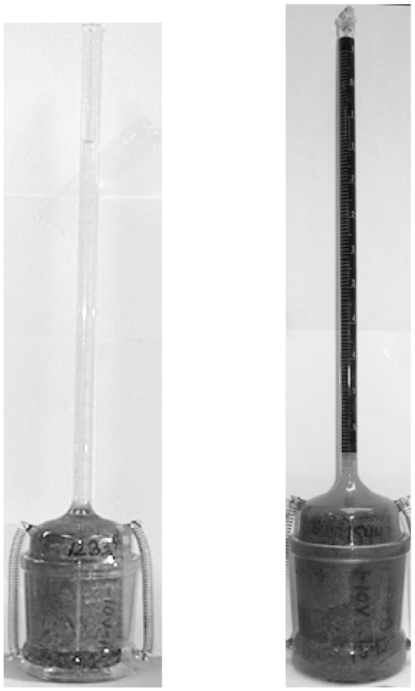

Fig. 4.2-1 Imbibition Cell Tests (Hirasaki *et al*., 2004)

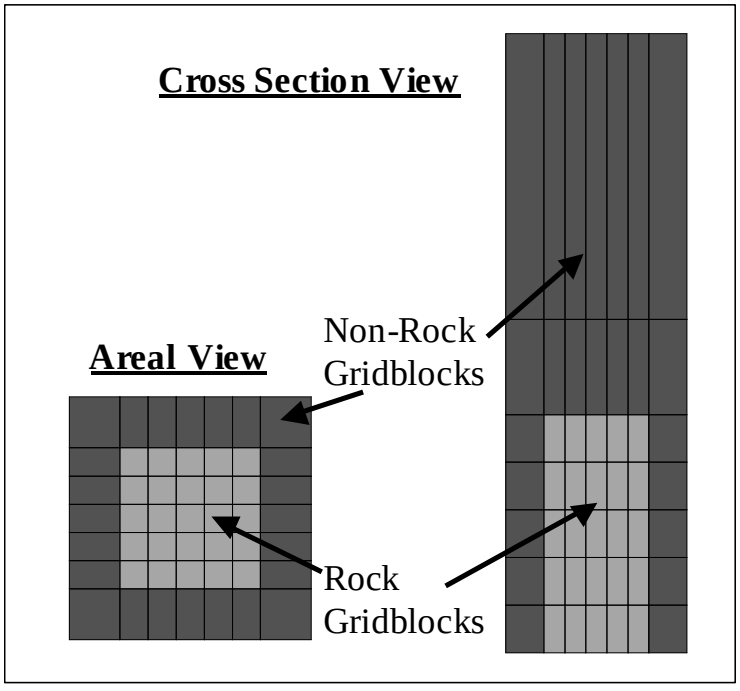

Fig. 4.2-2 View of Simulation Grid

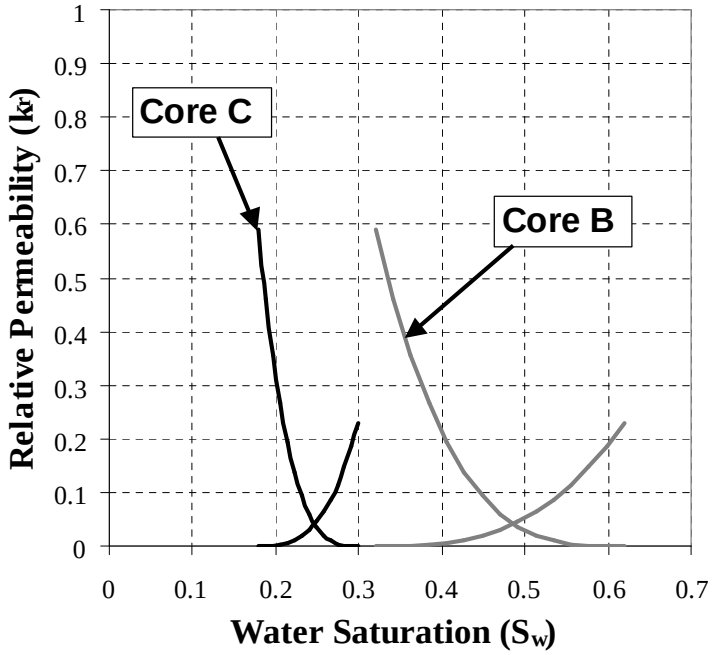

Fig. 4.2-3. Relative Permeability Curves for the Imbibition Simulations

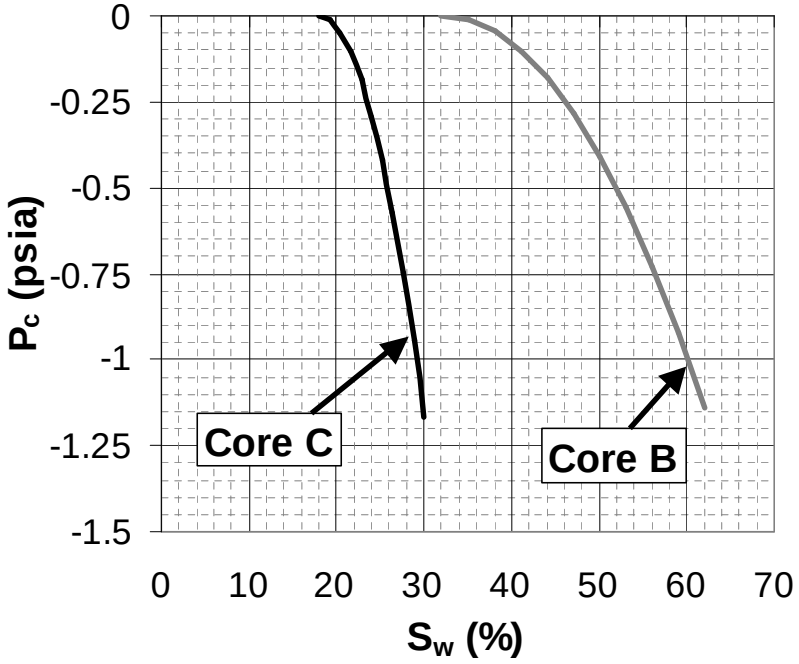

Fig. 4.2-4 Capillary Pressure Curve for the Imbibition Simulations

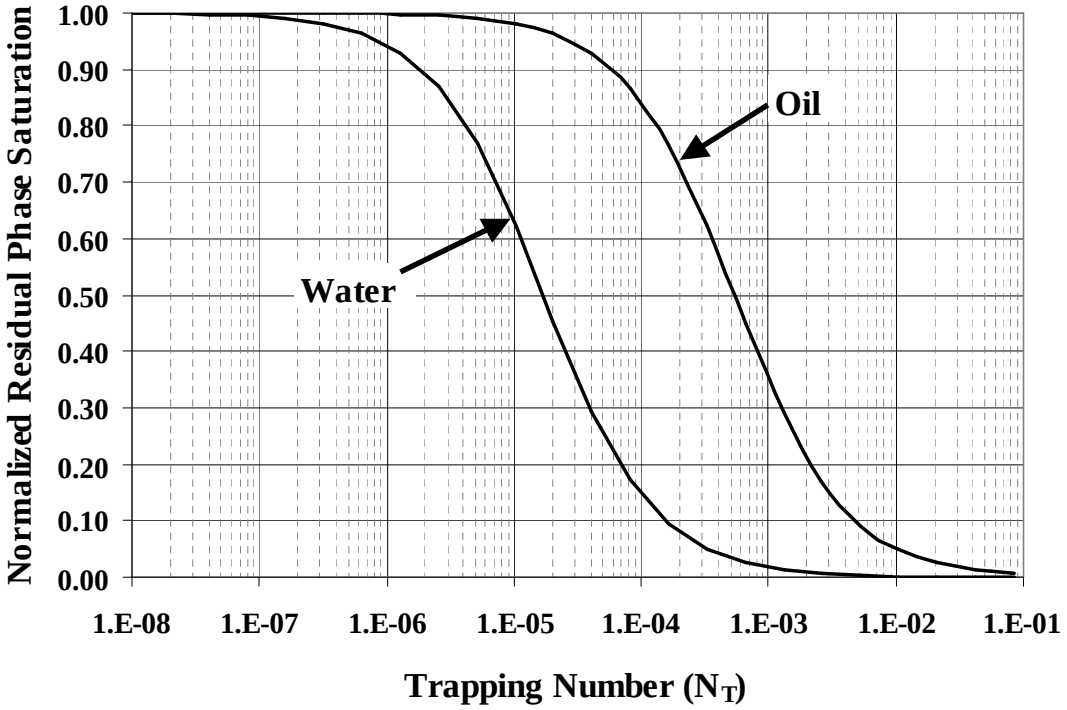

Fig. 4.2-5 Initial Oil Wet Capillary Desaturation Curve for the Imbibition Simulations

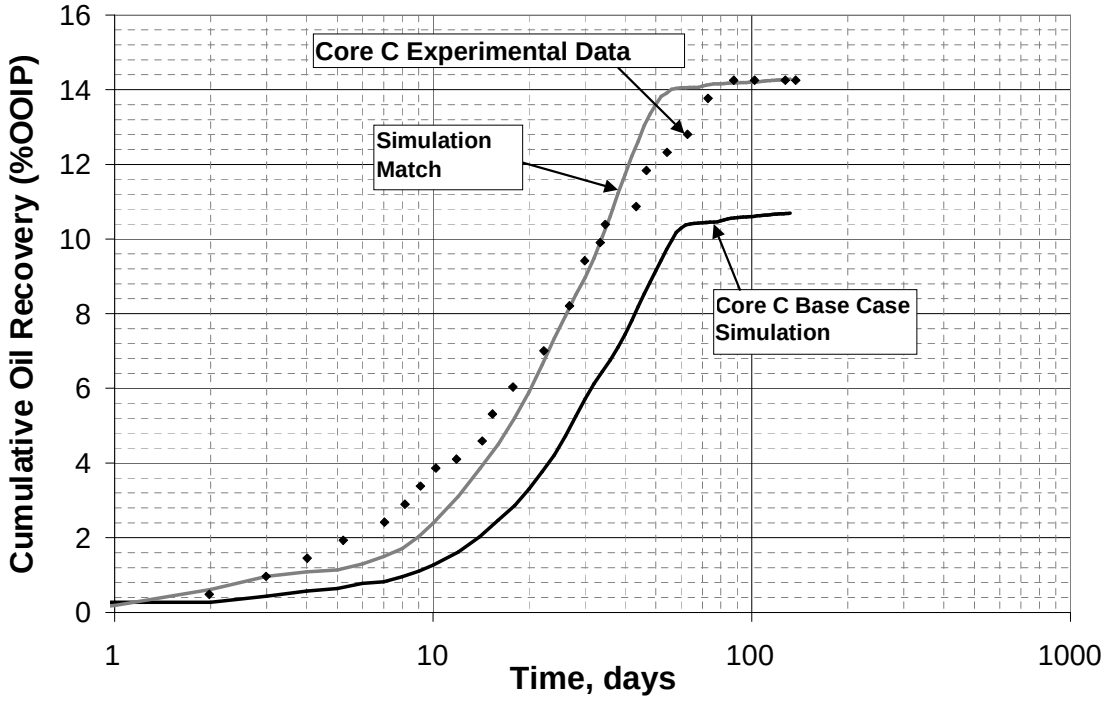

Fig. 4.2-6 Final Match for the Core C Simulation

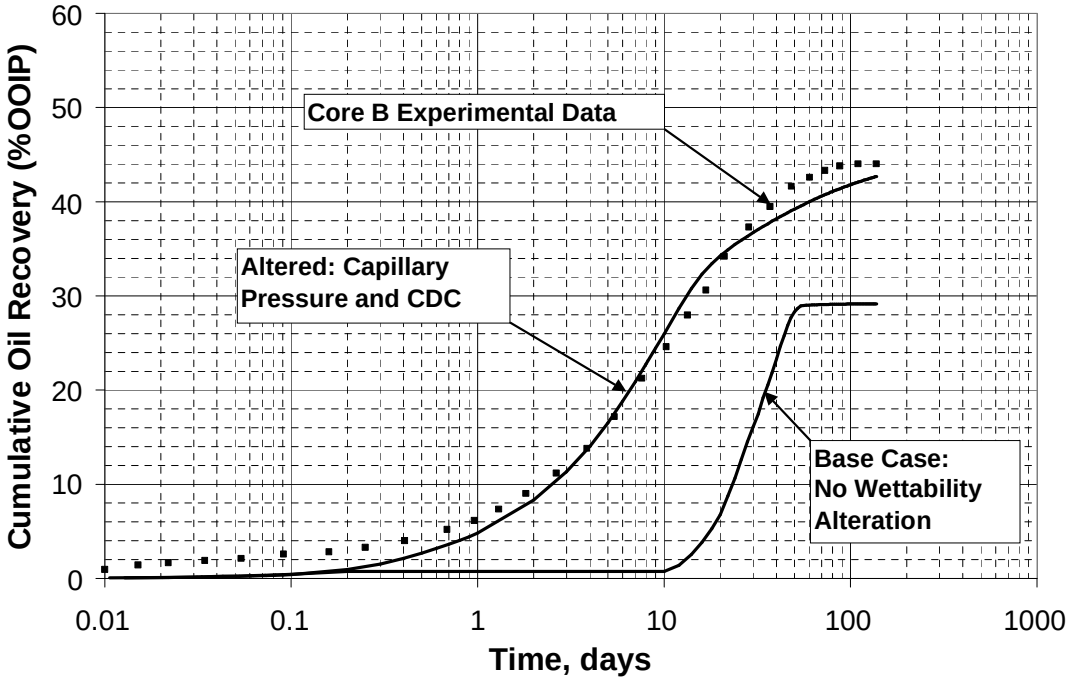

Fig. 4.2-7 Core B History Match

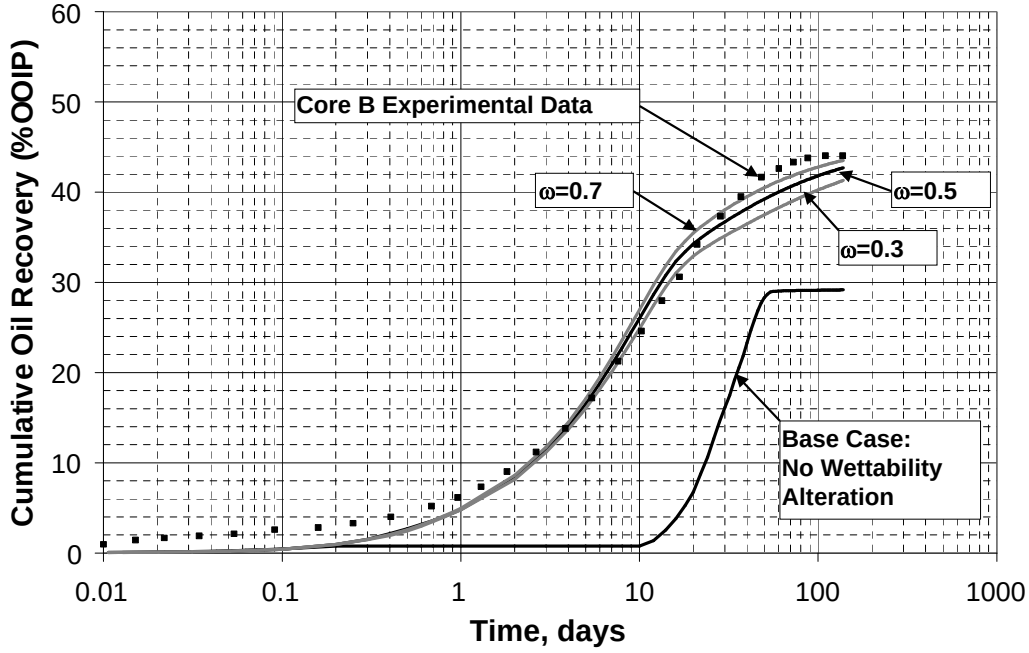

Fig. 4.2-8 Scaling Factor Sensitivity for Core B Simulations

Subtask 4.3 Field Scale Chemical Flooding with Effects of Reservoir Wettability

The purpose of this study was to determine the impact of wettability alteration on injectivity, sweep efficiency, and oil recovery for the heterogeneous carbonate reservoir. The reservoir is a mixed-wet dolomite within the Grayburg formation. The reservoir is currently undergoing waterflood recovery at a very high water cut. The reservoir also has a high remaining oil saturation and low reservoir pressure. This makes the reservoir a target for tertiary recovery. The reservoir is 4,700 feet deep, 100^{o}F, 100 feet thick, and has petrophysical properties indicative of a mixed-wet rock. A simulation model was developed according to these properties. The model was developed as a quarter 5-spot symmetry element with a pressure-constrained injector and producer. The symmetry element was based on a 40-acre well spacing, which is relatively large for chemical flooding. The field operator also provided the producer and injector well constraints (300 psi and 2,500 psi bottomhole, respectively), which were based on facility and reservoir fracture gradient limitations. The permeability field used in this model was developed by the field operator and is shown in Fig.4.3-1. As depicted in the figure, the reservoir is heterogeneous with high permeability layers in the middle and the top. The average post-waterflood saturations and pressure are listed in Table 4.3-1. Fluid properties are given in Table 4.3-2. Figure 4.3-2 shows the oil saturation distribution and the effect of the high permeability layers, which had the lowest post-waterflood oil saturation. A SP flood design was considered for this reservoir as given in Table 4.3-3.

The importance of simulating wettability alteration using this model is to study the effects of changes in mobility ratio, displacement efficiency, and injectivity in a non-fractured reservoir. As the use of chemical flooding spreads to new reservoirs, especially oil-wet and mixed-wet reservoirs, the importance of surfactant-based wettability alteration will become important, especially in naturally fractured reservoirs

The residual oil saturation, relative permeabilities, capillary pressure, and CDCs were adjusted to simulate different reservoir wettability conditions. The parameters used for the water-wet, mixed-wet, and oil-wet cases are provided in Table 4.3-4. The relative permeability curves are displayed in Figure 4.3-3. As depicted, the oil-wet case had the highest water relative permeability and lowest oil relative permeability. Conversely, the water-wet case had the lowest water relative permeability and highest oil relative permeability. The waterflood endpoint mobility ratios for these three scenarios are 1.3, 4.8, and 7.1 for the water-wet, mixed-wet, and oil-wet cases, respectively. The capillary pressure curves are shown in Figure 4.3-4. The water-wet capillary pressure curve had higher positive values and the oil-wet curve had negative values. The water CDCs for the three simulations are shown in Figure 4.3-5 and the oil CDCs in Figure 4.3-6.

4.3.1 Water-wet simulation

The first simulation analyzed was the case with water-wet properties. The water-wet simulation model was distinct because it had low water relative permeability, high oil relative permeability, high positive capillary pressure, and favorable CDCs. As

shown in Table 4.3-5, the breakthrough time was 0.08 PV (0.7 years). In addition, the surfactant breakthrough time was 0.26 PV (2.4 years).

The oil recovery and simulation length are also shown in Table 4.3-5. The water-wet case had a cumulative oil recovery of 33.8% OOIP and a simulation time of 33 years. The recovery for this simulation is quite high but the simulation time is extremely long. This occurrence is due to the loss of injectivity due to lower water relative permeability and low injection rates into the low permeability layers. A plot of the simulated injection rates is shown in Figure 4.3-7. In addition, plots of cumulative oil recovery, oil production rates, and produced surfactant concentration are shown in Figures 4.3-8 through 4.3-9.

4.3.2 Mixed-wet simulation

The next simulation was the case with mixed-wet properties. Compared to the water-wet case, the mixed-wet simulation model had slightly higher water relative permeability, lower waterflood residual oil saturation, lower oil relative permeability, low positive capillary pressure, and less favorable oil CDC. The results of this simulation are shown in Table 4.3-5. The oil bank breakthrough time was 0.13 PV (1.1 years) and the surfactant breakthrough time was 0.32 PV (2.8 years). The simulated oil breakthrough time was later than the water-wet case as expected.

The cumulative oil recovery and simulation length were 41.5% OOIP and 21 years, respectively. The oil recovery for this mixed-wet case was higher than the water-wet case and the simulation length was shorter. The primary reason for this result is the increase in injectivity as shown in Figure 4.3-7. A comparison of the cumulative oil recovery, oil production rates, and produced surfactant concentration are shown in Figures 4.3-8 through 4.3-10.

4.3.3 Oil-wet simulation

The last simulation with constant wettability was the case with oil-wet properties. Compared to the water-wet case, the oil-wet simulation model had higher water relative permeability, lower oil relative permeability, negative capillary pressure, and the least favorable oil CDC. Fractional flow theory predicted that this simulation would have the slowest oil bank breakthrough time. The results of this simulation are shown in Table 4.3-5. The oil bank breakthrough time was 0.24 PV (2.1 years) and the surfactant breakthrough time was 0.35 PV (3.1 years). The simulated breakthrough times were higher than the water-wet and mixed-wet cases as expected.

The cumulative oil recovery and simulation length were 31.2% OOIP and 20 years, respectively. The oil recovery for this oil-wet case was lower than the water-wet case and the simulation length was shorter. The primary reasons for the reduction in oil recovery are the less favorable mobility ratio and oil CDC. The reason for the reduction in simulation length was the increase in injectivity as shown in Figure 4.3-7. A comparison of the cumulative oil recovery, oil production rates, and produced surfactant concentration are shown in Figures 4.3-8 through 4.3-10.

4.3.4 Wettability alteration simulations

The next step for this study was to simulate an SP flood accounting for wettability alteration and compare to the results of the cases with constant wettability. The variations of wettability resulted in significant differences in oil recovery due to injectivity and sweep efficiency. The purpose of simulating wettability alteration was to test the modified UTCHEM simulator with a field scale application and to determine the importance of wettability alteration in a non-fractured reservoir.

Two pictures depicting the SP process in this quarter of a five-spot symmetry element are shown in Figures 4.3-11 and 4.3-12. Figure 4.3-11 is an areal view showing the oil bank, denuded zone, surfactant slug, and polymer drive between the injector and producer. The denuded zone was the region containing injected fluid that no longer contains chemicals due to adsorption or retention. Figure 4.3-12 shows the same fluid regions in a cross sectional view with a high permeability layer in the middle surrounded by low permeability layers on the top and bottom. This schematic was based on the permeability field of this reservoir model. It was also shown that the surfactant slug only partially invaded the low permeability layers. The primary difference between a simulation with wettability alteration and the one without was the rate at which the slug moves through the reservoir. The rate depends on the mobility ratio of the surfactant slug and the denuded water and the ratio of the denuded water and the oil bank. The water-wet case had more favorable mobility ratios compared to the oil-wet case. Therefore, the case with wettability alteration also had more favorable mobility ratios compared to the oil-wet case

The changes occurring during the wettability alteration process are expected to occur within the denuded zone. Within this zone, surfactant has invaded the gridblock and was adsorbed or retained. The presence of surfactant allows the model to alter the wettability within those gridblocks. Therefore, the wettability of the denuded zone would be water-wet for this study. As a result, the mobility ratio of the surfactant slug or polymer drive displacing the oil within the denuded zone would be lower compared to the original conditions. The wettability of the gridblocks swept by the surfactant slug and the polymer drive has also been altered to a water-wet condition. However, under ideal conditions, the oil saturation in these zones would be zero due to IFT reduction and capillary desaturation and the wettability is no longer important.

The UTCHEM input files for the wettability alteration simulations differ from those in the previous sections because wettability alteration parameters were required. In this section, two simulations were run. One simulation assumed a constant interpolation scaling factor (ω= 0.5) and the other simulation calculated the scaling factor based on the surfactant concentration and surfactant adsorption. The primary difference between these two cases was the rate at which the wettability was altered.

Relative permeability parameters, residual phase saturations, CDCs, and capillary pressure parameters representing the initial and final wettability condition were also required. For these two simulations, the initial condition parameters were assumed to be the same parameters as the oil-wet simulation and the final condition parameters were the water-wet parameters presented earlier. Therefore, high water

relative permeability, low oil relative permeability, negative capillary pressure, and an adverse oil CDC represented the initial reservoir conditions. The final or altered conditions were low water relative permeability, high oil relative permeability, positive capillary pressure, and a favorable oil CDC. Recall that the altered parameters are used within a gridblock once surfactant has reached the gridblock and its concentration exceeds CMC.

Compared to the constant oil-wet SP simulation, this wettability alteration simulation was expected to have a faster oil bank breakthrough time, lower residual oil saturation, and higher cumulative oil recovery. This was due to an expectation that the wettability of the reservoir swept by the surfactant slug and by the denuded surfactant front would be altered from oil-wet to water-wet. However, a decrease in injectivity was also expected.

The results of the two field scale wettability alteration simulations are provided in Table 4.3-6. In addition, plots of the injection rate, cumulative oil recovery, oil production rate, and produced surfactant concentration are shown in Figures 4.3-13 through 4.3-16. These figures also show the constant oil-wet and water-wet results for comparison. The changes in the results of the wettability alteration simulations were apparent in the injection rate and cumulative oil recovery. The differences were less apparent for the oil production rate and produced surfactant concentration.

An example areal profile of the simulated oil saturation is shown in Figure 4.32 for comparison with the schematic shown in Figure 4.3-11. Figure 4.3-17 shows that the oil saturation in the surfactant slug and polymer drive regions was zero. This is due to oil mobilization as a result of IFT reduction and capillary desaturation. The wettability alteration in this area is insignificant. However, the oil saturation within the denuded zone is non-zero and wettability alteration is significant.

The magnitude of changes in simulated injection rate was different for the two wettability alteration simulations. Both simulations had lower injection rates compared to the oil-wet case and higher rates compared to the water-wet case. Furthermore, the simulation with constant □ had higher injection rates than the variable □ case. This difference in injection rates was the reason for the variation in simulated project life. The primary cause of the changes in injection rate was rate of wettability alteration in the denuded zone. The equation used to calculate the interpolation scaling factor for the variable case is:

$$\omega = \frac{\hat{C}_{surf}}{\hat{C}_{surf} + C_{surf}}$$

where $\hat{C}_{surf}$ is the concentration of surfactant adsorbed in the gridblock and C_{surf} is the concentration of surfactant in the same gridblock. In the denuded zone, where the surfactant concentration was expected to be almost zero and the adsorbed concentration non-zero, □ would be close to 1. Conversely, □ was a value of 0.5 for the simulation with a constant scaling factor. Since, the initial and final conditions were the same for both simulations the variable scaling factor case would reach a water-wet state

faster within the denuded zone. Therefore, the water relative permeability would be lower ultimately causing lower injection rates.

Compared to the oil-wet and water-wet simulations in the previous section, both wettability alteration simulations had higher cumulative oil recovery. This result was similar to the mixed-wet case, which had the highest recovery. The two wettability alteration simulations had similar cumulative oil recovery. However, the case with constant □ had slightly higher recovery due to higher injectivity.

The oil production rate and produced surfactant concentration for the wettability alteration simulations were similar to the results of the oil-wet case. However, slight differences in breakthrough time of oil and surfactant are apparent in Figures 4.3-15 and 4.3-16 and are shown in Table 4.3-6. Both wettability alteration simulations had faster oil bank and surfactant breakthrough compared to the oil-wet case. This result can also be seen in the oil saturation profile comparisons (Figures 4.3-18, 4.3-20, and 4.3-22) and surfactant concentration profile comparisons (Figures 4.3-19, 4.3-21, and 4.3-23) at three different times. These profiles are areal views of layer 4 within the simulation model and the three times are 0.2, 0.35, and 0.85 pore volumes. Figure 4.3-18 shows that the front of the oil bank is closer to the producer in the wettability alteration simulations. These profile comparisons also depict differences in the size of the oil bank, size of the denuded zone, distance of invaded surfactant, and final oil saturation.

Table 4.3-1. Reservoir and Simulation Model Properties

Model physical dimensions	700' x 800' x 99.1'
Depth	4,700 feet
Porosity	Average = 0.16 Min = 0.06 Max = 0.273
Permeability	Average =156 md Min = 4.4 md Max = 870 md k_v/k_h = 0.05
Simulation model pore volume	1.610 MMbbl
Simulated post waterflood average saturations	Water = 0.53 Oil = 0.47
Simulated post waterflood oil in place	0.75 MMbbl
Simulated post waterflood average reservoir pressure	755 psi

Table 4.3-2. Fluid Properties

Density	Oil = 31 °API (0.87 g/ml) Water = 1 g/cc
Viscosity	Water = 0.72 cp Oil = 5 cp
Brine composition	Overall = 1 meq/mL Ca^{+2} = 2,066 ppm Mg^{+2} = 539 ppm Na^{+} = 20,533 ppm SO_4^{-2} = 4,540 ppm Cl^{-} = 32,637 ppm

Table 4.3-3. Base Case SP Design

Injection well constraints	Rate constraint = 2,000 bbl/day[1] Pressure control = 2,500 psi
Production well constraint	Pressure constraint = 300 psi
Surfactant slug	0.25 PV 1 vol% surfactant 1,000 ppm polymer 0.365 meq/mL (21,000 ppm TDS)
Polymer drive	1 PV 1,000 ppm polymer 0.2 meq/mL (11,700 ppm TDS)
Water postflush	0.5 PV 0.04 meq/mL (2,300 ppm TDS)
Surfactant adsorption	0.3 mg surfactant/g rock
Polymer adsorption	10 μg polymer/g rock
Capillary desaturation parameters	Water = 1,865 Oil = 59,074
Vertical permeability	k_v/k_h = 0.05

[1]Rate constraint is for full 5-spot pattern

Table 4.3-4. Properties for Constant Wettability Simulations

Case	Property	Value
Water-Wet	Waterflood Residual Oil Saturation	0.45
	Water Endpoint Relative Permeability	0.15
	Oil Endpoint Relative Permeability	0.8
	Water Relative Permeability Exponent	3
	Oil Relative Permeability Exponent	2
	Capillary Pressure Endpoint	6
	Capillary Pressure Exponent	2
	Water Trapping Parameter	1865
	Oil Trapping Parameter	59074
Mixed-Wet	Waterflood Residual Oil Saturation	0.4
	Water Endpoint Relative Permeability	0.4
	Oil Endpoint Relative Permeability	0.6
	Water Relative Permeability Exponent	2
	Oil Relative Permeability Exponent	2
	Capillary Pressure Endpoint	3
	Capillary Pressure Exponent	2
	Water Trapping Parameter	10000
	Oil Trapping Parameter	10000
Oil-Wet	Waterflood Residual Oil Saturation	0.45
	Water Endpoint Relative Permeability	0.5
	Oil Endpoint Relative Permeability	0.5
	Water Relative Permeability Exponent	2
	Oil Relative Permeability Exponent	2
	Capillary Pressure Endpoint	-3
	Capillary Pressure Exponent	2
	Water Trapping Parameter	59074
	Oil Trapping Parameter	1865

Table 4.3-5. Results of the Constant Wettability Simulations

Case	Oil B.T. (PV/Yr)		Surf B.T. (PV/Yr)		Cum. Oil Rec. (%OOIP)	Sim. Length (years)
	PV	Year	PV	Year		
Water-Wet	0.08	0.7	0.26	2.4	33.8%	33
Mixed-Wet	0.13	1.1	0.32	2.8	41.5%	21
Oil-Wet	0.24	2.1	0.35	3.1	31.2%	20

Table 4.3-6. Results of the Simulations with Wettability Alteration

Case	Oil B.T. (PV/Yr)		Surf B.T. (PV/Yr)		Cum. Oil Rec. (%OOIP)	Sim. Length (years)
	PV	Year	PV	Year		
Const. ω	0.19	1.7	0.33	2.9	37.8%	23
Varia. ω	0.2	1.8	0.32	2.8	36.9%	28

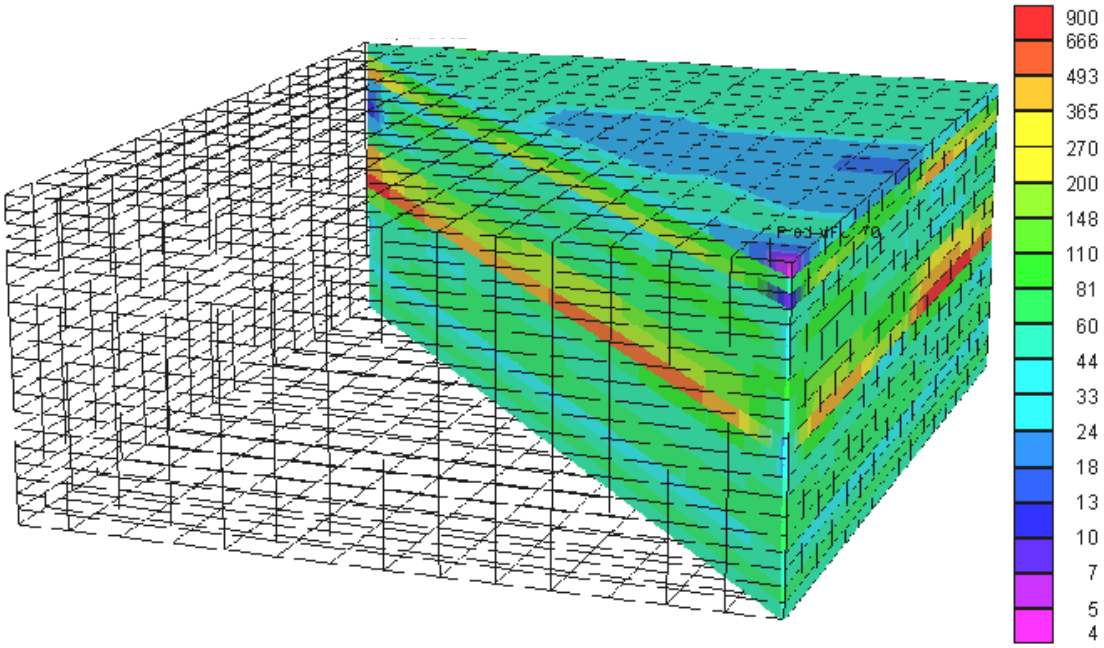

Fig. 4.3-1. Simulation Model Permeability (md)

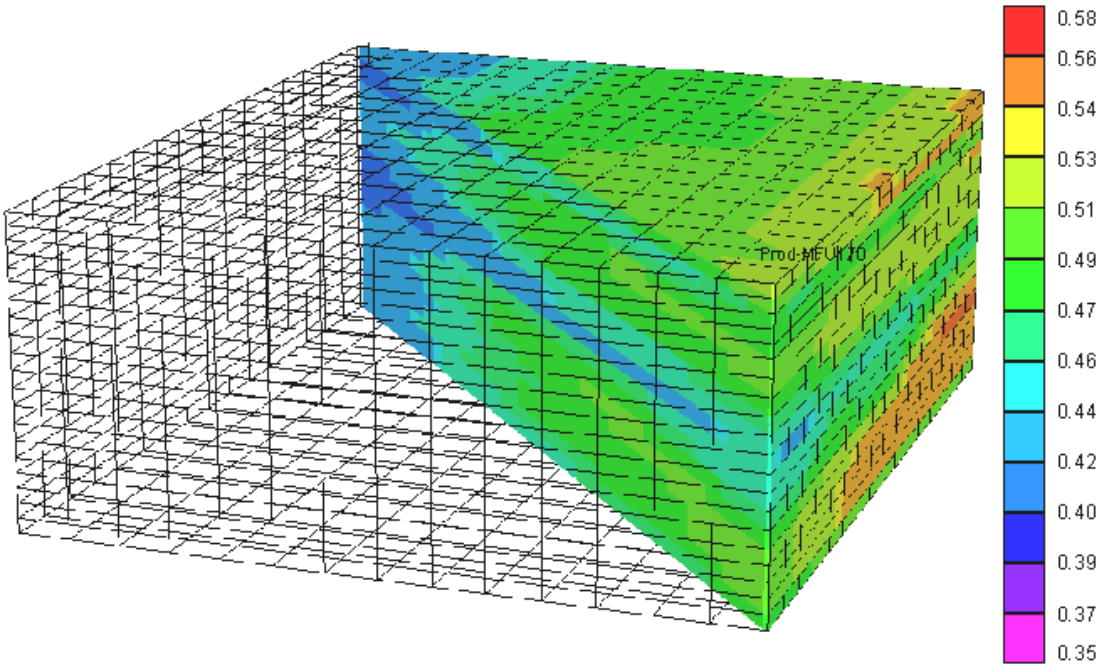

Fig. 4.3-2. Simulation Model Initial Oil Saturation

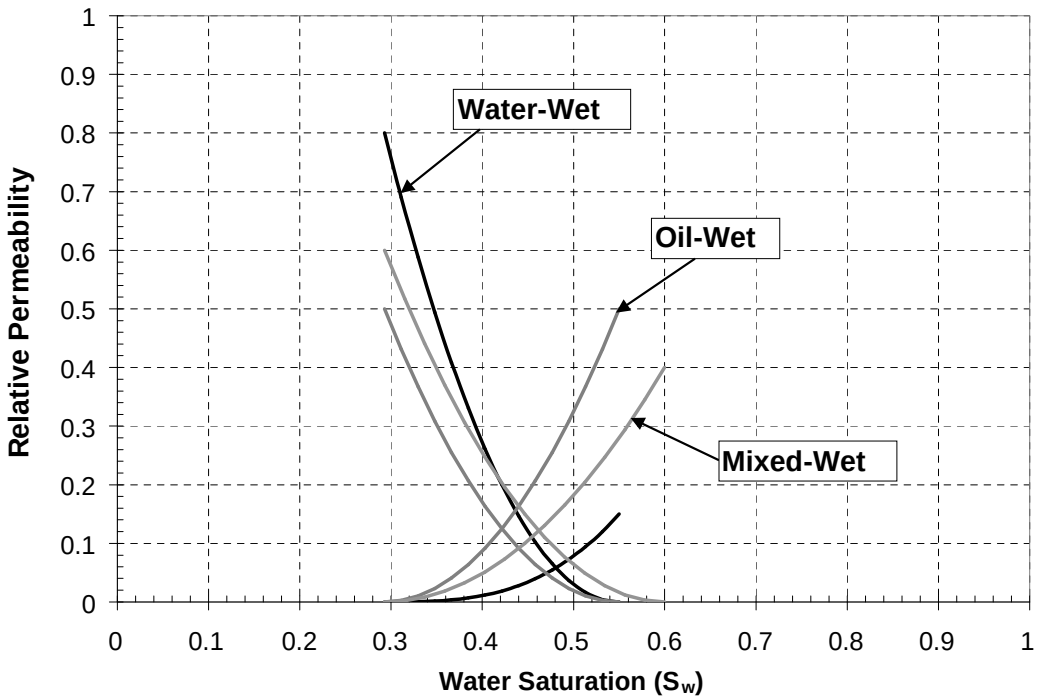

Fig. 4.3-3. Relative Permeability Curves for Constant Wettability Simulations

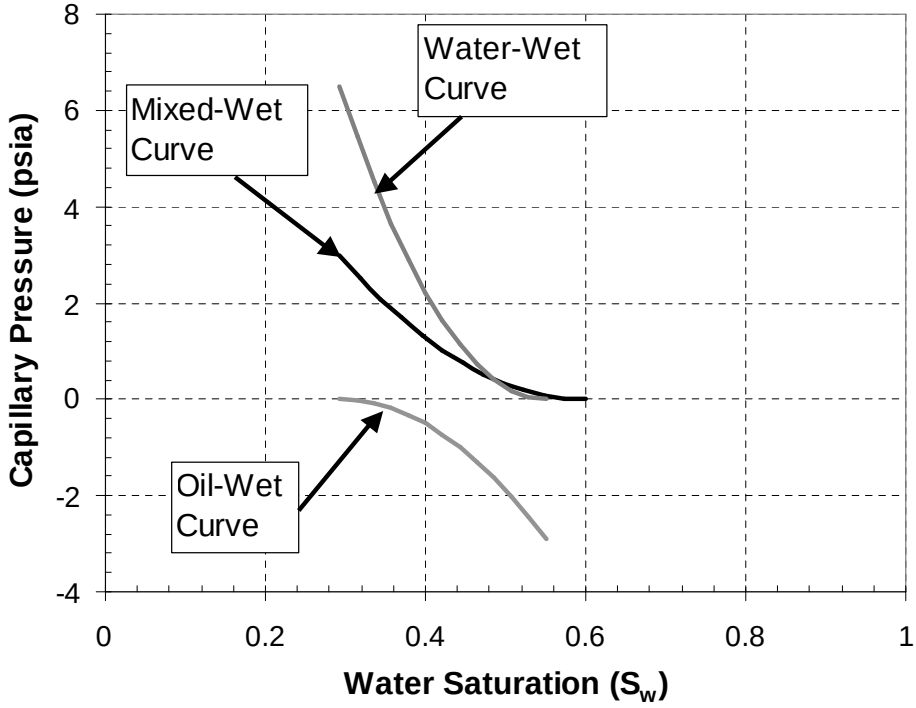

Fig. 4.3-4. Capillary Pressure Curves for Constant Wettability Simulations

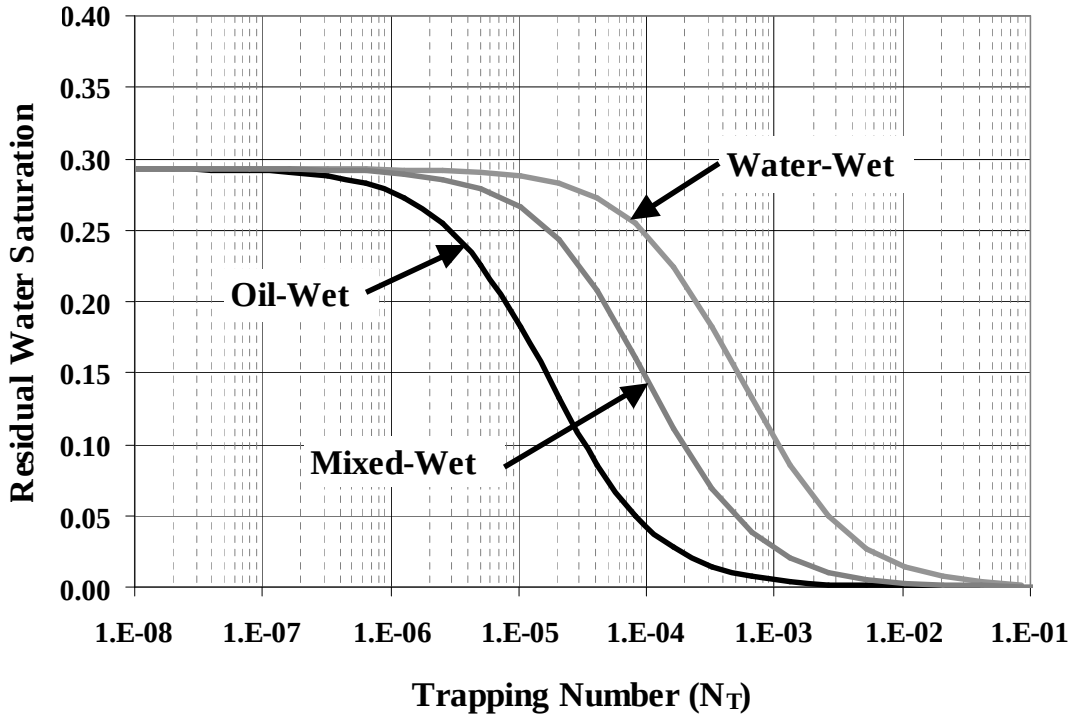

Fig. 4.3-5. Water CDCs for Constant Wettability Simulations

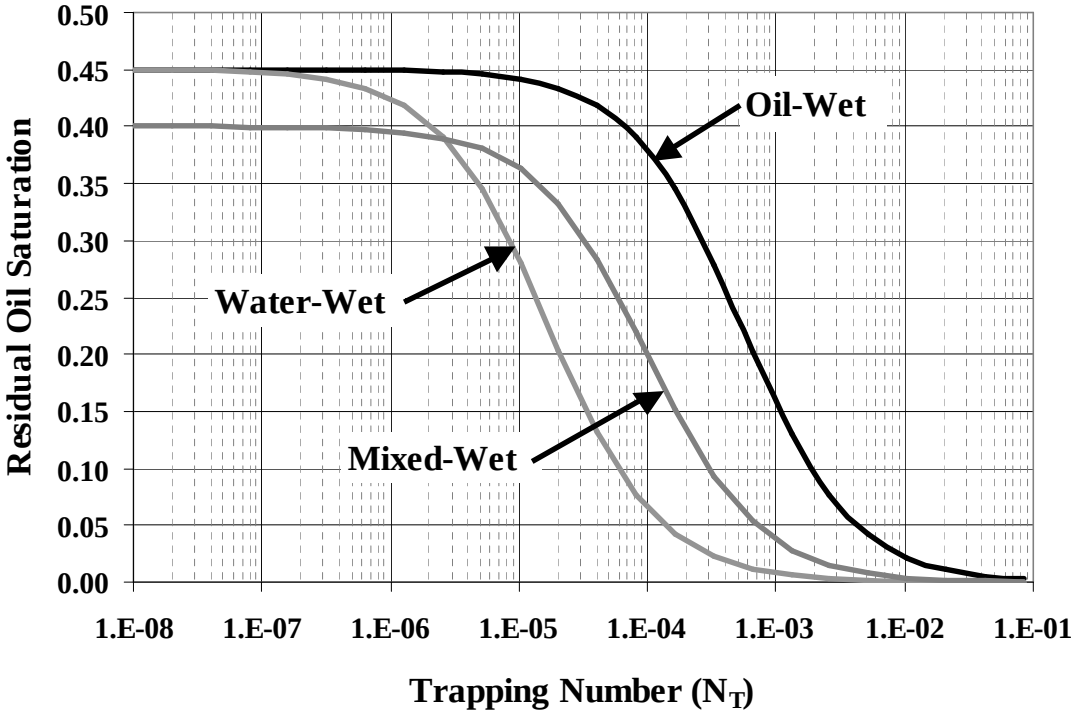

Fig. 4.3-6. Oil CDCs for Constant Wettability Simulations

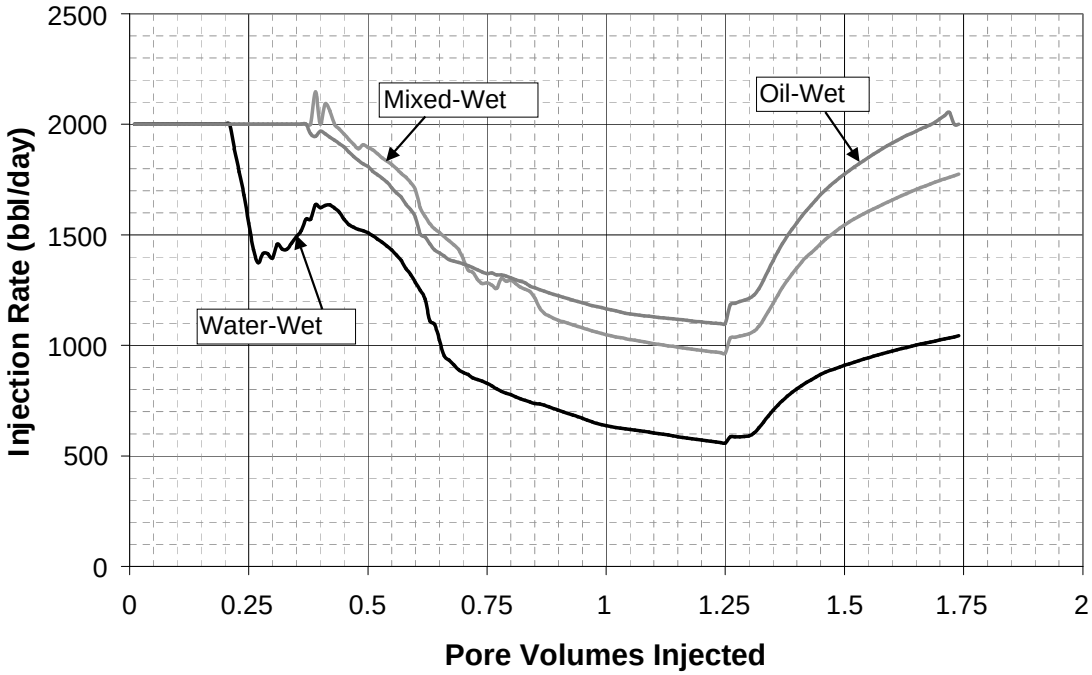

Fig. 4.3-7. Injection Rates for Constant Wettability Simulations

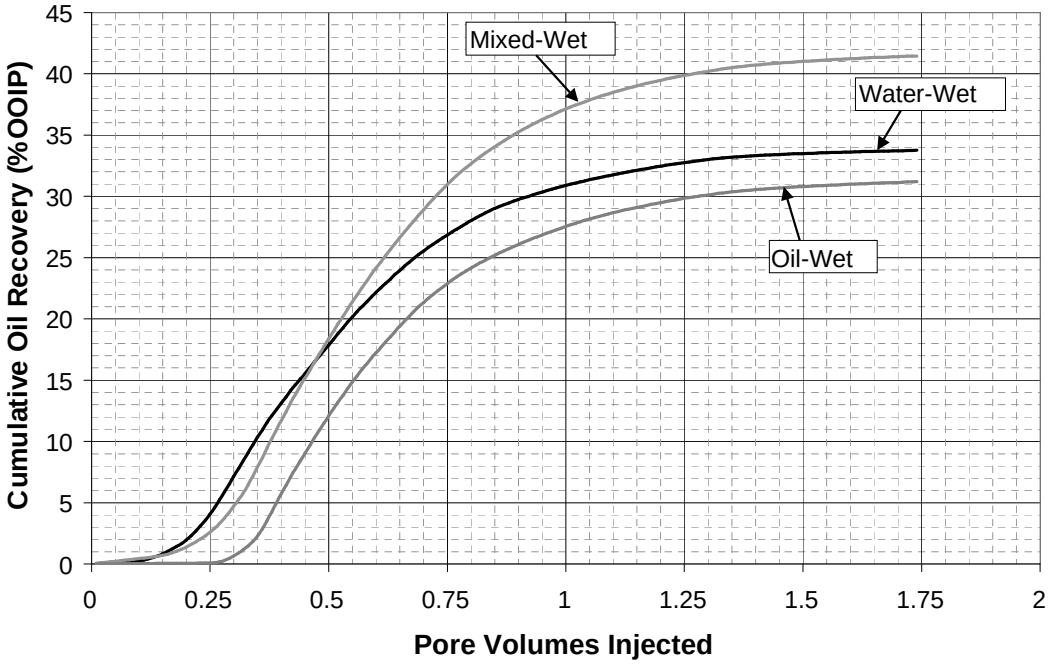

Fig. 4.3-8. Cumulative Oil Recovery for Constant Wettability Simulations

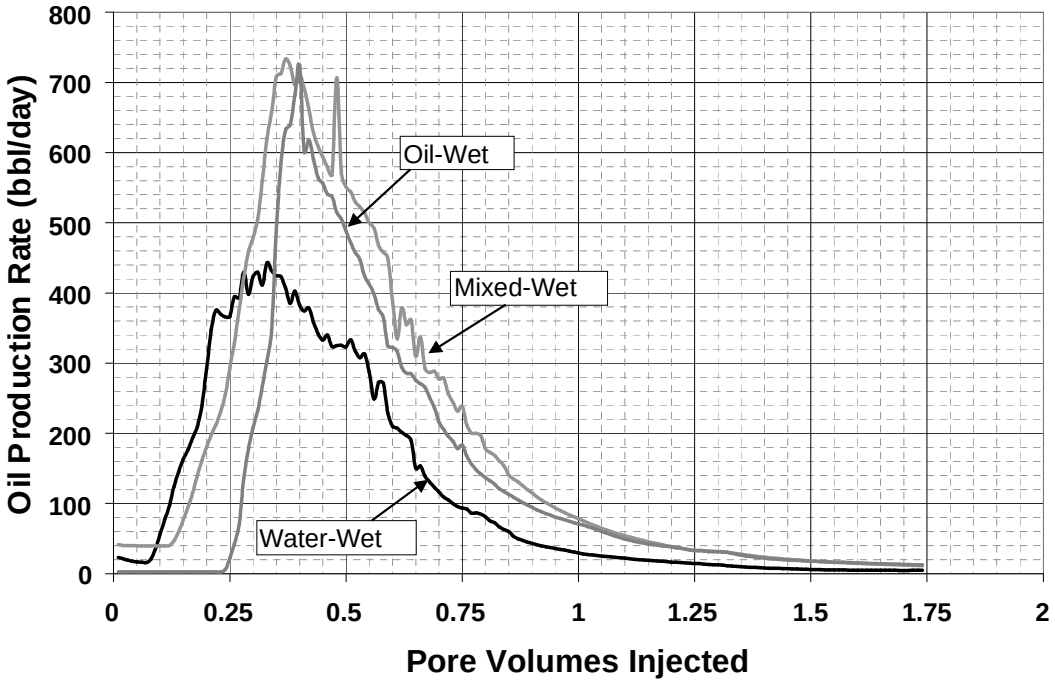

Fig. 4.3-9. Oil Production Rate for Constant Wettability Simulations

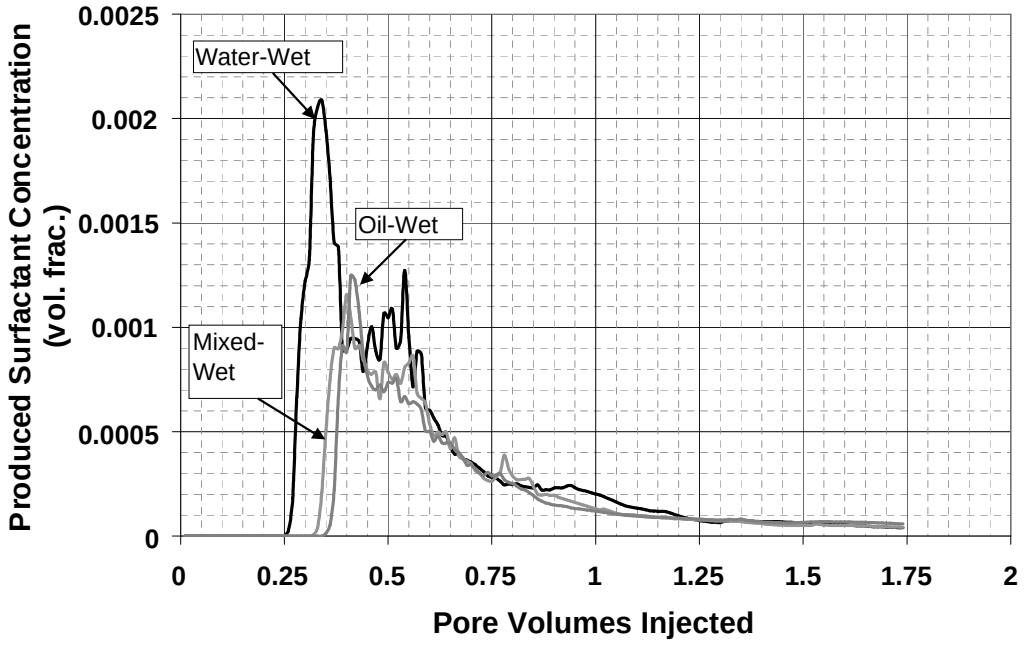

Fig. 4.3-10. Produced Surf. Conc. for Constant Wettability Simulations

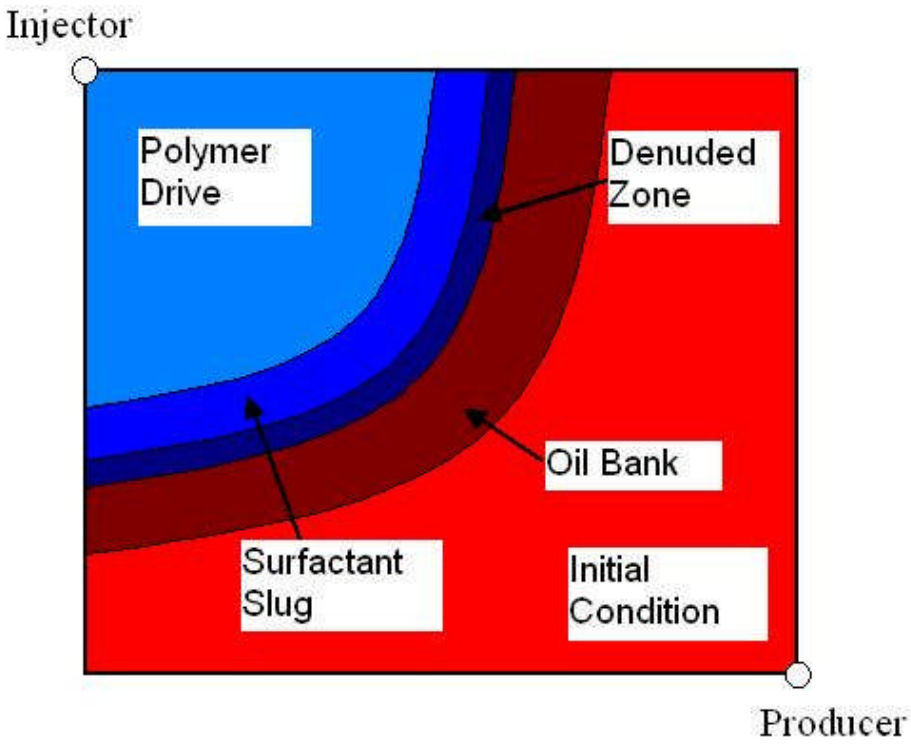

Fig. 4.3-11. Areal Schematic of the SP Process

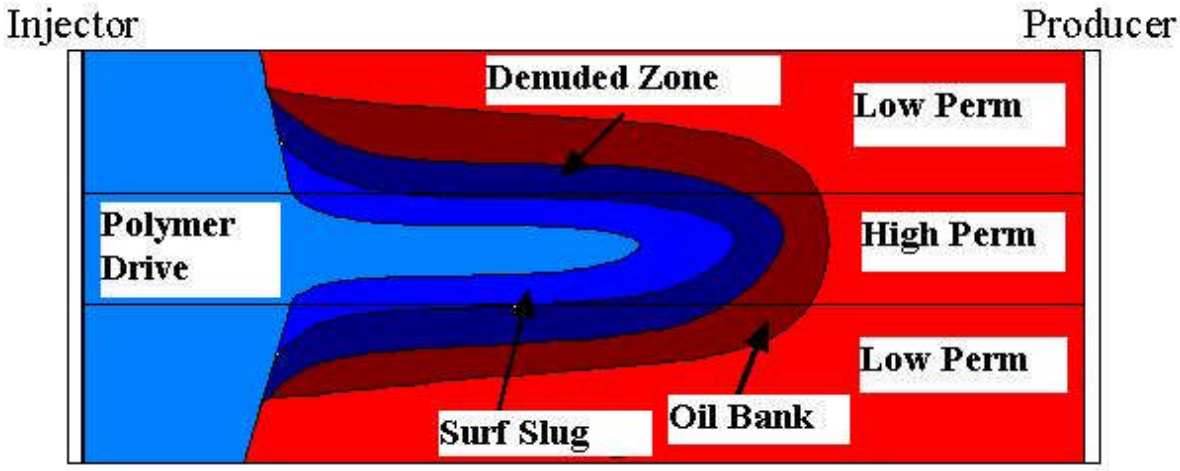

Fig. 4.3-12. Cross Section Schematic of the SP Process

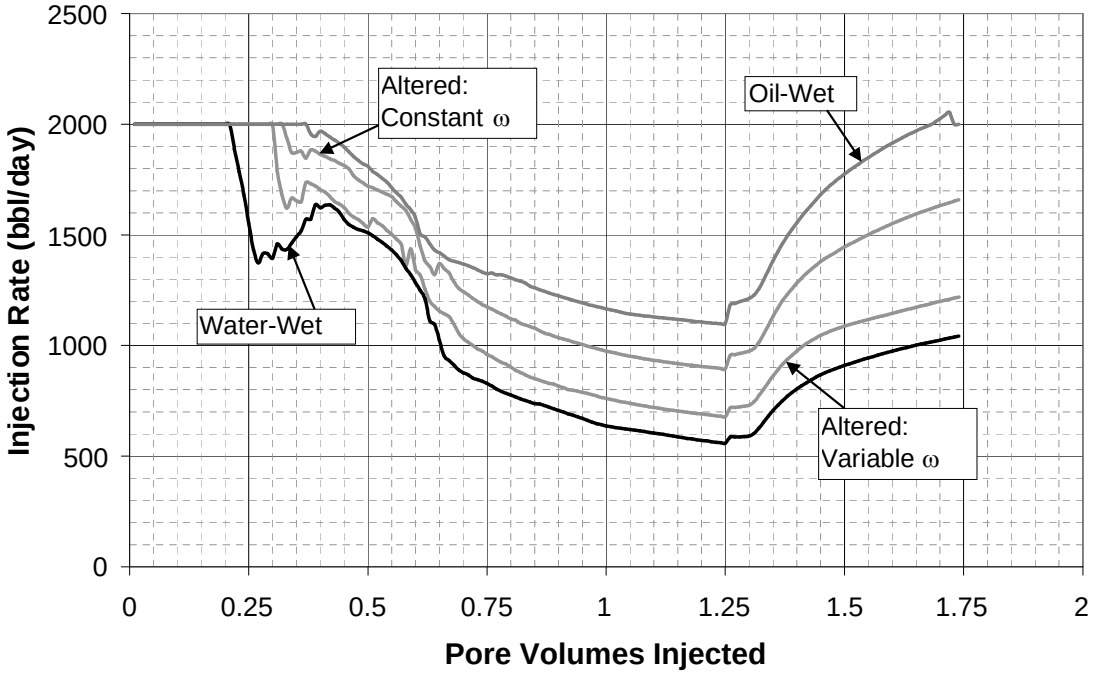

Fig. 4.3-13. Injection Rates for Wettability Alteration Simulations

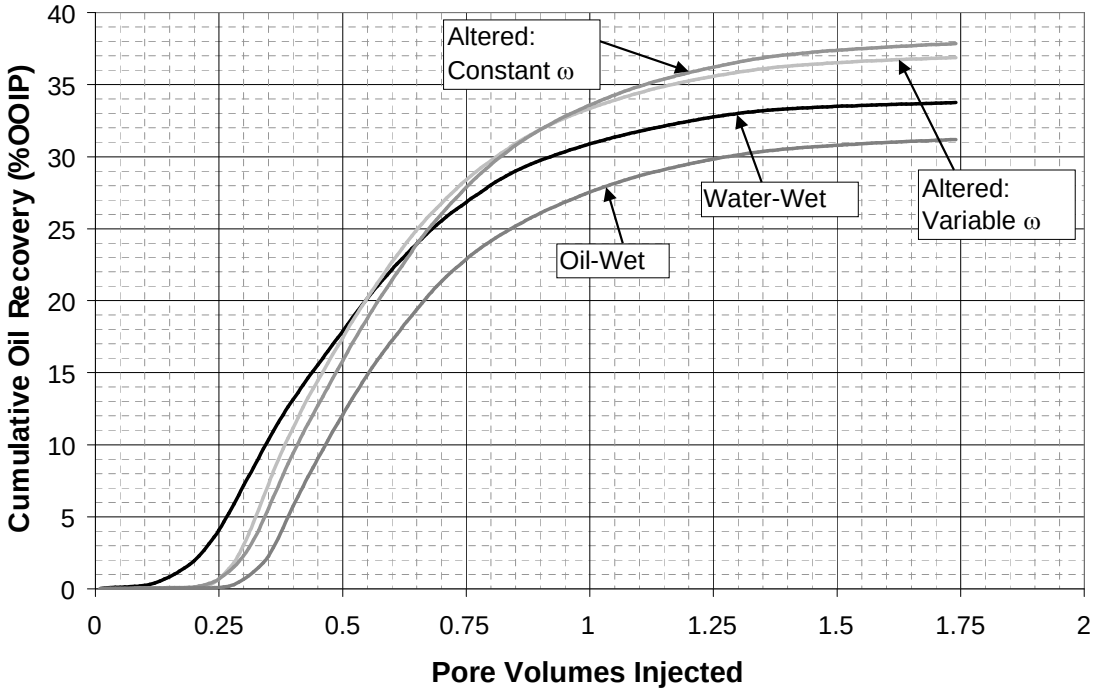

Fig. 4.3-14. Cumulative Oil Recovery for Wettability Alteration Simulations

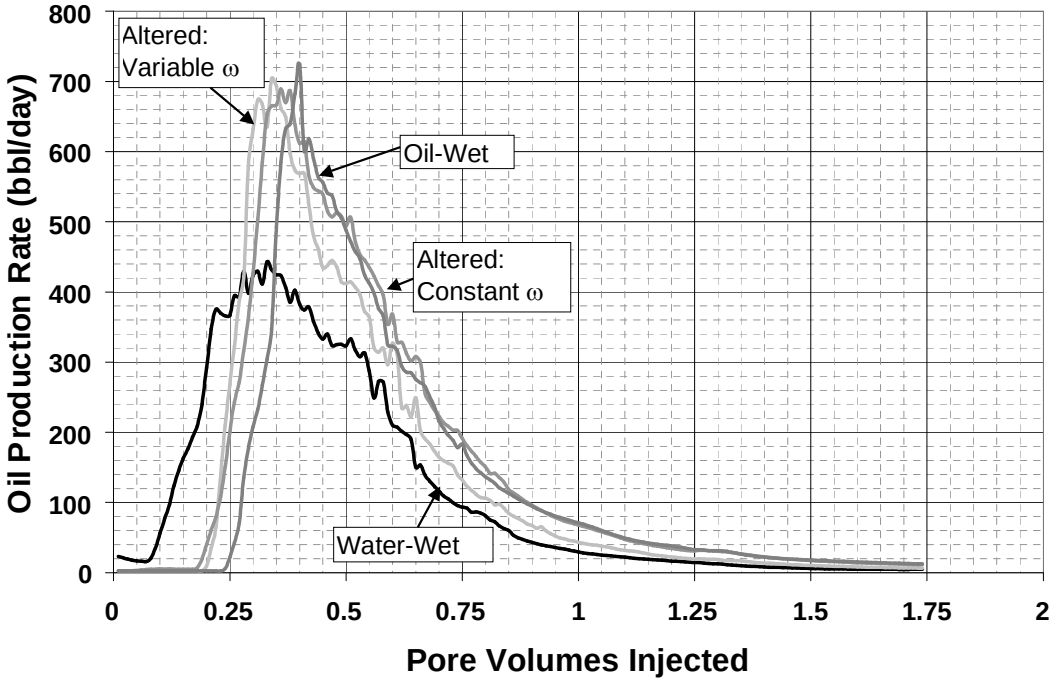

Fig. 4.3-15. Oil Production Rates for Wettability Alteration Simulations

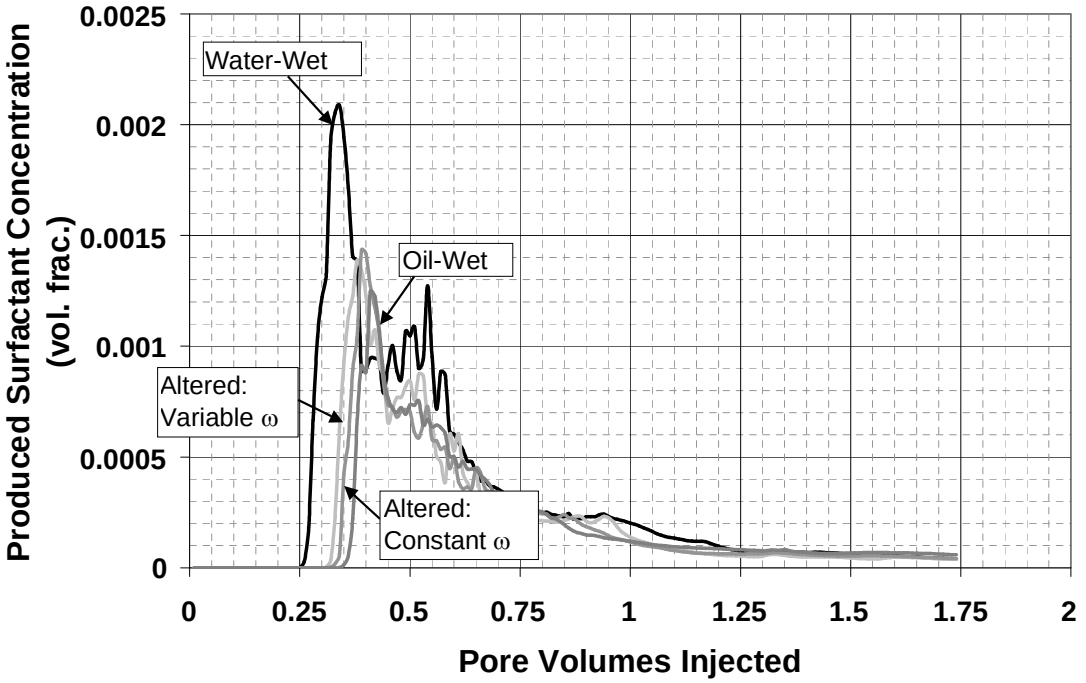

Fig. 4.3-16. Produced Surf. Conc. for Wettability Alteration Simulations

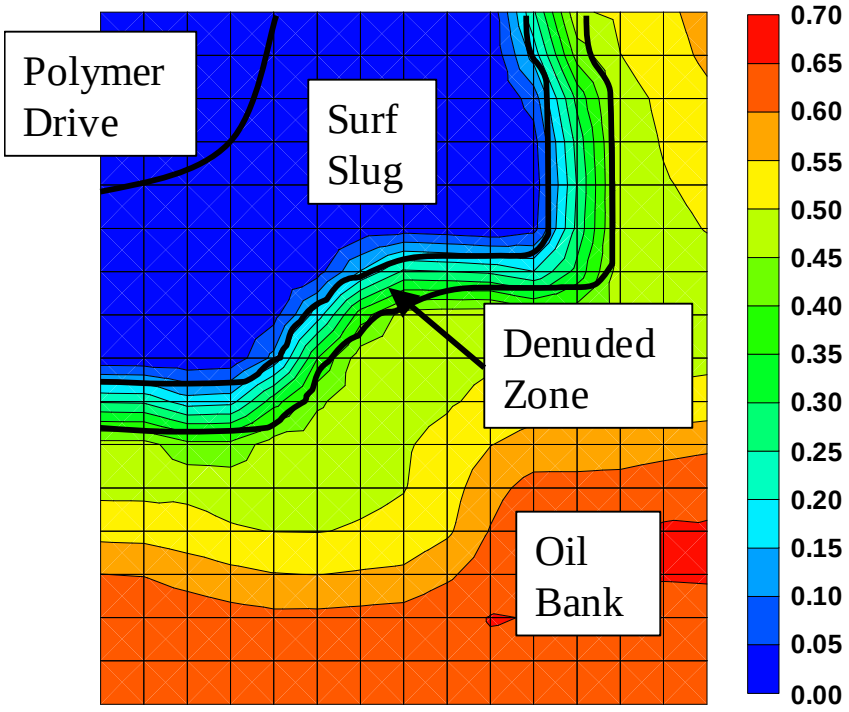

Fig. 4.3-17. Example Oil Saturation Profile

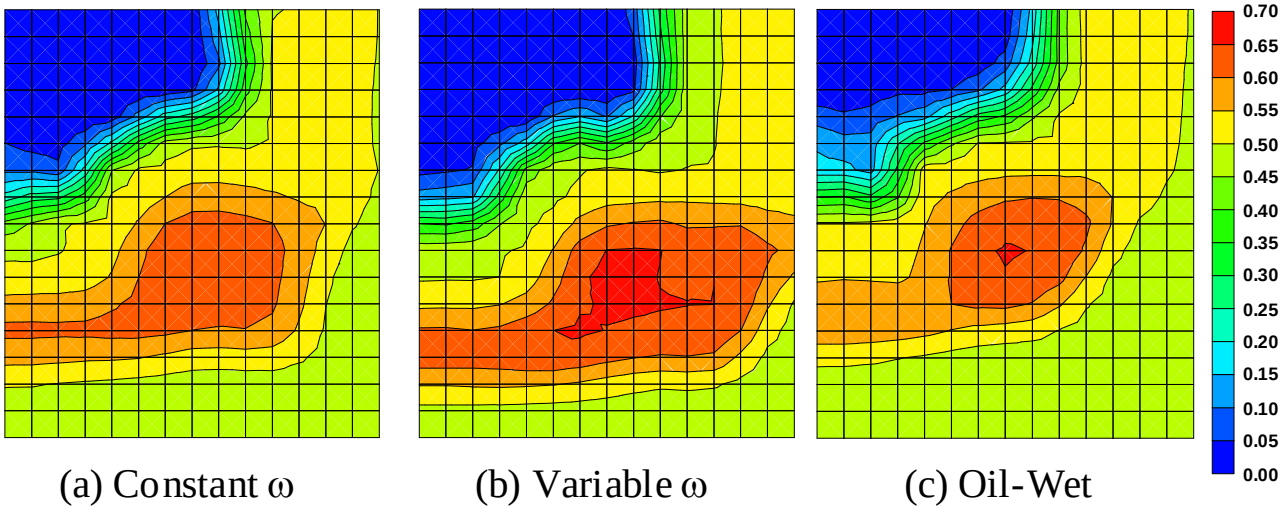

(a) Constant ω (b) Variable ω (c) Oil-Wet

Fig. 4.3-18. Comparison of Oil Saturation at 0.2 PV in Layer 4

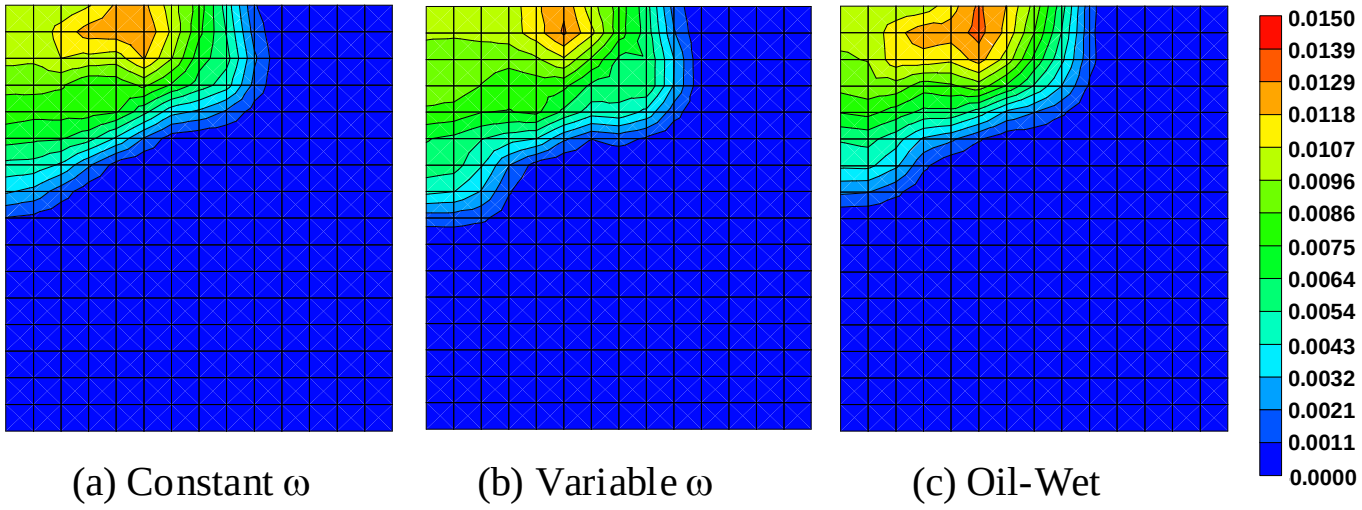

Fig. 4.3-19. Comparison of Surf. Conc. (vol frac) at 0.2 PV in Layer 4

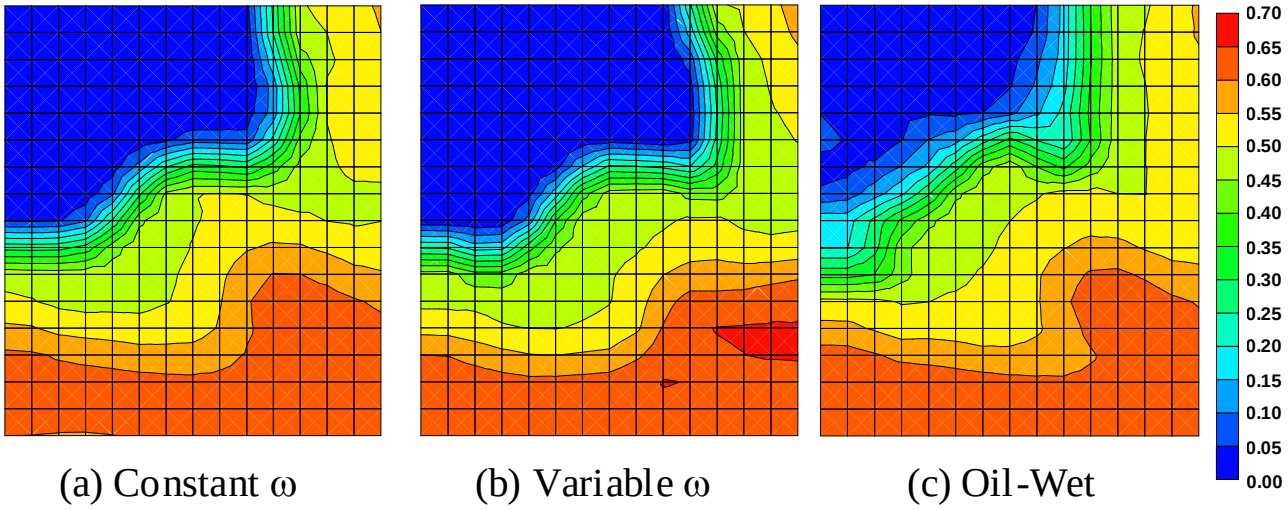

Fig. 4.3-20. Comparison of Oil Saturation at 0.35 PV in Layer 4

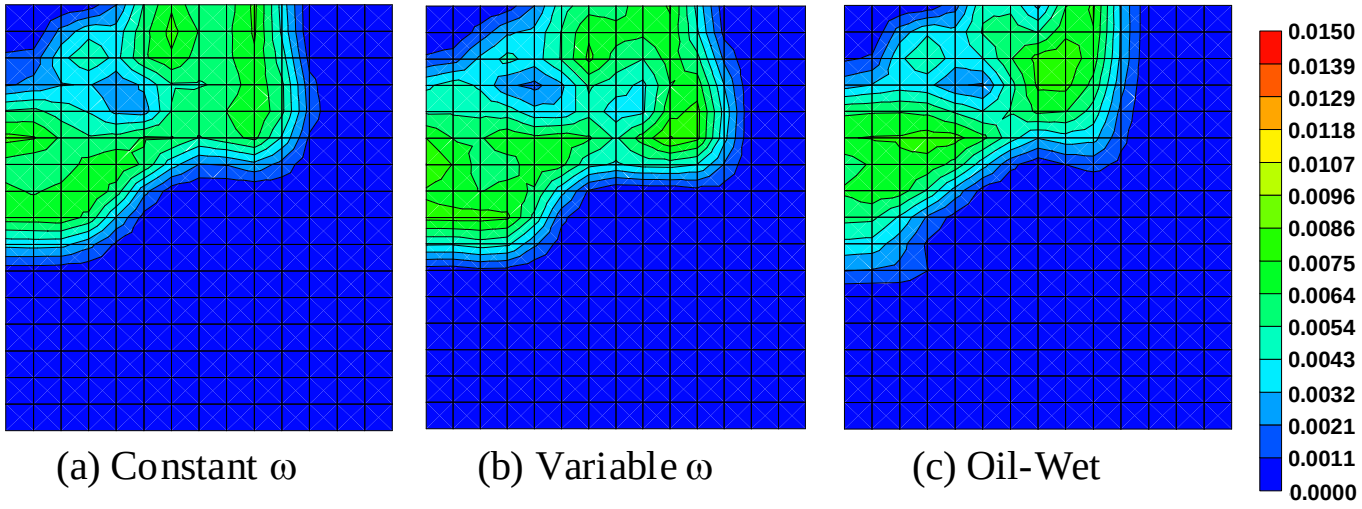

Fig. 4.3-21. Comparison of Surf. Conc. (vol frac) at 0.35 PV in Layer 4

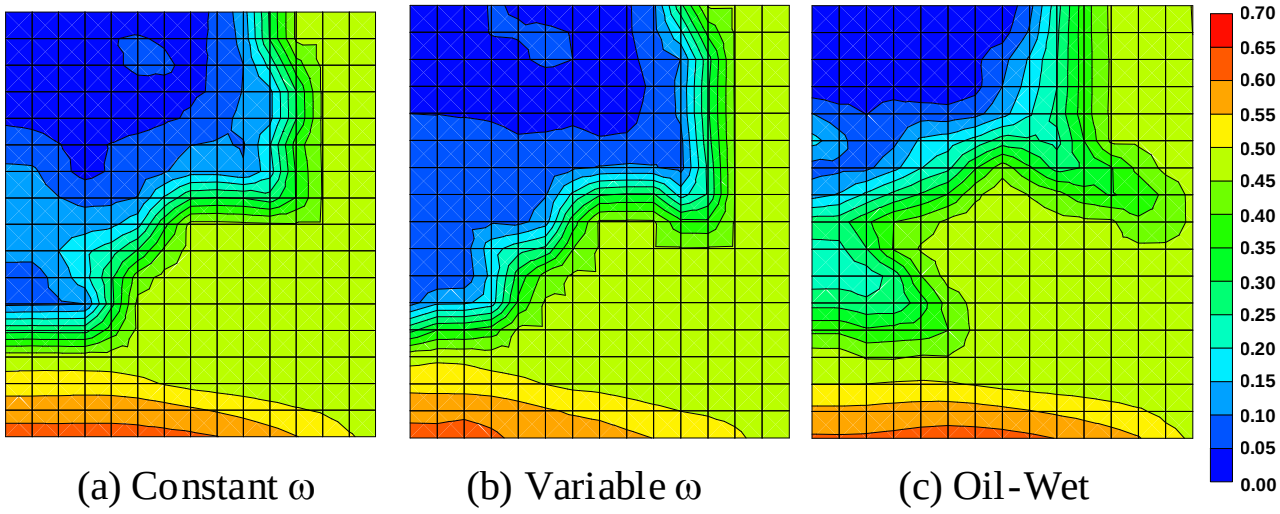

Fig. 4.3-22. Comparison of Oil Saturation at 0.85 PV in Layer 4

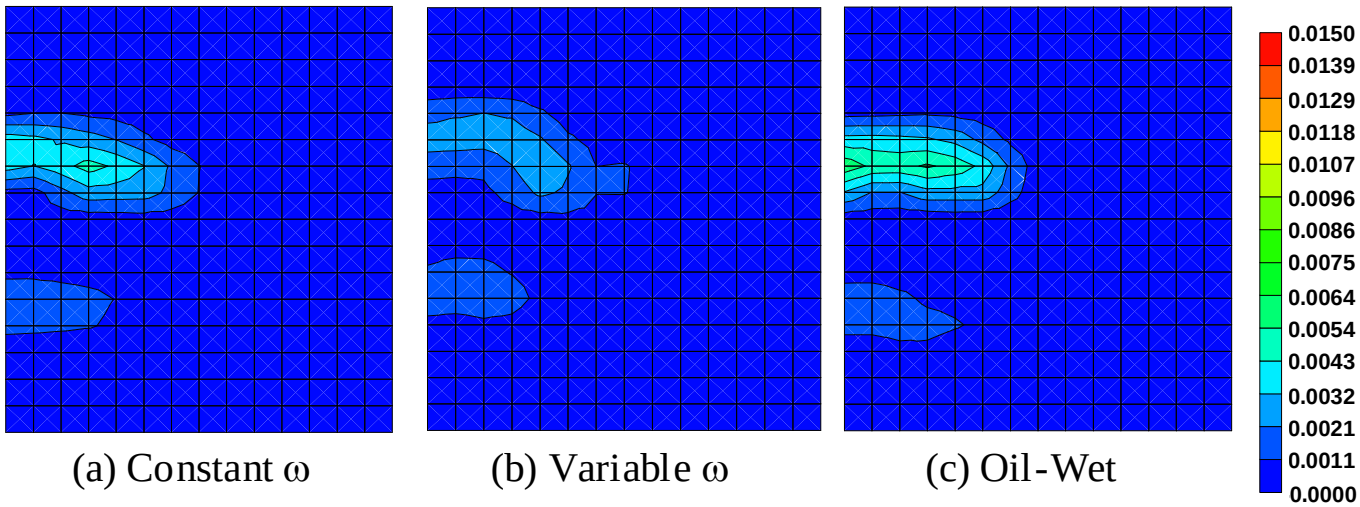

Fig. 4.3-23. Comparison of Surf. Conc. (vol frac) at 0.85 PV in Layer

Summary

Laboratory surfactant have shown a great potential in increasing oil recovery for reservoirs that are naturally fractured and have low permeability mixed-wet matrix rocks. Fractured, mixed-wet formations usually have poor waterflood performance because the injected water tends to flow in the fractures and spontaneous imbibition into the matrix is not very significant. Surfactants have been used to change the wettability for increasing the oil recovery by increased imbibition of the water into the matrix rock. The mechanisms for oil recovery are combined effects of reduced interfacial tension, reduced mobility ratio, and wettability alteration. The goal of this task was to adapt an existing numerical reservoir simulator to model chemical processes that lead to wettability alteration in naturally fractured reservoirs. Surfactants have been used to change the wettability with the goal of increasing the oil recovery by increased imbibition of the water into the matrix rocks. Reservoir simulation is required to scale up the process from laboratory to field conditions and to understand and interpret reservoir data. We have

adapted the chemical flooding simulator, UTCHEM, to model improved oil recovery processes that involve wettability alteration using surfactants. Multiple relative permeability and capillary pressure curves corresponding to different wetting states are used to model the wettability alteration. Simulations were performed to better understand and predict enhanced oil recovery as a function of wettability alteration and to investigate the impact of uncertainties in the fracture and matrix properties, reservoir heterogeneity, matrix diffusion, buoyancy driven flow, initial water saturation, and formation wettability.

To validate the wettability model and the implementation in the simulator, the laboratory alkaline/surfactant imbibition experiments conducted at Rice University were successfully modeled with UTCHEM. Three-dimensional simulations were then performed to determine the impact of wettability alteration on injectivity, sweep efficiency, and oil recovery for a heterogeneous carbonate reservoir. The importance of simulating wettability alteration using this model is to study the effects of changes in mobility ratio, displacement efficiency, and injectivity in a non-fractured reservoir. The results indicated the impact of wettability on fluid breakthrough times, oil production rate for the surfactant flooding process.

As the use of chemical flooding spreads to new reservoirs, especially oil-wet and mixed-wet reservoirs, the importance of surfactant-based wettability alteration will become important, especially in naturally fractured reservoirs.

Nomenclature

D = Depth, L

g = Gravitational constant, Lt^{-2}

$\vec{\vec{k}}$ = Permeability tensor, L^2

$k_{r\ell}$ = Relative permeability of phase ℓ

$k_{r\ell}^{o}$ = Endpoint relative permeability of phase ℓ

$k_{r\ell}^{o\,high}$ = Phase ℓ endpoint relative permeability at high trapping number

$k_{r\ell}^{o\,low}$ = Phase ℓ endpoint relative permeability at low trapping number

e_{ℓ}^{high} = Phase ℓ relative permeability exponents at high trapping number

e_{ℓ}^{low} = Phase ℓ relative permeability exponents at low trapping number

N_{T_ℓ} = Trapping number of phase ℓ

P_c = Capillary Pressure, $mL^{-1}t^{-2}$

P_{cow} = oil-water capillary pressure, $mL^{-1}t^{-2}$

S_ℓ = Saturation of phase ℓ, L^3/L^3 PV

$S_{\ell r}$ = Residual saturation of phase ℓ, L^3/L^3 PV

$S_{\ell r}^{high}$ = Residual saturation of phase ℓ at high N_T, L^3/L^3 PV

$s_{\ell r}^{low}$ = Residual saturation of phase ℓ at low N_T, L^3/L^3 PV

T_ℓ = Trapping parameter for phase ℓ

Greek Symbols

$\vec{\nabla}\Phi_{\ell'}$ = Flow potential gradient given by $\vec{\nabla}P_{\ell'} - g\,\rho_{\ell'}\vec{\nabla}D$

ρ_ℓ = Density of phase ℓ, mL^{-3}

$\sigma_{\ell\ell'}$ = Interfacial tension between phases ℓ and ℓ', mt^2

Φ_ℓ = Potential of phase ℓ, $mL^{-1}t^{-2}$

Subscripts

ℓ = Phase number (1: water, 2: oil, 3: microemulsion)

r = Residual

Superscripts

high = high trapping number

low = low trapping number

REFERENCES

Chen, Jiansheng, Hirasaki, George and Flaum, Mark: "Study of Wettability Alteration From NMR: Effect of OBM on Wettability and NMR Responses," 8th International Symposium on Reservoir Wettability, May 2004.

Delshad, M., G.A. Pope, and K. Sepehrnoori (1996) "A Compositional Simulator for Modeling Surfactant Enhanced Aquifer Remediation, 1. Formulation," *J. of Contaminant Hydrology* **23**, p.303-327.

Delshad, Mohammad (1990) "Trapping of Micellar Fluids in Berea Sandstone," Ph.D. dissertation, The University of Texas at Austin.

Delshad, Mojdeh, Mohammad Delshad, D. Bhuyan, G.A. Pope, and L.W. Lake (1986) "Effect of Capillary Number on the Residual Saturation of a Three-Phase Micellar Solution," Paper SPE 14911, Proceedings of the SPE/DOE Fifth Symposium on Enhanced Oil Recovery, Tulsa, OK, April 20-23.

Hirasaki, G. and D.L. Zhang (2004) "Surface Chemistry of Oil Recovery from Fractured, Oil-wet, Carbonate Formation, " *SPE Journal*, Vol. **9** (2), June 2004, p. 151-162.

Hirasaki, George and Zhang, Danhua Leslie "Surface Chemistry of Oil Recovery From Fractured, Oil-Wet, Carbonate Formation," *SPE* Paper 80988, International Symposium on Oilfield Chemistry, Houston, TX February 5-8, 2003.

Jin, M.: “A Study of Nonaqueous Phase Liquid Characterization and Surfactant Remediation,” Ph.D. dissertation, The University of Texas at Austin, 1995.

Kamath, J. and R.F. Meyer, F. M. Nakagawa (2001) "Understanding Waterflood Residual Oil Saturation of Four Carbonate Rock Types," Paper SPE 71505 presented at the SPE Annual Technical Conference and Exhibition, 30 Sept.-3 Oct., New Orleans, LA.

Mohanty, K. K (1983) "Multiphase Flow in Porous Media: III. Oil Mobilization, Transverse Dispersion, and Wettability," Paper SPE 12127 presented at the SPE Annual Technical Conference and Exhibition, 5-8 October, San Francisco, CA.

Morrow, N.R., P.J. Cram, and F.G. McCaffery (1973) "Displacement Studies in Dolomite with Wettability Control by Octanoic Acid," *SPE Journal*, Aug., p. 221-232.